# Investigation of the early age hydration of four calcium aluminates in the framework of radioactive waste conditioning

Birsen Budan

PSL UNIVERSITÉ PARIS

THÈSE DE DOCTORAT
DE L'UNIVERSITÉ PSL

Préparée à l'Ecole Supérieure de Physique et de Chimie Industrielle de la Ville de Paris

# Etude de l'hydratation au jeune âge de quatre aluminates de calcium dans le cadre du conditionnement des déchets radioactifs


Soutenue par

**Birsen Cansin BUDAN**

Le 22 octobre 2021


Ecole doctorale n° 397

**Physique et chimie des matériaux**

Spécialité

**Chimie des matériaux**

Composition du jury :

| | |
|---|---|
| Gwenn, Le SAOUT<br>Professeur, IMT Mines Alès | *Président*<br>*Examinateur* |
| Sandrine, GAUFFINET<br>Professeure, Université de Bourgogne | *Rapporteure* |
| Guillaume, RENAUDIN<br>Professeur, ICCF UMR 6296, SIGMA Clermont | *Rapporteur* |
| Stéphane, BERGER<br>Ingénieur, IMERYS Aluminates | *Examinateur* |
| Céline, CAU DIT COUMES<br>Ingénieure-chercheur HDR, CEA Marcoule | *Co-encadrante* |
| Jean-Baptiste, CHAMPENOIS<br>Ingénieur-chercheur, CEA Marcoule | *Encadrant* |
| Jean-Baptiste d'ESPINOSE de LACAILLERIE<br>Professeur, ESPCI Paris | *Directeur de thèse* |

ESPCI PARIS | PSL

*Dedicated to my family…*

**Acknowledgements**

This thesis was carried out thanks to the collaboration of two laboratories, the Cement and Bitumen for waste Conditioning Laboratory (LCBC) of CEA Marcoule and the Soft Matter Science and Engineering Laboratory (SIMM) of ESPCI Paris.

First, I would like to thank the jury members for accepting to evaluate this research work and for all discussions and ideas.

I would like to express my sincere gratitude to my supervisors Jean-Baptiste d'Espinose de Lacaillerie and Jean-Baptiste Champenois, for their guidance helped me in all the time of research and writing of this thesis. Thank you very much, Jean-Baptiste Champenois, for your support, your patience, and most of all your guidance and your availability on the experimental and scientific level which allowed me to progress and to learn more and more during these three years. Thank you very much, Jean-Baptiste d'Espinose de Lacaillerie, for your enthusiasm, great scientific rigor, patience, kindness, discussions and big support over these three years. It was a great pleasure to work with you both. I would like to give special thanks to Céline Cau-Dit-Coumes, always being there to answer my questions, to give me new insights on my work, but most of all thank you for passing on to me the passion for this research area over the past four years.

I thank the French Alternative Energies and Atomic Energy Commission for the financial support that enabled me to do this PhD work as well as to my laboratory chef, Stéphane Perrin, for hosting me during these three years at LCBC.

I am grateful to have worked in the LCBC. A huge thank you to the permanent staff (Pascal Antonucci "my big brother", David Chartier, David Lambertin, Arnaud Poulesquen, Jérémy Haas, Adeline Dannoux-Papin, Frédéric Chupin, Nicolas Courtois, Jennifer Sanchez-Canet, Arnaud Leclerc, Géraldine Dideron, Thomas Piallat, David Rudloff, Adrien Gerenton, Karine Ressayre, Myriam Capion) who have given me technical and human assistance.

I particularly thank my colleagues from LCBC and HERA: Jihane, Georges, Charles, Chengying, Pauline, Gabriel, Rachel, Priscillia, Matthieu, Julien, Svetlana, Marie, Lilas, Biwan, Fabrice, Kolani, Théo, Angel, Loïc, Thibault, Pierre-François, Jérémy and Antoine who have given me a great work environment. Thank you all for the support and good humor.

A huge thank you to my family in France. Thank you for the great support my lovely women: Aline (guria), Gabi (vizinha), Léa (wing), Leila (habibi), Miri, Norminha and ma Sara! I would like to also thank my beloved friends Başak, Simge, Ezgi, Pierre, Luiz, Ozan, Eglé, Lénaël, Frantz, Sophie, Armand, Jeanini, Maxime and Erik. Thank you for the great support.

I am forever grateful to my parents Hülya and Birol Budan who supported me, provided me good conditions to keep pushing forward my goals in life and chasing my dreams.

Thank you very much to all those who made this work possible.

Investigation of the early age hydration of four calcium aluminates in the framework of radioactive waste conditioning

## Abstract

### Investigation of the early age hydration of four calcium aluminates in the framework of radioactive waste conditioning

This Ph-D project takes place in the framework of nuclear waste conditioning in cementitious matrices. When an irradiating nuclear waste is stabilized and solidified in a cementitious matrix, the radiolysis of water molecules from the pore solution and from the hydrates themselves yields dihydrogen. In the case of highly irradiating wastes, the release of dihydrogen raises safety issues for storage and/or disposal facilities. The release of hydrogen gas by radiolysis can be limited by reducing the amount of water used for the elaboration of the cement or by choosing a cement binder with hydrates showing a good stability under irradiation. As far as radiolysis is concerned, calcium aluminate-based cements are of significant interest in comparison to calcium silicate cements. The hydration of calcium aluminate cements leads to mineralogical assemblages with a low radiolytic yield of dihydrogen. However, the hydration of these cements is sometimes too fast and incompatible with the industrial process requirements. The objective of this thesis is thus to better understand the underlying mechanisms of the hydration of the calcium aluminates present in calcium aluminate-based cements.

Specifically, the course of hydration of four synthetic anhydrous calcium aluminates, varying one from each other by their C/A ratio, is studied at 25°C from the point of view of their hydration rate, their degree of hydration and the resulting mineralogical assemblages by a combination of isothermal calorimetry, thermogravimetric analysis, x-ray diffraction and solid-state nuclear magnetic resonance. Monitoring the hydration by isothermal calorimetry in pastes and by conductometry in suspensions show that the higher the C/A ratio of the considered anhydrous phase, the higher the hydration rate. Finally, studying the hydration of each of these phases in suspension makes it possible to point out the reaction path followed by each studied system. This work also demonstrated that aluminium hydroxide formation limits the kinetics of hydration of anhydrous phases with a C/A ratio lower than or equal to 1. The results obtained in the framework of this thesis can help optimizing the design of a calcium aluminate cement-based matrix to be used for the conditioning of irradiating wastes.



**Keywords:** calcium aluminate cement, hydration, calcium aluminate hydrates, hydration degree, conductometry, isothermal calorimetry, solid-state NMR

## Résumé

### Étude de l'hydratation au jeune âge de quatre aluminates de calcium dans le cadre du conditionnement des déchets radioactifs

Lorsque des déchets nucléaires irradiants sont conditionnés en matrice cimentaire, l'eau contenue dans la solution porale et dans les hydrates peut être radiolysée, conduisant notamment à la production de dihydrogène. Dans le cas de déchets fortement irradiants, la maitrise de ce terme source hydrogène dans un site d'entreposage et/ou de stockage peut constituer un enjeu de sûreté. Ce terme source hydrogène peut-être limité en diminuant la quantité d'eau mise en œuvre pour élaborer les matrices cimentaires de conditionnement, ou en choisissant un liant cimentaire dont les produits d'hydratation présentent un faible rendement de production radiolytique de dihydrogène. De ce point de vue, les ciments alumineux pourraient présenter un intérêt significatif par rapport aux ciments silico-calciques. En effet, l'hydratation des ciments alumineux conduit à des assemblages minéralogiques dont les hydrates présentent une bonne stabilité sous irradiation. Toutefois, la vitesse d'hydratation de ces ciments est parfois élevée et incompatible avec les contraintes d'un atelier de cimentation industriel. Il convient donc de mieux comprendre les mécanismes d'hydratation de ces phases pour éventuellement mieux les contrôler.

Dans le cadre de ce travail, le déroulement de l'hydratation de quatre aluminates de calcium anhydres synthétiques, se distinguant l'un de l'autre par leur rapport C/A, a été étudié. En particulier, ont été examinés, leur vitesse d'hydratation, leur degré d'hydratation et l'assemblage minéralogique formé. Les suivis d'hydratation ont été réalisés par microcalorimétrie isotherme et conductimétrie quand les phases ont été caractérisées par analyse thermogravimétrique, par diffraction des rayons-x et par résonance magnétique nucléaire du solide. Toutes les expériences ont été réalisées à 25 °C. Les résultats du suivi de l'hydratation de pâtes de ciment et de suspensions cimentaires nous ont permis de conclure que les vitesses d'hydratation sont d'autant plus grandes que le rapport C/A de l'anhydre considéré est élevé. De plus, l'étude de l'hydratation de ces phases anhydres en suspension a permis d'identifier les chemins réactionnels suivis par chacun des systèmes étudiés. Notamment, il a été démontré que la formation d'hydroxyde d'aluminium limite la cinétique d'hydratation des phases anhydres dont le rapport C/A est inférieur ou égal à 1. Les résultats obtenus dans le cadre de ce travail pourront permettre à terme d'orienter le choix du ciment alumineux à mettre en œuvre pour le conditionnement de déchets irradiants.



**Mots-clefs:** ciment alumineux, hydratation, aluminates de calcium hydraté, degré d'hydratation, conductimétrie, microcalorimétrie, RMN du solide

# Table of contents

# List of figures

# List of tables

# Glossary

*Cementitious notation*

| | | | |
|---|---|---|---|
| C : CaO | A : $Al_2O_3$ | S : $SiO_2$ | Š : $SO_3$ |
| Č : $CO_2$ | H : $H_2O$ | F : $Fe_2O_3$ | T : $TiO_2$ |

*Abbreviations for the main anhydrous and hydrated phases*

| | | |
|---|---|---|
| **$CA_2$** | $CaAl_4O_7$ | Calcium dialuminate |
| **CA** | $CaAl_2O_4$ | Monocalcium aluminate |
| **$C_{12}A_7$** | $Ca_{12}Al_{14}O_{33}$ | Mayenite |
| **$C_3A$** | $Ca_9(Al_2O_6)_3$ | Tricalcium aluminate |
| **$CAH_{10}$** | $CaAl_2O_4 \cdot 10H_2O$ | Monocalcium aluminate decahydrate |
| **$C_2AH_8$** | $Ca_2Al_2O_5 \cdot 8H_2O$ | Dicalcium aluminate hydrates |
| **$C_2AH_{7.5}$** | $Ca_2Al_2O_5 \cdot 7.5H_2O$ | |
| **$C_4AH_{19}$** | $Ca_4Al_2(OH)_{12} \cdot 13(H_2O)$ | Tetracalcium aluminate hydrates |
| **$C_4AH_{13}$** | $Ca_4Al_2(OH)_{12} \cdot 7(H_2O)$ | |
| **$C_4AČH_{11}$** | $Ca_4Al_2(OH)_{12}(CO_3)(H_2O)_5$ | Calcium monocarboaluminate (Mc) |
| **$C_4AČ_{0.5}H_{12}$** | $(CaO)_4 \cdot (Al_2O_3) \cdot (CO_2)_{0.5} \cdot (H_2O)_{12}$ | Calcium hemicarboaluminate (Hc) |
| **$C_3AH_6$** | $Ca_3Al_2(OH)_{12}$ | Katoite |
| **$AH_3$** | $2Al(OH)_3$ | Aluminium hydroxide |
| **CH** | $Ca(OH)_2$ | Portlandite |
| **CČ** | $Ca(CO)_3$ | Calcite |
| **α-A** | α-$Al_2O_3$ | Alpha alumina |

*Abbreviations for the techniques*

| | |
|---|---|
| **XRD** | X-Ray Diffraction |
| **TGA** | Thermogravimetric Analysis |
| **NMR** | Nuclear Magnetic Resonance |
| **ICP-AES** | Inductively coupled plasma atomic emission spectroscopy |

*Other abbreviations*

| | |
|---|---|
| **CAC** | Calcium aluminate cement |
| **PC** | Portland cement |
| **w/c** | Water to cement ratio |
| **wt.%** | Weight percent |

# Introduction

A wide variety of radioactive wastes needs to be treated and conditioned for successful waste management, including transportation, storage and final disposal. The treatment process demands to minimize the volume of waste, which will be finally sent to disposal. The conditioning stage aims at reducing the potential hazard of the radioactive waste by providing an effective confinement. This means that the stabilization of the waste must either convert it into a form that excludes posterior evolution (e.g. incineration or mineralization of organic wastes), or eliminate its aggressive substances (e.g. neutralization of acids). In the end, the raw waste which is generated in solid and liquid form is immobilized and turned into "waste packages" in order to facilitate their transportation and to prevent dispersion in the surrounding environment [1].

Among the conditioning processes, there are different approaches to immobilize and stabilize radioactive wastes such as conditioning by cements, bitumens, polymers or glasses through mixing and/or encapsulating with the matrix material [2]. In particular, cementation is a widely applied process for the conditioning of low- and intermediate-level radioactive wastes.

The conditioning via solidification and stabilization in a cement matrix is a robust solution. However, the application of cementitious materials for radioactive waste conditioning demands special grout formulation adapted to the immobilization of the specific radioactive material, e.g. aqueous solutions, sludge, precipitates/gels, metals or ion exchange resins [3-5].

The conditioning of radioactive waste in a cementitious matrix raises the problem of the interaction between an ionizing particle and the cementitious material. Consequently, several studies have been carried out to determine the impact of radiation on cementitious matrices and to ensure the validity and durability of these solutions [6-11]. Indeed, the water naturally present in the cement matrix produces hydrogen gas when it is exposed to ionizing radiations emitted internally by the waste. To ensure the safety of the storage and/or of its disposal, the cement needs to be formulated to limit the release of the radiolytic gas to an acceptable level.

Portland Cement (PC) is a binder of reference for low- and intermediate-level radioactive wastes [12]. However, the gas release by radiolysis is a concern that may hinder the use of PC for the conditioning of some intermediate-level radioactive wastes containing high levels of alpha emitters. Indeed, when hydrated PC is exposed to ionizing radiation, the interstitial solution and hydrated cementitious phases produce hydrogen gas due to water decomposition.

In her thesis, L. Acher [9] investigated the production of radiolytic gas, in particular hydrogen gas, under γ and electron irradiations from three types of cement matrices and their hydration products. Hydrogen radiolytic yield $G(H_2)$ corresponds to the amount of hydrogen released by the material per amount of absorbed energy. The studies conducted on cement pastes showed that the production of hydrogen gas depends on the water-to-cement (w/c) ratio, but most importantly on the cement type. When calcium aluminate cement was used as cementitious

matrix, the global radiolytic hydrogen yield $G(H_2)$ was about three times lower than for Portland cement when submitted to irradiation. In contrast to what was generally accepted in the literature, this study evidenced a significant contribution of hydrates to hydrogen gas production in the cementitious matrices, in addition to the pore water. In brief, L. Acher demonstrated that Calcium Aluminate Cement (CAC) hydrates intrinsically produce less hydrogen, in comparison to PC hydrated phases [9]. For instance, the radiolytic production rate of katoite $C_3AH_6$ was ten times lower than that of a major hydrate formed during the hydration of PC i.e. C-S-H (calcium silicate hydrate) as shown in Figure 1.

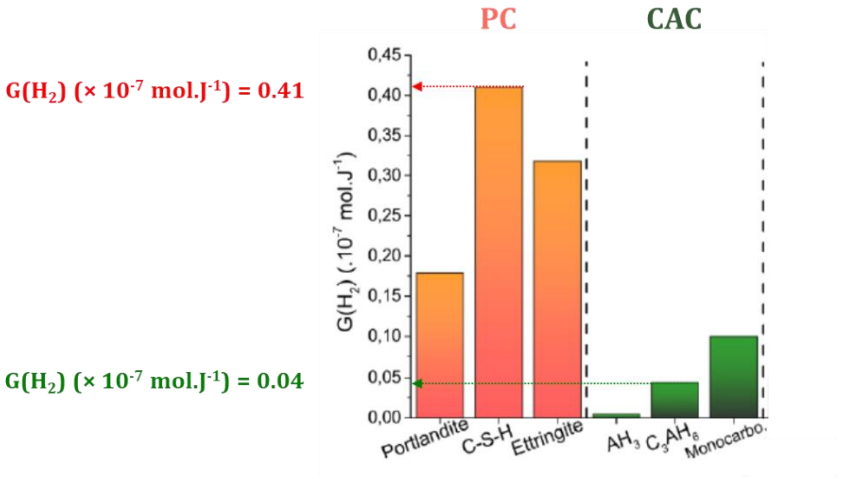


**Figure 1 : $G(H_2)$ values determined from Portland and Ciment Fondu® pastes and their hydrates, adapted from [9].**

When the cement is in contact with water, hydration starts. In CAC systems, formation of hydrates and hardening occur very rapidly. Previous studies have shown that the high reactivity of CACs results in short workability periods [13-16], unless an admixture is used. The dissolution kinetics of anhydrous calcium silicate cement phases and tricalcium aluminate have been widely investigated in suspensions or pastes [17-21]. However, in the field of calcium aluminate cements, the hydrations kinetics are still not so well-understood [22-26], which is a limit to widen their range of application for radwaste immobilization.

The main anhydrous components in CACs are grossite ($CaAl_4O_7$ or $CA_2$), monocalcium aluminate ($CaAl_2O_4$ or CA) and mayenite ($Ca_{12}Al_{14}O_{33}$ or $C_{12}A_7$). In addition, tricalcium aluminate ($Ca_3Al_2O_6$ or $C_3A$) is a principal phase of PC systems. Despite having similar chemistry in solution, these anhydrous phases lead to different early hydration kinetics. The present work aims at providing a better understanding of the early age hydration mechanisms of four calcium aluminates, varying one from each other by their C/A ratio. Thus, this work is rather a fundamental research and some of the basic questions are presented hereafter.

- The rapid reactions taking place during hydration of CACs make mechanisms difficult to study and may result in a short period of workability. We aim to understand how these calcium aluminates, varying one from each other by their $CaO/Al_2O_3$ ratio, react with water and describe the main reaction pathways.
- How do the precipitated hydrates evolve in the pastes and suspensions? How does the w/c ratio influence the mineralogical assemblages?
- What is the exact number of steps and the nature of the transient hydration products? The hydration process of CACs is a complex phenomenon. It involves several steps, but the exact number of steps and the nature of the transient hydration products remain debated, depending strongly on the applied conditions e.g. temperature, relative humidity, hydration time, water availability.
- Are the hydration mechanisms governed by the dissolution of anhydrous phases or the precipitation of hydrates?

In summary, the general aim of this PhD work is to "describe dissolution and precipitation processes that occur during the hydration of calcium aluminate phases, in order to widen their range of application to radwaste conditioning matrices with limited hydrogen production under irradiation, and help the design of materials with a well-controlled reactivity".

In this thesis manuscript, a state-of-art is first presented. It summarizes the knowledge about the composition of CACs, their properties and their early hydration process, and details each step, including hydration products and their structural properties (Chapter 1).

Afterward, we present the studied materials, the experimental procedures for the hydration investigations and the characterizations carried out (Chapter 2).

Chapter 3, 4, 5 and 6 are dedicated to the hydration studies of pure anhydrous calcium aluminate phases differing from each other by their C/A ratio: $CA_2$, CA, $C_{12}A_7$, $C_3A$. Each of the chapter treats one particular phase and is divided in two sections. First, the focus is on the hydration rates of the pastes prepared with the anhydrous phase under study. The influence of the w/c ratio is investigated. The pastes are then characterized in order to determine their mineralogical assemblages at early age and 7 days after mixing. Estimations are done on the hydration degree reached by the different systems. Second, the hydration studies are carried out in diluted media, which makes it possible to increase the duration of the different stages of hydration, thus allowing the characterization of liquid and solid fractions of rapidly-reacting systems.

Lastly, Chapter 7 concludes on the main findings of this PhD thesis and presents suggestions for future work.

## References


[1] C. S. a. G. Moniteur, J.-F. Parisot, Ed. *Nuclear Waste Conditioning*, Paris ed. (A Nuclear Energy Division Monograph). 2009.

[2] N. C. Hyatt and M. I. Ojovan, "Special Issue: Materials for Nuclear Waste Immobilization," *Materials*, vol. 12, no. 21, 2019.

[3] C. Cau Dit Coumes and S. Courtois, "Cementation of a low-level radioactive waste of complex chemistry Investigation of the combined action of borate, chloride, sulfate and phosphate on cement hydration using response surface methodology," *Cement and Concrete Research*, vol. 33, pp. 305–316, 2003.

[4] F. Bart, C. Cau Dit Coumes, F. Frizon, and S. Lorente, *Cement-Based Materials for Nuclear Waste Storage*. 2013.

[5] Z. Drace and M. I. Ojovan, "The Behaviours of Cementitious Materials in Long Term Storage and Disposal: An Overview of Results of the IAEA Coordinated Research Project," *MRS Proceedings*, vol. 1193, p. 663, 2009, Art. no. 663.

[6] C. J. Kertesz, P. R. Chenavas, and L. Auffret, "Conditioning of alpha and beta-gamma ashes of incinerator, obtained by radioactive wastes incinerating and encapsulation in several matrices," Commission of the European Communities (CEC)1993, Available: http://inis.iaea.org/search/search.aspx?orig_q=RN:24036288.

[7] C. Gallé *et al.*, "Concrete long-term behaviour in the context of nuclear waste management: Experimental and modelling research strategy," *J. Phys. IV France*, 10.1051/jp4:2006136004 vol. 136, pp. 25-38, 2006.

[8] K. Noshita, T. Nishi, and M. Matsuda, "Generation Mechanism of Hydrogen Gas from Hardened Cement Paste by γ-Irradiation," *MRS Proceedings*, vol. 353, p. 921, 1994, Art. no. 921.

[9] L. Acher, "Etude du comportement sous irradiation γ et électronique de matrices cimentaires et de leurs hydrates constitutifs," Doctorat École doctorale n°573 Interfaces Université Paris-Saclay, NNT : 2017SACLX045, 2017.

[10] D. Chartier, J. Sanchez-Canet, L. Bessette, S. Esnouf, and J. P. Renault, "Influence of formulation parameters of cement based materials towards gas production under gamma irradiation," *Journal of Nuclear Materials*, vol. 511, pp. 183-190, 2018/12/01/ 2018.

[11] P. Rotureau, "Etude de la radiolyse de l'eau en milieu poreux," Thèse de doctorat, Département de Recherche sur l'État Condensé, les Atomes et les Molécules, Ecole Nationale Superieure de Chimie de Mulhouse, 2004.

[12] C. Cau Dit Coumes, "Alternative Binders to Ordinary Portland Cement for Radwaste Solidification and Stabilization," in *Cement-Based Materials for Nuclear Waste Storage*, F. Bart, C. Cau-di-Coumes, F. Frizon, and S. Lorente, Eds. New York, NY: Springer New York, 2013, pp. 171-191.

[13] M. Heikal, M. S. Morsy, and M. M. Radwan, "Electrical conductivity and phase composition of calcium aluminate cement containing air-cooled and water-cooled slag at 20, 40 and 60 °C," *Cement and Concrete Research*, vol. 35, no. 7, pp. 1438-1446, 2005/07/01/ 2005.

[14] J. H. Ideker, "Early-age behavior of calcium aluminate cement systems," Doctor of Philosophy, Civil, Architectural, and Environmental Engineering, The University of Texas at Austin Austin, 2008.

[15] I. Stinnessen, A. Buhr, R. Kockegey-Lorenz, and R. Racher. (30 August). *High Purity Calcium Aluminate Cements, Production And Properties*. Available: https://almatis-umbraco.azurewebsites.net/media/3985/high_purity_calcium-aluminate-cements_production_and_properties.pdf

[16] J. Pourchez, P. Grosseau, and B. Ruot, "Current understanding of cellulose ethers impact on the hydration of C3A and C3A-sulphate systems," *Cement and Concrete Research,* vol. 39, no. 8, pp. 664-669, 2009/08/01/ 2009.

[17] F. Hueller, C. Naber, J. Neubauer, and F. Goetz-Neunhoeffer, "Impact of initial CA dissolution on the hydration mechanism of CAC," *Cement and Concrete Research,* vol. 113, pp. 41-54, 2018/11/01/ 2018.

[18] L. Nicoleau, A. Nonat, and D. Perrey, "The di- and tricalcium silicate dissolutions," *Cement and Concrete Research,* vol. 47, pp. 14-30, 2013/05/01/ 2013.

[19] F. Bellmann, T. Sowoidnich, H.-M. Ludwig, and D. Damidot, "Dissolution rates during the early hydration of tricalcium silicate," *Cement and Concrete Research,* vol. 72, pp. 108-116, 2015/06/01/ 2015.

[20] A. S. Brand *et al.*, "Dissolution and initial hydration behavior of tricalcium aluminate in low activity sulfate solutions," *Cement and Concrete Research,* vol. 130, p. 105989, 2020/04/01/ 2020.

[21] M. J. Sánchez-Herrero, A. Fernández-Jiménez, and A. Palomo, "Alkaline Hydration of Tricalcium Aluminate," *Journal of the American Ceramic Society,* vol. 95, no. 10, pp. 3317-3324, 2012/10/01 2012.

[22] N. Maach, "Kinetic modeling of the early age hydration of calcium aluminate cements : From chemical mechanism to the modeling by the Population Balance Equations," Thèse de doctorat, Mécanique, Energétique, Génie Civil, Acoustique (MEGA), l'INSA de Lyon, 2019LYSEI127, 2019.

[23] K. L. Scrivener and A. Nonat, "Hydration of cementitious materials, present and future," *Cement and Concrete Research,* vol. 41, no. 7, pp. 651-665, 2011/07/01/ 2011.

[24] S. Berger and H. Fryda, "Calcium aluminate cements for nuclear wastes conditioning: literature review and new approaches," presented at the NUWCEM-2011 Avignon (France), 2011. Available: https://www.osti.gov/etdeweb/biblio/22051442

[25] B. Lothenbach, L. Pelletier-Chaignat, and F. Winnefeld, "Stability in the system CaO–$Al_2O_3$–$H_2O$," *Cement and Concrete Research,* vol. 42, no. 12, pp. 1621-1634, 2012/12/01/ 2012.

[26] V. S. Ramachandran and R. F. Feldman, "Hydration characteristics of monocalcium aluminate at a low water/solid ratio," *Cement and Concrete Research,* vol. 3, no. 6, pp. 729-750, 1973/11/01/ 1973.

# Chapter 1: Literature review

# **Chapitre 1** : Étude Bibliographique

**Résumé:** L'état de l'art, présenté dans ce chapitre, porte sur les ciments alumineux calciques (CAC), leur hydratation et les mécanismes d'hydratation. Premièrement, est présenté l'état des connaissances sur la fabrication et la composition des ciments alumineux. Les caractéristiques des phases anhydres et de leurs produits d'hydratation sont successivement détaillées. Ensuite, une seconde partie est dédiée à l'hydratation d'aluminates de calcium purs qui feront l'objet d'une étude expérimentale dans la suite de ce travail. Nous présentons d'abord les réactions mises en jeu et la formation des hydrates qui en résulte. Puis, nous nous intéressons plus particulièrement à l'interprétation du suivi de l'hydratation par différentes techniques dans le but de dégager les mécanismes d'hydratation identifiés dans la littérature sur les ciments alumineux.

# Introduction

The state of the art presented in this chapter provides a background information about calcium aluminate phases, their hydration mechanisms and products.

This chapter outlines the relevant literature on calcium aluminate cements (CACs). The first part presents the composition and properties of calcium aluminate cements and their manufacturing processes. In addition, a second part is dedicated to the hydration of pure calcium aluminate phases studied during this work. We first present the chemical reactions of pure CACs and the formation of the resulting hydrates during hydration. Then, we focus on the interpretation of the hydration monitoring by different techniques in order to describe the hydration mechanisms of calcium aluminate phases reported in the literature.

## 1. Calcium aluminate cements – From the modern day manufacturing to their applications

Calcium aluminate cements were first documented from the observations of a reaction of alumina with marble by Ebelman (1848) and Saint-Claire Deville (1856) [1, 2]. In 1890, due to the corrosion of PLM (Paris, Lyon and Mediterranean) Railway in the south of France, studies led by Jules Bied were patented in 1908 in the Lafarge laboratories in France and then in UK. Consequently, their industrial applications were patented for the manufacturing process of bauxite, or other aluminous and ferruginous materials having a low silica content, fused with limestone [3]. The product of this manufacturing process was called High-alumina cement (HAC) due to their high alumina content. In these systems, calcium aluminate phases dominate the chemistry, thus in literature, HAC is referred as CAC.

From an historical timeline, at first, their resistance to environments containing calcium sulfate compared to Portland cements (PC) made them very interesting for constructions susceptible to sulfate attack. Further investigations proved another advantage of these cements: high early strength development because of rapid hardening in comparison to PC. Later on, from the 1980s on, CACs dominated the market for castable refractories [2]. An important economical characteristic is their high alumina content, sourced from bauxite – a limited resource – a fact that directly affects their cost making them significantly more expensive than PC. However, their distinct properties make them relevant for specific usage. Eventually, CACs are the most important family of non-Portland cements [4].

The cementitious materials for radioactive waste solidification and stabilization include a widely substantial amount of calcium silicate cements (PC, possibly blended with blastfurnace slag and/or fly ash). However, due to the complexity of nuclear waste compositions, when calcium silicate cement is hydrated, adverse waste-cement interactions sometimes occur and decrease the quality of the final product through, for example, swelling and cracking.

Approaches to suppress these undesired waste-cement interactions include pre-treatment of the waste by converting the interfering species into stable compounds within the cement matrix, or the selection of a cement showing a better chemical compatibility with the waste.

In this regard, CACs have been suggested as a possible alternative binder [5, 6] due to their potential for waste conditioning, as described in the following part.

## 1.1. Manufacturing of CACs

Calcium aluminate cements are mainly the product of limestone and bauxite used as raw materials. The main factor determining the manufacturing process is the $Al_2O_3$ content. By varying this content over a wide range, from 37.5 to over 82.5 %, different grades of CACs are manufactured [4]. There are two major methods to produce calcium aluminate cements in the cement factories:

- High purity CACs (60 to 82.5 % $Al_2O_3$) referred as "white" CACs. When demanded in a manufacturing process, pure raw materials are used i.e. low ferruginous bauxites, reactive alumina, low-silica lime-bearing compounds [4, 7, 8]. Manufacturing of these cements are processed by **sintering** limestone and alumina. First, raw materials are blended and grounded together, and second, fed to rotary kilns fired by fuel oil at about 1300 °C [9].
- Low purity CACs (37.5 to 40 % $Al_2O_3$) referred as "standard" CACs. Manufactured by **fusing** a mixture of limestone and bauxite in a reverberatory furnace at high temperatures up to 1400 °C [10]. As the mixture of raw materials is introduced to the furnace fired by pulverized coal, natural gas, oil or combination of them, the melting process occurs. The molten substance is then poured out constantly from a tap hole and slowly cooled. Once cooled, the clinker is produced then crushed by milling to reach required surface area [4].

Comparing these processes to the PC manufacturing process, the production of CAC results in lower $CO_2$ emission [11]. CAC requires lower lime content and less energy (fuel+electricity consumption) during the manufacturing processes than PC [12, 13]. Nevertheless, the annual production of CACs is about a thousand times less than that of Portland cement due to the cost of its manufacturing process (6-8 times more expensive than PC) and because of its use in specialized applications rather than in structural applications where PC is preferred.

Lastly, concerning the production of pure anhydrous phases, in general, their high-temperature synthesis are realized by using proper stoichiometric powder mixtures of $CaCO_3$ and $\alpha$-$Al_2O_3$ to obtain the desired compounds $C_3A$, CA, $CA_2$ and $C_{12}A_7$. The powder mixtures are placed in the heat-resistant crucibles, heated up to high temperatures (1360-1600 °C) and followingly cooled down inside the furnace. The resulting solids are ground and protected from air to minimize $CO_2$ contamination [14-16].

CACs are categorized in the market depending on their alumina content. Besides, the impurities e.g. iron and silica change the color of the CACs. High grades of CAC are white as they contain less impurities compared to lower grades of CAC [8]. The chemical compositions of several commercial CACs are summarized in Table 1.

**Table 1 : Typical oxide composition (wt. %) of common commercial CACs [17].**

| CAC | Color | $Al_2O_3$ | CaO | $SiO_2$ | $Fe_2O_3$ | Principal phases | Secondary phases |
|---|---|---|---|---|---|---|---|
| Fondu | Grey to black | 38-42 | 37-40 | 3-5 | 14-18 | CA | $C_{12}A_7$, $CA_2$, $C_2S$, $C_2AS$, $C_4AF$ |
| SECAR51 | Grey to white | 51-53 | 37-39 | 4-6 | - | CA | $C_{12}A_7$, $C_2AS$, CT |
| SECAR71 | White | 70-72 | 27-29 | - | - | CA, $CA_2$ | $C_{12}A_7$, α-A |
| SECAR80 | White | 80-83 | 16-18 | - | - | CA, $CA_2$, α-A | $C_{12}A_7$ |

During the manufacturing of CACs, C/A ratios are altered to produce different grades at different temperature ranges [4, 18, 19]. Figure 2 reveals how the formation of compounds such as $C_3A$, $C_{12}A_7$, CA, $CA_2$ and $CA_6$ occurs as the heating advances and by controlling the C/A ratios of the feed [11, 20]. These phases having different melting points can co-exist at same ranges [21]. It should be noted that $C_3A$ is not a normal constituent of CACs and $CA_6$ is rarely found.

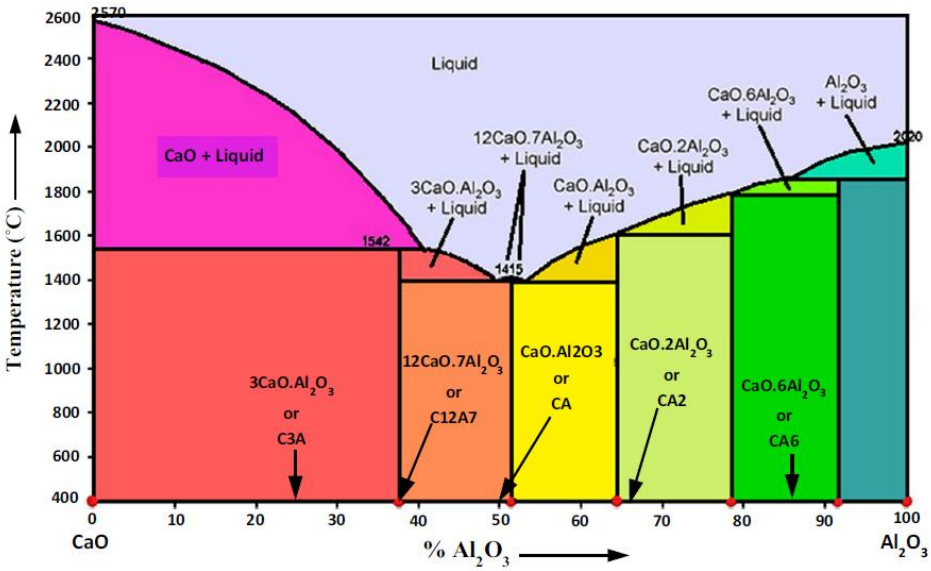


**Figure 2 : Phase diagram of $CaO$-$Al_2O_3$ system (molar fraction of $Al_2O_3$, %), reproduced from [20].**

## 1.2. Properties of CACs and their application areas

CACs differ from PC both chemically and physically [2]. In general, they are used by the construction industry as an alternative to PC due to their rapid setting and hardening even under sub-freezing weather conditions (around -10 °C). CACs can develop high early strength at 24 hours (compressive strength of ~50 MPa) while the PC needs at least 28 days to reach the same strength. That favors CAC application when high mechanical resistance in very short time is required e.g. rapid repairing grouts and mortars, foundation constructions, mining and tunnelling [2, 4, 22]. Also, mixtures of CACs and PC are used to make rapid hardening concretes and mortars i.e. ultra-fast setting concrete (in a few minutes) [23]. CACs are mainly used in a wide range of applications when specific properties are required, such as heat-resistance in refractory castables resisting up to 1600 °C [24, 25], high resistance against chemical corrosion particularly in acidic environments in the construction of sewage and wastewater pipelines, factory drains, coastal establishments, and factory chimneys [2, 4, 26].

Concerning nuclear waste conditioning, the potential of CACs as an alternative binder to PC arises from the following points:

- They contain chemical reactants that can form AFm or AFt phases with a flexible structure, which can uptake some deleterious species originated from radioactive wastes [3],
- They are compatible with compounds known to be strong retarders of PC such as heavy metals or borate ions [3],
- They have high thermal and chemical resistance, especially to acid attack [27],
- They have a high chemical water demand, thus leading to a dry internal environment due to the self-desiccation,
- The pore solution pH can be reduced allowing to mitigate the effect of adverse cement-waste interaction, in particular the corrosion of some metals [3].

Most interestingly, the amount of $H_2$ produced by Ciment Fondu pastes is found to be much lower than the amount produced by PC pastes containing the same amount of water, especially in the low range of water-to-cement ratios ($W/C \leq 0.4$). The $H_2$ production of the two major hydrates of Ciment Fondu®, gibbsite $AH_3$ and katoite $C_3AH_6$, is very low compared with that of the main hydrates of other cements as shown in Figure 3. Note that the normalized radiolytic yield represents the hydrogen radiolytic yield normalized with respect to the total mass of water present in the material [28].

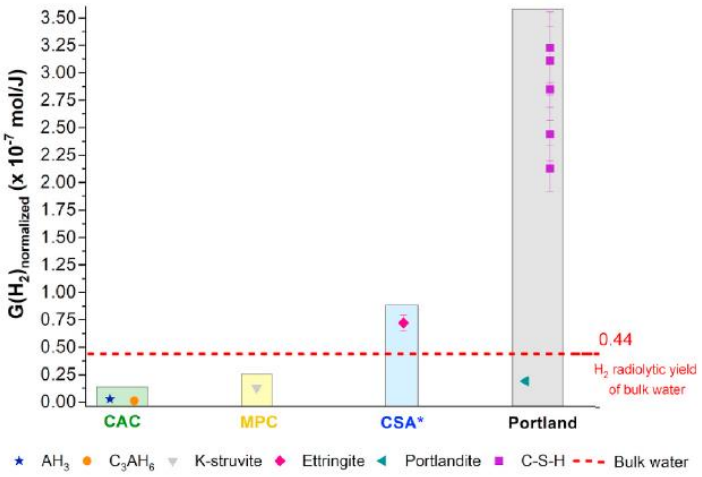


**Figure 3 : Normalized $H_2$ radiolytic yields for major hydrates of CAC, Magnesium Phosphate Cements (MPC), Calcium Sulfo-Aluminate cements (CSA *with calcium sulfate) and PC, reproduced from [28].**

Despite the advantageous characteristics of CACs, a problematic development can occur during their hydration: the conversion of metastable hydrates with low density into denser thermodynamically stable hydrates over time [29, 30]. As a consequence of this process, a reduction in solid volume and the formation of pores occur and result in strength loss [31]. In addition, this hydrates conversion releases water which can further react with the remaining anhydrous cement phases [32, 33]. Such a process might be problematic for practical applications as the macroscopic properties of the hardened cement-based material vary with time. Therefore, the use of calcium aluminate cements in mortars and concretes requires special precautions and their final properties should be predicted before their conception [34].

In the following section, the composition and structures of anhydrous and hydrated calcium aluminate phases are successively presented.

## 2. Characteristics of anhydrous calcium aluminate phases and their hydration products

### 2.1. Composition and structure of anhydrous phases

As described previously, commercial CACs contains mainly three anhydrous phases of interest [35]:

- Monocalcium aluminate CA, as the main hydraulic phase
- Mayenite $C_{12}A_7$
- Calcium dialuminate $CA_2$

The structure of the anhydrous phases and their main hydrates is detailed below. This information is be helpful for the interpretation of the results obtained by solid-state $^{27}Al$ NMR spectroscopy in the following chapters.

- *Monocalcium aluminate – CA*

The main reactive phase in the cement, the monocalcium aluminate ($CaAl_2O_4$), has its nomenclature derived from the CaO (C) to $Al_2O_3$ (A) ratio (1:1). Its proposed structure is monoclinic, from the space group $P2_1/n$ (14), with the parameters: a = 8.700 Å, b = 8.099 Å, c = 15.217 Å and $\alpha = 90°$, $\beta = 90°$, $\gamma = 90°$; z (number of formula units in the unit cell) = 12 [36]. Its asymmetric unit, i.e., the smallest structural unit that can be repeated (rotated or translated) to form the whole unit cell, has a ring composed of six non-equivalent $AlO_4^-$ tetrahedral units, and the calcium atoms occupy the voids of the rings (Figure 4a) [17, 37, 38]. The Ca atoms occupy three different sites: two of Ca are located between the rings in octahedral coordination (the orange octahedra in Figure 4b) and one Ca weakly bounded to nine O atoms [39]. In commercial CACs, CA is normally found in a solid solution with $Fe^{+3}$, which occupies a small portion of the $Al^{+3}$ tetrahedral sites, resulting in a composition of $Ca(Al_{1-x}Fe_x)_2O_4$ [17, 40].

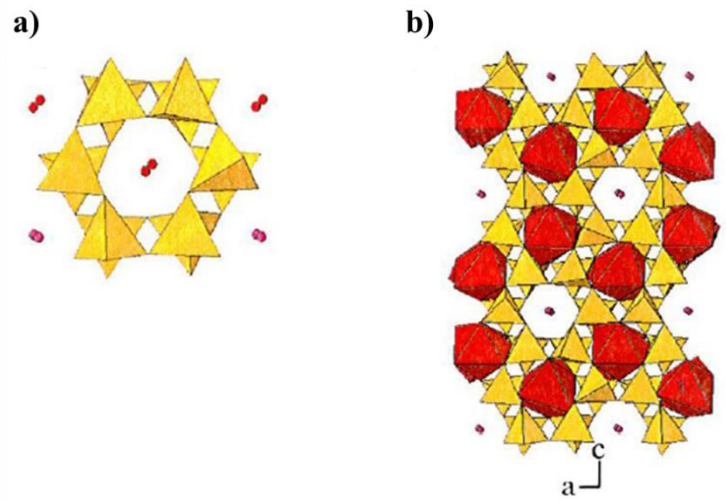


**Figure 4 : The CA structure: (a) six-membered rings of $AlO^{-4}$ tetrahedra (in yellow) and Ca atoms (orange spheres) in the voids of the rings, and (b) representation of the crystal structure with several asymmetric units showing the octahedral coordinated Ca ions (orange) composing two thirds of the interstices, reproduced from [17].**

- *Calcium dialuminate – $CA_2$*

Anhydrous $CA_2$ is also composed of a succession of $AlO_4^-$ tetrahedra bound to each other by calcium atoms [17]. There has been a long history of controversy about clarifying the structure

of this phase [20, 41, 42]. Based on X-ray diffraction (XRD), it has been initially reported that $CA_2$ crystalized in the monoclinic crystal system. However, further studies reported that this phase could belong to either the hexagonal or tetragonal system [42]. Hussain A. *et al.* has accepted the structure as monoclinic (Figure 5) in accordance to the research of Goodwin and Lindop [41]. The structure is described as Ca occurring in sevenfold coordination, whereas Al is distributed over two symmetrically independent tetrahedral sites, both of which are quite distorted [11, 41]. Skibsted *et al.* reported that in the crystal structure of $CA_2$, the main difference between the two crystallographically distinct tetrahedral Al sites is that one of the Al site, $Al_2$(IV), is linked to two tricoordinated O atoms whereas $Al_1$(IV) is linked to only one tricoordinated O atom [38]. A monoclinic unit cell has been proposed for $CA_2$ structure with the parameters: a = 12.866 Å, b = 8.879 Å, c = 5.440 Å and α = 90°, β = 107°, γ = 90°; z = 4. Whereas the $CA_2$ space group would be C2/c [41].

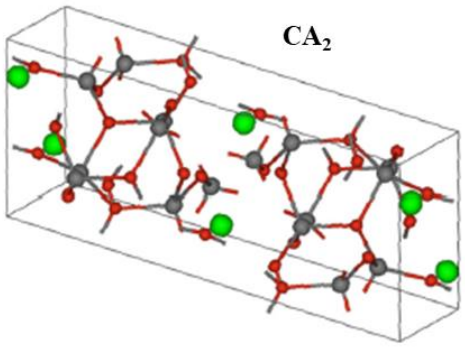


**Figure 5 : Crystal structure of the $CA_2$ phase (Al, grey; Ca, green; O, red), reproduced from [20].**

- *Dodecacalcium hepta-aluminate – $C_{12}A_7$*

Anhydrous $C_{12}A_7$ phase may exist as a major phase of commercial high-alumina cements [43]. In this structure, Al forms relatively regular $AlO_4^-$ tetrahedral that are partly interconnected by common corners (Figure 6) [20, 44]. Those partially connected tetrahedra build eightfold rings by bridging partly with Ca. The irregular Ca polyhedron has four short bonds (2.35 and 2.39 Å), two long bonds (2.59 Å) and a longer bond (2.73 Å) [20, 44]. The unit cell of $C_{12}A_7$ can be represented as two components: $[Ca_{24}Al_{28}O_{64}]^{4+}\cdot(O^{2-})_2$ [45]. The $[Ca_{24}Al_{28}O_{64}]^{4+}$ signifies a three dimensional lattice framework containing 12 cages. The two $O^{2-}$ ions denote extra-framework species as free ions and they are loosely bound to the lattice framework. These free ions can be replaced by various anions such as $OH^-$, $F^-$ and $Cl^-$ [46]. A cubic unit cell has been proposed for $C_{12}A_7$ structure with the parameters: a = 12 Å, b = 12 Å, c = 12 Å and α = 90°, β = 90°, γ = 90°; z = 2. Whereas $C_{12}A_7$ space group belongs to I4-3d (220) [47].

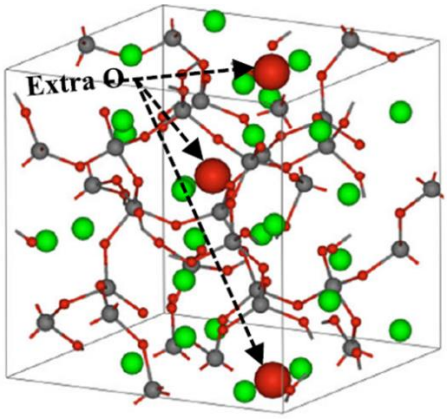


**Figure 6 : Crystal structure of the $C_{12}A_7$ phase (Al, grey; Ca, green; O, red), reproduced from [20].**

The structure of $C_3A$ is also described; below since the influence of C/A ratio of this anhydrous calcium aluminate phases was investigated in the scope of this thesis.

- *Tricalcium aluminate – $C_3A$*

The $C_3A$ is the most alumina-rich phase of PC. Different polymorphs of $C_3A$ exist: cubic, orthorhombic and monoclinic [40]. The cubic structure of $C_3A$ (Figure 7a) has a lattice constant of 15.263 Å , and belongs to the space group Pa3 (205) [48]. The asymmetric unit of $C_3A$ has six Ca, two A1 and six O atoms and the unit cell has 264 atoms. In this structure, the two types of $AlO_4^-$ tetrahedra are linked to form sixfold rings [49]. Figure 7b shows the structure of the ring detailing its two aluminium sites (Al1 and Al2) and six oxygen sites (O1, O2, O3, O4, O5, and O6) [50]. The $Ca^{2+}$ ions are located inside and in between the rings, and occupy 72 from the 80 interstices available. The average A1-O bond length is 1.750 Å for Al1 and 1.754 Å for Al2 [48].

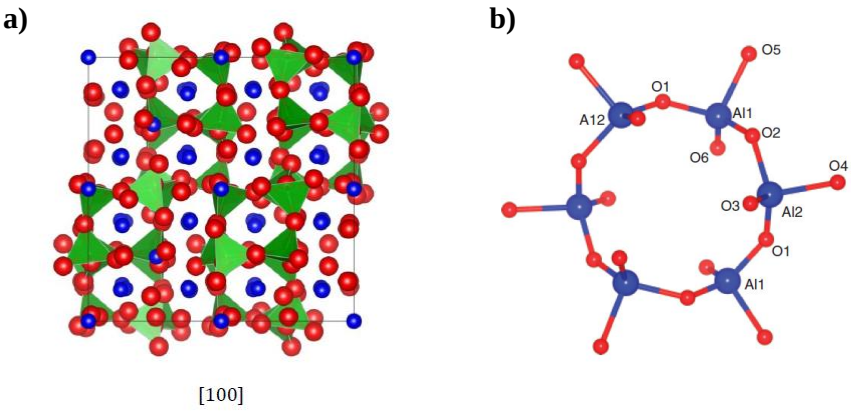


**Figure 7 : The cubic-$C_3A$ structure: (a) representation of the crystal structure along the [100] direction (Ca, in blue; Al and $AlO_4$, tetrahedra in green; O, in red) [51], and (b) structure of $Al_6O_{18}$ ring viewed along [-1,-1,-1] direction (Al, blue; O, red), reproduced from [50].**

## 2.2. Composition of hydrates and their structures

In the hydraulic reactions of the calcium aluminates $CA_2$, CA, $C_{12}A_7$ and $C_3A$, various hydration products called hydrates can be formed. When the anhydrous phases dissolve in water, calcium, aluminate and hydroxide ions are released in solution. Depending on the composition of the solution as well as of the temperature, different hydrated calcium aluminate phases precipitate from the aqueous interstitial solution [33].

The main hydration products that can be formed during the hydration of CACs are $CAH_{10}$, $C_2AH_{5\text{-}9}$, $C_4AH_{13\text{-}19}$ and $C_3AH_6$ [14, 33, 52]. In addition, aluminium hydroxide $AH_3$ precipitates and is sometimes formed as a by-product of the hydration of CACs.

Hydrated calcium aluminate phases can be categorized in two groups: metastable hydrates such as $CAH_{10}$, $C_2AH_{5\text{-}9}$, $C_4AH_{13\text{-}19}$, which undergo phase transformations into thermodynamically stable hydrate $C_3AH_6$. The formation of the metastable hydrates before their conversion reactions leading to stable hydrates has been extensively reported in the literature [33, 52-56]. Also, in the presence of carbonate, $C_4AH_{13\text{-}19}$ can form $C_4A\check{C}H_{11}$ [57, 58].

$C_2AH_{5\text{-}9}$ and $C_4AH_{13\text{-}19}$ are layered hydrates. Broadly speaking, the layer structure of these hydrates is composed of $[Al(OH)_6]^{3-}$ octahedra and seven coordinated Ca octahedra . The main layer composition is $[Ca_2Al(OH)_6]^{3+}$ (omitting the seventh apex of the Ca polyhedron, usually an interlayer water molecule oxygen) [59]. Hydrated calcium aluminate hydrate phases involve several aluminate-ferrite-monosubstituent phases (AFm) such as $C_4AH_{13\text{-}19}$ (OH-AFm phases) and $C_4A\check{C}H_{11}$ ($CO_3$-AFm). Their lamellar double hydroxides structure is composed of positively charged main layers $[Ca_2(Al,Fe)(OH)_6]^+$ and negatively charged interlayers $[X.nH_2O]^-$. X stands for monovalent ions such as $Cl^-$, $NO_3^-$, $NO_2^-$, $OH^-$ or half divalent ones such as $SO_4^{2-}$, $CO_3^{2-}$ but could also stand for the anionic group (such as an ionized carboxylic group) of an organic molecule [60-63]. These negatively charged ions balance the excess of

positive charge of the positively charged layers [64]. Furthermore, the distance between adjacent interlayers is affected by the nature of the anionic species and the water content. Most importantly, the crystallinity of these hydrates depends on various conditions such as temperature, humidity, grain size, hydration time [52, 65, 66]. Figure 8 illustrates a schematic of the lamellar AFm structure.

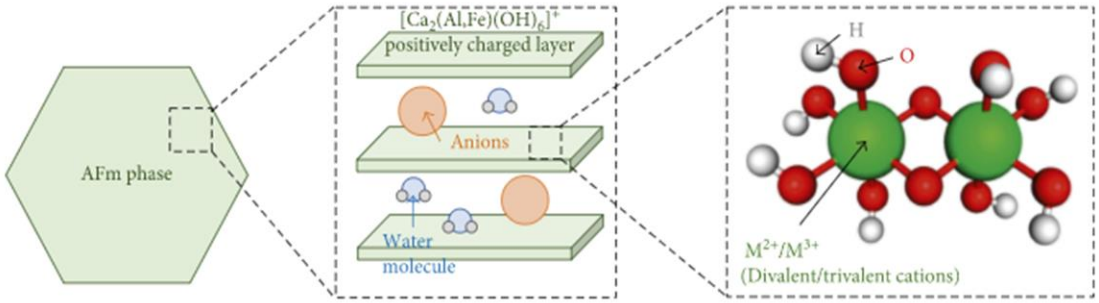


**Figure 8 : Schematic figure of the lamellar structure of an AFm phase, reproduced from [67].**

More specifically, the structure of $CAH_{10}$, $C_2AH_8$, $C_3AH_6$, $C_4A\check{C}H_{11}$ and $AH_3$ is detailed in the following bullet points.

- *Monocalcium aluminate decahydrate – $CAH_{10}$*

$CAH_{10}$ is known as the initial product of hydration of high-alumina cement, which is generally formed by hydration of $CA_2$ and CA at room temperature or below [68]. The $CAH_{10}$ structure is described in the hexagonal space group $P6_3/m$ (1 7 6) with the unit cell parameters a = b = 16.336 Å, c = 8.342 Å, α = β = 90°, γ = 120°; z = 6 [69, 70]. Christensen *et al.* determined the structure of $CaAl_2O_4.10D_2O$ by using Neutron and X-ray powder diffraction as illustrated in Figure 9 [70]. While the anhydrous phases have Al sites in tetrahedral coordination, the structure of $CAH_{10}$ has a single octahedrally-coordinated Al site. Together with $CaO_8$, the $AlO_6$ polyhedra form a framework with wide channels where water molecules could be located. [71]. The topological network of the interconnected $AlO_6$ octahedra and $CaO_8$ polyhedra of $CAH_{10}$ is represented in Figure 10 [72].

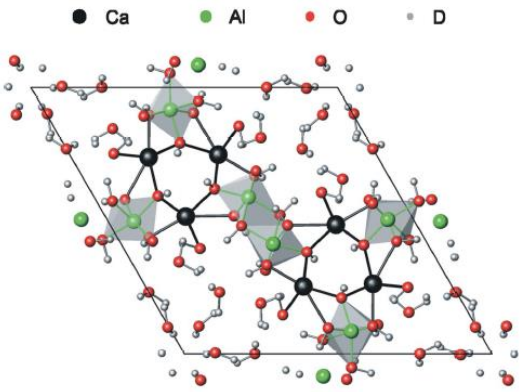


**Figure 9 : The crystal structure of $CaAl_2O_4.10D_2O$ with a projection on the ab plane of unit cell, proposed by Christensen *et al.*, reproduced from [70].**

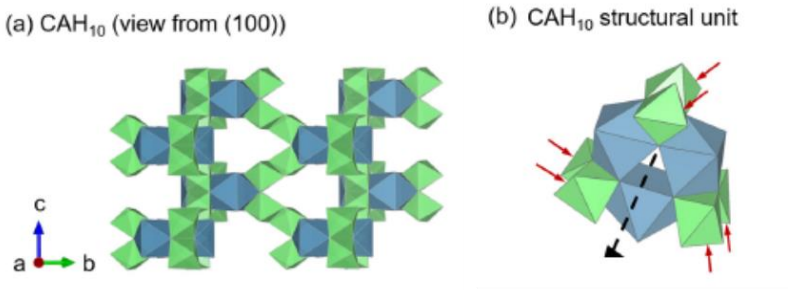


**Figure 10 : Representations of the topological structure of $CaO_8$ polyhedra (blue) and $AlO_6$ octahedra (green) in $CAH_{10}$ phase: (a) structure projected on (100), (b) red arrows represent the shared edges of $AlO_6$ octahedra, reproduced from [72].**

- *Dicalcium aluminate hydrates – $C_2AH_8$*

The $C_2AH_8$ is an important hydration product occurring during early age hydration of CACs [73]. It crystallizes as hexagonal or pseudo-hexagonal platelets (Figure 11).

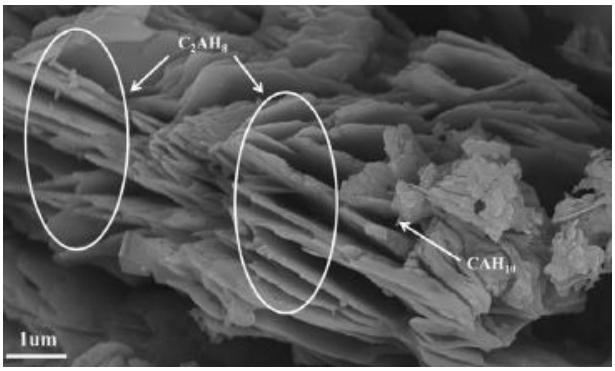


**Figure 11 : SEM image of a hydrated CAC : plate-shaped $C_2AH_8$ and hexagonal prism-shaped $CAH_{10}$ crystals, reproduced from [74].**

The $C_2AH_8$ structure is based on an hexagonal unit cell with parameters: a = 5.791 °A, b = 5.791 °A, c = 64.696 °A and α = 90°, β = 90°, γ = 120°; z = 6 [75]. However, the atomic positions in the $C_2AH_8$ structure are not completely determined yet [76]. Based on the description given by Ukrainczyk *et al.*, like AFm phases, $C_2AH_8$ consists of different main layers $[Ca_2Al(OH)_6]^+$ but with interlayer $[Al(OH)_4 \cdot 3H_2O]^-$ [77]. The number of water molecules in the interlayer of $C_2AH_8$ can be 4, 5, 7.5, 8 and 8.2 [78] depending on temperature, relative humidity and pressure [60, 79]. Therefore, the structural transformations can be observed by the loss of water from the interlayer and the spacing between layers vary. Figure 12 shows the (001) projection of the structure of $C_2AH_8$ published by Ukrainczyk N. [77]. Nevertheless, a complete description for the crystal structure of $C_2AH_8$ has not been published yet [80].

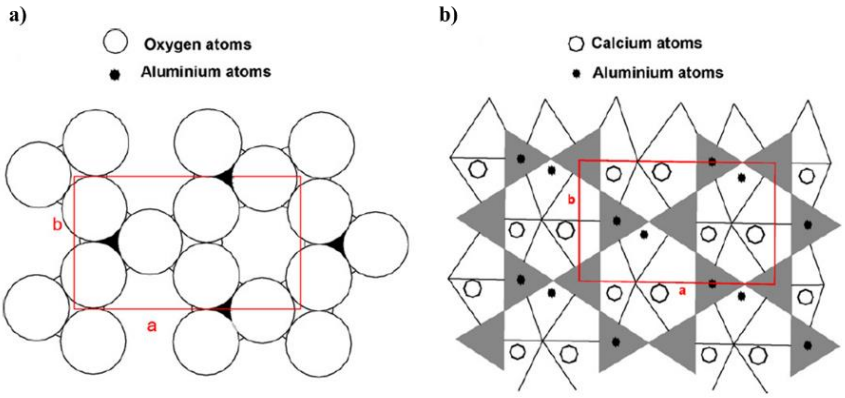


**Figure 12 : Projection (001) of the structure of $C_2AH_8$. a) Interlayer content, b) Stacking of tetrahedral interlayer above octahedral principal layer (water molecules are located below and above the centers of a six-membered tetrahedral rings), reproduced from [72].**

- *Hydrogarnet $C_3AH_6$*

$C_3AH_6$ has a cubic structure with a morphology of compact equiaxed crystals (Figure 13) [33]. $C_3AH_6$ is a thermodynamically stable phase formed by hydration of CAC [30, 62]. It is generally referred to as an end-member of the Al-containing hydrogarnet family [81, 82]. The $C_3AH_6$ unit cell contains a single octahedral Al site. The octahedral $Al(OH)_6$ units stack together and are linked by dodecahedral $Ca(OH)_8$, to build up a three dimensional framework as shown in Figure 14 [81, 83, 84]. $C_3AH_6$ crystallizes in the cubic system with Ia-3d (2 3 0) as space group [30]. The mesh parameters are a = 12.572 Å, α = 90°, z = 8 [82, 85, 86].

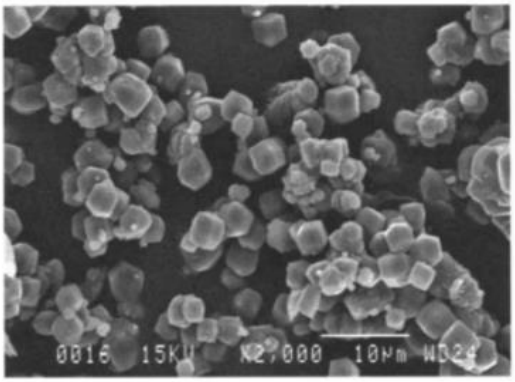


**Figure 13 : The microstructure of a 30-year-old concrete with a high w/c where the $C_3AH_6$ crystals are finely dispersed, reproduced from [33].**

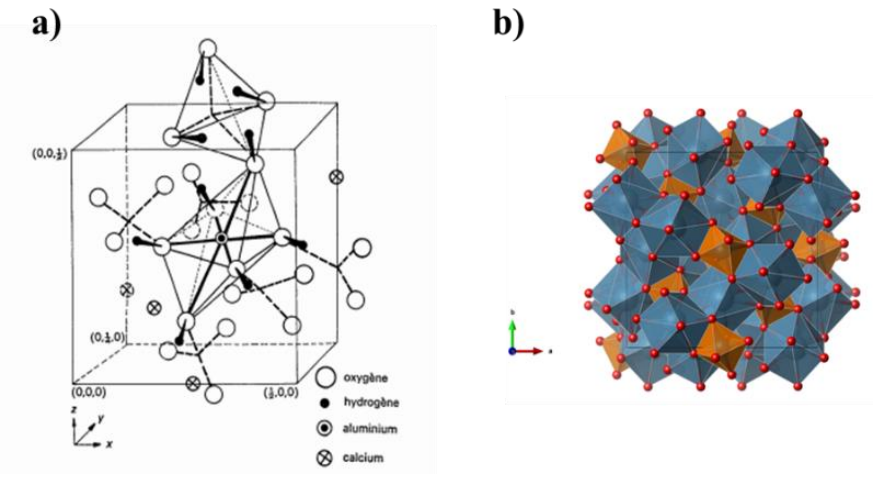


**Figure 14 : Schematic representation of the $C_3AH_6$ structure. a) representation of octahedral $Al(OH)_6$ and its environment, reproduced from [84], b) distorted $CaO_8$ cubes in blue and octahedra $AlO_6$ in orange, reproduced from [87].**

- *Monocarboaluminate – $C_4A\check{C}H_{11}$*

Monocarboaluminate $C_4A\check{C}H_{11}$ or $Ca_4Al_2(CO_3)(OH)_{12}.5H_2O$ is a carbonate-$AF_m$ ($CO_3$-$AF_m$) type phase. This hydrate forms due to the carbonation of the cementitious matrix. $C_4A\check{C}H_{11}$ crystallizes in the triclinic system with P1(1) as space group [83]. The mesh parameters are a = 5.775 Å, b = 8.469 Å, c = 9.923 Å and α = 64.77°, β = 82.75°, γ = 81.43°; z = 1 [88, 89]. This hydrate crystallizes in the form of thin hexagonal platelets. The structure is fully ordered and could be described as a layered compound constituted of positively charged $[Ca_4Al_2(OH)_{12}]^{2+}$ main layers and negatively charged $[CO_3.5H_2O]^{2-}$ interlayers, parallel to (011) [60, 90, 91]. The carbonate group is bonded to Ca atoms. Every oxygen atom of the carbonate groups provides strong hydrogen bounds with water molecules thus resulting in a strong cohesion between layers. Figure 15 shows the $C_4A\check{C}H_{11}$ structure projected on (100). In addition, hemicarboaluminate ($C_4A\check{C}_{0.5}H_{12}$) is another type of carbonated $AF_m$ phase. Its structure is similar to $C_4A\check{C}H_{11}$ but a hydroxyl group replaces half a carbonate group. M.Y. Hobbs explains that as the ratio of carbonate ions in the interlayers decreases below 0.8, monocarboaluminate cannot incorporate more hydroxyl ions in its structure and, as a consequence, hemicarboaluminate forms [92].

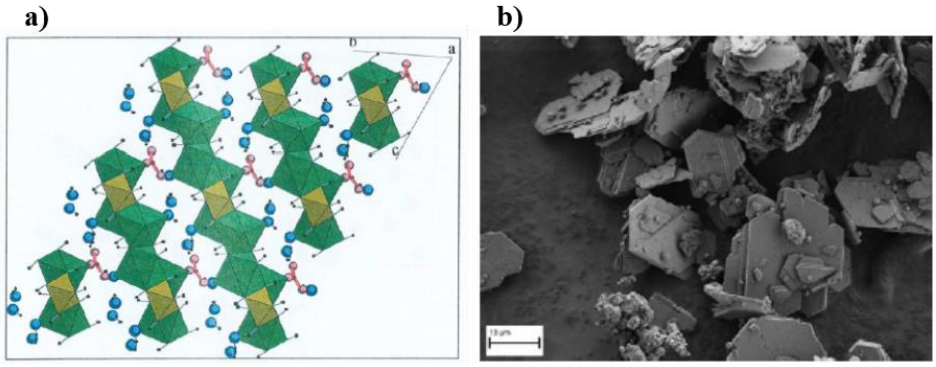


**Figure 15 : a) Schematic representation of the $C_4A\check{C}H_{11}$ structure projected on (100). The yellow octahedra are centered on the $Al^{3+}$ cations and the green polyhedra on $Ca^{2+}$. The water molecules are shown in blue, the carbonate ions in red and hydrogen atoms in black, reproduced from [83]. b) Secondary electron image of $AF_m$ hexagonal plates for monocarboaluminate, reproduced from [93].**

- *Aluminium hydroxide – $AH_3$*

Aluminium hydroxide ($AH_3$) exists in amorphous as well as in crystallized forms. The three crystalline polymorphs of $AH_3$ are gibbsite (α-$Al(OH)_3$), bayerite (β-$Al(OH)_3$) and nordstrandite (γ-$Al(OH)_3$) [93, 94]. The structures of these aluminium hydroxides consist of the stacking of double oxygen layers with the aluminium cations located in octahedrally coordinated interstices [95]. In Figure 16a, the atoms of aluminium are located at the center of octahedrons formed by hydroxyl groups occupying only two thirds of the octahedral sites within

the layers. A network of hydrogen bounds connects these layers: between the hydroxy ions of adjacent layers, interlayer hydrogen bonds and inside the double layers, intralayer hydrogen bonds are formed as shown in Figure 16b. This hydrogen bonds confers to $AH_3$ cohesion and stability [96].

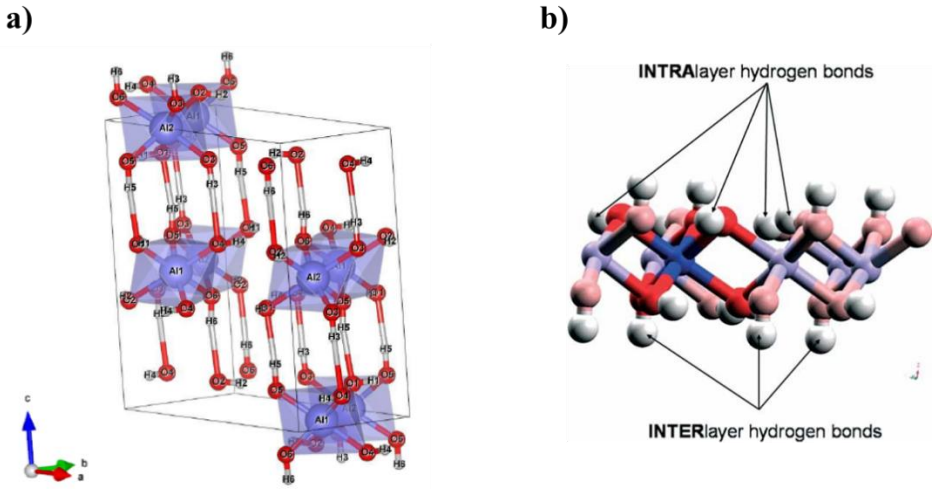


**Figure 16 : a) Representation of the gibbsite structure drawn via VESTA software, reproduced from [83], b) View of gibbsite sheet in the xz-plane with hydroxides participating in inter- and intralayer hydrogen bonds, reproduced from [97].**

Aluminium hydroxide polymorphs differ mainly as a result of different ways of stacking or superposition of octahedral layers [98]. At low temperatures (below 20 °C), aluminium hydroxide is poorly crystalline or amorphous whereas at high temperatures (above 40 °C), their crystallization occurs [30, 99].

Gibbsite crystalizes as monoclinical prisms within the space group $P2_1/c$ (14); z = 8. The cell parameters are a = 8.684 Å, b = 5.074 Å, c = 9.728 Å and $\alpha = 90°$, $\beta = 94.54°$, $\gamma = 90°$ [82, 89, 96]. The superposition of the double layers of hydroxyl groups enclosing a plane of aluminium atoms reveals that hydroxyl groups of two adjacent double layers are directly opposite to each other. Therefore, the ABBAABBA stacking sequence of gibbsite results in a crystal of hexagonal morphology and the bayerite ABABABAB stacking in conically shaped crystal as shown in Figure 17 and Figure 18 [100, 101]. As for the structure of nordstrandite, it is a combination of the two previous arrangements described for gibbsite and bayerite with a stacking sequence of the hydroxyl planes described by ABBABABA [102].

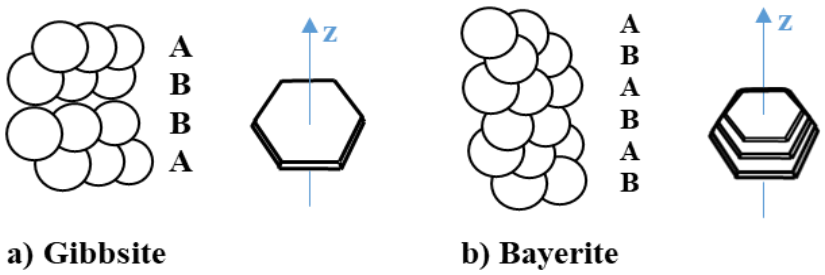


**Figure 17 : Stacking sequences of gibbsite and bayerite, adapted from [89, 101].**

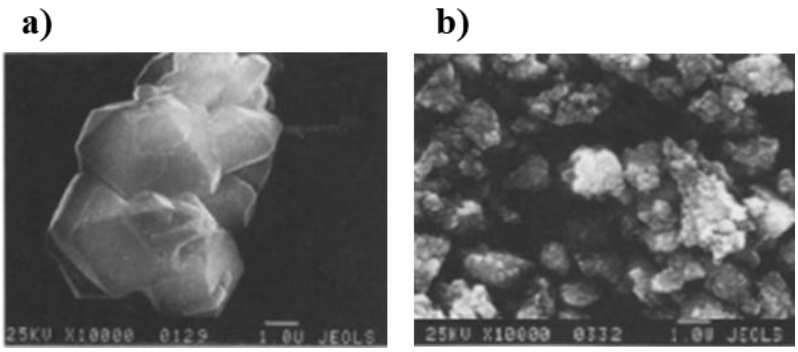


**Figure 18 : SEM micrographs of (a) gibbsite and (b) bayerite, reproduced from [103].**

## 2.3. Stability of hydrates and mineralogical assemblages

Mineralogical assemblages depend on the composition of the initial anhydrous phases and are related to the stability of hydrates precipitated within cementitious systems. Stability of hydrates varies according to several parameters. Precisely, it depends on the solution concentration of the species in equilibrium with the hydrate under consideration, the solution concentration of other species in solution and experimental conditions such as reaction time, pH, temperature and relative humidity.

*Stability of calcium aluminate hydrates*

In view of thermodynamics, hydration should lead to the assembly of the phases with the lowest solubility. In the case of CACs hydration nevertheless, different phases form temporarily, which are metastable. They have an intermediate energy between that of anhydrous and stable phases. From the anhydrous phases, there is thus a driving force for their formation but there is also one for their transformation into stable phases over time. This phenomenon is called a conversion reaction [33, 34].

The $CaO–Al_2O_3–H_2O$ system has been studied to understand and describe the hydration process of CACs. The behaviour of these systems may deviate strongly depending on the process conditions, in particular, the temperature. Solubility curves of the hydrates in $CaO-Al_2O_3-H_2O$ system at different temperatures are described in Figure 19.

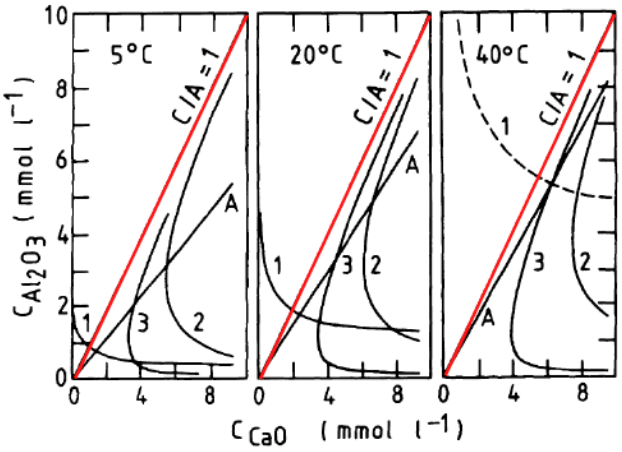


**Figure 19 : Solubility curves of the $CaO–Al_2O_3–H_2O$ system calculated at 5, 20 and 40 °C. (A) poorly crystalline $AH_3$, (1) $CAH_{10}$, (2) $C_2AH_8$ and (3) $C_3AH_6$ reproduced from [93].**

With the temperature, the solubility of metastable hydrates increases while on the contrary, the solubility of stable phases such as $C_3AH_6$ [93] generally decreases as illustrated in Figure 20 [102, 104].

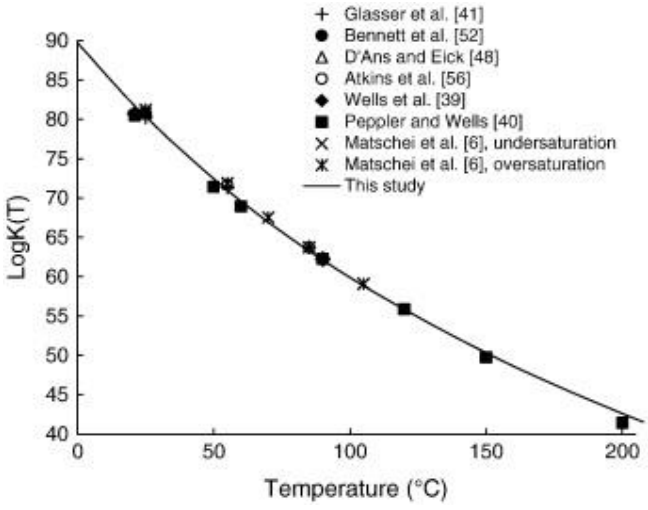


**Figure 20 : Equilibrium constant of hydrogarnet $C_3AH_6$ as a function of temperature, reproduced from [104].**

The formation of three other calcium aluminate hydrates such as $CAH_{10}$, $C_2AH_8$ and $C_4AH_{13}$ is mainly observed in the $CaO$-$Al_2O_3$-$H_2O$ system. These three hydrates are metastable phases. The solubility of the three hydrates at different temperatures is illustrated in Figure 21.

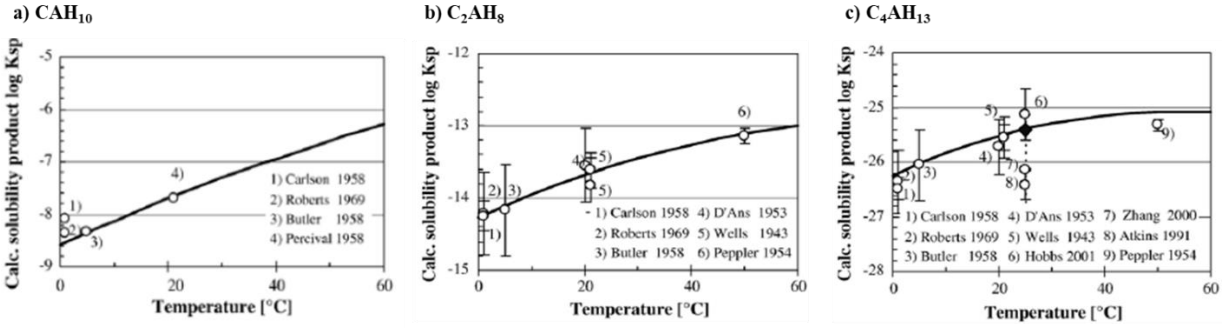


**Figure 21 : Calculated temperature dependent solubility products of (a) $CAH_{10}$, (b) $C_2AH_8$ and (c) $C_4AH_{13}$, reproduced from [105].**

Relatively coherent trends can be observed from the data obtained at 5 °C and 25 °C. For instance, the solubility curve of $CAH_{10}$ shows that it is less soluble at 5 °C than at 20 °C. The precipitation of this phase is thus favored at low temperature.

Matschei *et al*. have showed the relationships between the different phases in the $CaO$-$Al_2O_3$-$H_2O$ system and their results are reproduced in Figure 22 [105]. Hydrate assemblages can be predicted from these diagrams created from thermodynamical calculations and experimental data.

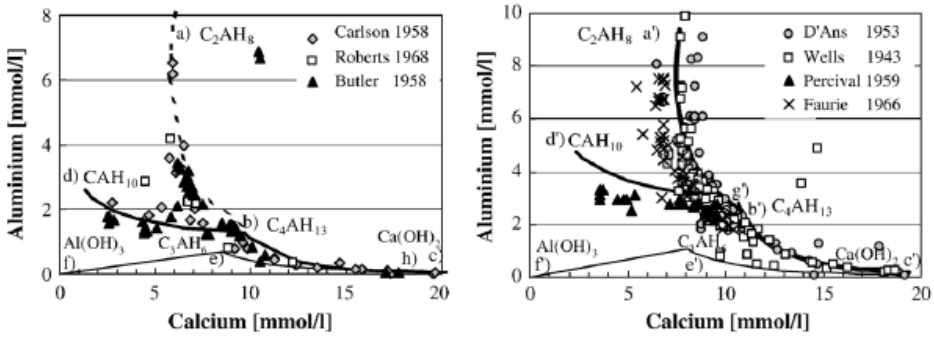


**Figure 22 : Solubility curves of different hydrates in the system $CaO$–$Al_2O_3$–$H_2O$ at 5 °C (left) and 25 °C (right), reproduced from [105].**

The differences regarding the solubility of hydrates affect the course of hydration. First hydrates formed in the system are the kinetically most favored ones. For instance, if the solution chemistry of a CAC system is closer to the solubility curve of $C_2AH_{7.5}$ phase, which nucleates faster than $CAH_{10}$ phase, than the one of $CAH_{10}$, the precipitation of $C_2AH_{7.5}$ occurs rather than $CAH_{10}$. That interferes directly to the hydration mechanism e.g. rapid setting of the CAC system [99].

Also apparent from Figure 23, the relative stability of hydrates in the $CaO–Al_2O_3–H_2O$ system depends on the ratio of CaO to $Al_2O_3$ of anhydrous phases. This fact is summarized in the pseudo phase diagram of Figure 23 [16]. Goetz-Neunhoeffer *et al.* studied the different hydration kinetics of synthetic $CA_2$ and CA resulting in different mineralogical assemblages over hydration time [14]. In addition, previous studies reported that the initial hydration product of CA, between 0 and 20 °C, is predominantly $CAH_{10}$ with amorphous $AH_3$. As the temperature was increased (below ca. 30 °C), the formation of crystalline phases such as $C_2AH_8$/$C_2AH_{7.5}$ and $AH_3$ occurred [106].

On the other hand, as the $C_{12}A_7$ phase, having higher C/A ratio than CA, is hydrated, the formation of $C_2AH_8$ is promoted. Furthermore, the fast hydration of $C_3A$ phase forms crystalline phases such as $C_2AH_8$, $C_4AH_{19}$ and $C_3AH_6$ [107].

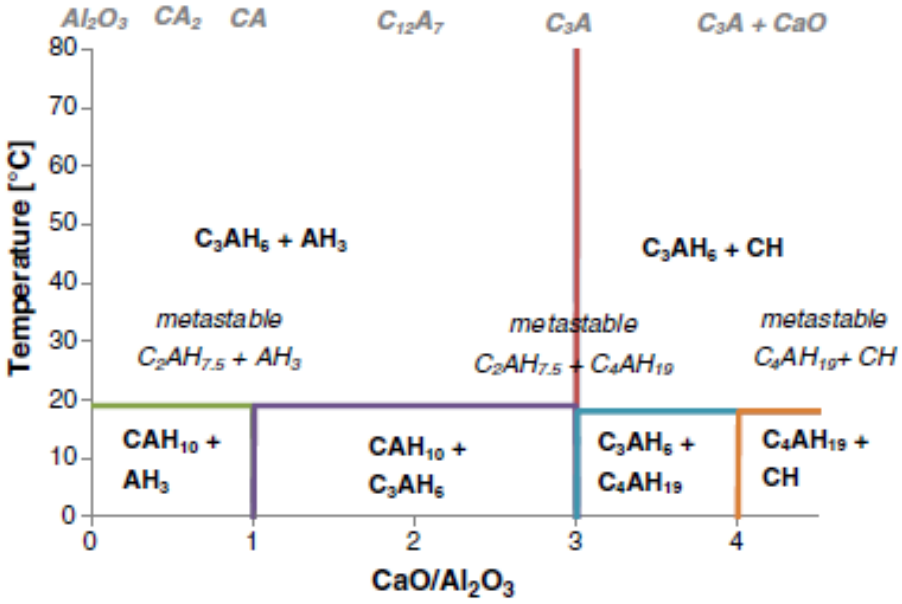


**Figure 23 : Stable hydrates in the $CaO–Al_2O_3–H_2O$ system, reproduced from [16].**

Various authors have described the hydration chemical equations pertaining to calcium aluminate cements [8, 55, 108]. At lower temperatures, below 15 °C, the hydration of CA leads

to the formation of $CAH_{10}$ [8, 34] according to equation (1). What is not shown in this equation is that the water content of this phase depends strongly on relative humidity [109]. As long as the temperature is constant and lower than 15 °C, $CAH_{10}$ can persist as such despite being a metastable phase, e.g. up to 574 days [110].

$$CA + 10\ H \rightleftharpoons CAH_{10} \quad (1)$$

At temperatures between 15 to 27 °C, the two metastable hydrates $CAH_{10}$ and $C_2AH_8$ coexist [76]:

$$CA + 10\ H \rightleftharpoons CAH_{10} \quad (2)$$
$$2\ CA + 11\ H \rightleftharpoons C_2AH_8 + AH_3 \quad (3)$$

For temperatures higher than 27 °C, only the metastable $C_2AH_8$ forms and above 50 °C, there is only the formation of $C_3AH_6$:

$$3\ CA + 12\ H \rightleftharpoons C_3AH_6 + 2\ AH_3 \quad (4)$$

Meanwhile, the conversion of metastable phases to the thermodynamically stable $C_3AH_6$ occurs during the hydration in two steps involving either $CAH_{10}$ or $C_3AH_6$ [32]:

$$6\ CA + 33\ H \rightleftharpoons 3\ AH_3 + 3\ C_2AH_8 \rightleftharpoons 4\ AH_3 + 2\ C_3AH_6 + 9\ H \quad (5)$$
$$3\ CA + 30\ H \rightleftharpoons 3\ CAH_{10} \rightleftharpoons 2\ AH_3 + C_3AH_6 + 16\ H \quad (6)$$

The water released because of these conversion reactions influences the porosity and causes a volume reduction resulting in the mechanical strength loss of the final products. These conversion reactions can be accelerated by curing at high temperatures above 50 °C.

*Stability of aluminium hydroxide*

Aluminium hydroxide is a hydration product of CACs and generally present in the form of gibbsite. This phase is however poorly crystallized at early ages [109]. It can even occur in a gel-like form at low temperatures (below 20 °C) [111]. The formation of aluminium hydroxide phase is particularly dependent on pH and temperature. With increase of the temperature, the crystalline forms appear but this is affected by the alkalinity of the system [17, 102]. The solubility diagrams of aluminium hydroxide in Figure 24 can be used to predict the aluminium concentration in solution at 25 °C. Whatever the form of the considered aluminium hydroxide, the solubility is minimal for pH values from 5 to 8. For a pH close to 12, the solubility of hydrated alumina remains low.

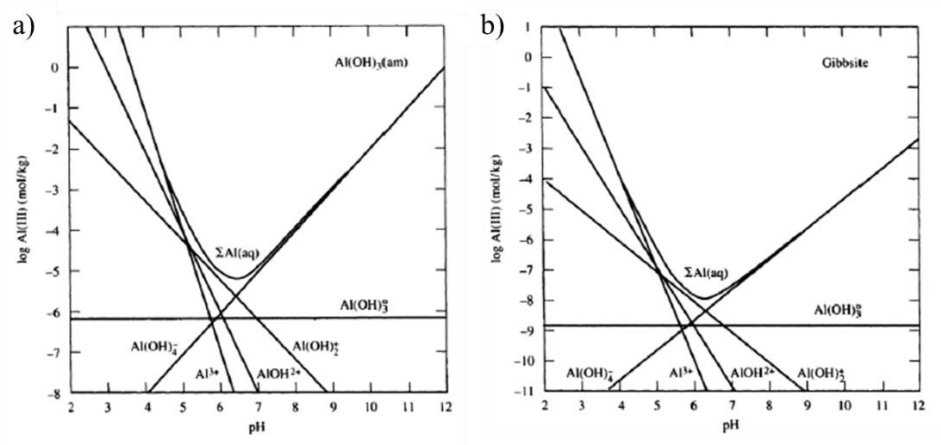


**Figure 24 : Aluminium aqueous species distribution and equilibrium solubility curve for (a) amorphous $Al(OH)_3$ and (b) gibbsite as a function of pH at 25 °C. Solid curved lines represent the solubility concentrations of $Al^{3+}$ and individual hydroxyl complexes, reproduced from [112]**

This hydrate is an amphoteric specie. Different possible aluminate species have been debated from as early as 1913. They are categorized as mononuclear and polynuclear aluminate species. Several polynuclear aluminate species can also be formed via "oligomerization" or formation of "hydroxo- or oxo-complexes" from mononuclear aluminate species [113]. In alkaline or acidic solution, aluminium can exist as the following forms: $Al^{3+}$, $Al(OH)_4^-$, $AlOH^{2+}$, $Al(OH)_2^+$, $Al(OH)_3^0$ [112, 114, 115]. In an alkaline environment, dissolved aluminium is predominantly in the form of mononuclear, tetrahedral aluminate ion, $Al(OH)_4^-$. At a very acidic medium, the $Al^{3+}$ cation predominates [113].

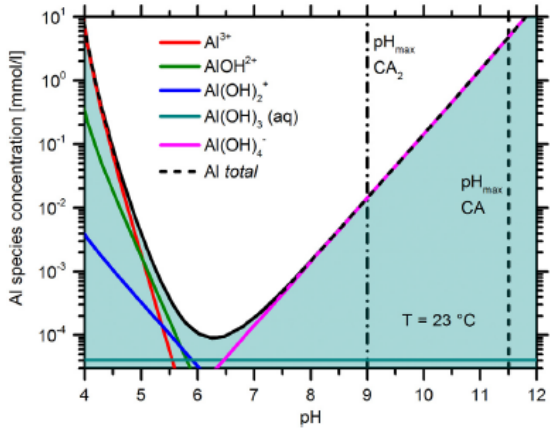


**Figure 25 : Aluminium aqueous species distribution and equilibrium solubility curve of amorphous $AH_3$, reproduced from [111].**

As already stated, $AH_3$ may exist as amorphous form, microcrystalline/nanocrystalline form, or one of the three crystallized forms known as aluminium trihydroxides: gibbsite, bayerite or nordstrandite (structure descriptions in Section 2.2) [110, 116]. Their polymorphs depend on the experimental conditions and the nature of materials initially used e.g. particle size and surface area [30, 112].

The phase transitions related to pH, aluminium concentration in the solution, temperature and synthesis time are defined in various studies [117-120]. Since aluminium hydroxide is amphoteric, it can be precipitated from acidic and basic environments [113, 121, 122]. Amorphous $AH_3$ can be obtained by rapid precipitation from neutralization of aluminate solutions [102]. Under alkaline conditions (pH>10), amorphous $AH_3$ is likely to precipitate but it evolves into crystalline phases such as bayerite (transient formation) and gibbsite with ageing (curing) [118, 123]. Under rapid precipitation from dilute sodium aluminate solutions, formation of bayerite predominates whilst slow precipitation from concentrated solutions favors the formation of gibbsite [123, 124]. Li *et al.* concluded that the NaOH concentration in aluminate solution significantly influences the form of the precipitated $AH_3$ at 22 °C. At low NaOH concentrations (NaOH $\leq$ 1.00 M), bayerite is formed while at higher concentrations (NaOH > 2.50 M) gibbsite precipitates [124]. The results showed that there is a precipitation sequence of aluminium hydroxide from thermodynamically less stable (amorphous) to more stable (bayerite) and subsequently the transformation of bayerite to gibbsite occurs by increasing pH and temperature (40-60 °C) [125]:

Amorphous aluminium hydroxide → Pseudo-boehmite (AlO(OH)) → Bayerite → Gibbsite

Van Straten *et al.* used the acid titration method to precipitate bayerite from supersaturated aluminate solutions. A similar method resulting in the precipitation of bayerite is the *slow* acidification of an aluminate solution with HCl, $HNO_3$ or $CO_2$ [117, 126, 127]. In brief, the initial aluminium concentration of the solution and the rate at which the pH is neutralized affect the crystal phase of aluminium hydroxide.

Furthermore, Du *et al.* studied the influence of the pH during the precipitation step on the formation of $AH_3$. It is reported that the amorphous phase, boehmite (aluminium monohydroxide, AlOOH) and bayerite are formed at pH = 5-6, 7, 8-11, respectively at different formation temperatures [118]. The formation of nordstrandite can be obtained at a temperature range of 60-75 °C [102, 128]. In addition, it can be precipitated from the neutralization of an aluminium salt solutions (in the intermediate pH range) [129].

Lothenbach *et al*. investigated the solubility of precipitated $AH_3$. Initially amorphous or poorly crystallized $AH_3$ precipitates and with time as the degree of ordering of $AH_3$ increases, the microcrystalline $AH_3$ forms are formed as shown in Figure 26. Besides, at high Ca and Al concentrations, amorphous $AH_3$ was found out to be more stable with respect to microcrystalline $AH_3$. Based on the Ostwald driving force, larger crystals are formed over time and consequently the solubility of $AH_3$ decreases.

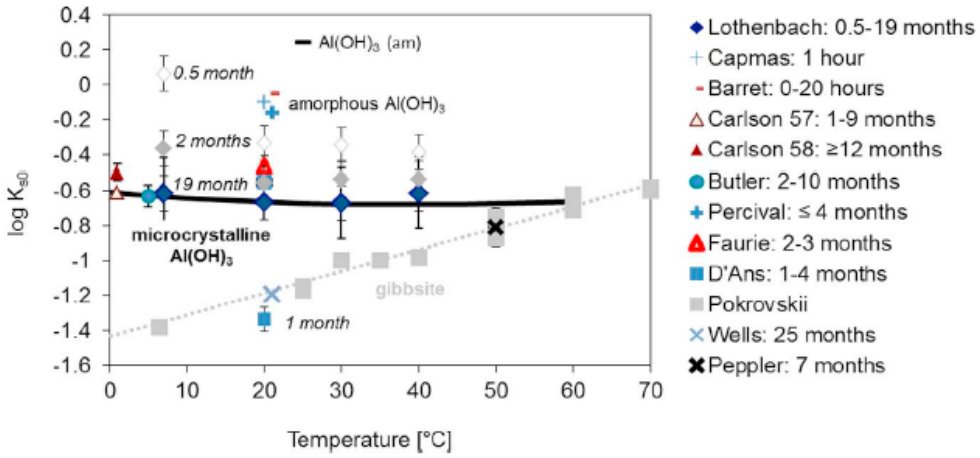


**Figure 26 : Logarithm of the solubility product of $Al(OH)_3$ as a function of time and temperature, reproduced from [130].**

When considering CAC hydration, Hueller F. *et al.* reported that the C/A ratio is a most significant factor that strongly alters the pH and thus the solubility of $AH_3$ (Figure 26). Their study showed that from the beginning of the hydration of $CA_2$ phase, crystalline gibbsite precipitated. For the hydration of CA phase, amorphous or poorly crystalline formation are observed [111]. Another relevant issue is the influence of the $AH_3$ solubility in calcium aluminate cement systems on the initial formation of $CAH_{10}$ or on the conversion reactions through stable phases such as $C_3AH_6$ and crystalline $AH_3$ [130].

## 3. Early-age hydration of anhydrous calcium aluminate cement phases

The hydration process is strongly dependent on the mineralogy of the anhydrous phases constituting the binder. Anhydrous phases react according to different mechanisms with different hydration kinetics. Therefore, in this section, the hydration mechanisms, including reaction equations of $CA_2$, CA, $C_{12}A_7$ and $C_3A$ and their subsequent hydration products are first described. Afterwards, two different technique used for the investigation of the hydration kinetics are explained for better comprehension of the following chapters.

### 3.1. Hydration reactions of anhydrous calcium aluminate phases

Hydration process begins when the anhydrous calcium aluminate phases are in contact with water. The hydration process occurs according to dissolution of anhydrous cement phases

through solution, followed by precipitation of hydrates. When the main reactive phase CA is mixed with water, it dissolves to give $Ca^{2+}$ and $Al(OH)_4^-$ ions in solution [93]. However, depending on mineralogical and structural characteristics of anhydrous cement phases, the reactivity of cements differs [11, 52]. Each of the anhydrous phases dissolves and releases ions in solution according to different dissolution reactions (Table 3).

**Table 2 : Dissolution reactions of anhydrous phases.**

| Anhydrous phase | Chemical reactions |
|---|---|
| **$CA_2$** | $CaAl_4O_7 + 2\ OH^- + 7\ H_2O \rightleftharpoons Ca^{2+} + 4\ Al(OH)_4^-$ |
| **CA** | $CaAl_2O_4 + 4\ H_2O \rightleftharpoons Ca^{2+} + 2\ Al(OH)_4^-$ |
| **$C_{12}A_7$** | $Ca_{12}Al_{14}O_{33} + 33\ H_2O \rightleftharpoons 12\ Ca^{2+} + 14\ Al(OH)_4^- + 10\ OH^-$ |
| **$C_3A$** | $Ca_3Al_2O_6 + 6\ H_2O \rightleftharpoons 3\ Ca^{2+} + 2\ Al(OH)_4^- + 4\ OH^-$ |

Dissolution of $CA_2$ consumes $OH^-$ while releasing $Ca^{2+}$ and $Al(OH)_4^-$, CA releases $Ca^{2+}$ and $Al(OH)_4^-$, whereas $C_{12}A_7$ and $C_3A$ release $Ca^{2+}$, $Al(OH)_4^-$ and $OH^-$ ions [52]. Since these anhydrous phases are more soluble than the hydration products, the solutions eventually become supersaturated with respect to the hydration products. Successively, hydrates precipitate: nucleation and crystal growth through solution and/or on the surface of grains occur by consuming released ions and water molecules. Furthermore, the formation of hydrates depends on various factors, principally the temperature and time of hydration. The hydration rate slows down when one of the reactants (water or anhydrous phase) is consumed or because of the lack of free space in which hydrated phases could precipitate.

The most significant and usual hydrates in calcium aluminate cements are $CAH_{10}$, $C_2AH_{5\text{-}9}$, $C_3AH_6$, $C_4AH_{13\text{-}19}$ and $AH_3$ [78, 93]. The water content of hydrates in the interlayers changes the structure of hydrate as mentioned in the previous section. For instance, $C_4AH_{19}$ may lose six water molecules from its interlayer thus often forming $C_4AH_{13}$ in the cementitious systems before further converting to more stable phases [82]. It should also be noted that the carbonation of the systems may change the hydrates assemblage. For example, carbonation of the originally precipitated hydocalumite OH-$AF_m$ yields monocarboaluminate $CO_3$-$AF_m$ ($C_4AČH_{11}$) or hemicarboaluminate (AFm containing $OH^-$ and $CO_3^{2-}$ with a molar ratio of 2:1) [131, 132].

After the dissolution of anhydrous phases leading to the passage of ions through solution, the precipitation of hydrates occur from the solution according to the chemical reactions given in Table 3 [34, 130]. It should be noted that the first hydrate to form is the most kinetically favored. However, that does not make them necessarily the most stable hydrate.

**Table 3 : Precipitation reactions of common hydration products.**

| Hydration products | Chemical reactions |
|---|---|
| **$CAH_{10}$** | $Ca^{2+} + 2\ Al(OH)_4^- + 6\ H_2O \rightleftharpoons (CaO) \cdot (Al_2O_3) \cdot (H_2O)_{10}$ |
| **$C_2AH_8$** | $2\ Ca^{2+} + 2\ Al(OH)_4^- + 2\ OH^- + 3\ H_2O \rightleftharpoons (CaO)_2 \cdot (Al_2O_3) \cdot (H_2O)_8$ |
| **$C_3AH_6$** | $3\ Ca^{2+} + 2\ Al(OH)_4^- + 4\ OH^- \rightleftharpoons (CaO)_3 \cdot (Al_2O_3) \cdot (H_2O)_6$ |
| **$C_4AH_{13}$** | $4\ Ca^{2+} + 2\ Al(OH)_4^- + 6\ OH^- + 6\ H_2O \rightleftharpoons (CaO)_4 \cdot (Al_2O_3) \cdot (H_2O)_{13}$ |
| **$C_4AH_{19}$** | $4\ Ca^{2+} + 2\ Al(OH)_4^- + 6\ OH^- + 12\ H_2O \rightleftharpoons (CaO)_4 \cdot (Al_2O_3) \cdot (H_2O)_{19}$ |
| **$C_4AČH_{11}$** | $4\ Ca^{2+} + 2\ Al(OH)_4^- + CO_3^{2-} + 4\ OH^- + 5\ H_2O \rightleftharpoons (CaO)_4 \cdot (Al_2O_3) \cdot (CO_3) \cdot (H_2O)_{11}$ |
| **$AH_3$** | $2\ Al(OH)_4^- \rightleftharpoons (Al_2O_3) \cdot (H_2O)_3 + 2\ OH^-$ |

In particular, the formation of hydration products is highly dependent on the initial C/A ratio of the solids, concentration of ions in solution, solubility of solid phases and surface area of the grains exposed to the solution during the hydration phenomenon [133-135].

## 3.2. Early-age hydration monitoring of anhydrous calcium aluminate phases by calorimetry

Isothermal heat flow calorimetry has been extensively used to monitor the hydration kinetics of cement over time, essentially because the dissolution of the anhydrous phases is an exothermic process. This technique, maintaining isothermal conditions, ensures that the heat received or released by the reactions does not influence neither the hydration rate, nor the type of hydrates formed [136].

Gosselin C. [137] studied the microstructural development of a calcium aluminate cement. The studied CAC here is a Secar 51 binder supplied by IMERYS (France) and mainly composed of CA phase (63.5 wt. %) and gehlenite "$C_2AS$" (21.5 wt. %). Figure 27 shows the normalized heat flow curves (by mass of CA) of the pastes prepared with different w/c ratios.

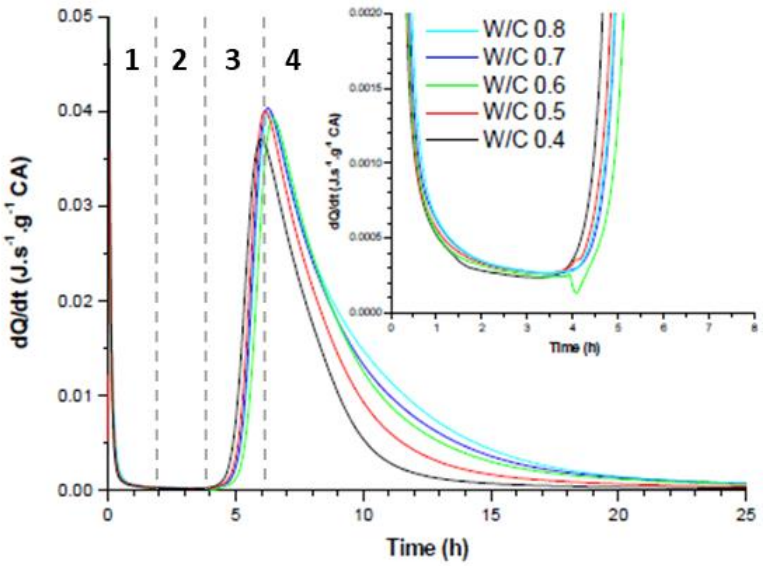


**Figure 27 : Heat flow curves of CAC hydrated at 20 °C for different w/c ratios, reproduced from [30].**

The early hydration mechanisms of the studied CAC can be divided into four periods:

1. Initial period: The first exothermic signal is related to the initial dissolution of CAC beginning upon wetting of the anhydrous grains with water. It should be noted that due to the cement paste mixing method (here "ex-situ mixing" of the isothermal calorimeter) only the end of the initial dissolution of the anhydrous phases contributed to the signal.
2. Induction period: Following the first exothermic signal, the initial rate drastically slows down within the first minutes. This period of low thermal activity is called induction period. The physical origin of the slowing down of the reaction rate during the induction period is largely debated but finds its explanation in dissolution and nucleation theory [108]. As reported by Gosselin C. [30], during this period, the concentration of calcium and aluminates are high in the aqueous solution before the rate increases again 4 hours after mixing (see Figure 27). It should be noted that this period can be regulated by the addition of accelerating or retarding admixtures [138].
3. Acceleration period: This period corresponds to the increase of heat flow values until a maximum level. It is mostly understood that this period corresponds to a competition between nucleation and crystal growth process on the one hand, and diffusion on the other hand [139, 140]. Massive precipitation of hydrates occurs during this period. In Figure 27, it corresponds to the sharp edge of the heat flow peak.
4. Deceleration period: This period begins from the time after the massive precipitation period. The heat flow slowly decreases on the right of the main peak. The deceleration period of hydrated CAC paste (w/c=0.5, T=30 °C) mainly constituted of CA and $CA_2$ phases has been investigated by Wang *et al.* [141]. It is reported that increasing formation of $C_3AH_6$ and $AH_3$ gels in the pore structure (about 16-19 hours of hydration) hinders ions migration, which causes the slowdown of the cement hydration rate.

The induction period of anhydrous calcium aluminate cements especially CA is still an object of investigation and debate in the literature. There are various hypotheses [142-145] concerning its origin, such as the nucleation of calcium aluminate hydrates and $AH_3$, or the formation of a coating layer around the anhydrous grains. Fujii *et al.* [146] indicated the formation of a dense layer of hydration products around the CA grains during the hydration of CA paste (w/c=0.5). Concerning the initial hydration of $C_3A$, a barrier around the anhydrous grains is considered to be formed by the rapid precipitation of hexagonal hydrates [147]. Capmas *et al.* explained the long setting time of hydrated CA (w/c=10 at 20 °C) with the presence of an amorphous $CAH_{10}$ gel layer around unreacted CA phases by scanning electron microscopy (SEM) [56]. However, Scrivener K. and Nonat A. [143] emphasized the absence of barrier layers when the most reactive phases such as $C_3A$ is hydrated. The slowdown of the dissolution rate is related to the concentrations of calcium and aluminium reaching high-levels. In addition, Damidot D. *et al.* [148], from hydration experiments of Ciment Fondu in diluted media (w/c=10) at 20 °C, conclude that the induction period is kinetically controlled by a nucleation and growth process of $AH_3$ instead of $CAH_{10}$ or of $C_2AH_8$. During the hydration studies on $CA_2$ and CA performed by Hueller F. *et al.* [78], the mineralogical assemblage and the duration of the induction periods are significantly influenced by the degree of crystallinity of $AH_3$ formed.

In brief, the heat flow development during the hydration of anhydrous phases reflects the global kinetics of the anhydrous phase hydration with all its features and characteristic periods. From isothermal calorimetry results, an experimental plan can be adapted in order to define the mineralogical and chemical evolutions of the sample for different periods of time and to understand the corresponding hydration steps. For instance, Klaus S. [14] investigated different mixes of CA/$CA_2$ using heat flow calorimetry and quantitative XRD. The dissolution of CA is not changed by the presence of $CA_2$ phase in the mixes however different kinetics are occurred during the hydration of each phases. The hydration of $CA_2$ lasts longer than CA due to the very slow precipitation of $C_2AH_{7.5}$/$C_2AH_8$ from pore solution. Šoukal *et al.* [149] studied the influence of pH buffers (pH 6 to 13) on the hydration of synthetic $CA_2$, CA, $C_{12}A_7$ and $C_3A$ at 26 °C. The combination of isothermal calorimetry to follow the hydration kinetics with hydrates characterization by XRD and thermogravimetric analysis (TGA) allowed them to establish that pH influences the hydration products of $CA_2$, CA and $C_{12}A_7$ whereas it was not the case for $C_3A$. However, the pH influenced the total hydration heat of $C_3A$. Furthermore, based on the quantitative phase analysis and isothermal calorimetry results, a degree of hydration can be calculated. Ukrainczyk N. [108] studied the influence of the increase in temperature from 5 to 10 °C on the hydration of a commercial CAC (mainly constituted of CA) paste prepared with a w/c of 0.4. The results obtained from quantitative XRD and isothermal calorimetry showed that the rate of nucleation and growth of $CAH_{10}$ decreased and retarded the setting time, and enhanced the final experimentally obtained hydration degree. Joseph S. *et al.* [150] investigated the hydration of $C_3A$ by using a combination of several experimental techniques (isothermal calorimetry, TGA, XRD, $^{27}$Al MAS-NMR) and numerical modelling. From to studies of pastes with w/c ratios varying from 0.5 to 1.0, the overall hydration degree after 7 days of hydration is found to increase with the w/c ratio, which is explained by a higher water content available for hydration. All of these examples from the literature show the benefits and success of the monitoring of hydration kinetics by calorimetric observations.

Monitoring the chemical composition of the solution during the hydration of a cement paste gives many insights. For example, the chemical composition of the liquid phase determines which hydrates are thermodynamically stable and can thus probably precipitate. However, because of the rapid stiffening and fast hardening of calcium aluminate-based cements, it is challenging to follow the chemical evolutions occurring in the pore solution of calcium aluminate cement pastes. Consequently, a simplification of these systems is needed to be able to follow the chemical evolution within these systems. Investigating diluted systems is a way to overcome the difficulties raised from rapid hydration process as long as saturation of the solution with respect to the cement hydrates can be reached. It makes possible a regular titration of the calcium, aluminate and hydroxide ions resulting from the dissolution of CAC, which would be more difficult in a cement paste. Moreover, it increases the duration of the different stages of hydration, which is of great help to investigate highly reactive systems.

## 3.3. Early-age hydration monitoring of anhydrous calcium aluminate phases by conductometry

Techniques based on the measurement of electrical conductivity enables the investigation of the early-age stages of hydration in detail. The duration of the different stages of hydration increases and that makes the composition changes of the aqueous phase easier to follow over hydration time. The electrical conductivity mirrors the calcium, aluminate and hydroxide concentrations in solution. For instance, Damidot D. *et al.* [148] measured the conductivity of stirred and diluted suspensions of Ciment Fondu® with a w/c ratio of 10 at 20 °C.

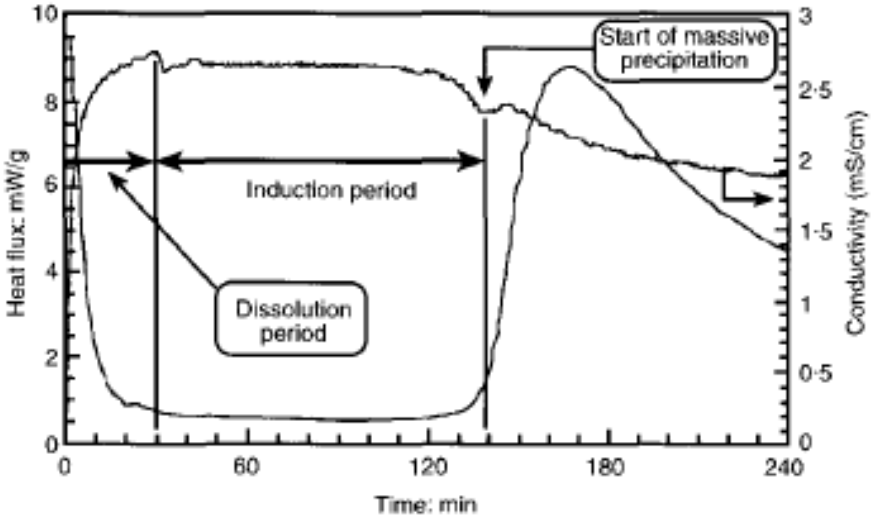


**Figure 28 : Monitoring of the hydration of Ciment Fondu® (w/c=10) by conductimetric and calorimetric measurements at 20 °C, reproduced from [148].**

Three stages of hydration are defined as follows:

- Dissolution period: Ions release from the dissolution of anhydrous phases into the solution. Consequently, the electrical conductivity increases.
- Induction period: The electrical conductivity reaches a plateau, highlighting that the chemical composition of the solution might remain constant. The reaction rate slows down. In the study of Damidot D. *et al.* [148], the aqueous phase composition is close to the minimum instability curves of $AH_3$ and $C_2AH_8$. In addition, it is supposed to reach the equilibrium with respect to the CA phase. Therefore, it is concluded that the kinetics are likely to be governed by the rate of nucleation of the hydrates and not by the dissolution rate of the anhydrous phases. It should be noted that the formation of $AH_3$ correlates with an increase in the reaction rate before the end of the conductivity plateau.
- Massive precipitation period: The rapid decrease in the electrical conductivity is characterized by the consumption of ions from the solution due to the massive precipitation of hydrates. Therefore, the undersaturation with respect to anhydrous CA increases. A small increase in conductivity is observed at 140 min (Figure 28) showing that to overcome the undersaturation of CA, the dissolution is reaccelerated for a second time. Afterwards, the conductivity drops and stays quasi-constant reflecting a reaction rate slow-down.

These results obtained by Damidot D. *et al.* also confirmed the good agreement between the monitoring on pastes and on suspensions across all hydration stages.

More interestingly for this PhD study, Maach N. [151] investigated the hydration of pure CA at 10 $g.L^{-1}$ at 35 °C by conductometry (Figure 29).

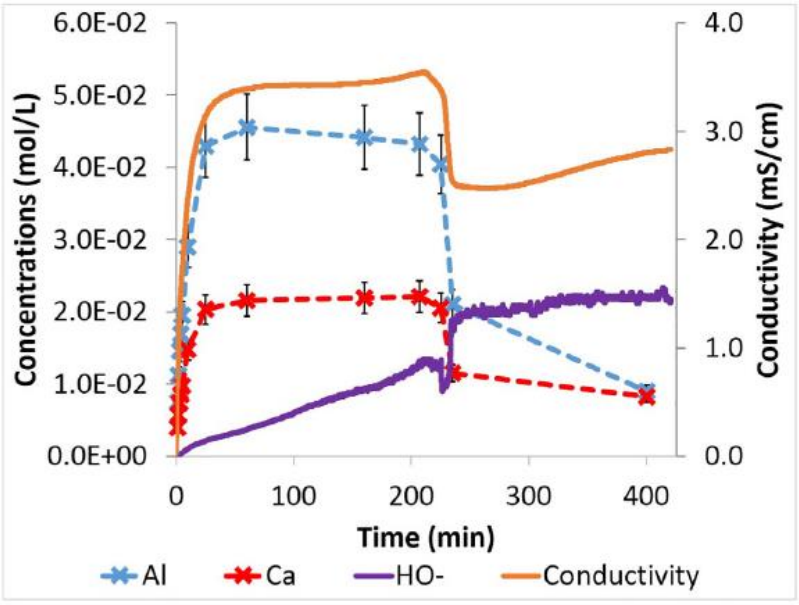


**Figure 29 : Aqueous phase monitoring of the pure CA hydration at 10 $g.L^{-1}$ at 35 °C, reproduced from [151].**

The calcium concentration increases during the first 0.5 hours revealing CA dissolution, and then remains stable until 4 hours of hydration. Meanwhile, the increase in the hydroxide concentration is related here to the formation of $AH_3$ which is the only reaction contributing to a pH increase following the reaction " $2\ Al(OH)_4^- \rightleftharpoons AH_3\ (gibbsite) + 2\ OH^-$ ". After 4 hours of hydration, the conductivity decrease, mirroring the concentration drop in calcium, aluminium and hydroxide due to the formation of a calcium aluminate hydrate. In brief, Maach N. summarized these events as follows: first, the anhydrous phase dissolves without precipitation at low hydroxide content, then the precipitation of $AH_3$ brings hydroxide ions into the solution; subsequently, higher concentrations of hydroxide are reached allowing hydrates precipitation.

One can obtain important information about the kinetics of hydration by following the solution evolutions, as their conductivity profiles reflect accurately the hydration events at different hydration periods. The next section is devoted to the advantages of a thermodynamic approach by the interpretation of saturation indexes.

## 3.4. Understanding of the early-age hydration mechanisms of anhydrous calcium aluminate phases by saturation indexes

The saturation index with respect to a solid phase is defined by $\log(IAP/K_{s0})$, where IAP is the ion activity product, calculated from the activities derived from the experimentally obtained concentrations, and $K_{s0}$ is the solubility product of the considered solid phase [16, 130].

SI values are interpreted as follows. If $SI > 0$, the solution is supersaturated and the solid phase tends to precipitate. If $SI < 0$, the solution is undersaturated and the solid phase tends to dissolve. At equilibrium, $SI = 0$ [152].

The following studies highlight how an approach based on saturation indices allows to successfully interpret experimental data.

Hueller F. *et al.* [111] discussed the hydration mechanism of $CA_2$. First, the solution C/A ratio is calculated from experimentally obtained Ca and Al concentrations. The C/A ratio is found to be far from 0.5, a value which would have been reached if a simple congruent dissolution of $CA_2$ occurred. Hence, the changes in the C/A ratio are interpreted as originating from either the precipitation of an alumina-rich phase or an incongruent dissolution of $CA_2$. In Figure 30, positive saturation indices for $AH_3$ from the time of water addition means that a potential precipitation could explain the high C/A ratio in solution. In addition, the pore solution is found to be highly undersaturated with respect to $CAH_{10}$ and $C_2AH_x$. Therefore, $AH_3$ reported as the first and only hydrate which might form until the beginning of the main hydration period. Besides, the earlier precipitation of $AH_3$ compared to other hydrates is confirmed from in-situ XRD analysis. Meanwhile, very low amount of dissolved $CA_2$ is calculated at the end of the

induction period. That is explained by the fact that low degree of oversaturation for $AH_3$ results in low driving force for $CA_2$ dissolution during the first 120 min.

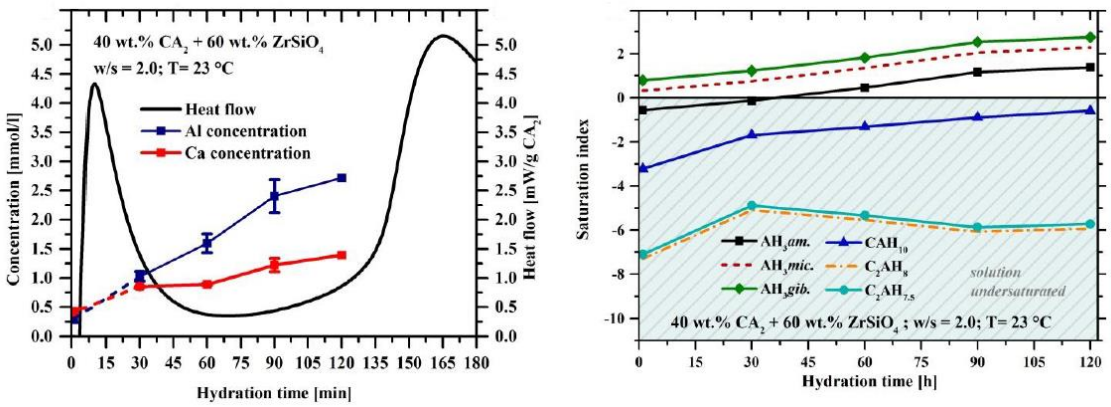


**Figure 30 : Saturation indexes for relevant hydrates in pore solutions of $CA_2$, reproduced from [111].**

Manninger *et al.* [153] studied the hydration of CA-cement in presence of low concentrations of phosphoric acid. The mineralogical assemblages are determined by in-situ XRD and afterwards compared to the saturation indices calculated from the data obtained by pore water analysis of the samples. During this study, CA-cement, mainly composed of CA phase (small amounts of $CA_2$ and amorphous phase), is hydrated at 23 °C with a w/c of 1. In Figure 31, step 1 stops after reaching to the maximum heat flow, and step 2 to the main reaction period. The concentrations of calcium and aluminium remain constant until the end of step 1 after an initial dissolution of CA during mixing and first minutes of hydration. Saturation indexes predicted the precipitation of $CAH_{10}$ and $AH_3$ (gibbsite form) together with $C_2AH_x$. However, XRD analysis detects only the presence of unreacted CA-cement at this period. After 10 hours of hydration, with renewed dissolution of CA, these latter hydrates are detected by XRD in agreement with the saturation indices. After 15 hours of hydration, the massive precipitation of hydrates is observed from the heat flow results. Noticeably, the $C_2AH_x$ phase is detected as $C_2AH_8$ then after about 5 hours it is converted to $C_2AH_{7.5}$. Overall, this study including further studies with phosphates confirms the coherence between different methods to monitor hydration of calcium aluminate phases including saturation indices calculated from pore solution data.

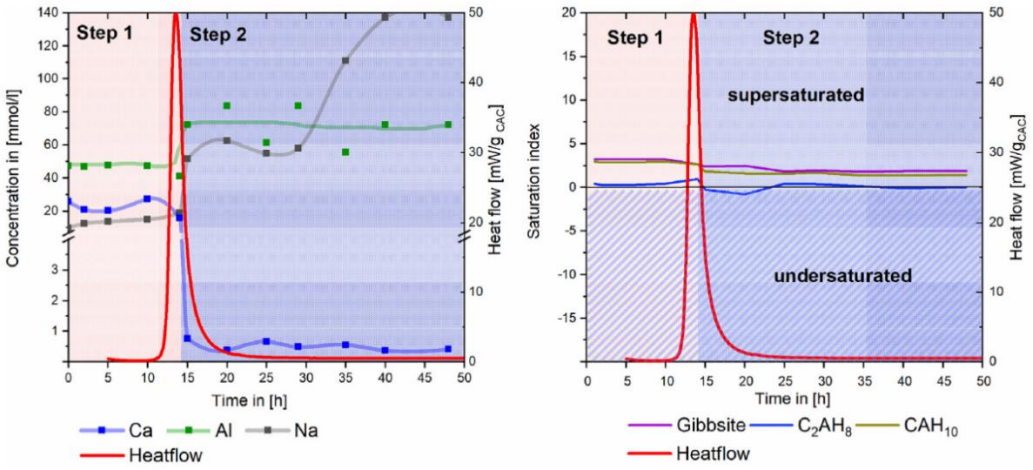


**Figure 31 : Pore solution composition and calculated saturation indexes during the two periods observed by heat flow measurement of CA-cement hydration (w/c=1) at 23 °C, reproduced from [153].**

Another study of Manninger *et al.* [154] where the hydration mechanism is defined by using experimentally obtained pore solution data, solubility curves and quantitative XRD on the samples is particularly interesting for our purposes. The hydration mechanism of a CA-cement with/without calcite is defined. Two kinds of materials are used in this study. The first one is a mixture of industrial CA-cement with an industrial grade calcite, and the second one is a mixture of synthetized CA and pure calcite. These mixtures are prepared with a 70/30 ratio and a water-to-solid ratio of 1 is chosen. The calorimetry measurements showed similar reaction paths except for the duration of the induction period. Most interestingly concerning this literature review, is the approach followed. It combines the solubility curves calculated using cemdata18 [130] and the concentration values obtained from pore solution evolution at different periods of time. The Ca/Al ratio varies and passes from different stability zones according to the plot in Figure 32. At the beginning of hydration, the pore solution is found to be mainly driven by the dissolution of the mixture. The composition of the first solution falls in the zone where the solubilities of $C_2AH_{7.5}$, hemicarboaluminate (HC), monocarboaluminate (MC) and $AH_3$ phases having very close values. Manninger *et al.* interpreted the formation of these hydrates as the fact that they are reached to supersaturation at the early hydration. Afterwards, the pore solution composition is found to be following the solubility curve of the most thermodynamically stable phase monocarboaluminate in the system under study.

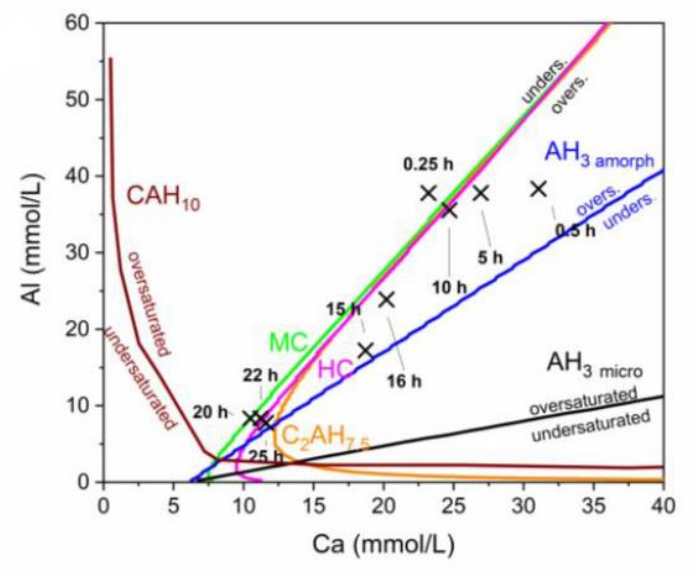


**Figure 32 : Calculated solubility curves at low alkali contents (0.05 mmol/L of K and 0.5 mmol/L of Na) and with considering a small amount of S in the pore solution (0.9±0.3 mmol/L), plotted with Ca and Al ion contents over time in the mixture of pure CA and calcites, reproduced from [154].**

## 4. Summary

The current state of the art allowed identifying different hydration mechanisms of anhydrous calcium aluminate phases as well as several parameters influencing this process. First, a short history on the calcium aluminate cements including their manufacturing processes was presented. Afterwards, the interests of the use of calcium aluminate phases especially for the radioactive waste conditioning compared to widely used calcium silicate cement, was discussed.

Then, the reactive components of calcium aluminate cements were presented, as well as the crystalline structures of hydrates. The goal of this particular section devoted to the crystalline structures of phases is to set the context for the following chapters where XRD and $^{27}$Al MAS-NMR characterization methods are used to identify and/or quantify the compounds present in the studied systems. The mineralogical assemblage obtained on the course of hydration depends on the composition of the anhydrous cement constituents, and is related to the hydration degree and the stability of the hydrates in the studied environment. Thus, the stability of several hydrates that could precipitate in a $CaO$-$Al_2O_3$-$H_2O$ system was introduced.

The hydration of CACs is difficult to control and to understand because of the formation of metastable phases/transient states raised from the early age of hydration reactions. Compared to systems based on PC, the knowledge on the hydration mechanisms of CACs remains limited. An extensive literature review of the available research opens this manuscript to support the experimental approach applied for this PhD research.

The different hydration reactions occurring through the physicochemical phenomena that were taking place during the liquid-solid interactions involved in the hydration of CACs were summarized. The dissolution and precipitation reactions were given, which are useful for the following chapters. However, neither the main reaction pathways for pure calcium aluminate phases when their $CaO/Al_2O_3$ ratio is varied, nor their related mineralogical assemblages on the course of hydration at 25 °C have been yet described in detail. In the literature, these phases have been investigated in general with the presence of additives. However, the use of admixtures should be avoided because of the complexity with the radionuclides decreasing the confining properties of the cemented waste packages.

A good understanding of the early-age hydration of anhydrous calcium aluminates is needed to provide controlled and reasoned formulations for the cement matrices of waste packages. As an important parameter, the influence of the w/c ratio on pastes and suspensions is carefully assessed in this PhD research. Afterwards, w/c ratios were determined for experiments on pastes and suspensions allowing us to focus on the investigation of the hydration degree of the different systems with tailored approaches. For the first time, the hydration degrees of these anhydrous phases were estimated and compared together, under the same experimental conditions, to evaluate the early-age hydration and contribute to the knowledge on calcium aluminate phases.

Lastly, the research of this PhD thesis is originated from the potential of CAC for the conditioning of the nuclear wastes to overcome the problematic related the limiting of the $H_2$ production. More precisely, resulting mineralogical assemblages of hydrated calcium aluminate phases contribute to its potential as a confining material [83]. Thus, in this chapter, monitoring techniques, interest in studying pastes and/or suspensions, resulting mineralogical assemblages, advantages and contributions of thermodynamic calculations based on the solution composition were summarized. This review enabled to form a set of helpful information supporting our experimental approach to investigate early-age hydration mechanisms of anhydrous calcium aluminates, varying from each other by their C/A ratio, and their hydration products. In particular, among the works published in the literature about the hydration of anhydrous calcium aluminates, Maach N. *et al.* [151] reported in 2019 a similar approach to the one applied in PhD thesis, with a point of view of identifying chemical mechanisms in diluted suspensions.

In the next chapter, the compositions of the studied anhydrous calcium aluminate phases, their physical-chemical characterizations as well as the experimental procedures are presented.

## 5. References


[1] P. D. Swift, "The Development of Calcium Aluminate Phosphate Cement for Radioactive Waste Encapsulation," PhD, Department of Materials Science and Engineering, University of Sheffield, 2013.

[2] J. Bensted, "Milestones in the History of Concrete Technology: The development and usage of high alumina cement," in *ICT Yearbook 2003-2004*, T. I. o. C. Technology, Ed., ed, 2003-2004, pp. 13-23.

[3] R. O. Abdel Rahman, R. Rakhimov, N. Rakhimova, and M. Ojovan, "Alternative Binders," 2014, pp. 79-104.

[4] J. H. Ideker, K. L. Scrivener, H. Fryda, and B. Touzo, "12 - Calcium Aluminate Cements," in *Lea's Chemistry of Cement and Concrete (Fifth Edition)*, P. C. Hewlett and M. Liska, Eds.: Butterworth-Heinemann, 2019, pp. 537-584.

[5] C. Cau Dit Coumes, "Alternative Binders to Ordinary Portland Cement for Radwaste Solidification and Stabilization," in *Cement-Based Materials for Nuclear Waste Storage*, F. Bart, C. Cau-di-Coumes, F. Frizon, and S. Lorente, Eds. New York, NY: Springer New York, 2013, pp. 171-191.

[6] M. I. Ojovan, W. E. Lee, and S. N. Kalmykov, "Chapter 17 - Immobilisation of Radioactive Waste in Cement," in *An Introduction to Nuclear Waste Immobilisation (Third Edition)*, M. I. Ojovan, W. E. Lee, and S. N. Kalmykov, Eds.: Elsevier, 2019, pp. 271-303.

[7] I. Stinnessen, A. Buhr, R. Kockegey-Lorenz, and R. Racher. (30 August). *High Purity Calcium Aluminate Cements, Production And Properties*. Available: https://almatis-umbraco.azurewebsites.net/media/3985/high_purity_calcium-aluminate-cements_production_and_properties.pdf

[8] J. H. Ideker, "Early-age behavior of calcium aluminate cement systems," Doctor of Philosophy, Civil, Architectural, and Environmental Engineering, The University of Texas at Austin Austin, 2008.

[9] AZoM. (2002). *Calcium Aluminate Cements - History, Manufacture and Grades*. Available: https://www.azom.com/article.aspx?ArticleID=1634

[10] M. F. Zawrah, A. B. Shehata, E. A. Kishar, and R. N. Yamani, "Synthesis, hydration and sintering of calcium aluminate nanopowder for advanced applications," *Comptes Rendus Chimie*, vol. 14, no. 6, pp. 611-618, 2011/06/01/ 2011.

[11] C. Qi, D. Spagnoli, and A. Fourie, "Structural, electronic, and mechanical properties of calcium aluminate cements: Insight from first-principles theory," *Construction and Building Materials*, vol. 264, p. 120259, 2020/12/20/ 2020.

[12] E. Gartner, "Industrially interesting approaches to “low-CO2” cements," *Cement and Concrete Research*, vol. 34, no. 9, pp. 1489-1498, 2004/09/01/ 2004.

[13] Z. He, X. Zhu, J. Wang, M. Mu, and Y. Wang, "Comparison of CO2 emissions from OPC and recycled cement production," *Construction and Building Materials*, vol. 211, pp. 965-973, 2019/06/30/ 2019.

[14] S. R. Klaus, J. Neubauer, and F. Goetz-Neunhoeffer, "Hydration kinetics of CA2 and CA—Investigations performed on a synthetic calcium aluminate cement," *Cement and Concrete Research*, vol. 43, pp. 62-69, 2013/01/01/ 2013.

[15] S. R. Klaus, J. Neubauer, and F. Goetz-Neunhoeffer, "How to increase the hydration degree of CA — The influence of CA particle fineness," *Cement and Concrete Research,* vol. 67, pp. 11-20, 2015/01/01/ 2015.

[16] B. Lothenbach, L. Pelletier-Chaignat, and F. Winnefeld, "Stability in the system CaO–$Al_2O_3$–$H_2O$," *Cement and Concrete Research,* vol. 42, no. 12, pp. 1621-1634, 2012/12/01/ 2012.

[17] I. Martin, "Développement d'une matrice à base d'aluminate de calcium pour la cimentation de boues issues de la décontamination d'effluents actifs," Doctorat, Laboratoire Matériaux et Durabilité des Constructions (LMDC), EA 3027, Université Toulouse III Paul Sabatier, 2016.

[18] M.-N. de Noirfontaine, S. Tusseau-Nenez, C. Girod-Labianca, and V. Pontikis, "CALPHAD formalism for Portland clinker: thermodynamic models and databases," *Journal of Materials Science*, journal article vol. 47, no. 3, pp. 1471-1479, February 01 2012.

[19] B. P. Mahiaoui and J. E. Jacques, "Composition comprenant un aluminate de calcium amorphe et procédé de fabrication associé," France Patent FR3037061A1, 2015.

[20] A. Hussain, S. Mehmood, M. N. Rasool, S. Aryal, P. Rulis, and W. Y. Ching, "Electronic structure, mechanical, and optical properties of CaO·Al2O3 system: a first principles approach," *Indian Journal of Physics,* vol. 90, no. 8, pp. 917-929, 2016/08/01 2016.

[21] R. Salomão, V. Ferreira, I. Oliveira, A. Souza, and W. Correr, "Mechanism of pore generation in calcium hexaluminate (CA6) ceramics formed in situ from calcined alumina and calcium carbonate aggregates," *Journal of the European Ceramic Society,* vol. 36, 06/01 2016.

[22] D. Torréns-Martín, L. Fernández-Carrasco, and S. Martínez-Ramírez, "Hydration of calcium aluminates and calcium sulfoaluminate studied by Raman spectroscopy," *Cement and Concrete Research,* vol. 47, pp. 43-50, 2013/05/01/ 2013.

[23] B. Touzo, "Ultra-fast setting cement based on amorphous calcium aluminate," United States, 2017. Available: https://www.freepatentsonline.com/10196306.html.

[24] J. Alex, "Effect of Sodium on the Microstructure and Properties of Calcium Aluminate Cement Bonded Refractories," Doctor of Philosophy (PhD), Department of Materials, Imperial College London, 2015.

[25] K. Baltakys, A. Eisinas, J. Doneliene, T. Dambrauskas, and G. Sarapajevaite, "The impact of Al2O3 amount on the synthesis of CASH samples and their influence on the early stage hydration of calcium aluminate cement," *Ceramics International,* vol. 45, no. 2, Part B, pp. 2881-2886, 2019/02/01/ 2019.

[26] G. Li, A. Zhang, Z. Song, C. Shi, Y. Wang, and J. Zhang, "Study on the resistance to seawater corrosion of the cementitious systems containing ordinary Portland cement or/and calcium aluminate cement," *Construction and Building Materials,* vol. 157, pp. 852-859, 2017/12/30/ 2017.

[27] K. L. Scrivener, J.-L. Cabiron, and R. Letourneux, "High-performance concretes from calcium aluminate cements," *Cement and Concrete Research,* vol. 29, no. 8, pp. 1215-1223, 1999/08/01/ 1999.

[28] L. Acher *et al.*, "H2 production under gamma irradiation of a calcium aluminate cement: An experimental study on both cement pastes and its stable hydrates," *Radiation Physics and Chemistry*, vol. 189, p. 109689, 2021/12/01/ 2021.

[29] E. Litwinek and D. Madej, "Structure, microstructure and thermal stability characterizations of C3AH6 synthesized from different precursors through hydration," *Journal of Thermal Analysis and Calorimetry*, vol. 139, no. 3, pp. 1693-1706, 2020/02/01 2020.

[30] C. Gosselin, "Microstructural development of calcium aluminate cement based systems with and without supplementary cementitious materials," PhD Theses, Faculte Sciences et Techniques de l'ingénieur, École Polytechnique Fédérale De Lausanne, Suisse, N.4443, 2009.

[31] H. Pöllmann, "Calcium Aluminate Cements – Raw Materials, Differences, Hydration and Properties," *Reviews in Mineralogy and Geochemistry*, vol. 74, no. 1, pp. 1-82, 2012.

[32] T. Manninger, "Early hydration of CA and CA-cement in interaction with calcite and additives," PhD, Naturwissenschaftliche Fakultät, Friedrich-Alexander-Universität Erlangen-Nürnberg, Friedrich-Alexander-Universität Erlangen-Nürnberg, 2020.

[33] K. Scrivener, "Calcium aluminate cements," in *Advanced Concrete Technology*, vol. 3, J. C. Newman, B.S., Ed. 1 ed. Oxford, England: Butterworth-Heinemann Elsevier Ltd., 2003, pp. 1-31.

[34] H. T. Nguyen, "Transfert hydrique dans le milieu poreux réactif : Application à l'étude de séchage d'une pâte pure ettringitique au jeune âge," Doctorat, Mécanique, Energétique, Génie Civil, Acoustique, INSA Lyon, Ecole Doctorale ED162, INSA Lyon, 2018LYSEI124, 2018.

[35] M. C. G. Juenger, F. Winnefeld, J. L. Provis, and J. H. Ideker, "Advances in alternative cementitious binders," *Cement and Concrete Research*, vol. 41, no. 12, pp. 1232-1243, 2011/12/01/ 2011.

[36] C. Ma *et al.*, "Krotite, CaAl2O4, a new refractory mineral from the NWA 1934 meteorite," *American Mineralogist*, vol. 96, no. 5-6, pp. 709-715, 2011.

[37] M. C. Ball, C. M. Marsh, R. E. Simmons, I. Sutherland, and M. C. R. Symons, "Surface composition of anhydrous monocalcium aluminate, CaAl2O4," *Journal of Materials Science*, vol. 23, no. 4, pp. 1431-1435, 1988/04/01 1988.

[38] J. H. Skibsted, E.; Jakobsen, H.J., "Characterization of Calcium Aluminate Phases in Cements by 27Al MAS NMR Spectroscopy," *Inorg. Chem.*, vol. 32, pp. 1013-1027, 1993.

[39] V. Kahlenberg, "On the Al/Fe substitution in iron doped monocalcium aluminate — the crystal structure of CaAl1.8Fe0.2O4," *European Journal of Mineralogy*, vol. 13, no. 2, pp. 403-410, 2001.

[40] J. Bensted and P. Barnes, *Structure and performance of cements*, (2nd Edition) ed. London; New York: Spon Press, 2002.

[41] D. W. L. Goodwin, A. J., "The crystal structure of CaO.2Al2O3," *Acta Crystallographica*, vol. 26, pp. 1230-1235, 1970.

[42] A. Altay, C. B. Carter, P. Rulis, W. Y. Ching, I. Arslan, and M. A. Gülgün, "Characterizing CA2 and CA6 using ELNES," *Journal of Solid State Chemistry,* vol. 183, no. 8, pp. 1776-1784, 2010/08/01/ 2010.

[43] J. A. McLeod *et al.*, "Spectroscopic characterization of a multiband complex oxide: Insulating and conducting cement 12CaO7Al2O3," *Physical Review B,* vol. 85, no. 4, p. 045204, 01/13/ 2012.

[44] H. Boysen, M. Lerch, A. Stys, and A. Senyshyn, "Structure and oxygen mobility in mayenite ($Ca_{12}Al_{14}O_{33}$): a high-temperature neutron powder diffraction study," *Acta Crystallographica Section B,* vol. 63, no. 5, pp. 675-682, 2007.

[45] J. E. Medvedeva, E. N. Teasley, and M. D. Hoffman, "Electronic band structure and carrier effective mass in calcium aluminates," *Physical Review B,* vol. 76, no. 15, p. 155107, 10/09/ 2007.

[46] K. Hayashi, M. Hirano, S. Matsuishi, and H. Hosono, "Microporous Crystal 12CaO·7Al2O3 Encaging Abundant O- Radicals," *Journal of the American Chemical Society,* vol. 124, no. 5, pp. 738-739, 2002/02/01 2002.

[47] L. Palacios *et al.*, "Crystal Structures and in-Situ Formation Study of Mayenite Electrides," *Inorganic Chemistry,* vol. 46, no. 10, pp. 4167-4176, 2007/05/01 2007.

[48] P. J. Mondal, J. W. , "The crystal structure of tricalcium aluminate, Ca3Al2O6," *Acta Crystallographica,* vol. B31, pp. 689-697, 1975.

[49] V. Rheinheimer, S. R. Chae, E. D. Rodríguez, G. Geng, A. P. Kirchheim, and P. J. M. Monteiro, "A Scanning Transmission X-ray Microscopy Study of Cubic and Orthorhombic C3A and Their Hydration Products in the Presence of Gypsum," *Materials,* vol. 9, no. 9, 2016.

[50] H. Manzano, J. S. Dolado, and A. Ayuela, "Structural, Mechanical, and Reactivity Properties of Tricalcium Aluminate Using First-Principles Calculations," *Journal of the American Ceramic Society,* https://doi.org/10.1111/j.1551-2916.2009.02963.x vol. 92, no. 4, pp. 897-902, 2009/04/01 2009.

[51] N. Garg, "Structure, Reactivity, and Dissolution of Calcined Clays by Solid-state NMR," 2015.

[52] N. Maach, "Kinetic modeling of the early age hydration of calcium aluminate cements : From chemical mechanism to the modeling by the Population Balance Equations," Thèse de doctorat, Mécanique, Energétique, Génie Civil, Acoustique (MEGA), l'INSA de Lyon, 2019LYSEI127, 2019.

[53] S. M. Park, J. G. Jang, H. M. Son, and H. K. Lee, "Stable conversion of metastable hydrates in calcium aluminate cement by early carbonation curing," *Journal of CO2 Utilization,* vol. 21, pp. 224-226, 2017/10/01/ 2017.

[54] C. Bradbury, P. M. Callaway, and D. D. Double, "The conversion of high alumina cement/concrete," *Materials Science and Engineering,* vol. 23, no. 1, pp. 43-53, 1976/04/01/ 1976.

[55] Y. Zhang, G. Ye, W. Gu, D. Ding, L. Chen, and L. Zhu, "Conversion of calcium aluminate cement hydrates at 60°C with and without water," vol. 101, no. 7, pp. 2712-2717, 2018.

[56] A. Capmas, D. Sorrentino, and D. Damidot, "The effect of temperature on the setting time of calcium aluminate cements," in *Calcium Aluminate Cements: Proceedings of a*

*Symposium*, R. J. Mangabhai, Ed. London: Taylor&Francis, CRC Press, 1990, pp. 65-80.

[57] D. Damidot, S. Stronach, A. Kindness, M. Atkins, and F. P. Glasser, "Thermodynamic investigation of the $CaO$-$Al_2O_3$-$CaCO_3$-$H_2O$ closed system at 25 °C and the influence of $Na_2O$," *Cement and Concrete Research,* vol. 24, no. 3, pp. 563-572, 1994.

[58] V. Rahhal *et al.*, "Red Ceramic Wastes: A Calcined Clay Pozzolan," in *Calcined Clays for Sustainable Concrete*, Dordrecht, 2015, pp. 179-187: Springer Netherlands.

[59] W. Kurdowski, *Cement and Concrete Chemistry*. Krakow, Poland: Springer, Netherlands, New York, 2014, p. 705.

[60] L. G. Baquerizo, T. Matschei, K. L. Scrivener, M. Saeidpour, and L. Wadsö, "Hydration states of AFm cement phases," *Cement and Concrete Research,* vol. 73, pp. 143-157, 2015/07/01/ 2015.

[61] N. C. M. Marty, S. Grangeon, E. Elkaïm, C. Tournassat, C. Fauchet, and F. Claret, "Thermodynamic and crystallographic model for anion uptake by hydrated calcium aluminate (AFm): an example of molybdenum," *Scientific Reports,* vol. 8, no. 1, p. 7943, 2018/05/21 2018.

[62] M. Balonis, M. Mędala, and F. P. Glasser, "Influence of calcium nitrate and nitrite on the constitution of AFm and AFt cement hydrates," vol. 23, no. 3, pp. 129-143, 2011.

[63] G. Puerta-Falla, M. Balonis, G. Falzone, M. Bauchy, N. Neithalath, and G. Sant, "Monovalent Ion Exchange Kinetics of Hydrated Calcium-Alumino Layered Double Hydroxides," *Industrial & Engineering Chemistry Research,* vol. 56, no. 1, pp. 63-74, 2017/01/11 2017.

[64] A. Duran, R. Sirera, M. Pérez-Nicolás, I. Navarro-Blasco, J. M. Fernández, and J. I. Alvarez, "Study of the early hydration of calcium aluminates in the presence of different metallic salts," *Cement and Concrete Research,* vol. 81, pp. 1-15, 2016/03/01/ 2016.

[65] V. S. Ramachandran and R. F. Feldman, "Hydration characteristics of monocalcium aluminate at a low water/solid ratio," *Cement and Concrete Research,* vol. 3, no. 6, pp. 729-750, 1973/11/01/ 1973.

[66] T. R. Jensen, A. N. Christensen, and J. C. Hanson, "Hydrothermal transformation of the calcium aluminum oxide hydrates CaAl2O4·10H2O and Ca2Al2O5·8H2O to Ca3Al2(OH)12 investigated by in situ synchrotron X-ray powder diffraction," *Cement and Concrete Research,* vol. 35, no. 12, pp. 2300-2309, 2005/12/01/ 2005.

[67] Y. Lee, M. Kim, Z. Chen, H. Lee, and S. Lim, "Chloride-Binding Capacity of Portland Cement Paste Blended with Synthesized CA2," *Advances in Materials Science and Engineering,* vol. 2018, p. 5418930, 2018/03/25 2018.

[68] F. Guirado, S. Galí, and J. S. Chinchón, "Thermal Decomposition of Hydrated Alumina Cement (CAH10)," *Cement and Concrete Research,* vol. 28, no. 3, pp. 381-390, 1998/03/01/ 1998.

[69] A. N. Christensen, T. R. Jensen, B. Lebech, J. C. Hanson, H. J. Jakobsen, and J. Skibsted, "Thermal decomposition of monocalcium aluminate decahydrate (CaAl2O4•10H2O) investigated by in-situ synchrotron X-ray powder diffraction, thermal analysis and 27Al, 2H MAS NMR spectroscopy," *Dalton Transactions,* Article vol. 8, no. 4, pp. 455-462, 2008.

[70] A. N. Christensen, B. Lebech, D. Sheptyakov, and J. C. Hanson, "Structure of calcium aluminate decahydrate (CaAl2O4.10D2O) from neutron and X-ray powder diffraction data," *Acta Crystallogr B*, vol. 63, no. Pt 6, pp. 850-61, Dec 2007.

[71] F. Guirado, S. Galí, S. Chinchón, and J. Rius, "Crystal Structure Solution of Hydrated High-Alumina Cement from X-ray Powder Diffraction Data," vol. 37, no. 1-2, pp. 72-75, 1998.

[72] G. Geng *et al.*, "A high-pressure X-ray diffraction study of the crystalline phases in calcium aluminate cement paste," *Cement and Concrete Research*, vol. 108, pp. 38-45, 2018/06/01/ 2018.

[73] B. Raab and H. Pöllmann, "$C_2AH_8$ – $2CaO{\cdot}Al_2O_3{\cdot}(8\pm n)H_2O$ – main hydration products of CAC," in *European Powder Diffraction Conference*, Darmstadt, Germany, 2011, vol. 1, pp. 349-354: Oldenbourg Wissenschaftsverlag.

[74] J. Chen, C. Liang, B. Li, E. Wang, G. Li, and X. Hou, "The effect of nano-γAl2O3 additive on early hydration of calcium aluminate cement," *Construction and Building Materials*, vol. 158, pp. 755-760, 2018/01/15/ 2018.

[75] H. S. Poellmann, J.; Goske, J.; Kuzel, H.-J., "$Ca_2Al_2O_5.8H_2O$," ed. Friedrich-Alexander-Univ., Erlangen-Nurnberg, Erlangen, Germany: ICDD Grant-in-Aid, 1994.

[76] G. Geng, J. Li, Y.-S. Yu, D. A. Shapiro, D. A. L. Kilcoyne, and P. J. M. Monteiro, "Nanometer-Resolved Spectroscopic Study Reveals the Conversion Mechanism of CaO·Al2O3·10H2O to 2CaO·Al2O3·8H2O and 3CaO·Al2O3·6H2O at an Elevated Temperature," *Crystal Growth & Design*, vol. 17, no. 8, pp. 4246-4253, 2017/08/02 2017.

[77] N. Ukrainczyk, T. Matusinovic, S. Kurajica, B. Zimmermann, and J. Sipusic, "Dehydration of a layered double hydroxide—$C_2AH_8$," *Thermochimica Acta*, vol. 464, no. 1, pp. 7-15, 2007/11/25 2007.

[78] F. Hüller, "Hydration mechanisms of CA2 and alumina-rich calcium aluminate cements: Effects of mechanical activation, critical CA contents and crystallinity of AH3," PhD, Geographie und Geowissenschaften, Friedrich-Alexander-Universität Erlangen-Nürnberg (FAU), 2019.

[79] A. M. Cuesta García, "Preparation and hydration of model ecocement phases. Characterization by diffraction and cognate methods," PhD, Inorganic Chemistry, Crystallography and Mineralogy Department, University of Málaga, Málaga, 2015

[80] S. Stöber and H. Pöllmann, "Crystallograpy and crystal chemistry of $AF_m$ phases related to cement chemistry," in *Cementitious Materials: Composition, Properties, Application*, H. Pöllmann, Ed. Germany: De Gruyter, 2017, pp. 191-240.

[81] B. Z. Dilnesa, "Fe-containing hydrates and their fate during cement hydration: thermodynamic data and experimental study " Docteur, Faculté Sciences et Techniques de l'Ingénieur, École de Polytechnique Fédérale de Lausanne, Suisse, 5262, 2011.

[82] M. Balonis, "The Influence of Inorganic Chemical Accelerators and Corrosion Inhibitors on the Mineralogy of Hydrated Portland Cement Systems," PhD, Chemistry, University of Aberdeen United Kingdom, 2010.

[83] L. Acher, "Etude du comportement sous irradiation γ et électronique de matrices cimentaires et de leurs hydrates constitutifs," Doctorat École doctorale n°573 Interfaces Université Paris-Saclay, NNT : 2017SACLX045, 2017.

[84] C. Cohen-Addad, P. Ducros, and E. F. Bertaut, "Etude de la substitution du groupement SiO4 par (OH)4 dans les composés Al2Ca3(OH)12 et Al2Ca3(SiO4)2,16(OH)3,36 de type grenat," *Acta Crystallographica,* vol. 23, pp. 220-230, 1967.

[85] E. P. M. Flint, H.F.; Wells, L.S., "Standard x-ray diffraction powder patterns: Section 11 - data for 70 substances," *National Bureau of Standards Monograph 25,* vol. 11, p. 16, 1974.

[86] J. M. Rivas Mercury, P. Pena, A. H. De Aza, X. Turrillas, I. Sobrados, and J. Sanz, "Solid-state 27Al and 29Si NMR investigations on Si-substituted hydrogarnets," *Acta Materialia,* vol. 55, no. 4, pp. 1183-1191, 2007/02/01/ 2007.

[87] G. A. D. Lager, R.T.; Origlieri, M.; Garoutte, R., "High-pressure single-crystal X-ray diffraction study of katoite hydrogarnet: Evidence for a phase transition from Ia3d →$I\bar{4}3d$ symmetry at 5 GPa," *American Mineralogist,* vol. 87, pp. 642-647, 2002.

[88] M. R. François, G. and Evrard, O., "A Cementitious Compound with Composition $3CaO.Al_2O_3.CaCO_3.11H_2O$," *Acta Crystallographica,* vol. C54, pp. 1214-1217, 1998.

[89] G. Renaudin, "I/ Etude d'un hydroxyde simple d'aluminium : La bayerite II/ Etude d'une famille d'hydroxydes doubles lamellaires d'aluminium et de calcium : les phases AFM (Aluminates Tétracalciques Hydrates)," Université Henri Poincaré - Nancy 1, 1998NAN10302, 1998.

[90] G. Renaudin, M. Francois, and O. Evrard, "Order and disorder in the lamellar hydrated tetracalcium monocarboaluminate compound," *Cement and Concrete Research,* vol. 29, no. 1, pp. 63-69, 1999/01/01/ 1999.

[91] M. François, G. Renaudin, and O. Evrard, "A cementitious compound with composition 3CaO.Al2O3.CaCO3.11H(2)O," *Acta Crystallographica Section C,* vol. 54, 09/15 1998.

[92] M. Y. Hobbs, "Solubilities and ion exchange properties of solid solutions between the OH, CI and CO, end members of the monocalcium aluminate hydrates," PhD, Earth Sciences, University of Waterloo Waterloo, Ontario, Canada, 2001.

[93] J. Bizzozero, "Hydration and dimensional stability of calcium aluminate cement based systems," Theses 2014 2014, Art. no. 6336.

[94] J. Chang, Y. Zhang, X. Shang, J. Zhao, and X. Yu, "Effects of amorphous AH3 phase on mechanical properties and hydration process of $C4A3\bar{S}$-$C\bar{S}H2$-CH-H2O system," *Construction and Building Materials,* vol. 133, pp. 314-322, 2017/02/15/ 2017.

[95] I. Levin and D. Brandon, "Metastable Alumina Polymorphs: Crystal Structures and Transition Sequences," *Journal of the American Ceramic Society,* https://doi.org/10.1111/j.1151-2916.1998.tb02581.x vol. 81, no. 8, pp. 1995-2012, 1998/08/01 1998.

[96] D. A. Ksenofontov and Y. K. Kabalov, "Structure refinement and thermal stability of gibbsite," *Inorganic Materials,* vol. 48, no. 2, pp. 142-144, 2012/02/01 2012.

[97] A. Vyalikh, K. Zesewitz, and U. Scheler, "Hydrogen bonds and local symmetry in the crystal structure of gibbsite," *Magnetic Resonance in Chemistry,* https://doi.org/10.1002/mrc.2682 vol. 48, no. 11, pp. 877-881, 2010/11/01 2010.

[98] G. Y. B. Chao, J.; Sabina, A.P.; Roberts, A.C., "Doyleite, a new polymorph of $Al(OH)_3$, and its relationship to bayerite, gibbsite and nordstrandite," *Canadian Mineralogist,* vol. 23, pp. 21-28, 1985.

[99] M. Zajac, J. Skocek, F. Bullerjahn, B. Lothenbach, K. Scrivener, and M. Ben Haha, "Early hydration of ye'elimite: Insights from thermodynamic modelling," *Cement and Concrete Research,* vol. 120, pp. 152-163, 2019/06/01/ 2019.

[100] H. a. W. Saalfed, M., "Refinement of the crystal structure of gibbsite, $Al(OH)_3$," *Zeitschrift für Kristallographie,* vol. 139, no. 1-2, pp. 129-135, 1974.

[101] S. Goldberg, J. A. Davis, and J. D. Hem, "The Surface Chemistry of Aluminum Oxides and Hydroxides," in *The Environmental Chemistry of Aluminum*, G. Sposito, Ed. Second ed. California: CRC Lewis Publisher, 1996, pp. 271-333.

[102] J.-B. Champenois, "Etude de l'hydratation des ciments sulfo-alumineux par des solutions de borate de sodium : de la spéciation du bore au retard à l'hydratation.," Doctorat thèse de doctorat, Chimie et Physicochimie des matériaux, Université de Montpellier 2 2012.

[103] T. Tsuchida and N. Ichikawa, "Mechanochemical phenomena of gibbsite, bayerite and boehmite by grinding," *Reactivity of Solids,* vol. 7, no. 3, pp. 207-217, 1989/08/01/ 1989.

[104] P. Blanc, X. Bourbon, A. Lassin, and E. C. Gaucher, "Chemical model for cement-based materials: Thermodynamic data assessment for phases other than C–S–H," *Cement and Concrete Research,* vol. 40, no. 9, pp. 1360-1374, 2010/09/01/ 2010.

[105] T. Matschei, B. Lothenbach, and F. P. Glasser, "Thermodynamic properties of Portland cement hydrates in the system CaO–Al2O3–SiO2–CaSO4–CaCO3–H2O," *Cement and Concrete Research,* vol. 37, no. 10, pp. 1379-1410, 2007/10/01/ 2007.

[106] A. G. Rettel, W.; Mueller, D.; Scheler, G. , "On the hydration of calcium aluminate ($CaAl_2O_4$) at various temperatures," *British Ceramic Transactions Journal*, vol. 84 pp. 25–28, 1985.

[107] A. P. Kirchheim, V. Fernàndez-Altable, P. J. M. Monteiro, D. C. C. Dal Molin, and I. J. J. o. M. S. Casanova, "Analysis of cubic and orthorhombic C3A hydration in presence of gypsum and lime," journal article vol. 44, no. 8, pp. 2038-2045, April 01 2009.

[108] N. Ukrainczyk, "Kinetic modeling of calcium aluminate cement hydration," *Chemical Engineering Science,* vol. 65, no. 20, pp. 5605-5614, 2010/10/15/ 2010.

[109] S. Berger, "Etude des potentialités des ciments sulfo-alumineux bélitiques pour le conditionnement du zinc De l'hydratation à la durabilité," Université des Sciences et Technologie de Lille - Lille I, 2009.

[110] W. Ding, Y. He, L. Lu, F. Wang, and S. Hu, "Mechanical property and microstructure of quaternary phase paste blended with metakaolin," *Cement and Concrete Composites,* vol. 118, p. 103934, 2021/04/01/ 2021.

[111] F. Hueller, C. Naber, J. Neubauer, and F. Goetz-Neunhoeffer, "Impact of initial CA dissolution on the hydration mechanism of CAC," *Cement and Concrete Research,* vol. 113, pp. 41-54, 2018/11/01/ 2018.

[112] J. Zhang, M. Klasky, and B. C. Letellier, "The aluminum chemistry and corrosion in alkaline solutions," *Journal of Nuclear Materials,* vol. 384, no. 2, pp. 175-189, 2009/02/15/ 2009.

[113] P. Sipos, "The structure of Al(III) in strongly alkaline aluminate solutions — A review," *Journal of Molecular Liquids,* vol. 146, no. 1, pp. 1-14, 2009/05/31/ 2009.

[114] B. Mitrović, R. Milačič, and B. Pihlar, "Speciation of Aluminium in Soil Extracts by Employing Cation-exchange Fast Protein Liquid Chromatography-Inductively Coupled Plasma Atomic Emission Spectrometry " *Analyst,* vol. 121, pp. 627-634, 1996.

[115] S. Dong, W. Shi, J. Zhang, and S. Bi, "$^{27}$Al NMR Chemical Shifts and Relative Stabilities of Aqueous Monomeric $Al^{3+}$ Hydrolytic Species with Different Coordination Structures," *ACS Earth and Space Chemistry,* vol. 3, no. 7, pp. 1353-1361, 2019/07/18 2019.

[116] H. van Gog, "First-principles study of dehydration interfaces between diaspore and corundum, gibbsite and boehmite, and boehmite and γ-Al2O3: Energetic stability, interface charge effects, and dehydration defects," *Applied Surface Science,* vol. 541, p. 148501, 2021/03/01/ 2021.

[117] H. A. van Straten, B. T. W. Holtkamp, and P. L. de Bruyn, "Precipitation from supersaturated aluminate solutions: I. Nucleation and growth of solid phases at room temperature," *Journal of Colloid and Interface Science,* vol. 98, no. 2, pp. 342-362, 1984/04/01/ 1984.

[118] X. Du, Y. Wang, X. Su, and J. Li, "Influences of pH value on the microstructure and phase transformation of aluminum hydroxide," *Powder Technology,* vol. 192, no. 1, pp. 40-46, 2009/05/15/ 2009.

[119] A. Kocjan, A. Dakskobler, and T. Kosmač, "Evolution of Aluminum Hydroxides in Diluted Aqueous Aluminum Nitride Powder Suspensions," *Crystal Growth & Design,* vol. 12, no. 3, pp. 1299-1307, 2012/03/07 2012.

[120] T. Isobe, T. Watanabe, J. B. d'Espinose de la Caillerie, A. P. Legrand, and D. Massiot, "Solid-state 1H and 27Al NMR studies of amorphous aluminum hydroxides," *Journal of Colloid and Interface Science,* vol. 261, no. 2, pp. 320-324, 2003/05/15/ 2003.

[121] R. J. Stol, A. K. Van Helden, and P. L. De Bruyn, "Hydrolysis-precipitation studies of aluminum (III) solutions. 2. A kinetic study and model," *Journal of Colloid and Interface Science,* vol. 57, no. 1, pp. 115-131, 1976/10/01/ 1976.

[122] D. A. Palmer and D. J. Wesolowski, "Aluminum speciation and equilibria in aqueous solution: II. The solubility of gibbsite in acidic sodium chloride solutions from 30 to 70°C," *Geochimica et Cosmochimica Acta,* vol. 56, no. 3, pp. 1093-1111, 1992/03/01/ 1992.

[123] G. Lefèvre and M. Fédoroff, "Synthesis of bayerite (β-Al(OH)3) microrods by neutralization of aluminate ions at constant pH," *Materials Letters,* vol. 56, no. 6, pp. 978-983, 2002/11/01/ 2002.

[124] H. Li, J. Addai-Mensah, J. C. Thomas, and A. R. Gerson, "The crystallization mechanism of Al(OH)3 from sodium aluminate solutions," *Journal of Crystal Growth,* vol. 279, no. 3, pp. 508-520, 2005/06/01/ 2005.

[125] H. A. Van Straten and P. L. D. Bruyn, "Precipitation from supersaturated aluminate solutions. II. Role of temperature," *Journal of Colloid and Interface Science,* vol. 102, no. 1, pp. 260-277, 1984/11/01/ 1984.

[126] W. J. T. McHardy, A. P., "Conditions for the formation of bayerite and gibbsite," *Mineralogical Magazine,* vol. 38, pp. 358-368, 1971.

[127] V. a. S. Aghazadeh, S., "Decomposition of Aluminate Solution for Aluminum Hydroxide Precipitation by Carbonation: A Thermodynamic and Experimental Studies," *Journal of Chemical Technology and Metallurgy,* vol. 56, pp. 149-160, 2021.

[128] V. A. Lipin, "A New Technique for Synthesis of Nordstrandite," *Russian Journal of Applied Chemistry,* vol. 74, pp. 184-187, 2001.

[129] K. P. Prodromou and A. S. Pavlatou-Ve, "Formation of Aluminum Hydroxides as Influenced by Aluminum Salts and Bases," *Clays and Clay Minerals,* vol. 43, no. 1, pp. 111-115, 1995/02/01 1995.

[130] B. Lothenbach *et al.*, "Cemdata18: A chemical thermodynamic database for hydrated Portland cements and alkali-activated materials," *Cement and Concrete Research,* vol. 115, pp. 472-506, 2019/01/01/ 2019.

[131] R. J. Myers, G. Geng, E. D. Rodriguez, P. da Rosa, A. P. Kirchheim, and P. J. M. Monteiro, "Solution chemistry of cubic and orthorhombic tricalcium aluminate hydration," *Cement and Concrete Research,* vol. 100, pp. 176-185, 2017/10/01/ 2017.

[132] M. Balonis, B. Lothenbach, G. Le Saout, and F. P. Glasser, "Impact of chloride on the mineralogy of hydrated Portland cement systems," *Cement and Concrete Research,* vol. 40, no. 7, pp. 1009-1022, 2010/07/01/ 2010.

[133] B. Pacewska and M. Nowacka, "Studies of conversion progress of calcium aluminate cement hydrates by thermal analysis method," *Journal of Thermal Analysis and Calorimetry,* vol. 117, no. 2, pp. 653-660, 2014/08/01 2014.

[134] H. Minard, "Etude intégrée des processus d'hydratation, de coagulation, de rigidification et de prise pour un système C3S-C3A - sulfates - alcalins," 2003.

[135] J. Goergens, T. Manninger, and F. Goetz-Neunhoeffer, "In-situ XRD study of the temperature-dependent early hydration of calcium aluminate cement in a mix with calcite," *Cement and Concrete Research,* vol. 136, p. 106160, 2020/10/01/ 2020.

[136] G. Le Saout, "Contribution to the characterisation of cementitious materials and hydration follow-up," Université de Montpellier, 2015.

[137] C. Gosselin, E. Gallucci, and K. Scrivener, "Influence of self heating and Li2SO4 addition on the microstructural development of calcium aluminate cement," *Cement and Concrete Research,* vol. 40, no. 10, pp. 1555-1570, 2010/10/01/ 2010.

[138] S. A. Rodger and D. D. Double, "The chemistry of hydration of high alumina cement in the presence of accelerating and retarding admixtures," *Cement and Concrete Research,* vol. 14, no. 1, pp. 73-82, 1984/01/01/ 1984.

[139] J. He, G. Long, K. Ma, and Y. Xie, "Influence of fly ash or slag on nucleation and growth of early hydration of cement," *Thermochimica Acta,* vol. 701, p. 178964, 2021/07/01/ 2021.

[140] B. Zhu, Y. Song, X. Li, P. Chen, and Z. Ma, "Synthesis and hydration kinetics of calcium aluminate cement with micro MgAl2O4 spinels," *Materials Chemistry and Physics,* vol. 154, pp. 158-163, 2015/03/15/ 2015.

[141] A. She, K. Ma, P. Zhao, and J. Wang, "Characterisation of calcium aluminate cement hydration: comparison of low-field NMR and conventional methods," *Advances in Cement Research,* pp. 1-8, 2021.

[142] P. P. Barret, D. Ménétrier, and D. Bertrandie, "Contribution to the study of the kinetic mechanism of aluminous cement setting I — Latent periods in heterogeneous and homogeneous milieus and the absence of heterogeneous nucleation," *Cement and Concrete Research,* vol. 4, no. 4, pp. 545-556, 1974/07/01/ 1974.

[143] K. L. Scrivener and A. Nonat, "Hydration of cementitious materials, present and future," *Cement and Concrete Research,* vol. 41, no. 7, pp. 651-665, 2011/07/01/ 2011.

[144] L. Prasittisopin and I. Sereewatthanawut, "Dissolution, nucleation, and crystal growth mechanism of calcium aluminate cement," *Journal of Sustainable Cement-Based Materials,* vol. 8, no. 3, pp. 180-197, 2019/05/04 2019.

[145] S. R. Klaus, J. Neubauer, and F. Goetz-Neunhoeffer, "Influence of the specific surface area of alumina fillers on CAC hydration kinetics," vol. 28, no. 1, pp. 62-70, 2016.

[146] K. Fujii, W. Kondo, and H. Ueno, "Kinetics of Hydration of Monocaldum Aluminate," *Journal of the American Ceramic Society,* vol. 69, no. 4, pp. 361-364, 1986/04/01 1986.

[147] J. F. Young, "Effect of Organic Compounds on the Interconversions of Calcium Aluminate Hydrates: Hydration of Tricalcium Aluminate," *Journal of the American Ceramic Society,* https://doi.org/10.1111/j.1151-2916.1970.tb12011.x vol. 53, no. 2, pp. 65-69, 1970/02/01 1970.

[148] D. Damidot, A. Rettel, and A. Capmas, "Action of admixtures on Fondu cement: Part 1. Lithium and sodium salts compared," vol. 8, no. 31, pp. 111-119, 1996.

[149] F. Šoukal *et al.*, "The influence of pH buffers on hydration of hydraulic phases in system CaO–Al2O3," *Journal of Thermal Analysis and Calorimetry,* Article vol. 124, no. 2, pp. 629-638, 2016.

[150] S. Joseph, J. Skibsted, and Ö. Cizer, "A quantitative study of the C3A hydration," *Cement and Concrete Research,* vol. 115, pp. 145-159, 2019/01/01/ 2019.

[151] N. Maach, J. F. Georgin, S. Berger, and J. Pommay, "Chemical mechanisms and kinetic modeling of calcium aluminate cements hydration in diluted systems: Role of aluminium hydroxide formation," *Cement and Concrete Research,* vol. 143, p. 106380, 2021/05/01/ 2021.

[152] G. L. Saoût, B. Lothenbach, P. Taquet, H. Fryda, and F. Winnefeld, "Hydration of calcium aluminate cement blended with anhydrite," vol. 30, no. 1, pp. 24-36, 2018.

[153] T. Manninger, D. Jansen, J. Neubauer, and F. Goetz-Neunhoeffer, "The retarding effect of phosphoric acid during CAC hydration," *Cement and Concrete Research,* vol. 122, pp. 83-92, 2019/08/01/ 2019.

[154] T. Manninger, D. Jansen, J. Neubauer, and F. Goetz-Neunhoeffer, "Phase Solubility Changes during Hydration of Monocalciumaluminate and Calcite—The Influence of Alkali Accumulation," *Materials,* vol. 13, no. 6, 2020.

# Chapter 2: Materials, characterization of materials and methods

# **Chapitre 2** : Matériaux, caractérisation des matériaux et méthodes

**Résumé:** L'objectif de cette thèse est de décrire le processus d'hydratation au jeune âge de quatre aluminates de calcium, et en particulier d'évaluer l'influence du rapport C/A sur le déroulement de l'hydratation. Pour cela, quatre phases synthétiques d'aluminates de calcium anhydres fournies par la société Mineral Research ont été étudiées:

- Dialuminate monocalcique - $CA_2$
- Aluminate monocalcique - CA
- Mayenite - $C_{12}A_7$
- Aluminate tricalcique - Cubic-$C_3A$

Tout d'abord, ce chapitre est consacré à la présentation des matériaux utilisés au cours de cette thèse et de leurs propriétés physico-chimiques. Dans la première partie de ce chapitre, les caractéristiques physiques et la composition chimique des phases anhydres d'aluminate de calcium utilisées sont présentées. Ensuite, une analyse minéralogique est réalisée afin d'évaluer la pureté de chaque poudre. Les deuxième et troisième parties de ce chapitre sont consacrées à la description des méthodes expérimentales mis en œuvre et des techniques analytiques utilisées pour caractériser l'hydratation des pâtes et suspensions étudiées.

# Introduction

Commercial calcium aluminate cements are a mixture of different phases as mentioned in the literature review section. The reactive anhydrous phases of these commercial cements are monocalcium dialuminate $CA_2$, monocalcium aluminate CA, tricalcium aluminate $C_3A$ and mayenite (dodecacalcium hepta-aluminate) $C_{12}A_7$. From a chemical point of view, these calcium aluminate phases differ from each other by their calcium/aluminium ratio.

The objective of this thesis is to describe separately the hydration process of these anhydrous calcium aluminate phases, and in particular to determine the influence of the C/A ratio on the course of hydration. For this reason, four synthetic anhydrous calcium aluminate phases were purchased from Mineral Research Processing:

- Monocalcium dialuminate – $CA_2$
- Calcium monoaluminate – CA
- Mayenite – $C_{12}A_7$
- Tricalcium aluminate – Cubic-$C_3A$

Their physical characteristics and chemical composition are presented in the first part of this chapter. Then, a mineralogical analysis is carried out in order to evaluate the purity of each powder.

The second and third parts of this chapter are dedicated to the description of the experimental procedures and analytical techniques used to characterize the hydration of the pastes and of the suspensions under investigation.

# 1. Characterization of calcium aluminate anhydrous phases

## 1.1 Physical characteristics and chemical composition

All four synthetic anhydrous calcium aluminate phases were characterized by laser granulometry, helium pycnometry and nitrogen adsorption measurements in order to determine their particle size distribution, absolute density and specific surface area respectively. Analytical procedures for each of these measurements are described in Appendix A.1. Results from these measurements are reported in Table 4. Particle size distribution is presented in Figure 33.

**Table 4 : Particle size distribution of the anhydrous phases.**

| | Particle size distribution | | | Absolute density ($g/cm^3$) | Specific Surface Area ($m^2/g$) |
|---|---|---|---|---|---|
| **Anhydrous phase** | **$d_{10}$ (µm)** | **$d_{50}$ (µm)** | **$d_{90}$ (µm)** | | |
| $CA_2$ | 2.5 | 9.4 | 31.1 | 3.1 | 1.0 |
| CA | 3.7 | 10.3 | 22.2 | 3.1 | 1.1 |
| $C_{12}A_7$ | 6.3 | 22.1 | 73.8 | 2.8 | 1.1 |
| Cubic-$C_3A$ | 3.7 | 9.8 | 20.6 | 3.1 | 1.6 |

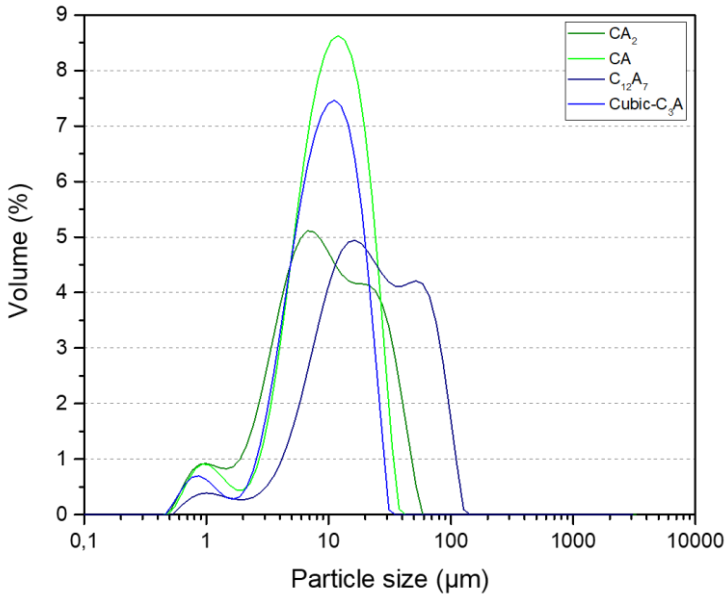


**Figure 33 : Particle size distribution of the anhydrous phases used in this study.**

In order to determine their chemical composition, each of synthetic anhydrous phases was first dissolved under acidic conditions. The composition of the resulting solution was then determined by using ICP-AES measurements. The measured C/A ratios were consistent with the ratios expected from the mineral stoichiometry (Table 5).

**Table 5 : Comparison between expected and measured C/A ratio for each anhydrous calcium aluminate phase.**

| | $CA_2$ | CA | $C_{12}A_7$ | Cubic-$C_3A$ |
|---|---|---|---|---|
| **Stoichiometric C/A** | 0.25 | 0.50 | 0.86 | 1.50 |
| **Measured C/A** | 0.29 | 0.54 | 0.84 | 1.47 |

## 1.2 Mineralogical characterization of anhydrous phases

Prior to any hydration study, the mineralogical composition of each anhydrous calcium aluminate phase was verified. Three analytical techniques were used to complete such a mineralogical characterization. First, X-ray diffraction (XRD) analysis was carried out in order to identify the crystalline phases in presence. Thermogravimetric analysis (TG) analysis was then used in order to quantify bound water. Experimental details for both techniques are given in Appendix A.2 and Appendix A.3. Finally, $^{27}$Al solid-state nuclear magnetic resonance (NMR) experiments were carried out in order to quantify the mineralogical compositions. Self-consistency of the results from the three methods was evaluated, in particular with respect to hydration advancement and bound water content.

### 1.2.1 Powder X-ray diffraction analysis

Collected Powder XRD patterns of each anhydrous calcium aluminate phase are presented in Figure 34, Figure 35, Figure 36 and Figure 37.

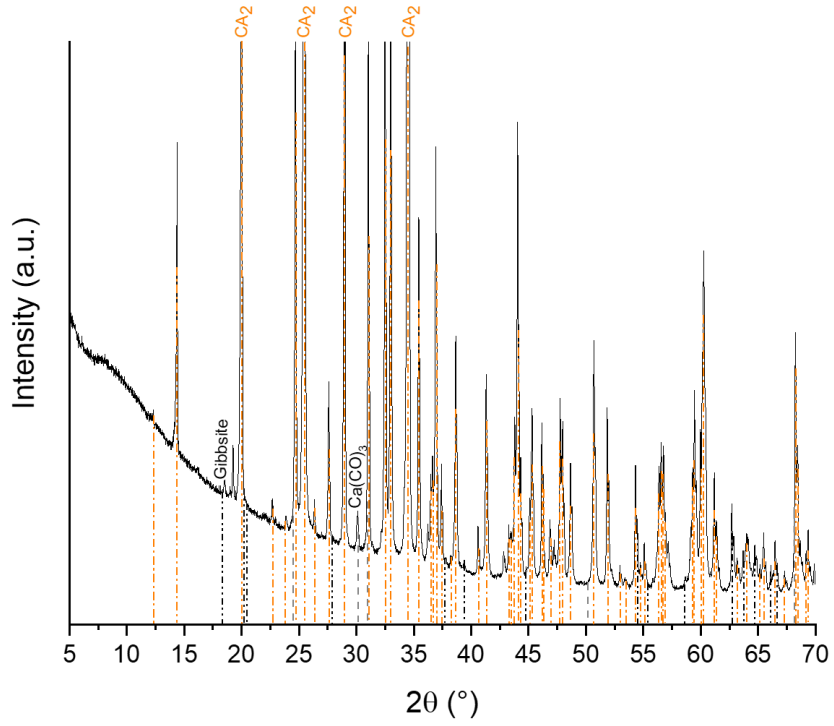


**Figure 34 : XRD pattern of the anhydrous $CA_2$ phase as received (CuKα radiation).**

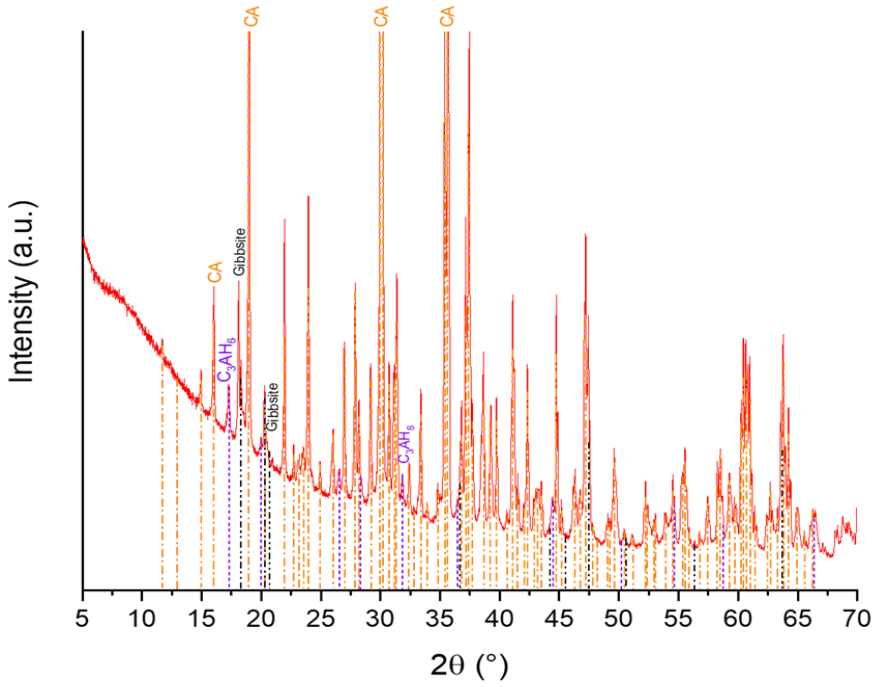


**Figure 35 : XRD pattern of the anhydrous CA phase as received (CuKα radiation).**

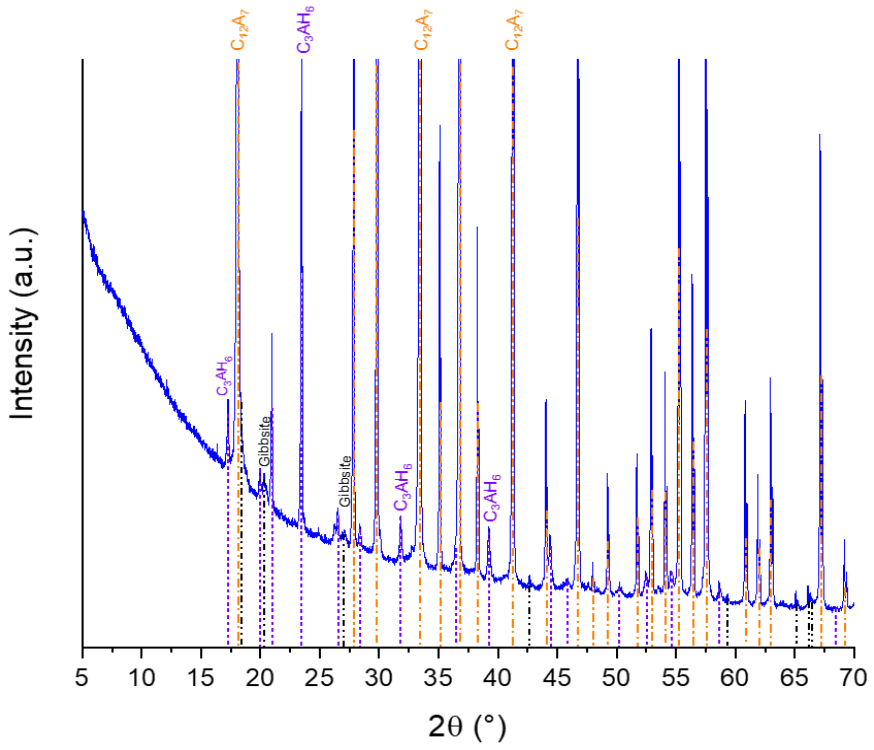


**Figure 36 : XRD pattern of the anhydrous $C_{12}A_7$ phase as received (CuKα radiation).**

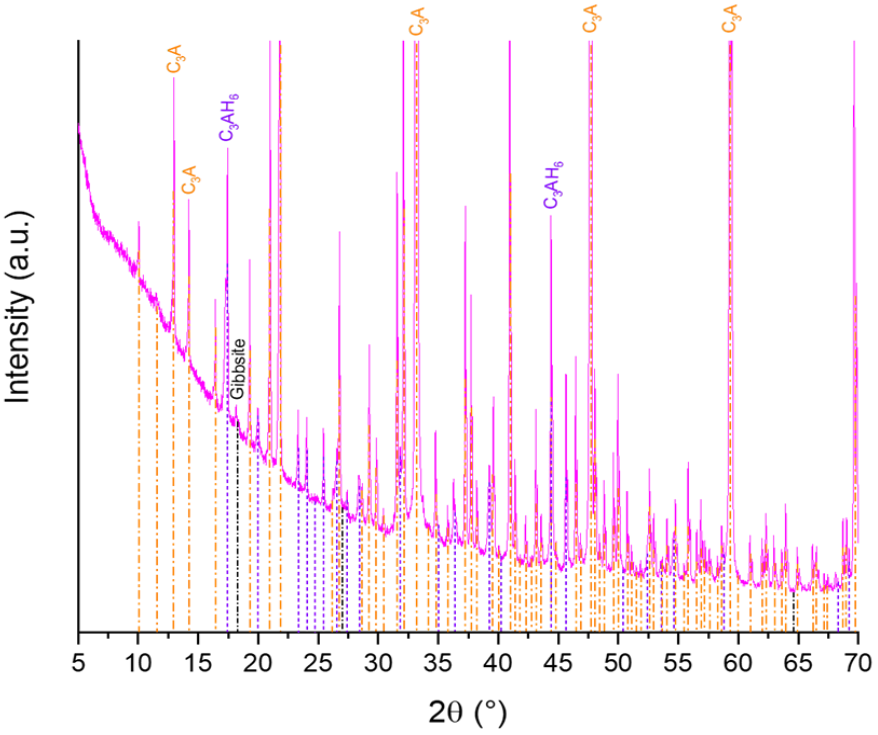


**Figure 37 : XRD pattern of the anhydrous cubic-$C_3A$ phase as received (CuKα radiation).**

The powder XRD patterns confirmed the presence of the expected phases for each of the anhydrous calcium aluminate phases. However, hydrated phases were also identified. Table 6 recapitulates the observed phases together with the number of the powder diffraction file (PDF) used to identify them – figured as dotted lines in Figure 34, Figure 35, Figure 36 and Figure 37.

**Table 6 : Identified phases from XRD patterns of synthetic anhydrous calcium aluminate phases.**

| XRD pattern | $CA_2$ | CA | $C_{12}A_7$ | Cubic-$C_3A$ |
|---|---|---|---|---|
| Identified phases | $CaAl_4O_7$ (01-072-0767) | $CaAl_2O_4$ (01-080-3836) | $Ca_{12}Al_{14}O_{33}$ (00-009-0413) | $Ca_9Al_6O_{18}$ (01-070-0839) |
| | Gibbsite, $Al(OH)_3$ (00-033-0018) | Gibbsite, $Al(OH)_3$ (01-080-6432) | Gibbsite, $Al(OH)_3$ (01-080-6432) | Gibbsite, $Al(OH)_3$ (01-080-6432) |
| | | Katoite, $Ca_3Al_2(OH)_{12}$ (00-024-0217) | Katoite, $Ca_3Al_2(OH)_{12}$ (00-024-0217) | Katoite, $Ca_3Al_2(OH)_{12}$ (01-074-6226) |

The identification of hydrated phases such as katoite and/or gibbsite revealed a small level of hydration despite the curing of the anhydrous calcium aluminates in sealed flasks under nitrogen atmosphere.

### 1.2.2 Thermogravimetric analysis

Thermogravimetric analysis of the four calcium aluminate phases confirmed the XRD conclusions. The analysis was performed from 30 °C to 1000 °C at a heating rate of 10 °C/min under nitrogen atmosphere to prevent carbonation (see Appendix A.3). Mass loss curves and corresponding derivative curves are plotted in Figure 38 for $CA_2$, CA, $C_{12}A_7$ and $C_3A$ powders.

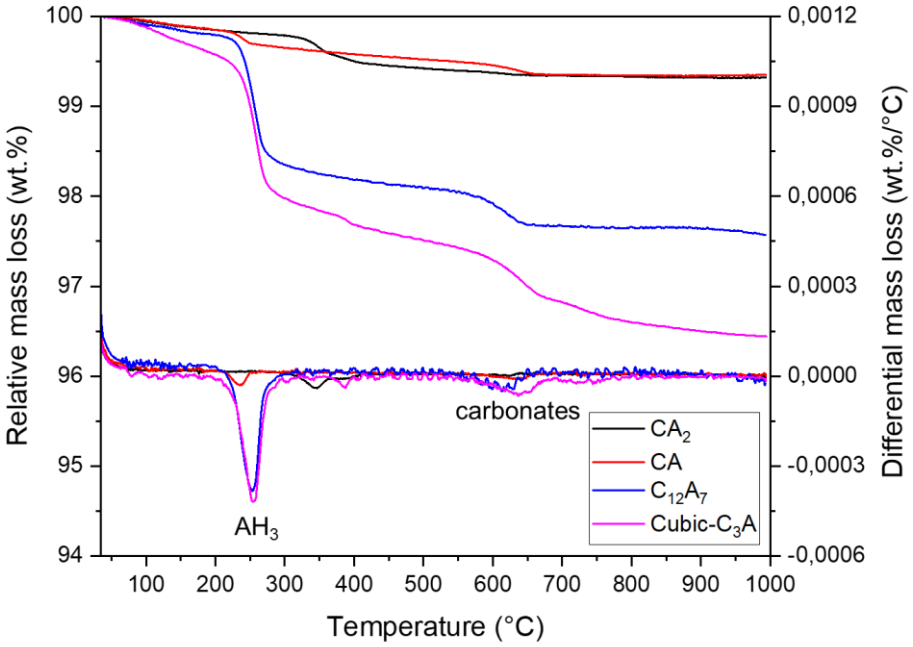


**Figure 38 : Thermogravimetric curves of the anhydrous phases used in this study.**

On these thermograms, weight losses occurring below 500 °C were attributed to the water loss from thermal decomposition of hydrated phases. More precisely, a sharp weight loss occurring around 250 °C was attributed to the thermal decomposition of aluminium hydroxide, as already reported in literature [1-4] and described by the following reaction equation (7).

$$2Al(OH)_3 \rightleftharpoons Al_2O_3 + 3H_2O \text{ (in cement notation } AH_3 \rightleftharpoons A + 3H) \quad (7)$$

For all calcium aluminate powders, weight losses measured up to 550 °C and weight losses measured between 175 °C and 325 °C are reported in the second and third column of Table 7 respectively. Weight losses measured between 175 °C and 325 °C were then used in order to calculate the corresponding amount of aluminium hydroxide in all four samples. Knowing that the $AH_3$ has three moles of water per mole of phase, the amount of aluminium hydroxide is obtained by using the following equation (8).

$$AH_{3,measured} = WL_{175°C \rightarrow 325°C} \cdot \frac{M(AH_3)}{3 \cdot M(H_2O)} \quad (8)$$

where, $AH_{3,measured}$ is aluminium hydroxide amount, $WL_{175°C \rightarrow 325°C}$ is the weight loss between 175 °C and 325 °C obtained by TGA, $M(AH_3)$ is the molar mass of $AH_3$, and $M(H_2O)$ is the molar mass of $H_2O$.

**Table 7 : Bound water amount of the anhydrous phases used for the study.**

| Anhydrous phase | Mass loss between 30 and 550 °C (wt. %) | Mass loss between 175 and 325 °C (wt. %) | Calculated $AH_3$ content (wt. %) |
|---|---|---|---|
| $CA_2$ | 0.6 | 0.1 | 0.3 |
| CA | 0.5 | 0.2 | 0.6 |
| $C_{12}A_7$ | 1.9 | 1.5 | 4.3 |
| Cubic-$C_3A$ | 2.6 | 1.7 | 4.9 |

The thermal decomposition of $C_3AH_6$ occurs between 260 and 310 °C, with a main decomposition event occurring at 300 °C [3, 5]. The identification and quantification of $C_3AH_6$ are difficult because of low weight loss values at this temperature and overlapping with the thermal decomposition of the aluminium hydroxide.

Finally, weight losses at temperatures above 550 °C are related to the decarbonation of the calcium carbonate (CČ) [6, 7] or monocarboaluminate ($C_4AČH_{11}$) [8-10]. Small weight losses are observed (≤ 1 wt. %) [6, 9]. To get an estimate of the amount of carbonates present, the maximum content of calcium carbonate and monocarboaluminate phases was calculated considering hypothetically that the decarbonation peak corresponded solely to one or the other, using the molar masses of each of the expected carbonated phases (100 g/mol for calcium carbonate and 568 g/mol, for monocarboaluminate) and of $CO_2$ (44 g/mol). The results are summarized in Table 8. It should be noted that the presence of crystalline carbonated phases was not identified by powder XRD analysis.

**Table 8 : Amount of the carbonated phases when present assuming that it is either CČ or $C_4AČH_{11}$.**

| Anhydrous phase | Mass loss between 550 and 1000 °C (wt. %) | Calculated CČ content (wt. %) | Calculated $C_4AČH_{11}$ content (wt. %) |
|---|---|---|---|
| $CA_2$ | 0.1 | 0.2 | 1 |
| CA | 0.1 | 0.2 | 1 |
| $C_{12}A_7$ | 0.5 | 1 | 6 |
| Cubic-$C_3A$ | 1 | 2 | 13 |

### 1.2.3 $^{27}$Al solid-state nuclear magnetic resonance

$^{27}$Al solid-state NMR analysis was performed on all four calcium aluminate phases. Experimental procedure for spectra acquisition is detailed in Appendix A.4. Spectra were then decomposed into their individual spectral components using the DMFIT freeware [11] fitted with a second order quadrupolar lineshape for the central transition (Q mas ½) model [11, 12]

using parameters from the literature (Table 9). In addition, the crystal structure of each anhydrous phase is described in the Literature Review chapter.

**Table 9 : $^{27}$Al quadrupolar coupling constants, asymmetry parameters and isotropic chemical shifts for the synthetic anhydrous phases from the literature [13-15].**

| Anhydrous phase | Site | $\delta_{iso}$ (ppm) | Quadrupole coupling constant, $C_Q$ (MHz) | Asymmetry parameter, $\eta$ |
|---|---|---|---|---|
| $CA_2$ | $Al_1^{(IV)}$ | 75 | 6.2 | 0.88 |
| | $Al_2^{(IV)}$ | 69 | 9.5 | 0.82 |
| CA | $Al_1^{(IV)}$ | 82 | 2.5 | 0.20 |
| | $Al_2^{(IV)}$ | 84 | 2.6 | 0.75 |
| | $Al_3^{(IV)}$ | 86 | 2.6 | 0.95 |
| | $Al_4^{(IV)}$ | 83 | 3.3 | 0.53 |
| | $Al_5^{(IV)}$ | 82 | 3.4 | 0.39 |
| | $Al_6^{(IV)}$ | 81 | 4.3 | 0.47 |
| $C_{12}A_7$ | $Al_1^{(IV)}$ | 86 | 9.7 | 0.40 |
| | $Al_2^{(IV)}$ | 80 | 3.8 | 0.70 |
| Cubic-$C_3A$ | $Al_1^{(IV)}$ | 79 | 8.7 | 0.32 |
| | $Al_2^{(IV)}$ | 78 | 9.3 | 0.54 |

Figure 39 shows the simulated $^{27}$Al solid-state NMR central bands of the central transition for tetrahedral Al sites of anhydrous phases based on the literature.

First, anhydrous $CA_2$ phase has overlapping resonances corresponding to two tetrahedrally coordinated Al sites. Anhydrous CA phase contains six non-equivalent $AlO_4$ tetrahedra in the asymmetric unit [13, 16]. Anhydrous $C_{12}A_7$ phase contains two different tetrahedrally coordinated Al sites: the intensity ratio of $Al_1$(IV) to $Al_2$(IV) is reported as 4:3 by Gessner *et al.* [17]. Anhydrous cubic-$C_3A$ phase exhibits overlapping resonances from two tetrahedral Al sites [13].

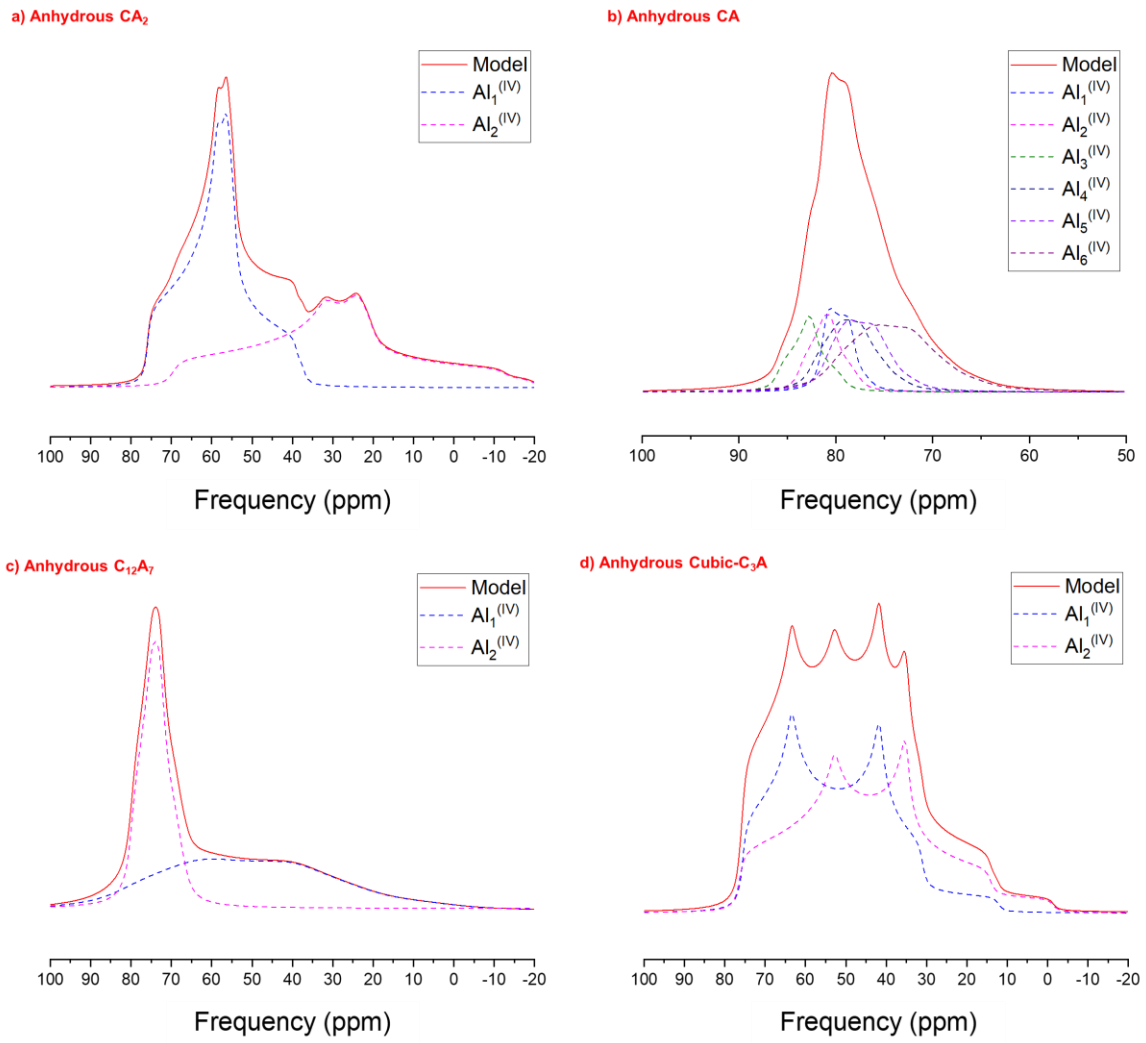


**Figure 39 : $^{27}$Al solid-state NMR simulated spectrum using the parameters of Table 9. a) anhydrous $CA_2$, b) anhydrous CA, c) anhydrous $C_{12}A_7$ and d) anhydrous cubic-$C_3A$.**

By using the relative data for each Al site found in literature for the studied anhydrous phases (see Table 9), a convincing simulation for each anhydrous phase was done (Figure 40). The fitted spectra showed a remarkably good agreement with data obtained from literature (see Table 10).

**Table 10 : Fitted spectra values of each anhydrous phase.**

| Anhydrous phase | Identified phase | Chemical shift (ppm) | Model | Peak intensity (a.u.) | Quadrupole coupling constant (MHz) | Asymmetry parameter | Width (ppm) |
|---|---|---|---|---|---|---|---|
| **$CA_2$** | $CaAl_4O_7$ | 76 | Q mas 1/2 | 24200 | 6.25 | 0.88 | - |
| | | 70 | Q mas 1/2 | 8400 | 9.55 | 0.82 | - |
| | $AH_3$ (gibbsite) | 9 | Lorentzian | 900 | - | - | 7.00 |
| **CA** | $CaAl_2O_4$ | 82 | Q mas 1/2 | 33000 | 2.50 | 0.20 | - |
| | | 84 | Q mas 1/2 | 30000 | 2.60 | 0.75 | - |
| | | 86 | Q mas 1/2 | 29000 | 2.60 | 0.95 | - |
| | | 83 | Q mas 1/2 | 29000 | 3.30 | 0.53 | - |
| | | 82 | Q mas 1/2 | 29000 | 3.40 | 0.39 | - |
| | | 81 | Q mas 1/2 | 27000 | 4.30 | 0.47 | - |
| | $AH_3$ (gibbsite) | 9.0 | Lorentzian | 120 | - | - | 10 |
| **$C_{12}A_7$** | $Ca_{12}Al_{14}O_{33}$ | 86 | Q mas 1/2 | 5400 | 9.70 | 0.40 | - |
| | | 80 | Q mas 1/2 | 26500 | 3.80 | 0.70 | - |
| | $C_3AH_6$ | 12.4 | Lorentzian | 1550 | - | - | 2.80 |
| | $AH_3$ (gibbsite) | 9.0 | Lorentzian | 957 | - | - | 8.93 |
| | $AH_3$ (amorphous) | 5.3 | Lorentzian | 250 | - | - | 1.64 |
| **Cubic-$C_3A$** | $Ca_3Al_2O_6$ | 79 | Q mas 1/2 | 4500 | 8.7 | 0.32 | - |
| | | 78 | Q mas 1/2 | 3900 | 9.3 | 0.54 | - |
| | $C_3AH_6$ | 12.4 | Lorentzian | 3514 | - | - | 2.70 |
| | $AH_3$ (gibbsite) | 9 | Lorentzian | 184 | - | - | 5.81 |

However, a signal of low intensity signal around 10 – 9 ppm established the occurrence of octahedral Al sites. This finding reflected the partial hydration of the anhydrous phases, as already evidenced from XRD and TG analysis. It should be reminded that the identification and quantification of hydrated calcium aluminate phases are difficult because of their overlapping signals on the spectrum. From literature, the signal around 9.0 ± 0.3 ppm was ascribed to $AH_3$ (gibbsite). Nevertheless, it should be noted that the values corresponding to the chemical shift of aluminium hydroxide vary in literature. This is due to the fact that differences in crystallinity of aluminium hydroxide results in variation of Al octahedral environments [18]. Skibsted *et al.* reported two Al atoms in octahedral environments at 10.4 ± 0.3 ppm for $Al_1$(IV) and 11.5 ± 0.3 ppm $Al_2$(IV) in synthetic $Al(OH)_3$ (magnetic field strength of 9.4 T) [13]. On the other hand,

Al in amorphous alumina gel has a chemical shift values below 8 ppm [19, 20]. Finally, Zhang and Chang [21] assigned the signal at 9.3 ppm to $Al(OH)_3$ whereas Pena *et al.* [22] assigned it at 8.1 ± 0.5 ppm. Moreover, the chemical shift observed at 12.3 ppm [22] was determined for the stable $C_3AH_6$ phase. Lastly, the chemical shift located at 5.3 ppm in the spectrum of anhydrous $C_{12}A_7$ was considered as an artefact and neglected due to its low intensity.

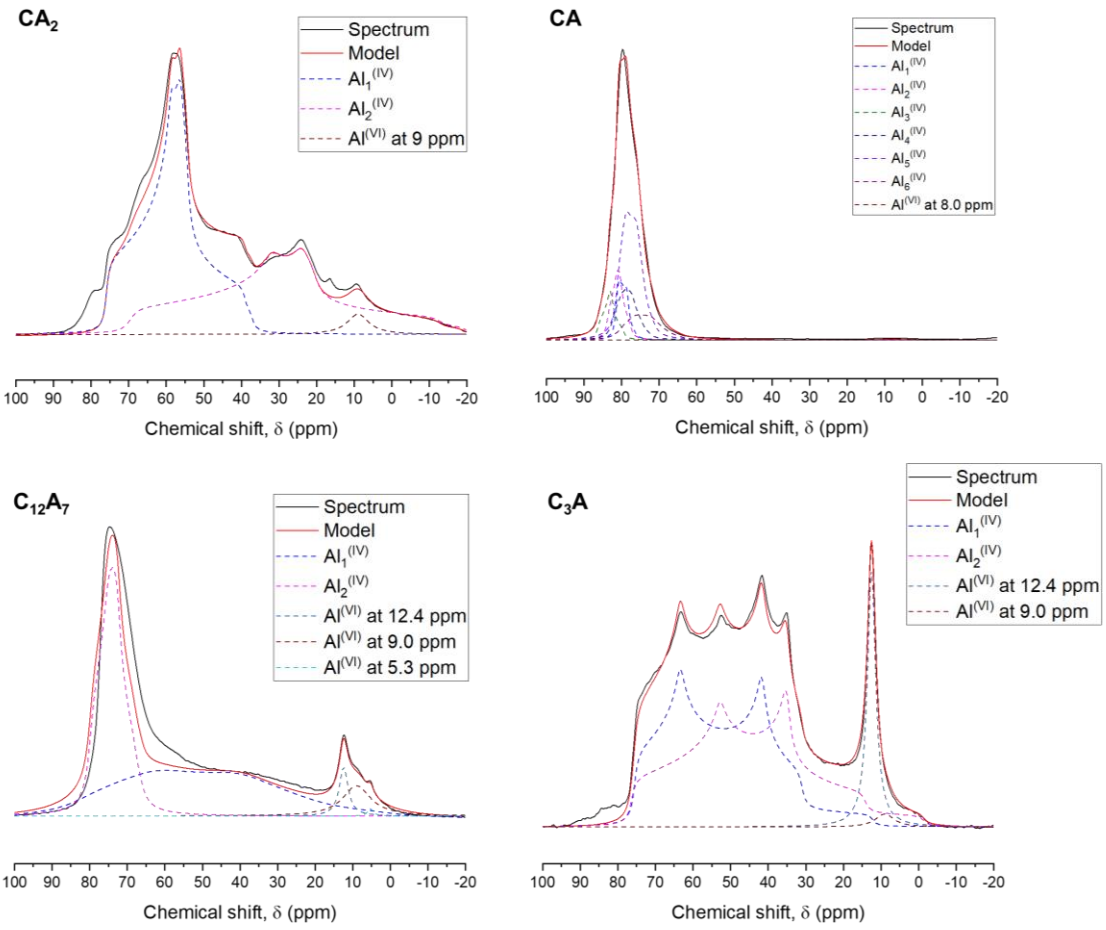


**Figure 40 : $^{27}$Al NMR spectra (black lines) and fit decomposition of the anhydrous phases with a second order quadrupolar lineshapes and of the octahedral Al sites of the hydrates with Lorentzian lineshapes [23].**

Mineralogical composition estimations from $^{27}$Al NMR signals for synthetic powders used as raw materials in this study are listed in Table 11. Considering the quality of the fits, the necessary baseline corrections and the fact that the spinning side-band pattern was not taken into account in the models, these estimates were probably accurate within +/- 5%.

**Table 11 : Quantitative estimations from $^{27}Al$ NMR signals for anhydrous phases ($Al^{(IV)}$ sites) and hydrated phases ($Al^{(VI)}$).**

| Anhydrous phase | Phases | Chemical shift (ppm) | Molar fraction of Al present in the identified phase (%) | Weight fraction (wt. %) |
|---|---|---|---|---|
| $CA_2$ | $CaAl_4O_7$ | 76/70 | 97 | 99 |
| | $AH_3$ (gibbsite) | 9.0 | 3 | 1 |
| CA | $CaAl_2O_4$ | 82/84/86/83/82/81 | 99.5 | 99.5 |
| | $AH_3$ (gibbsite) | 8.0 | 0.5 | 0.5 |
| $C_{12}A_7$ | $Ca_{12}Al_{14}O_{33}$ | 86/80 | 90 | 99.8 |
| | $C_3AH_6$ | 12.4 | 3 | 0.1 |
| | $AH_3$ (gibbsite) | 9.0 | 6.7 | 0.1 |
| | Artefact | 5.3 | 0.3 | |
| Cubic-$C_3A$ | $Ca_3Al_2O_6$ | 79/78 | 89.4 | 86 |
| | $C_3AH_6$ | 12.4 | 9.6 | 13 |
| | $AH_3$ (gibbsite) | 9.0 | 1 | 1 |

As already observed by using XRD and TG analysis, apart from the expected calcium aluminate anhydrous phases, $^{27}Al$ solid-state NMR highlighted the presence of hydrated phases in all raw materials used in this study. The presence of gibbsite has been confirmed for $CA_2$, CA, $C_{12}A_7$ and cubic-$C_3A$ and its content was estimated as being equal to 1, 3, 0.1 and 1 wt. % respectively. From NMR estimation, small amounts of $C_3AH_6$ were also present in the $C_{12}A_7$ and cubic-$C_3A$ samples. These results confirmed that synthetic calcium aluminate phases were slightly hydrated despite all precautions taken to avoid this phenomenon. However, anhydrous calcium aluminates still remain as the main component of the studied powders, with contents higher than 89 % of the total Al content representing over 99 wt.% of the sample mass (except for $C_3A$ were it was only 86 wt.%).

**To sum up:**

| | **Anhydrous phases** | | | |
|---|---|---|---|---|
| | **$CA_2$** | **CA** | **$C_{12}A_7$** | **Cubic-$C_3A$** |
| *Particle size distribution* | 9.4 µm < $d_{50}$ < 22.1 µm | | | |
| *Density* | Similar values around 3 g/cm$^3$ | | | |
| *Specific surface area* | $CA_2$, CA and $C_{12}A_7$ around 1 m$^2$/g and cubic-$C_3A$ 1.6 m$^2$/g | | | |
| *Measured C/A values* | 0.29 | 0.54 | 0.84 | 1.47 |
| *Bound water amount (wt. %)* | 0.6 | 0.5 | 1.9 | 2.6 |
| *Purity (wt. % - from NMR)* | 99 | 99 | > 99 | 86 |
| *Impurities* | Mainly $AH_3$ and small presence of $C_3AH_6$<br>* Possible presence of carbonate phases that has not been identified neither by XRD analysis nor by $^{27}$Al solid-state NMR analysis | | | |

In the following part of this manuscript, hydration of the previously described calcium aluminate anhydrous phases will be studied under two different conditions.

Firstly, pastes will be elaborated by using a water/cement ratio comprised between 0.3 and 0.6. The hydration of anhydrous phases will be monitored by using isothermal calorimetry, and mineralogical assemblages will be characterized. The objective is to evaluate if the C/A ratio has any influence on the mineralogical assemblage taking into account the degree of hydration reached. Secondly, suspensions will be elaborated by using an unusually high water/cement ratio comprised between 15 and 75. In this part, a specific focus will be placed on the evolution of the interstitial solution composition to evaluate if the C/A ratio has any influence on the reaction path followed during hydration.

The two following parts of this chapter are dedicated to the description of the experimental procedures used to follow hydration kinetics, namely calorimetry and conductometry. Instrumental details of the solid phases characterization methods will not be reported there but in the Appendices.

## 2. Hydration monitoring of pastes by isothermal conduction calorimetry

It is well known that hydration of cementitious phases is an exothermic process [6]. Isothermal conduction calorimetry is thus a technique of choice for monitoring their hydration. It consists in measuring the heat released by a sample as a function of time. The integration of the measured heat flow over time yields the cumulative heat released by chemical reaction under consideration, here hydration. When considering a single reaction, the measured cumulative heat is proportional to the degree of a reaction weighted by its enthalpy of reaction, as described by the equation (9):

$$Q(t) = \Delta_r H . \xi(t) \tag{9}$$

In the case of simultaneous reactions, as it can be the case during hydration of cementitious phases, the resulting cumulative heat release of the whole process is then equal to the sum of the heat released by each single reaction. This kind of consideration highlights the need of measuring accurately the whole heat release from the beginning of the process.

In this study, from an experimental point of view, paste samples (with a total volume of paste around 10 mL) were prepared in a cylindrical polypropylene recipient of 125 mL (inner diameter: 52 mm) by mixing for 90 seconds with an IKA agitator equipped with an anchor type blade of 45 mm (shaft: 8 mm, height: 350 mm) at 600 rpm each anhydrous phases, in decarbonated ultrapure water using water/cement (w/c) ratios ranging from of 0.3 to 0.6, and in laboratory conditions (ambient temperature around 22±2 °C). About 1.2 ±0.2 g of the elaborated paste was then cast in a sealed glass ampoule and introduced in the calorimeter. Such an ex-situ mixing procedure introduces an artefact on the heat measurement at the beginning of the process, since sample introduction leads to a heat variation unrelated to the hydration reaction.

In the present study, an inert paste composed of quartz and water with the same w/c ratio as that of the studied paste was systematically considered to evaluate and factor out this artefact. In Figure 41, the heat flow released during the first five hours after the introduction of an inert sample of quartz is compared to that measured for the $CA_2$, CA, $C_{12}A_7$ and cubic-$C_3A$ samples at identical w/c ratio (0.5).

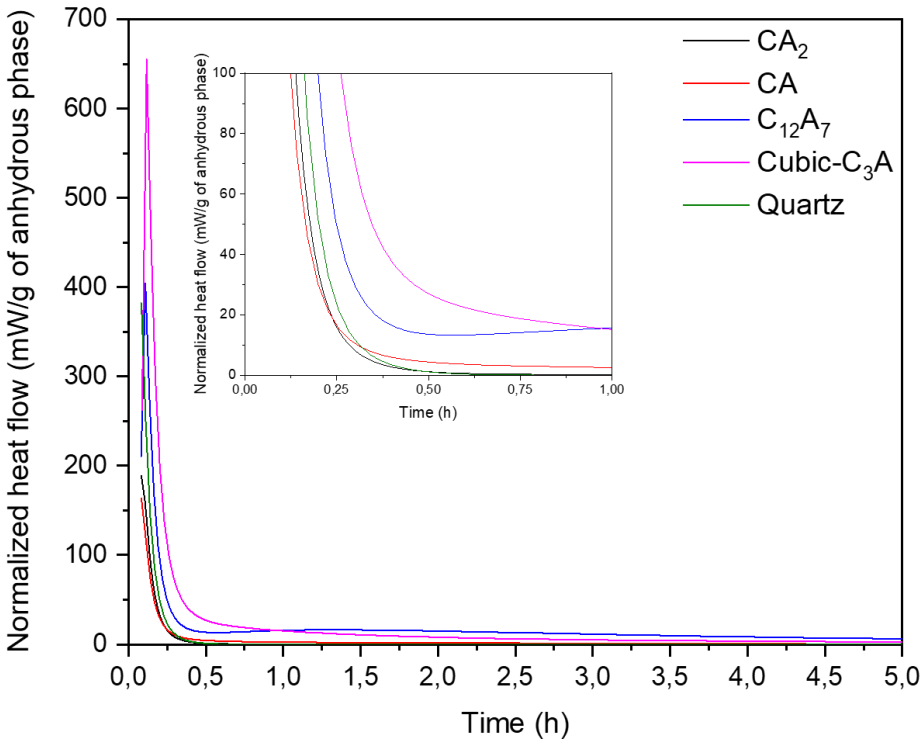


**Figure 41 : Heat flow results of the pastes with a w/c ratio of 0.5 including inert quartz paste for the first 5 hours of hydration (the inset shows an expanded view of the data for the first hour).**

In Figure 41, the heat flows are normalized per mass of anhydrous phases. The results showed that the heat flow measured after CA and $CA_2$ samples introduction were close to that measured during the introduction of an inert paste sample composed of quartz. On the contrary, the heat flow measured after the introduction of $C_{12}A_7$ and cubic-$C_3A$ paste samples was higher than the one measured for the quartz reference sample. This meant that early heat release overlapped with the artefact resulting from the introduction of the paste in the calorimeter. Therefore, accurate determination of cumulative heat by integration of the heat flow profiles of $C_{12}A_7$ and cubic-$C_3A$ paste samples was difficult. Consequently, the protocol was modified and an in-situ mixing technique was performed to evaluate the amount of heat released from early hydration.

For in-situ mixing (i.e. mixing directly inside the calorimeter), a special commercial apparatus (Admix Ampoule Stirrer, TA Instruments) combined with two syringes of 1 ml was used. 2 g of anhydrous phase were weighted in a glass ampoule and introduced in the adiabatic chamber of the calorimeter. After ~1.5 h, once thermal equilibrium was reached, 1 mL of water was introduced with a syringe to the glass ampoule and mixed for 90 seconds. Heat flow measurements were started immediately after the injection. In Figure 42, heat flow and cumulative heat are plotted as a function of time for both procedures for the sake of comparison.

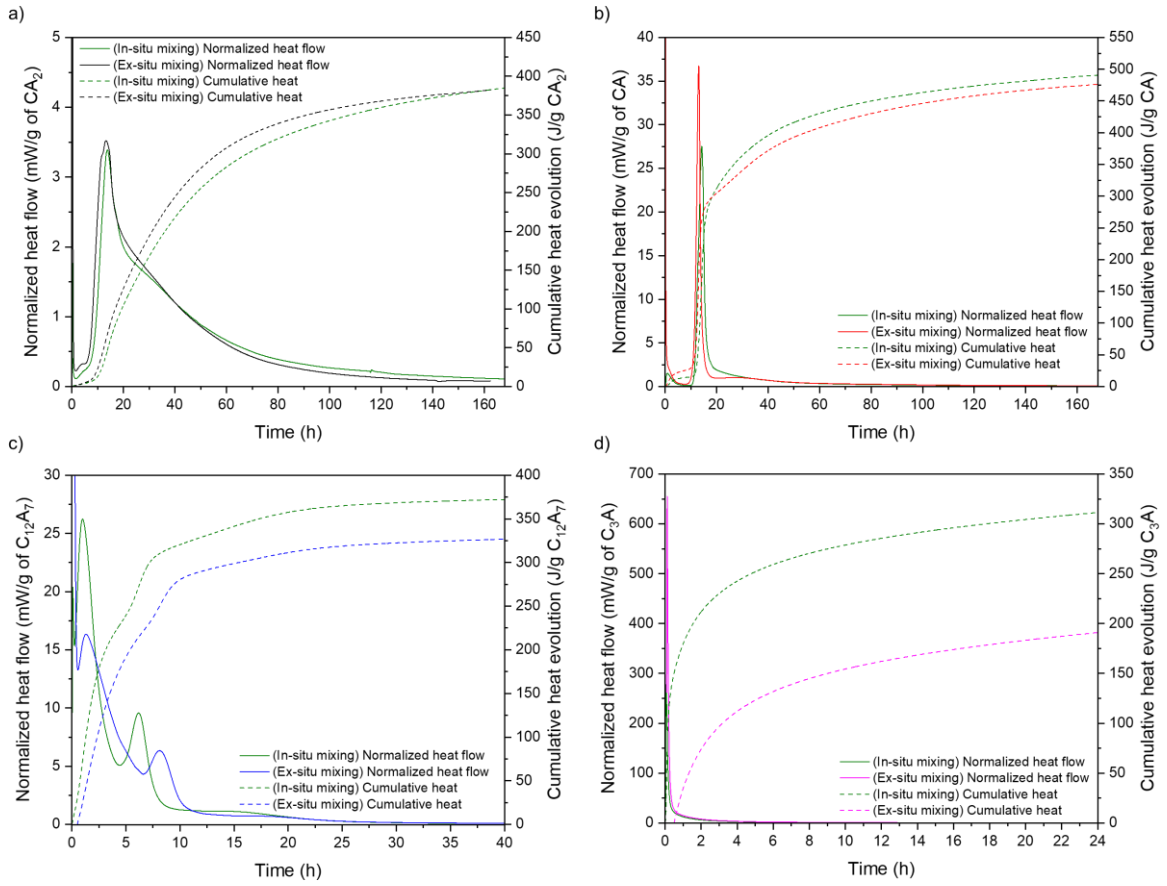


**Figure 42 : Comparison of isothermal calorimetry measurements of the pastes (w/c=0.5) prepared with the in-situ and ex-situ mixing methods at 25 °C for 7 days of hydration. a) $CA_2$ paste, b) CA paste, c) $C_{12}A_7$ paste and d) Cubic-$C_3A$ paste (only results from the first 24 h of hydration monitoring).**

From these experiments, the underestimation of heat release is clearly evidenced for the quickly reacting cementitious phases ($C_{12}A_7$ and cubic-$C_3A$) when ex-situ mixing of pastes employed. In Table 12, cumulative heats measured after 7 days of hydration are compared for each anhydrous phase and both procedures.

**Table 12 : Cumulative heat measured after 7 days of hydration of each paste prepared with the two different methods of mixing (w/c = 0.5, 25 °C).**

| | | **Cumulative heat values (J/g)** | |
|---|---|---|---|
| | Time (day) | In-situ mixing | Ex-situ mixing |
| **$CA_2$** | 7 | 385 | 382 |
| **CA** | | 491 | 477 |
| **$C_{12}A_7$** | | 376 | 341 |
| **Cubic-$C_3A$** | 1 | 311 | 191 |

From Table 12, it can be seen that, within 5 %, the experimental procedure does not affect the cumulative heat measurement when hydrating $CA_2$ and CA. Such a result confirms the observations made by comparing the heat flow released during early hydration of these pastes and the one released by an inert sample. For these minerals, the ex-situ mixing procedure thus leads to accurate measurements of the heat release during their hydration.

Concerning $C_{12}A_7$ pastes, the cumulative heat released 40 hours after mixing was underestimated by about 10 % (50 J/g) when using the ex-situ mixing procedure. Such an underestimation is still acceptable when compared to the uncertainty on cumulative heat measurements, which was estimated to be close to 5 % (see Appendix A.5).

For $C_3A$, the cumulative heat released 24 hours after mixing measured using the ex-situ mixing procedure was lower this time by about 40 % compared to value obtained by in-situ mixing. This must be the result of the well-known quick reactivity of $C_3A$ with water. This will be further discussed in the concerned chapter 6.

There is a practical interest for studying the hydration of cementitious phases in paste that are hydrated under conditions close to those used industrially. However, for water content corresponding to a real cement hydration, extraction of the pore solution from the paste is often difficult to perform and can furthermore destabilize the mineralogical assemblages. The composition of the pore solution cannot then be easily measured as a function of time. To circumvent this difficulty, it was decided to depart from realistic w/c ratio. Hydration monitoring was performed with strongly increased w/c ratios, going from a paste to a dispersed suspension in which conductivity can be directly measured. Therefore, experiments in suspensions were carried out in this study, with the aim to identify whether the C/A ratio of calcium aluminate phases has any influence on the reaction path followed during their hydration.

## 3. Hydration monitoring of suspensions by using conductometry

The hydration of cementitious phases is a general process involving the dissolution of anhydrous phases into the solution and the precipitation of hydrated phases from ions in solution. Monitoring the conductivity of the solution thus provides information on the course of hydration, since it reflects the evolution of the solution composition as a function of time. Indeed, the electrolytic conductivity is in fact the sum of the concentration of ionic species weighted by their specific ionic conductivity.

First, the influence of the w/c ratio on the course of hydration of the studied anhydrous phases was evaluated by monitoring the conductivity of the suspensions.

Different suspensions were elaborated by mixing decarbonated milli-Q water (18.2 MΩ.cm) and anhydrous phases using water/cement ratios ranging from 12.5 to 75. Note that decarbonated milli-Q water was prepared by boiling one liter of milli-Q water for three hours and then bubbling with nitrogen gas down to room temperature. The experiments were performed using a Multicad CDM 210 conductometer (CAD Instruments). The cell was composed of a cylindrically shaped Plexiglas cell (inner radius of 20 mm, total volume of 175 mL) with two annular stainless steel electrodes, which was filled with the solution (see in Figure 43). The cell was thermostated at 25 °C by circulation of cooling water in a double envelope. A specific data acquisition software (Consort Dis Data) was used to collect conductivity measurements every 5 minutes. The conductivity cell was calibrated with a standard 0.1 M KCl solution (1280 µS/cm at 20 °C) at 25 °C before every trial. First, 100 g of decarbonated milli-Q water were introduced in the cell and thermostated at 25 °C. Then, the cement was added to reach the desired water/cement ratio. The suspension was stirred at 500 rpm by using a magnetic bar and quickly covered with Parafilm® to avoid any evaporation.

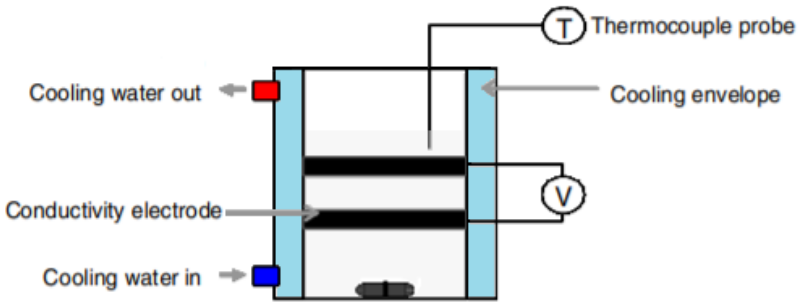


**Figure 43 : Scheme the electrical conductivity cell ($V_{cell}$ = 175 mL).**

Second, the evolution of liquid and solid fractions was characterized as a function of the hydration time for a given w/c ratio by sampling the reacting medium. To perform such a sampling, a suspension reactor with a higher volume than the one previously described was needed. Suspensions were elaborated by mixing 20 g of each anhydrous phase and 500 g of decarbonated milli-Q water, to reach a water/cement ratio of 25. Suspensions were stirred by using a magnetic bar and their temperature was kept constant at 25 °C by using a double wall jacketed reactor. Sampling of suspensions was done at first every minute, then hour, during the first 7 hours after mixing. In this setup, the conductivity of the interstitial solution was also monitored by using a commercial probe (SENTEK conductivity probe operated with a multi-parameter analyzer CONSORT C3010). The experimental scheme is shown in Figure 44.

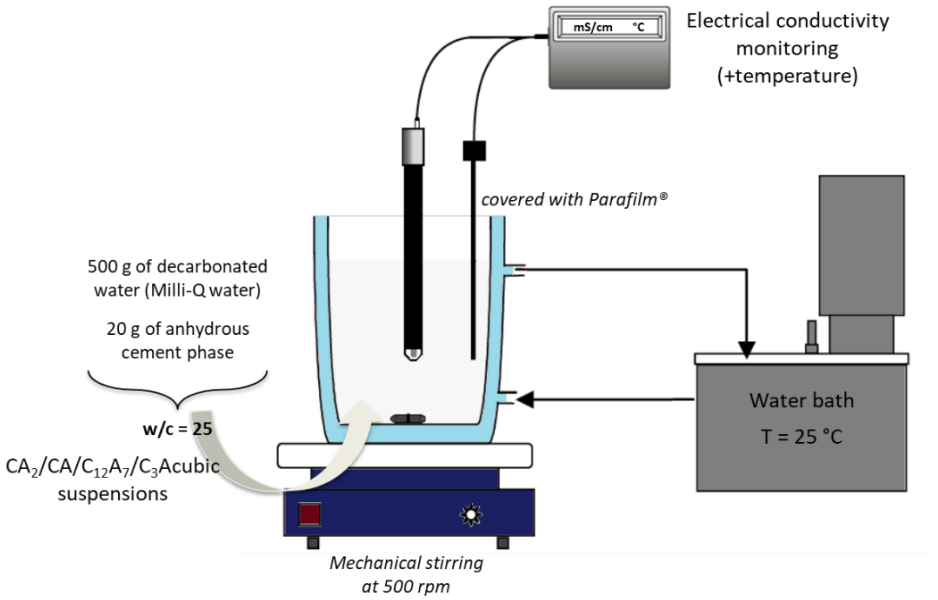


**Figure 44 : Experimental protocol of the hydration monitoring experiments conducted with a water/cement ratio of 25 for 7 hours.**

In Figure 45 , conductivity monitoring for both experimental setup done during the hydration of CA in pure water (w/c = 25) are compared, in order to evaluate if the experimental set up

and/or the sampling has any influence on the course of hydration. For both experimental set-ups, a similar electrical conductivity profile was obtained. Such a result showed that differences in the experimental procedure and sampling did not affect significantly the course of hydration. However, measurements of the electrical conductivity of the suspensions with a volume of 500 mL using the probe method were systematically higher (maximum at 3.23 mS/cm) than those for the 100-mL suspension in the conductivity cell (maximum at 2.96 mS/cm). Such a difference might be due to inaccuracies in the cell calibrations.

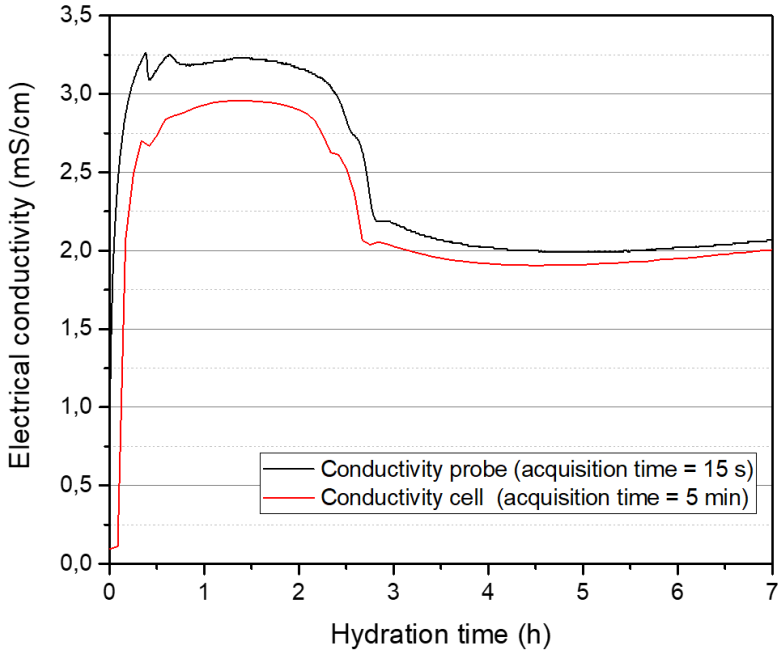


**Figure 45 : Example of monitoring of the early hydration by both conductivity methods. Data from the early hydration monitoring of anhydrous CA phase with a w/c ratio of 25 at 25 °C.**

The liquid and solid fractions of the sampled suspension were then separated by using a polyethersulfone syringe filter (pore size 0.2 µm). The pH and temperature of the collected aqueous fractions were measured immediately after sampling. pH of liquid fractions was measured with a pH electrode calibrated against two IUPAC standard solutions at pH 12.45 (25 °C) and 9.18 (25 °C). Then, the liquid fractions of the suspensions were acidified with 2% (w/w) nitric acid ($HNO_3$) to prevent their carbonation. Analysis by inductively coupled plasma atomic emission spectrometry (ICP-AES) (see Appendix A.6) was performed for quantifying aluminium ($Al^{3+}$) and calcium ($Ca^{2+}$) ions concentration.

The characterization of liquid and solid fractions collected during hydration studies in suspensions and/or pastes is detailed in Appendix A.7.

## 4. Conclusion and summary

In this work, the hydration of four anhydrous aluminate phases is studied. The starting materials were purchased from Mineral Research and were expected to be pure. Mineralogical analysis performed by thermal analysis, XRD and solid-state NMR on all four phases confirmed the purity of these phases from the point of view of the anhydrous phase. However, minor amounts of hydration products were also detected in all raw powders despite the precautions taken to avoid their hydration. The higher the C/A ratio, the higher the amount of hydration products. Such an observation already provided an indication on the reactivity of each of the studied anhydrous phases. In the worst case of $C_3A$, the amount of anhydrous phase was quantified to be around 86 wt. %.

In the following parts of this work, the hydration of these synthetic anhydrous phases is investigated, each phase being the object of one chapter.

In each chapter, each phase is studied under two different conditions.

First, the hydration of pastes elaborated with a w/c ratio ranging from 0.3 to 0.6 was monitored by using isothermal calorimetry and mineralogical assemblages analysis.

Second, the hydration of suspensions elaborated with a w/c ratio ranging from 12.5 to 75.0 was carried out and the composition evolution of the interstitial solution was characterized as a function of time.

In the last chapter of this manuscript, the results obtained for each phases will be recalled and compared, in order to evaluate if similars reaction are followed regardless of the C/A ratio of the anhydrous phase.

## 5. References

[1] K. Irisawa, I. Garcia-Lodeiro, and H. Kinoshita, "Influence of mixing solution on characteristics of calcium aluminate cement modified with sodium polyphosphate," *Cement and Concrete Research*, vol. 128, p. 105951, 2020/02/01/ 2020.

[2] P. Lura, F. Winnefeld, and X. Fang, "A simple method for determining the total amount of physically and chemically bound water of different cements," *Journal of Thermal Analysis and Calorimetry*, vol. 130, no. 2, pp. 653-660, 2017/11/01 2017.

[3] T. Dos Santos *et al.*, "Gluconate action in the hydration of calcium aluminate cements: Theoretical study, processing of aqueous suspensions and hydration reactivation," *Journal of the European Ceramic Society*, vol. 39, no. 8, pp. 2748-2759, 2019/07/01/ 2019.

[4] K. J. D. MacKenzie, J. Temuujin, and K. Okada, "Thermal decomposition of mechanically activated gibbsite," *Thermochimica Acta*, vol. 327, no. 1, pp. 103-108, 1999/03/08/ 1999.

[5] E. Litwinek and D. Madej, "Structure, microstructure and thermal stability characterizations of C3AH6 synthesized from different precursors through hydration," *Journal of Thermal Analysis and Calorimetry*, vol. 139, no. 3, pp. 1693-1706, 2020/02/01 2020.

[6] K. Scrivener, R. Snellings, and B. Lothenbach, *A Practical Guide to Microstructural Analysis of Cementitious Materials*. Boca Raton: CRC Press, Taylor & Francis Group, 2016.

[7] E. E. Chang, A.-C. Chiu, S.-Y. Pan, Y.-H. Chen, C.-S. Tan, and P.-C. Chiang, "Carbonation of basic oxygen furnace slag with metalworking wastewater in a slurry reactor," *International Journal of Greenhouse Gas Control*, vol. 12, pp. 382-389, 2013/01/01/ 2013.

[8] M. R. Nilforoushan and N. Talebiaan, "The hydration products of a refractory calcium aluminate cement at low temperatures," (in English), *Iranian Journal of Chemistry and Chemical Engineering (IJCCE)*, Article vol. 26, no. 2, pp. 71-76, 2007.

[9] P. T. Durdziński, "Hydration of multi-component cements containing cement clinker, slag, calcareous fly ash and limestone," PhD, Faculté Sciences et Techniques de l'Ingénieur, EPFL, Suisse, 6834, 2016.

[10] V. S. Ramachandran, R. M. Paroli, J. J. Beaudoin, and A. H. Delgado, "10 - Non-Portland Rapid Setting Cements," in *Handbook of Thermal Analysis of Construction Materials*, V. S. Ramachandran, R. M. Paroli, J. J. Beaudoin, and A. H. Delgado, Eds. Norwich, NY: William Andrew Publishing, 2002, pp. 403-448.

[11] D. Massiot *et al.*, "Modelling one- and two-dimensional solid-state NMR spectra," *Magnetic Resonance in Chemistry*, https://doi.org/10.1002/mrc.984 vol. 40, no. 1, pp. 70-76, 2002/01/01 2002.

[12] D. Massiot, C. Bessada, J. P. Coutures, and F. Taulelle, "A quantitative study of 27Al MAS NMR in crystalline YAG," *Journal of Magnetic Resonance (1969)*, vol. 90, no. 2, pp. 231-242, 1990/11/01/ 1990.

[13] J. H. Skibsted, E.; Jakobsen, H.J., "Characterization of Calcium Aluminate Phases in Cements by 27Al MAS NMR Spectroscopy," *Inorg. Chem.*, vol. 32, pp. 1013-1027, 1993.

[14] J. M. Rivas Mercury, P. Pena, A. H. De Aza, X. Turrillas, I. Sobrados, and J. Sanz, "Solid-state 27Al and 29Si NMR investigations on Si-substituted hydrogarnets," *Acta Materialia,* vol. 55, no. 4, pp. 1183-1191, 2007/02/01/ 2007.

[15] P. Faucon, T. Charpentier, D. Bertrandie, A. Nonat, J. Virlet, and J. C. Petit, "Characterization of Calcium Aluminate Hydrates and Related Hydrates of Cement Pastes by 27Al MQ-MAS NMR," *Inorganic Chemistry,* vol. 37, no. 15, pp. 3726-3733, 1998/07/01 1998.

[16] J. J. F. Faucon P., Adenot F., Gautier N., Massiot D., Virlet J. , *$^{27}$Al MAS NMR Study on Cement Paste Degradation by Water* (Nuclear Magnetic Resonance Spectroscopy of Cement-Based Materials). Springer, Berlin, Heidelber, 1998.

[17] W. Gessner, D. Müller, H.-J. Behrens, and G. Scheler, "Zur Koordination des Aluminiums in den Calciumaluminathydraten $2CaO{\cdot}Al_2O_3{\cdot}8H_2O$ und $CaO{\cdot}Al_2O_3{\cdot}10H_2O$," *Zeitschrift für anorganische und allgemeine Chemie,* https://doi.org/10.1002/zaac.19824860122 vol. 486, no. 1, pp. 193-199, 1982/03/01 1982.

[18] P. Padilla-Encinas, A. Palomo, M. T. Blanco-Varela, and A. Fernández-Jiménez, "Calcium sulfoaluminate clinker hydration at different alkali concentrations," *Cement and Concrete Research,* vol. 138, p. 106251, 2020/12/01/ 2020.

[19] B. Walkley and J. L. Provis, "Solid-state nuclear magnetic resonance spectroscopy of cements," *Materials Today Advances,* vol. 1, p. 100007, 2019/03/01/ 2019.

[20] M. D. Andersen, H. J. Jakobsen, and J. Skibsted, "A new aluminium-hydrate species in hydrated Portland cements characterized by 27Al and 29Si MAS NMR spectroscopy," *Cement and Concrete Research,* vol. 36, no. 1, pp. 3-17, 2006/01/01/ 2006.

[21] Y. Zhang and J. Chang, "Microstructural evolution of aluminum hydroxide gel during the hydration of calcium sulfoaluminate under different alkali concentrations," *Construction and Building Materials,* vol. 180, pp. 655-664, 2018/08/20/ 2018.

[22] P. Pena, J. M. Rivas Mercury, A. H. de Aza, X. Turrillas, I. Sobrados, and J. Sanz, "Solid-state 27Al and 29Si NMR characterization of hydrates formed in calcium aluminate–silica fume mixtures," *Journal of Solid State Chemistry,* vol. 181, no. 8, pp. 1744-1752, 2008/08/01/ 2008.

[23] J.-B. d'Espinose de Lacaillerie, C. Fretigny, and D. Massiot, "MAS NMR spectra of quadrupolar nuclei in disordered solids: The Czjzek model," *Journal of Magnetic Resonance,* vol. 192, no. 2, pp. 244-251, 2008/06/01/ 2008.

# Chapter 3: Investigation of pure $CA_2$ hydration at early age

# **Chapitre 3** : Étude de l'hydratation au jeune âge de $CA_2$ pur

**Résumé:** Ce chapitre est dédié à l'étude de l'hydratation au jeune âge de $CA_2$ pur à 25°C. Dans un premier temps, la vitesse d'hydratation des pâtes de $CA_2$ avec différents rapports massiques eau/ciment (e/c) a été étudiée par calorimétrie isotherme. Il a été observé que plus le rapport e/c est élevé, plus la chaleur libérée est importante. Les pâtes résultantes ont ensuite été caractérisées afin de définir leurs assemblages minéralogiques 7 jours après le mélange. Une estimation du degré d'hydratation en fonction du temps a été faite en supposant que la dissolution de $CA_2$ contribue principalement à la libération de chaleur. Cette hypothèse s'est avérée cohérente par rapport aux assemblages minéralogiques quantifiés par RMN. Du point de vue des hydrates et pour une pâte élaborée avec un rapport e/c de 0.5, l'assemblage minéralogique est composé majoritairement d'hydroxyde d'aluminium et de phases métastables (20% en masse). La vitesse d'hydratation s'est avérée faible sur environ 80 heures. Enfin, la dissolution d'environ 75 % du $CA_2$ a été obtenue après 7 jours d'hydratation. Dans un second temps, l'étude de l'hydratation par conductimétrie a été menée en suspension diluée avec un rapport massique e/c fixé à 25 à 25°C. L'évolution de la composition de la solution interstitielle et de la minéralogie a été étudiée en fonction du temps, ce qui a permis de définir trois étapes principales au cours de l'hydratation. Les résultats obtenus au cours de la première étape suggèrent que le taux d'hydratation du $CA_2$ est d'abord limité par la précipitation des hydrates, la limite de solubilité de $CA_2$ étant rapidement atteinte en solution. Le déclenchement de la deuxième étape pourrait être lié à la précipitation d'une phase d'hydroxyde d'aluminium. Concernant la troisième étape, la dissolution du $CA_2$ et la précipitation de l'hydroxyde d'aluminium sont supposées comme étant des étapes limitantes, au contraire de la précipitation du $C_2AH_x$.

# Introduction

So far, the hydration of $CA_2$ has not been investigated as deeply as the one of other calcium aluminate phases such as CA or $C_3A$ because of its very slow hydration kinetics within the first 2 days. $CA_2$ is even assumed in some studies to be a non reactive material over long periods of times [1]. Negro et al. [2] have shown that, after several hours, a very low hydration degree was reached in comparison to CA due to the lower solubility of $CA_2$. The hydration reactions of $CA_2$ were found out to be slow at ambient temperature, but they accelerated when the temperature increased up to 40 °C [3]. Despite the low hydraulic property of $CA_2$ as compared to the other CAC phases, Klaus [4] demonstrated the significant influence of $CA_2$ during the course of CAC hydration based on calculated and measured heat flow results. Furthermore, it was reported that the first hydrate formed during the hydration of $CA_2$ at ambient temperature is aluminium hydroxide $AH_3$. As the hydration degree increases, so does the concentration of calcium ions leading to the precipitation of metastable $C_2AH_8$ [1]. Nevertheless, the need for further research was highlighted to better understand the $CA_2$ hydration process and in particular the influence of precipitation or crystallinity of their hydration products ($AH_3$ especially) [5]. The hydration products of $CA_2$ phase are described in details in the Literature review of this manuscript (Chapter 1, section 2.3).

This third chapter is dedicated to the study of $CA_2$ hydration and is divided into two sections.

In the first section, the study is focused on the hydration of $CA_2$ pastes at 25 °C. The hydration rate of $CA_2$ pastes was studied by isothermal microcalorimetry. The influence of the w/c ratio on the course of $CA_2$ hydration was investigated. The resulting pastes were then characterized in order to define their mineralogical assemblages 7 days after mixing.

In the second section, the hydration of $CA_2$ was investigated in diluted media at 25 °C. For a given w/c ratio of 25, the evolution of the solution composition and of the mineralogy was studied as a function of time.

In summary, the objectives of the study are to:

- evaluate the influence of the w/c ratio on heat release during hydration;
- characterize the hydration products and mineralogical assemblages 7 days after mixing as a function of the w/c ratio;
- estimate an hydration degree of $CA_2$ based on mineralogical analysis and calorimetric measurements;
- characterize the composition evolution of the interstitial solution as a function of time under diluted conditions.

The following chapters, Chapter 4, 5 and 6, have the same objectives but addressing different anhydrous calcium aluminate phases. The same procedures were applied in all those chapters.

# 1. Hydration study of $CA_2$ pastes at early age

## 1.1. Investigation of the influence of the w/c ratio on the early age hydration of $CA_2$ pastes

### 1.1.1. Heat flow monitoring

The influence of a w/c ratio ranging from 0.40 to 0.60 on the early age hydration of calcium dialuminate $CA_2$ was monitored during 7 days by isothermal calorimetry at 25 °C. These pastes were prepared with ex-situ mixing and thus introduced into the calorimeter prior to mixing. All the curves were normalized with respect to the initial weight of synthetic anhydrous phase ($CA_2$) in the paste. The heat flow profiles are reported in Figure 46. A more detailed view of the first 24 hours of hydration is given on the right of the figure.

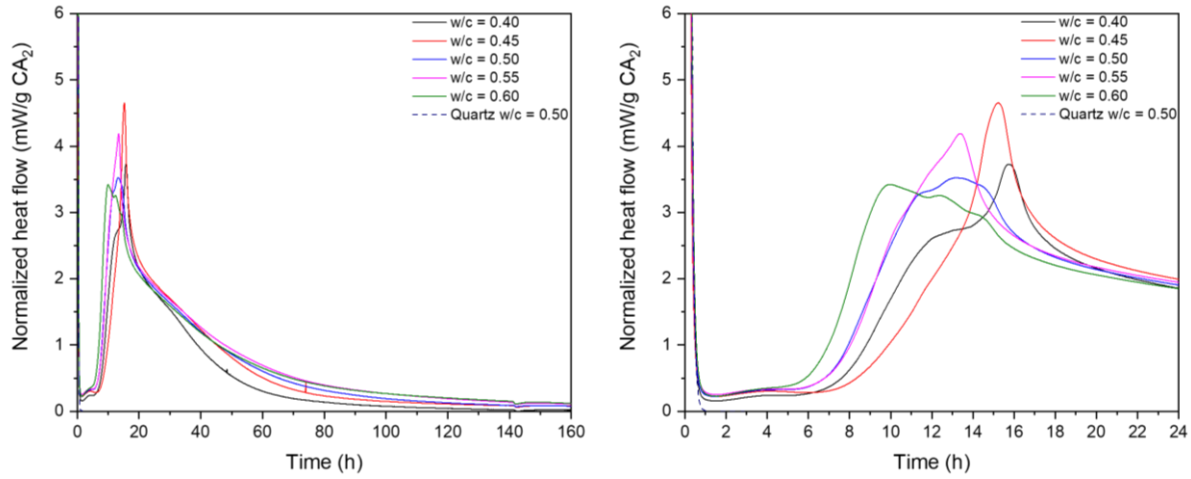


**Figure 46 : Heat flow measurements on pure $CA_2$ pastes with different w/c ratios at 25 °C for 7 days of hydration. On the right, zoom on the first 24 hours of hydration.**

Heat flow profiles observed during $CA_2$ hydration could be divided into three main periods.

After the introduction of the sample into the calorimeter, the first period was characterized by a small heat release during the first six hours after mixing, whatever the w/c ratio.

A second period was characterized by an increase in the heat flow that expressed an acceleration of $CA_2$ hydration. The increase in the w/c ratio from 0.40 up to 0.60 led to a decrease in the maximum measured heat flow, from 5.0 down to 3.4 mW/g but in a non-monotonic way. Moreover, the time corresponding to the maximum measured heat flow varied between 16 h and 10 h independently of the studied w/c ratios. The low hydraulic activity of $CA_2$ makes the hydration process slower compared to other calcium aluminate phases [6]. The non-monotonous variation of the maximum measured heat flow with the increase in the w/c ratio from 0.40 up to 0.60 could be explained by the low hydraulic activity of $CA_2$ influencing directly the rate of the hydration process [6]. Slow continuing hydration reactions would in first analysis result in a gradually evolving acceleration period. However, the potential formation of

different precipitated phases with different precipitation kinetics might occur, resulting in fine complex details that are apparent because of to the extended reaction time.

The third period was characterized on heat flow profiles by a decrease in the measured heat flow, and corresponded to the deceleration of $CA_2$ hydration. During this period, the heat flow released by the samples continuously decreased down to the baseline. However, the heat flows were still producing very low heat values of about 0.1 mW/g for a very long time and for all of the pastes except the one prepared with the lowest w/c ratio (0.40). To this exception, this proved that hydration was still ongoing 7 days after mixing.

The cumulative heat evolution, expressed in J/g related to the weight of anhydrous phase ($CA_2$), over the first week of hydration is shown in Figure 47. As described in the previous chapter, integration of $CA_2$ heat flow profiles was carried out with a good confidence since a low amount of heat is released during the first 30 minutes after ex-situ mixing.

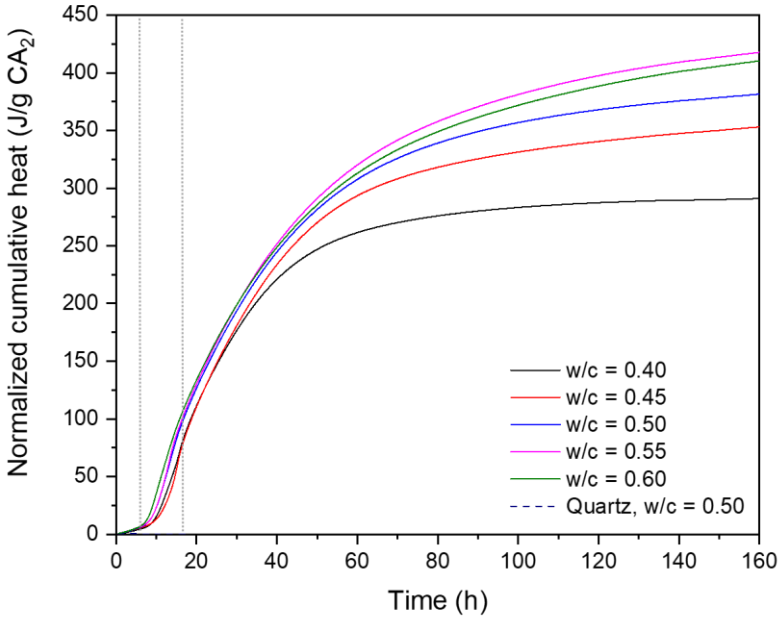


**Figure 47 : Normalized cumulative heat of $CA_2$ pastes prepared with different w/c ratios during seven days of hydration at 25 °C.**

The same three periods as those described previously could be identified on the cumulative heat plots. Furthermore, the cumulative heat released at seven days was strongly affected by the w/c ratio: increased with the w/c ratio.

In Figure 48, the heat released after 7 days of hydration is plotted as a function of the w/c ratio. It increased with the w/c ratio in the range [0.40; 0.55] and seemed to level off at 420 J/g for higher w/c values.

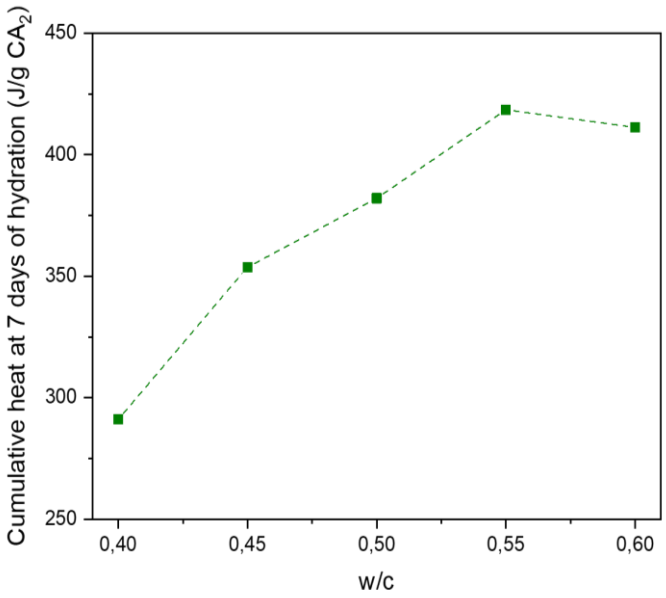


**Figure 48 : Cumulative heat values measured after 7 days of $CA_2$ hydration as a function of w/c ratio (at 25 °C).**

Two kinds of information can be derived from these calorimetric analyses.

First, using similar calorimetric data, Lura *et al.* developed a simple approach to assess the water demand of a cementitious anhydrous material. In their approach, the water demand is defined as the minimum w/c ratio leading to the highest hydration degree of the considered anhydrous cementitious phase. Such a water demand is then estimated by evaluating the critical w/c ratio leading to a break or a plateau in the graph plotting the cumulative heat as a function of the w/c ratio [7]. The reliability of this approach was established for Portland cement pastes, CAC pastes and CSA pastes [7, 8]. From Figure 48, the water demand as defined previously is evaluated to be close to 0.55.

Then, a hydration degree of $CA_2$ can be evaluated at first order by formulating a rough hypothesis. By assuming that only the dissolution of $CA_2$ contributes to the heat release (reaction equation (10), and thus neglecting the heat that could be released by hydrated phases precipitation), a hydration degree of $CA_2$ can be estimated by normalizing the cumulative heat Q by the $CA_2$ dissolution enthalpy $\Delta_{diss}H$ as described by equation (10).

$$CA_2 + 2\,OH^- + 7\,H_2O \rightleftharpoons Ca^{2+} + 4\,Al(OH)_4^- \qquad \Delta_{diss}H = -309.8\ J/g \qquad (10)$$

When only the dissolution of anhydrous $CA_2$ was considered to be contributing to the heat release, hydration degrees exceeding 100 % were obtained. Therefore, the enthalpy of reaction ($\Delta_rH$) of $CA_2$ as reported by Klaus *et al.* was applied to estimate the hydration degree in this section. Indeed, Klaus *et al.* calculated an enthalpy of reaction by assuming a simultaneous

hydration of the anhydrous $CA_2$ and precipitation of hydrates. The resulting $\Delta_r H$ for the hydration of $CA_2$ was found to be equal to -498 J/g [9, 10].

In Figure 49, the cumulative heat of Figure 48 is replotted following the approach normalizing the cumulative heat Q by the $CA_2$ reaction enthalpy in terms of hydration degree. It shows that increasing the w/c ratio from 0.50 to 0.60 raised the hydration degree of $CA_2$ 7 days after mixing from 50 % up to 80 %.

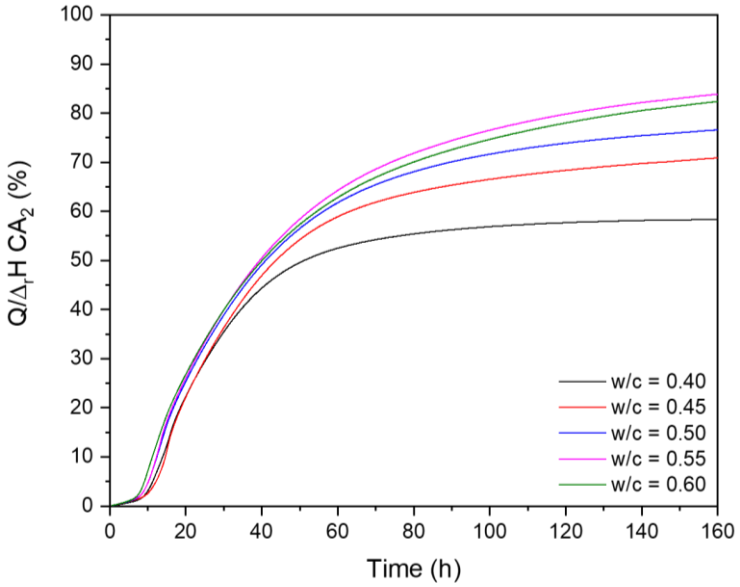


**Figure 49 : Influence of the w/c ratio on the degree of hydration of the pastes, assuming that the heat release is due to the dissolution of anhydrous $CA_2$ and precipitation of hydrates – 25 °C.**

To complement these results based on calorimetry, mineralogical assemblages of pastes were characterized 7 days after mixing by using TGA and XRD in order to quantify the amount of bound water and identify the crystalline phases in presence. The mineralogical composition of a sample elaborated with a w/c ratio of 0.50 was further investigated by $^{27}Al$ solid-state NMR spectroscopy.

### 1.1.2. Influence of w/c ratio on mineralogical assemblages after 7 days of hydration

In the studied system, the linear relationship between the cumulative heat released at 7 days and the w/c ratio suggested that a similar mechanism drew the $CA_2$ dissolution at all w/c ratios. It was thus important to verify if the same mineralogical assemblage precipitated in all cases, as already reported by Klaus S.R. *et al.* [10]. Further characterization by using XRD analysis was carried out for that purpose.

Figure 50 shows the powder XRD patterns of the $CA_2$ pastes hydrated at 25 °C for 7 days. The qualitative comparison of the peak areas suggests that the amount of hydrates increased with

the w/c ratio. Moreover, in all samples, unreacted $CA_2$ was detected. The PDF used to identified the phases have been listed in Appendix A.7.

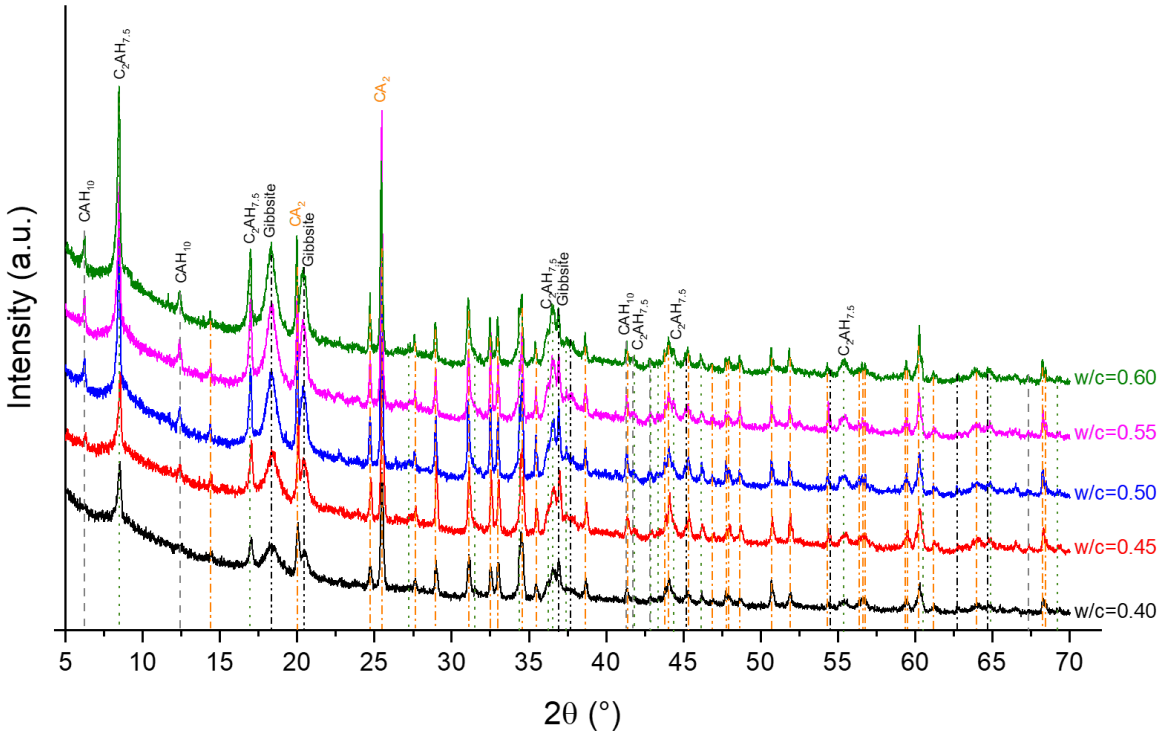


**Figure 50 : XRD patterns representing hydration products after hydrating $CA_2$ with w/c ratios ranging from 0.4 to 0.6 at 25 °C for 7 days.**

First of all, the XRD results showed the presence of $CAH_{10}$, $C_2AH_{7.5}$ (partially dehydrated form of $C_2AH_8$) and aluminium hydroxide. The reflection located at 18.3° 2θ showed that gibbsite precipitated in all the systems. However, it seems that the width of this peak decreased as the w/c ratio increased. This could suggest an increased crystallinity of the aluminium hydroxide polymorph under formation.

The pastes prepared with different w/c ratios were also analyzed by thermogravimetry in order to quantify the bound water content 7 days after initial mixing. Figure 51 shows the resulting the TGA and DTG curves.

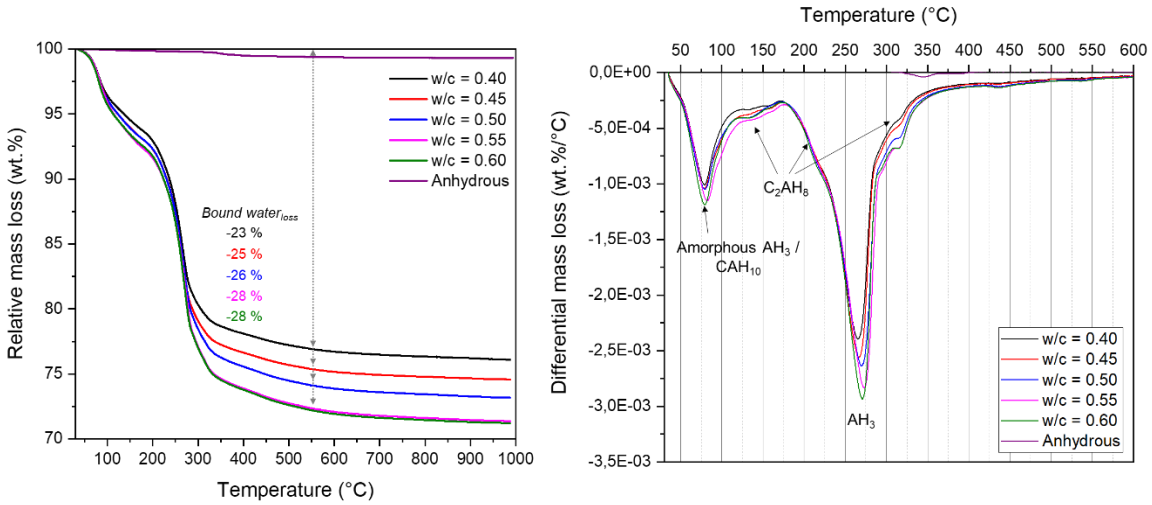


**Figure 51 : TGA and DTG curves obtained from hydrated $CA_2$ pastes with different w/c ratios at 25 °C for 7 days. On the TGA curves, the arrow shows the mass loss in the range of temperatures between 25 and 550 °C.**

The thermal events can be interpreted as follows:

- Close to 100 °C: decomposition of metastable $CAH_{10}$ and/or amorphous aluminium hydrates [11-15],
- Between 110 and 170 and then at 300 °C: decomposition of metastable $C_2AH_8$ proceeding in three main steps [16, 17] ; $C_2AH_8$ is also responsible for the shoulder at 230 °C on the left side of the peak corresponding to dehydration of $AH_3$ [13],
- Close to 250 °C: a main DTG peak related to the decomposition of $AH_3$ [7, 13, 18].

Due to peak overlaps, phase quantification using TGA is a hard task. However, since the weight losses are solely due to water departure, it is possible to assess the total amount of bound water. This parameter is plotted as a function of the w/c ratio in Figure 52. A linear relationship is observed between the measured bound water and the w/c ratio up to 0.55. The fraction of bound water then tended to stabilize at 27.5 wt. % for w/c ratios ranging from 0.55 to 0.60.

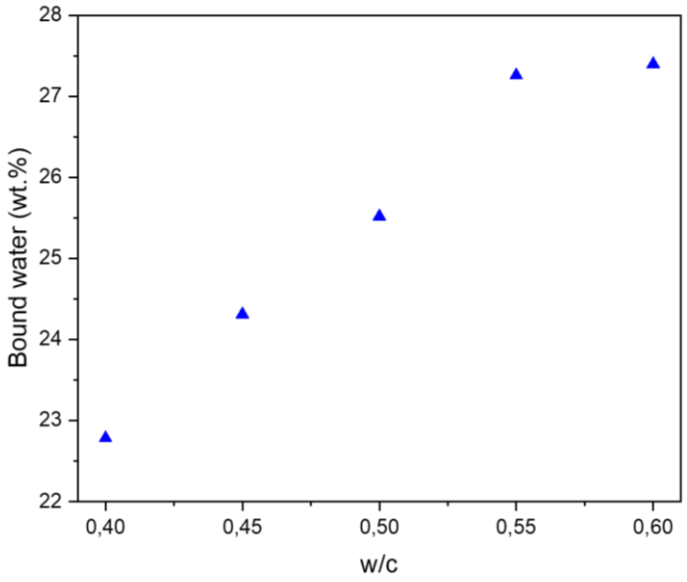


**Figure 52 : Bound water amount of $CA_2$ pastes with different w/c ratios hydrated at 25 °C for 7 days.**

This result was consistent with the calorimetry results (Figure 48). Consequently, the bound water contents after 7 days of hydration, obtained by TGA, were plotted as a function of the cumulative heat and the estimated hydration degree, obtained by calorimetry (Figure 53). A clear linear relationship is observed. This correlation highlights the influence of the initial w/c ratio on the hydration degree reached after 7 days.

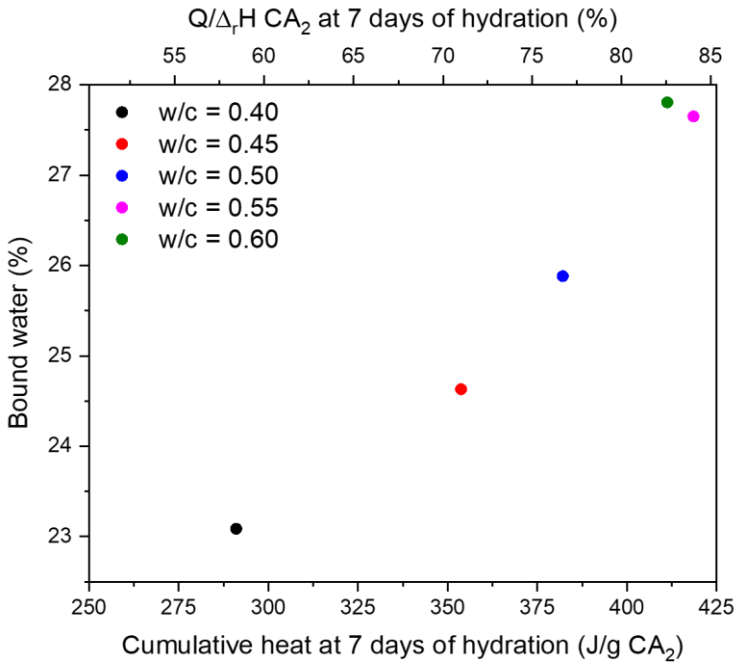


**Figure 53 : Bound water content of $CA_2$ pastes from TGA results as a function of maximum cumulative heat values after reaching a plateau.**

Following TGA and powder XRD analysis, $^{27}$Al MAS-NMR spectrometry was performed on a 7 day-old $CA_2$ sample prepared with a w/c ratio of 0.50 in order to determine as quantitatively as possible its mineralogical composition. The collected spectrum (Figure 54) and its decomposition are shown in Figure 55.

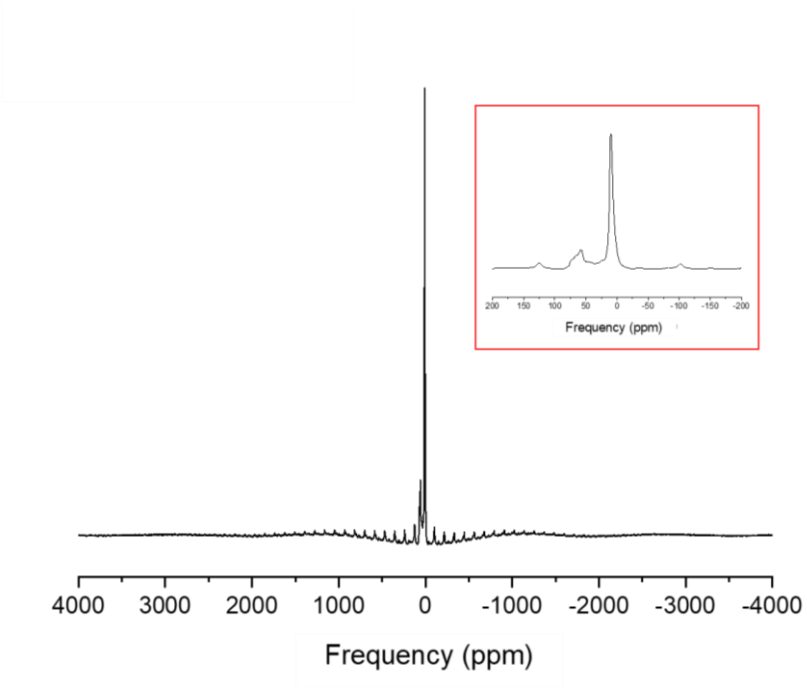


**Figure 54 : $^{27}$Al MAS NMR spectrum of the 7 d-old $CA_2$ paste (w/c = 0.5).**

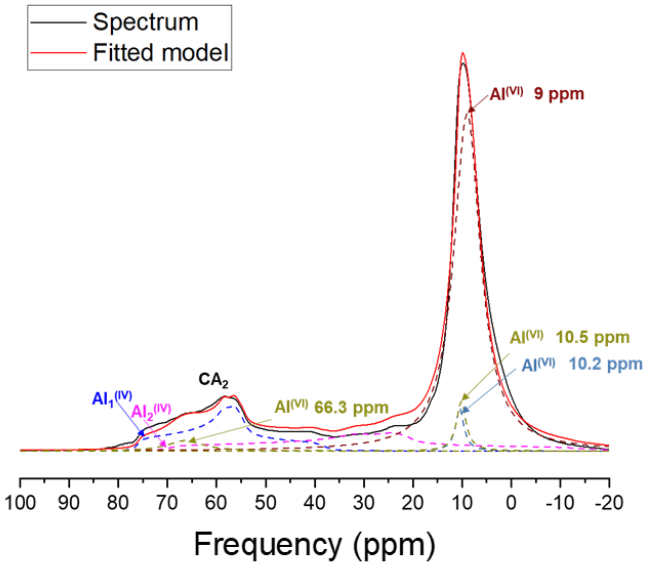


**Figure 55 : Decomposition of the $^{27}$Al MAS-NMR spectrum central bands of the 7 d-old $CA_2$ paste (w/c = 0.5).**

According to the literature, the two tetrahedral Al sites in $CA_2$ resonate with equal weight at 76 ppm for $Al_1^{(IV)}$ and 70 ppm for $Al_2^{(IV)}$ [19]. The fitted model resulting from these two sites is in agreement with the experimental spectrum and the quadrupolar parameters attributed to $CA_2$ (see Chapter 2, Figure 39a and Table 10). Additional resonances in the octahedral range were also observed and assigned to the hydrates. From the decomposition of the $^{27}$Al MAS-NMR

spectrum of the 7 d-old $CA_2$ paste (w/c = 0.5), the following hydrates were identified with the data obtained from literature as summarized in Table 13:

- $CAH_{10}$
- $C_2AH_8$
- $AH_3$

The fitted model (Figure 55) comprised four peaks assigned to:

- $CAH_{10}$ ($\delta$ = 10.2 ppm),
- $C_2AH_8$ (sharp peak at 10.3 ppm and broader peak at 66 ppm),
- Gibbsite (peak at 9 ppm corresponding to the octahedrally coordinated Al site).

**Table 13 : Summary of chemical shifts, intensities and quadrupolar parameters corresponding to the identified hydrates from the decomposition of the $^{27}$Al MAS-NMR spectrum of the 7 d-old $CA_2$ paste (w/c = 0.5).**

| Phase | Site | $\delta_{iso}$ (ppm) | Model | Peak intensity | Quadrupole coupling constant, $C_Q$ (MHz) | Asymmetry parameter, $\eta$ | Width | Reference |
|---|---|---|---|---|---|---|---|---|
| $CA_2$ | $Al_1^{(IV)}$ | 76 | Q mas 1/2 | 5500 | 6.25 | 0.88 | - | [19] |
| | $Al_2^{(IV)}$ | 70 | Q mas 1/2 | 2300 | 9.55 | 0.82 | - | |
| $CAH_{10}$ | $Al^{(VI)}$ | 10.2 | Lorentzian | 2822 | - | - | 2.3 | [19] |
| $C_2AH_8$ | $Al^{(IV)}$ | 10.5 | Lorentzian | 2450 | - | - | 2.02 | [16, 20, 21] |
| | $Al^{(VI)}$ | 66.5 | Lorentzian | 600 | - | - | 8.5 | |
| $AH_3$ | $Al^{(VI)}$ | 9 | Lorentzian | 19130 | - | - | 6.6 | [22-24] |

The choice of Lorentzian lineshapes for the hydrates rather than Gaussians or residual quadrupolar lineshapes can be disputed on theoretical grounds but was deemed empirically reasonable for quantitative purposes considering that the lines were unresolved and featureless.

Such a decomposition of the spectrum yields the mineralogical composition described in Table 14.

**Table 14 : Quantification of Al-containing phases in the 7 d-old $CA_2$ paste (w/c = 0.5).**

| Phase | Chemical shift (ppm) | Al atomic fraction (%) | Phase weight fraction (wt. %) | Corresponding bound water content (wt. %) |
|---|---|---|---|---|
| $CA_2$ | 76 / 70 | 28.5 | 22 | - |
| $AH_3$ | 9 | 63 | 60 | 21 |
| $CAH_{10}$ | 10.2 | 3.4 | 7 | 4 |
| $C_2AH_8$ | 10.5 / 66.3 | 5.1 | 11 | 4 |

The results obtained from the decomposition of the NMR spectrum indicated a residual amount of $CA_2$ equal to 22 wt. %. By defining the hydration as the amount of reacted anhydrous phases, a hydration degree of 71.5 % would thus have been achieved 7 days after mixing pure water and $CA_2$ for this w/c ratio and keeping the temperature at 25 °C. It has to be noted that such a value is close to the 75 % hydration degree estimated by using calorimetry. The consistency of these results supported the hypothesis consisting in neglecting the contribution of hydrates precipitation in the total heat released during $CA_2$ hydration. Moreover, still by using the mineralogical composition inferred from the $^{27}$Al NMR spectrum decomposition, the calculated total bound water content was equal to 29 wt. % whereas bound water content was measured to be equal to 25.7 wt. % by TGA in this sample (Figure 52).

However and despite the whole consistency of the results obtained and presented in the above section, the mineralogical assemblage estimated by using $^{27}$Al NMR spectrum could be seen as surprising. First, the theoretical fraction of $AH_3$ expected by the stoichiometry of equations (11) and (12) was calculated by taking into account the Al molar fractions of $CAH_{10}$ and $C_2AH_8$ measured from the NMR results as reported in Table 14. The led to an expected molar fraction of $AH_3$ (18 %) much smaller than the actually measured one (63 %). These equations thus do not seem well adapted to describe the hydration process at early age.

$$CA_2 + 13\,H \rightleftharpoons CAH_{10} + AH_3 \tag{11}$$

$$2\,CA_2 + 17\,H \rightleftharpoons C_2AH_8 + 3\,AH_3 \tag{12}$$

Similarly, this stoichiometric approach can be applied to the Ca molar fractions. From the NMR results, 71.5 % of anhydrous $CA_2$ was found to have reacted 7 days after hydration, *i.e.* 71.5 % of the initially available Ca had reacted. However, the quantity of Ca embedded in the measured quantities of $CAH_{10}$ and $C_2AH_8$ was only 13.6 %. Such a difference between the Ca molar fraction obtained from the stoichiometric calculations and the one measured from NMR results

indicated that there was a significant missing amount of Ca in the solid fraction of 7 d-old $CA_2$ paste as seen by $^{27}Al$ NMR. This can be interpreted in two ways. First such a difference could arise from the presence of Ca bearing but Al exempt phases such as portlandite CH and/or calcite CČ. However, these two latter phases were not observed neither by XRD nor by TGA. Therefore, this brought us to the second explanation. Despite the fact that quantification of the hydrates by NMR led to a reasonable amount of bound water, it underestimated the amount of Ca and overestimated the amount of Al in the hydrates. This meant that the decomposition underestimated the amount of calcium aluminium hydrates in favour of $AH_3$. This is clearly the limit of trying to decompose unresolved resonance lines with width (2-8 ppm) exceeding their frequency shift difference (about 1 ppm).

Further studies were thus clearly needed to better understand the relative role of the hydrates in the overall hydration process. This is addressed in the following section by focussing on solution chemistry.

**To sum up:**

From TGA, XRD and NMR results, it was concluded that after 7 days of hydration at 25°C, the mineralogical assemblage was mainly composed of $CA_2$ and $AH_3$, with the presence of smaller amounts of metastable calcium aluminate hydrates $CAH_{10}$ and $C_2AH_8$ (respectively $C_2AH_{7.5}$ for XRD analysis).

The $CA_2$ hydration degrees estimated by using calorimetric data were consistent with the mineralogical composition obtained by NMR and the bound water obtained by TGA. $CA_2$ reacts slowly, in agreement with literature, since the acceleration period started after 6 to 10 hours depending on the w/c ratio, and the hydration was still in progress 7 days after mixing. However, quite a high hydration degree, ranging from 50 % to 85 %, was achieved during the first 7 days of hydration. For w/c ratio up to 0.55, the hydration degree increased with the w/c ratio before levelling off. Thus, this ratio of 0.55 was interpreted as corresponding to the hydraulic water demand of this synthetic anhydrous phase.

From the comparison between the theoretical amount of calcium and aluminium calculated by the stoichiometry of hydration reactions and the one measured by $^{27}Al$ NMR resulted in significant differences. That confirmed the interest in determining the solution composition and the hydration pathway followed on the course of $CA_2$ hydration at 25 °C.

## 2. Hydration study of $CA_2$ suspensions at early age

Studying hydration in diluted conditions allows to sample the reacting medium and to collect the liquid fraction more easily than in paste conditions. However, the main drawback lies in the fact that an increase in the w/c ratio might disturb the hydration if the system becomes undersaturated with respect to some hydrates which thus do not precipitate anymore. As a first step, the influence of an increase in the w/c ratio from 12.5 up to 75.0 on the hydration progress and on mineralogical assemblage was thus evaluated. Then, the composition evolution of the interstitial solution was measured as a function of time for a w/c ratio of 25.

### 2.1 Influence of the w/c ratio on the early age hydration of $CA_2$ elaborated in suspensions

#### 2.1.1. Electrical conductivity monitoring

Suspensions containing $CA_2$ phase were prepared with decarbonated Milli-Q water (18.2 MΩcm) using different w/c ratios, namely, 12.5, 25, 50 and 75. The evolution of the electrical conductivity of the suspensions at 25 °C is shown as a function of time in Figure 56. Measurements were performed every 5 min.

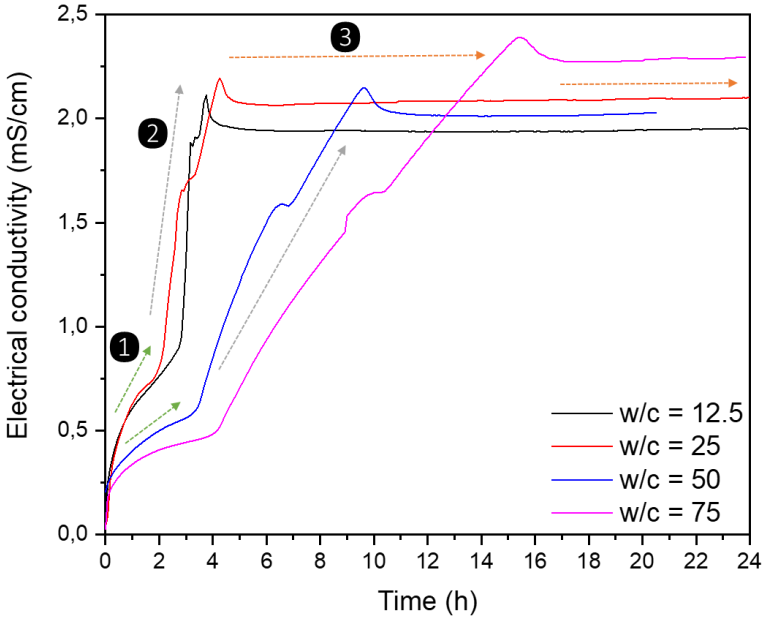


**Figure 56 : Electrical conductivity monitoring of $CA_2$ suspensions prepared with different w/c ratios at 25 °C. The arrows show the assigned periods (1st period: green, 2nd period: grey and 3rd period: orange).**

Electrical conductivity profiles can be divided into three main periods as for heat flow profiles. During the first period, the conductivity increased instantaneously, as soon as the $CA_2$ anhydrous phase was in contact with pure water. A second period was then observed,

characterized by a sharp increase in the conductivity up to a maximum. The third period was characterized by a conductivity decrease down to a plateau. Characteristic times and conductivity values corresponding to these three periods are summarized in Table 15.

**Table 15 : Characteristic parameters of the electrical conductivity curves recorded on $CA_2$ suspensions with variable w/c ratios.**

| Water-to-solid ratio | Time to reach the maximum conductivity value (h) | Maximum conductivity value (mS/cm) | Time to reach the plateau (h) | Conductivity value at the end of the experiment (mS/cm) |
|---|---|---|---|---|
| **12.5** | 3.8 | 2.11 | 5.0 | 1.95 |
| **25** | 4.3 | 2.19 | 5.6 | 2.10 |
| **50** | 9.6 | 2.15 | 11.5 | 2.03 |
| **75** | 15.5 | 2.39 | 17.0 | 2.29 |

Broadly speaking, the higher the w/c ratio, the slower the conductivity increase. The maximum conductivity value of the studied suspensions shifted to longer hydration times as the w/c ratios increased from 12.5 to 75. Such a behaviour could be explained by the fact that higher amounts of anhydrous phase had to be dissolved to reach a saturation index that might enable hydrates precipitation. Regardless, conductivity profiles were similar whatever the w/c ratio, suggesting that the hydration progress was also similar. A characterization of the mineralogical assemblages was needed to support this hypothesis.

### 2.1.2. Characterization of the solid fraction of suspensions

According to the XRD patterns of the solid fractions of suspensions hydrated for 24 h at 25 °C, the following mineralogical phases were identified (Figure 57) regardless of the w/c ratio:

- $C_2AH_{7.5-8}$,
- $C_4AČH_{11}$,
- $AH_3$ indexed by using Gibbsite reflections
- unreacted $CA_2$.

The mineralogical assemblage was thus not qualitatively modified by a variation in the w/c ratio. However, the crystallinity of the aluminium hydroxide formed seemed to be affected since the width of its main diffraction peak decreased when the w/c ratio increased. The XRD pattern suggested the presence of $C_2AH_8$ (main reflections at 8.2 ° 2θ and 24.7 ° 2θ), but also of its partly dehydrated form $C_2AH_{7.5}$ (8.5 ° 2θ and 25.6 ° 2θ). In the literature, it was reported that $C_2AH_8$ can undergo- partial depletion to form $C_2AH_{7.5}$ or $C_2AH_{8-x}$ within a few hours of

hydration [25]. Asterisk symbols are used in Figure 57 to point out the peaks that can be assigned to a $C_2AH_x$-type phase.

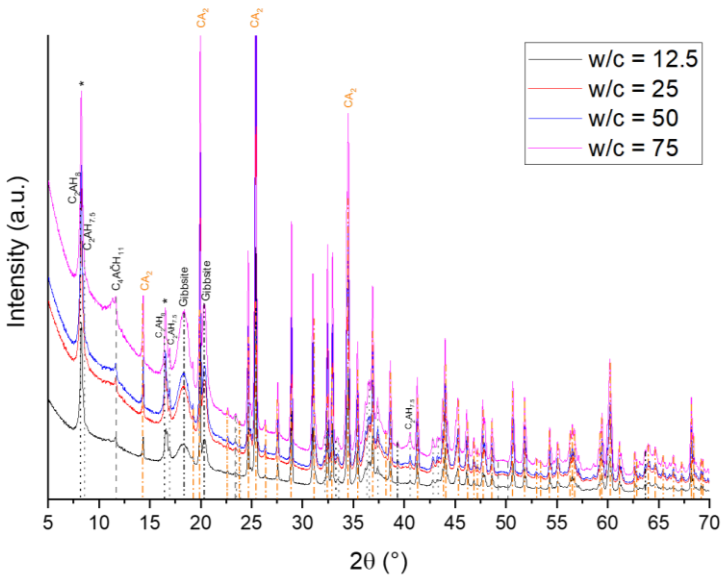


**Figure 57 : XRD patterns representing mineralogical assemblages of $CA_2$ suspensions after 24 hours of hydration at 25 °C.**

The thermal decomposition of the solid fractions collected and characterized by TGA occurred in several steps as already described in Table 16. Thermograms are presented in Figure 58.

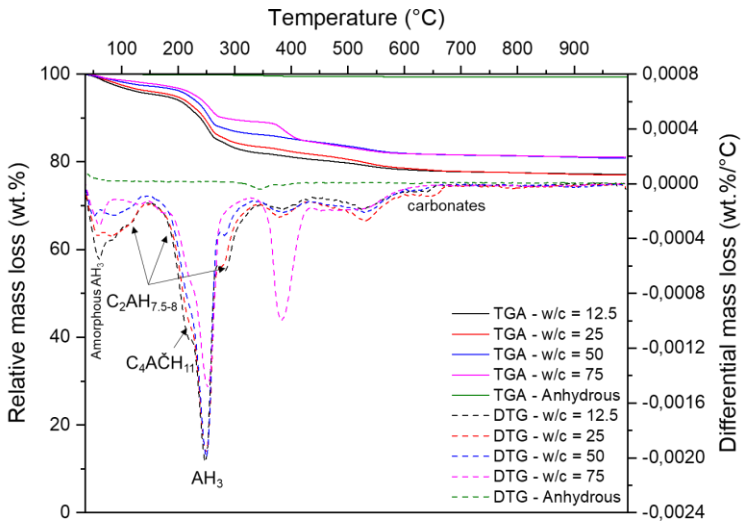


**Figure 58 : TGA and derivative TGA results obtained from $CA_2$ suspensions with various w/c ratios after 24 hours of hydration at 25 °C.**

A shown in the Table 16, the thermal events observed could be assigned to the thermal decomposition of $AH_3$, $C_4AČH_{11}$ and $C_2AH_{7.5\text{-}8}$. The main DTG peak related to the decomposition of $AH_3$ was observed close to 250 °C [7, 13, 18]. However, the thermal events around 380 °C and 530 °C were unexpected based on XRD results. Collier N. [26] described the decomposition of $AH_3$ in three successive steps. First a minor decomposition close to 230 °C corresponding to gibbsite to boehmite transition, then a major decomposition between 310 and 325 °C related to gibbsite to alumina transition, and finally a minor loss can be attributed to boehmite to alumina transition between 495 and 525 °C.

These observations were not in full agreement with ours but led us to attribute the DTG peaks around 380 °C and 525 °C also to $AH_3$, beside the main 250 °C peak already observed for gibbsite in section 1.1.2 (Figure 51). The mass loss below 100 °C was also attributed to $AH_3$ but in amorphous form.

**Table 16 : Decomposition temperatures of hydrates relevant for calcium aluminate systems.**

| Temperature (°C) | Phase | Reference |
|---|---|---|
| ≤ 100 | $AH_3$ (amorphous) | [11, 27] |
| 110 – 170 – 300 | $C_2AH_8$ | [16, 28, 29] |
| 60 – 200 | $C_4AČH_{11}$ | [30-32] |
| 200 – 300 | | |
| 650 | | |
| 220 – 320 | $AH_3$ (gibbsite) | [7, 13, 18] |
| 220 – 230 | $AH_3$ (gibbsite) | [26] |
| 310 – 325 | | |
| 495 – 525 | | |

The exact attribution of each DTA event is difficult due to overlaps and the occurrence of $AH_3$ polymorphs. Regardless, as already underlined in section 1.1.2, knowing that the decomposition of hydrates mostly occurs below 550 °C, the bound water can be calculated overall from TGA. The mass loss up to 550 °C was 21, 21, 17 and 26 % for the suspensions with a w/c ratio of 12.5, 25, 50 and 75 respectively. The mass loss obtained between 500 and 700 °C established the presence of carbonates in the samples most likely due to the carbonation of some hydrated phases during the drying or grinding stages. From these TGA results, the increase of the w/c ratio from 12.5 up to 75 did not seem to affect the mineralogical composition since the bound water content was approximately constant and the DTG curves close to each other.

When comparing the mineralogical assemblages observed here with the ones observed in the sample prepared with a w/c ratio of 0.5 in the first section of this chapter, the main difference laid in the absence of $CAH_{10}$ in the hydration products formed in suspension. Increasing the w/c ratio from 0.5 up to a value higher than 12.5 thus modified the precipitated phases. Such a result was consistent with the influence of the w/c ratio on mineralogical assemblages already reported in literature [33, 34]. However, it should be recalled that the w/c ratio ranging from 0.40 to 0.60 did not change the mineralogical assemblages of resulting $CA_2$ pastes hydrated for 7 days at 25 °C.

### 2.2. Course of $CA_2$ hydration during the first 24 hours – w/c = 25

In order to investigate the early age hydration of $CA_2$ phase, a suspension with a w/c ratio of 25 was monitored with an electrical conductivity probe during the first 7 hours at 25 °C, as detailed in Chapter 2, section 3. The evolution of the liquid fraction composition and of the mineralogical assemblage was characterized after fixed periods as follows: 30, 60, 90, 120, 150, 180, 240, 300 and 420 min. These periods are shown on the conductivity plot in Figure 59.

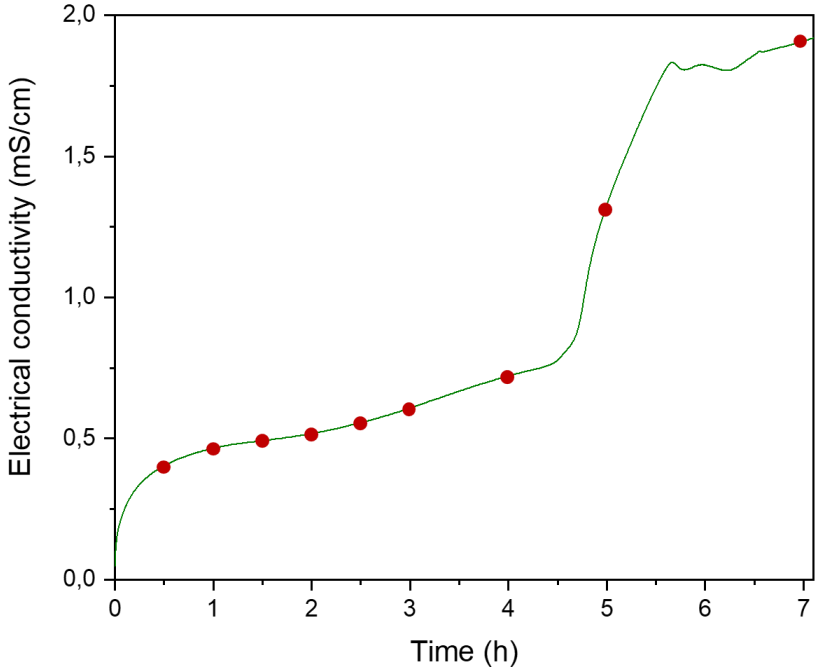


**Figure 59 : Definition of characterization times (red dots) based on the variation of the electrical conductivity during $CA_2$ hydration with a w/c = 25.**

### 2.2.1. Characterization of the solid fraction of suspensions

After each of the described periods, hydration was stopped using the solvent displacement method (Appendix A.7) and the collected solid fraction was characterized by XRD, TGA and $^{27}$Al MAS-NMR spectroscopy.

In Figure 60, the XRD patterns show the presence of only two crystalline phases, $CA_2$ and traces of monocarboaluminate. This latter phase was evidenced only on the 420 min-pattern and may result from carbonation occurring during the hydration stoppage stage and/or drying prior to XRD analysis.

On the 420 min-pattern, the small broad reflections close to 18.3° 2θ and 20.4° 2θ were assigned to aluminium hydroxide (Figure 60).

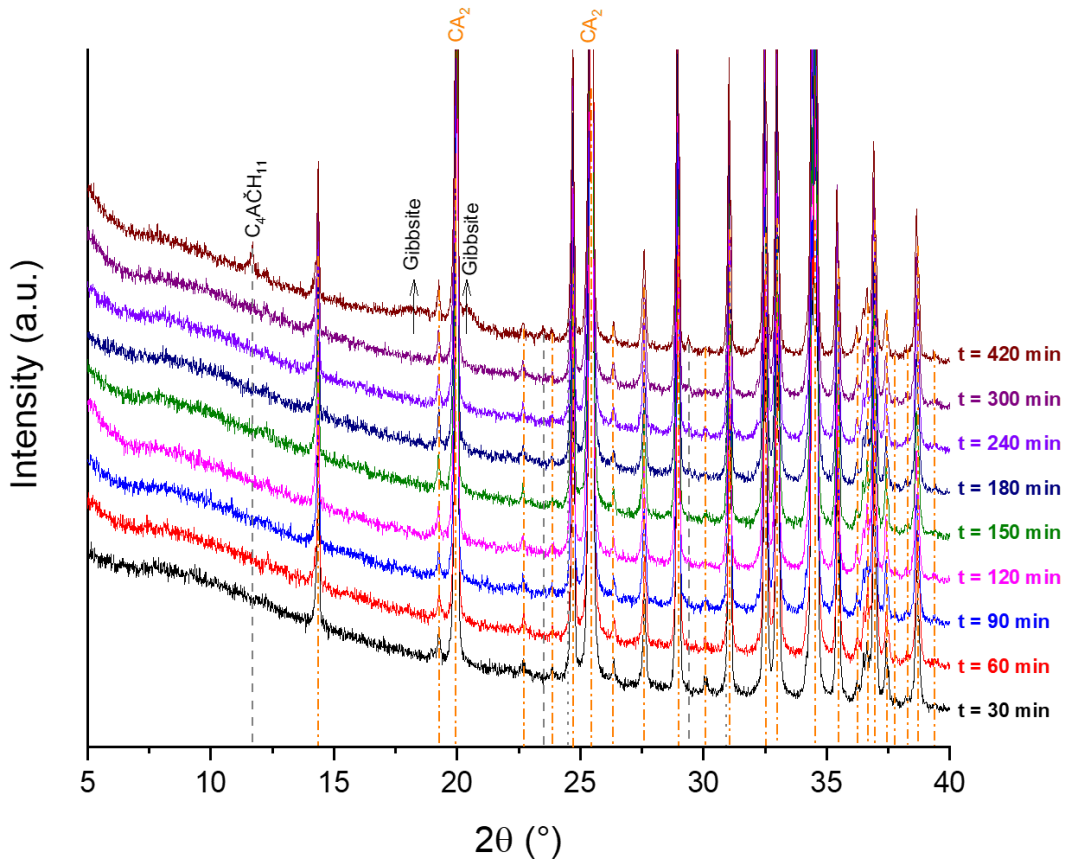


**Figure 60 : XRD patterns of the solid fractions of $CA_2$ suspension with a w/c of 25 after increasing periods of hydration at 25 °C.**

The thermograms of the studied samples and their derivatives are plotted in Figure 61. Measured weight losses were quite small (below 1 wt. %) until 240 min of hydration, highlighting a low degree of hydration. The fraction of bound water reached 1.5% and 4% after 5 hours and 7 hours of hydration respectively.

The presence of $C_4AČH_{11}$, pointed out by XRD, could be also evidenced on DTG by the presence of three thermal decompositions:

- a first thermal decomposition between 60 and 200 °C, corresponding to the loss of five interlayer water molecules from monocarboaluminate ($CO_3$-$AF_m$) [35],
- a second one between 200 and 300 °C, corresponding to the mass loss of six water molecules from the octahedral layer of monocarboaluminate ($CO_3$-$AF_m$) [35],
- a third thermal decomposition around 650 °C, corresponding to the mass loss of $CO_2$.

The thermal decomposition of aluminium hydroxide was also identified in the thermograms by the mass loss at approximately 250 °C [36].

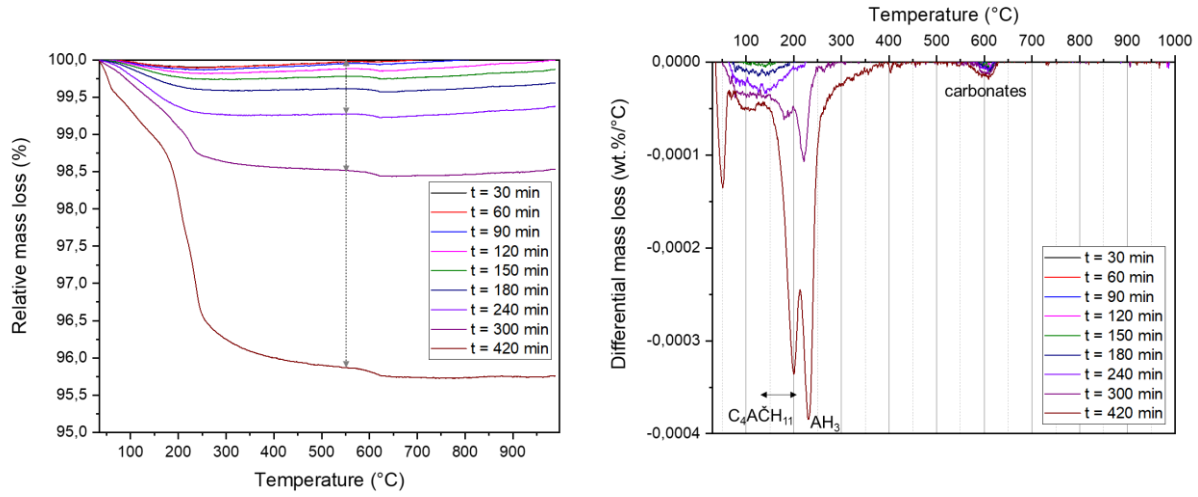


**Figure 61 : TGA and DTG curves obtained from $CA_2$ suspension with a w/c ratio of 25 after increasing periods of hydration at 25 °C.**

As a complement to XRD and TGA studies, $^{27}$Al MAS-NMR spectroscopy was carried out to characterize and more importantly quantify the hydration products found in the solid fractions of the suspension. The distinction between tetrahedrally and octahedrally coordinated Al sites is observed in Figure 62. Nevertheless, the approximate chemical shift values of hydrates led to ambiguous assignment of the phases if only based on $^{27}$Al NMR results. Thus, the peak attribution was based on the hydrates phases detected by XRD and TGA. Considering these phases, a model was fitted to the spectrum for each sampling time in order to quantify the precipitated hydrates.

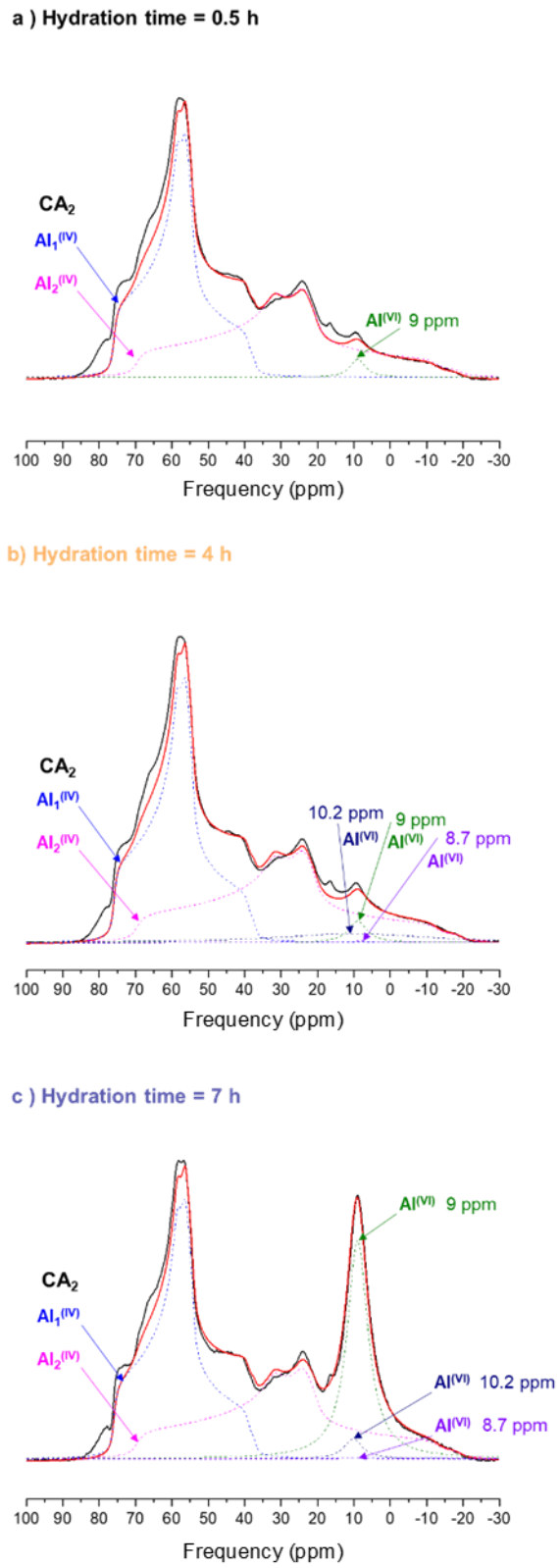


**Figure 62 : $^{27}$Al NMR spectra of $CA_2$ suspension with a w/c of 25 at different hydration times: a) 0.5 h, b) 4 h and c) 7 h.**

For each of the solid fractions, two overlapping centerbands of unreacted $CA_2$ related to the two tetrahedrally coordinated Al sites of this phase appeared as shown in Figure 62. As observed in the spectra from 0.5 h to 7 h of hydration, the content of unreacted $CA_2$ decreased. 30 minutes after the beginning of hydration, the presence of small amounts (2 %) of aluminate from an aluminium hydroxide was observed. That would correspond to a bound water amount of 0.7 wt. % if a $Al(OH)_3$ stoichiometry was assumed. The presence of poorly crystalline $CAH_{10}$ that could not be detected by XRD analysis was also suspected. This was consistent with the weight loss at around 120 °C associated to the decomposition of $CAH_{10}$ in Figure 61. Results with ongoing hydration are summarized in Table 17.

**Table 17 : Quantification by $^{27}$Al NMR of Al-containing phases present in $CA_2$ suspensions (w/c = 25) after 0.5 h, 4 h and 7 h of hydration.**

| Hydration stoppage time (h) | Phase | Chemical shift (ppm) | Al atomic fraction (%) | Phase weight fraction (wt. %) | Corresponding bound water content (wt. %) |
|---|---|---|---|---|---|
| **0.5** | $CA_2$ | 76/70 | 98 | 98 | - |
| | $AH_3$ | 9 | 2 | 2 | 1 |
| **4** | $CA_2$ | 76/70 | 91 | 86 | - |
| | $AH_3$ | 9 | 6.5 | 7 | 3 |
| | $CAH_{10}$ | 10 | 2.3 | 6 | 3 |
| | $C_4AČH_{11}$ | 8.7 | 0.2 | 1 | 0.3 |
| **7** | $CA_2$ | 76/70 | 76.2 | 71 | - |
| | $AH_3$ | 9 | 22 | 25 | 9 |
| | $CAH_{10}$ | 10 | 1.7 | 4 | 2 |
| | $C_4AČH_{11}$ | 8.7 | 0.1 | 0.4 | 0.1 |

Based on these mineralogical compositions, the bound water amount was calculated and found equal to 1 wt. %, 6 wt. % and 11 wt. % for the solid fractions of 0.5 h-, 4 h- and 7 h-old $CA_2$ mixtures, respectively. The bound water content derived from TGA (0, 0.8 and 4.3 wt. % respectively) was much smaller. Such discrepancy remains unexplained at this stage.

The measured bound water content and the mineralogical composition obtained from NMR are superimposed on the conductivity curve in Figure 63.

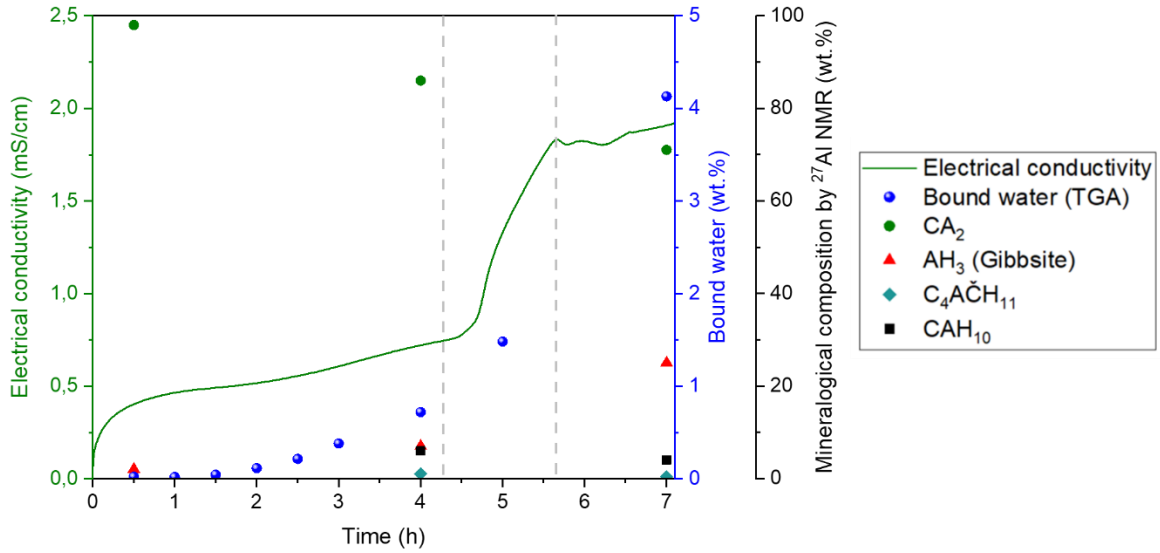


**Figure 63 : Investigation of $CA_2$ hydration at early age: electrical conductivity and phase evolution.**

Based on this figure, the acceleration stage of hydration started 5 hours after mixing, as shown by the sharp increase in conductivity and bound water content. After 7 h of hydration, the analyzed sample contained approximately 4 wt. % of $CAH_{10}$, 25 wt. % of aluminium hydroxide, 0.4 wt. % of monocarboaluminate and 71 wt. % of anhydrous $CA_2$. From the NMR results, 2 %, 9 % and 24 % of anhydrous $CA_2$ were found to have reacted 0.5 h, 4 h and 7 h after hydration respectively. In theory, the calcium fraction issued from $CA_2$ should be found in the identified calcium aluminate hydrates (Table 17). However, difference of the calcium molar fractions between the ones theoretically calculated and the ones measured from NMR results was significant. As the absence of any calcium-containing compounds e.g. $C\check{C}$ and CH was evidenced by XRD and TGA results, the same considerations than in section 1.1.2 of this chapter can be evoked. Either the NMR decomposition overvalued the amount of $AH_3$ compared to other calcium aluminium hydrates, or the missing calcium amounts should be in the aqueous fractions. After 7 h of hydration, this latter hypothesis was consistent with calcium concentration measured in solution (8.0 mmol/L measured experimentally versus 9.8 mmol/L calculated). Based on this discrepancy, the next step would be to characterize the liquid fraction of suspensions.

### 2.2.2. Characterization of the liquid fraction of suspensions

The evolution of the liquid fraction composition with ongoing hydration was measured by ICP-AES. pH values were also measured and corresponding $OH^-$ concentrations were calculated. Results are plotted in Figure 64.

Four periods could be defined on the graphs. The Ca and Al concentrations first increased rapidly. A levelling-off was then noticed, before a new acceleration. Finally, the concentrations reached a plateau. The pH evolution showed a similar trend, with a two-step increase.

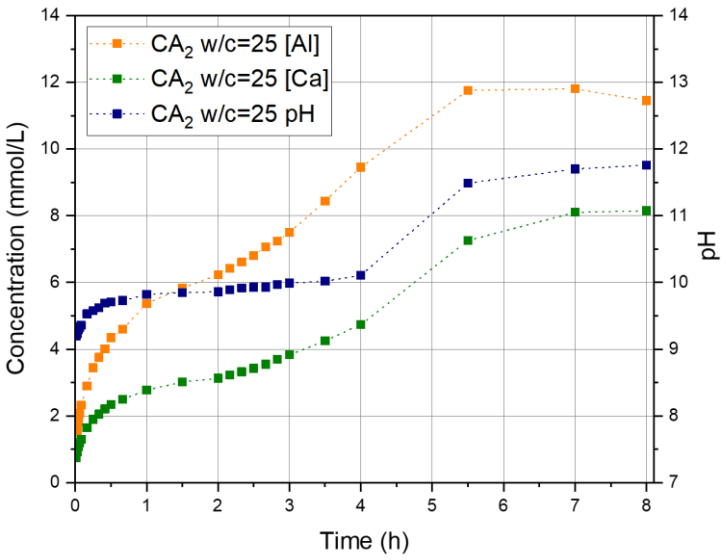


**Figure 64 : Characterization of the liquid fractions of $CA_2$ suspension (w/c ratio = 25, T = 25 °C) during the first eight hours of hydration: evolution of pH and chemical composition.**

From these raw results, the ratio between calcium and aluminate ions was plotted as a function of time (Figure 65). This $[Ca^{2+}]/[Al_{tot}]$ ratio in solution decreased from the beginning of hydration down to a value of 0.50 and remained constant at this value from 2 to 4 hours. Noticeably, this ratio value differed significantly from the 0.25 value that would correspond to the congruent dissolution of $CA_2$ following equation (13):

$$CA_2 + 2\,OH^- + 7\,H_2O \rightleftharpoons Ca^{2+} + 4\,Al(OH)_4^- \qquad (13)$$

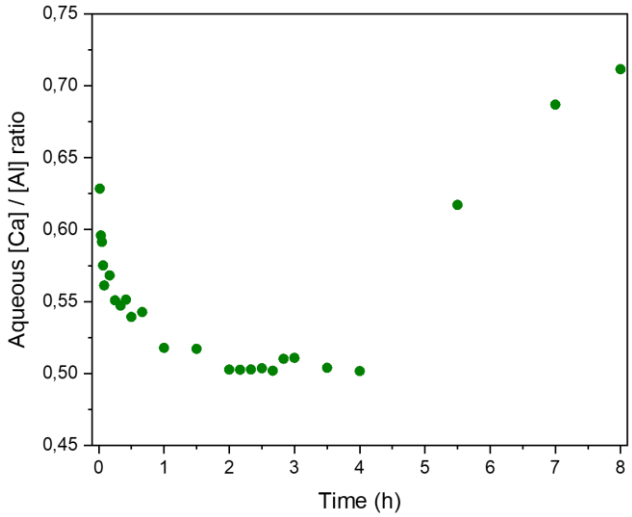


**Figure 65 : Evolution of Ca/Al ratio in the liquid fraction as a function of time during $CA_2$ hydration in suspension (w/c = 25 – T = 25 °C).**

In the following section, saturation index are calculated first and the hydration path followed by calcium and aluminate ions is then reported on the {$CaO$-$Al_2O_3$-$H_2O$} diagram in order to identify a limiting step during $CA_2$ hydration.

### 2.2.3. Investigation of the hydration pathway

Nicoleau *et al.* [37] have recently underlined the importance of some concepts of heterogeneous kinetics which are relevant for investigations of the hydration of a mineral (A) into another one (B) by dissolution / precipitation. The driving force for the reactions is the deviation from equilibrium: $\mu_i^A > \mu_i^{solution} > \mu_i^B$, where $\mu_i$ is the chemical potential of species *i* common to A and B. The equilibrium state is the solubility of solid in a solution. A deviation from equilibrium is called either undersaturation, driving the dissolution reaction, or supersaturation, driving the precipitation reaction. The lower the undersaturation is with respect to solid A, the slower it dissolves. The lower the supersaturation is with respect to solid B, the slower it precipitates. The rates of dissolution and precipitation are coupled when solids A and B contain common species. Indeed, the precipitation of solid B increases the level of undersaturation with respect to solid A and inversely, the dissolution of solid A increases the level of supersaturation with respect to solid B. The evolution of the composition during the transformation of A into B defines the kinetic pathway, which can be plotted as an ion activity product vs. time diagram that always remains within the limits defined by the solubility products of A and B. If the kinetic pathway is close to the solubility product of A and far from that of B, the transformation is driven by the precipitation of B. On the contrary, if the pathway is close to the solubility product of B and far from that of A, the transformation is driven by the dissolution of A.

*2.2.3.1.First approach: calculation of the saturation indexes*

Based on these considerations, we calculated the evolution over time of the ion activity products associated with the main reactions involved in $CA_2$ hydration. The results were expressed in terms of saturation indexes for the phases of interest, as defined by equation (14).

$$SI = log\ (IAP/K_{So}) \quad (14)$$

with IAP the ion activity product and $K_{So}$ the solubility product for the phase under consideration.

The saturation indexes were calculated using the CHESS software [38] with the following input data:

- the pH as well as the aqueous Al and Ca concentrations determined experimentally (Appendix A.10),
- the CEMDATA 2018 database [39] containing the solubility products of the relevant minerals and the formation constants of the aqueous species in the {CaO, $Al_2O_3$, $H_2O$} system (Appendix A.9).

Figure 66 shows their evolution over time for the main phases of interest.

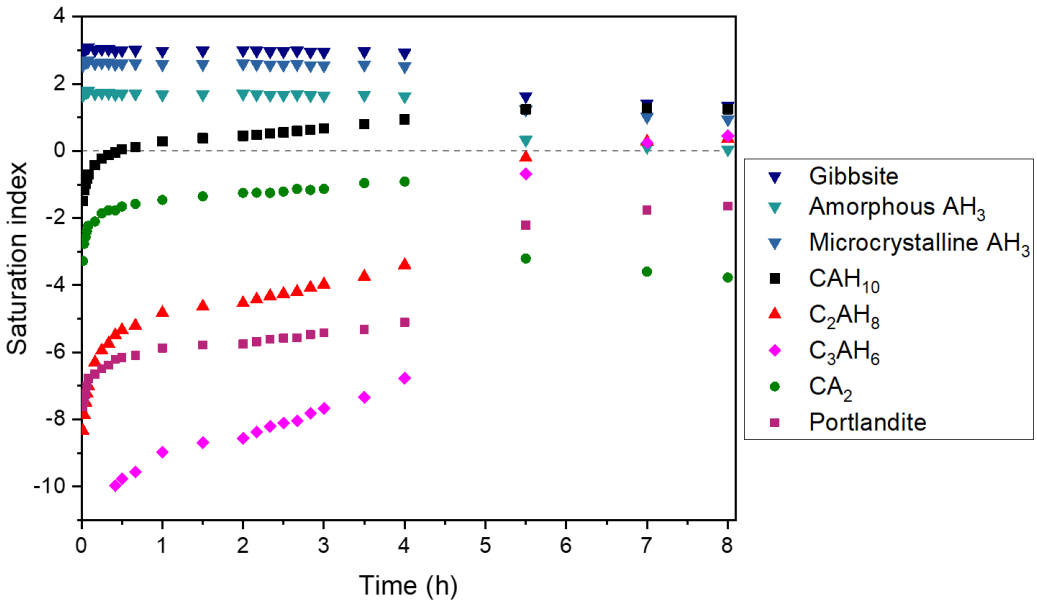


**Figure 66: Evolution of saturation indexes in the $CaO$-$Al_2O_3$-$H_2O$ system as a function of time during the hydration of $CA_2$ in suspension (w/c = 25 – T = 25 °C).**

From mixing and up to 4 hours of hydration:

- The saturation index of portlandite, $C_2AH_8$ and $C_3AH_6$ remained negative. The precipitation of these phases was thus not expected within the studied period.

- The $CAH_{10}$ saturation index became slightly positive 30 minutes after the beginning of hydration, making the precipitation of this phase possible at this stage. The $CAH_{10}$ saturation index value went on increasing up to 4 hours of hydration.
- The saturation index of aluminium hydroxide polymorphs was positive and remained constant within the whole period, despite the increase in calcium, aluminate and hydroxide ions concentration.
- The $CA_2$ saturation index increased right from the beginning of hydration and remained approximately constant from 30 minutes up to 4 hours, despite the increase in the calcium, aluminate and hydroxide ions concentrations.

These results suggest that precipitation of $CAH_{10}$ might play a key role in the control of the kinetics from 30 min to 4 h. However, the presence of this phase, which was evidenced by NMR in the 4h-old sample, still needs to be confirmed experimentally at earlier age.

Nevertheless, our results pointed out the calculated saturation index of $CA_2$ should be closer to zero during the first period. In parallel with this fact, very low saturation indices of the main phases of interest (Figure 66) are calculated. That would support a bad/limited description of the aluminate phases by the thermodynamic database, especially in respect with calculated pH values.

The relevance of the calculated saturation index values discussed above is however questionable since electroneutrality of the solution was not reached from speciation calculations. As a reminder, these calculations simply consisted in determining the electrical balance of the system at equilibrium using the solution composition as input. For each composition, ionic speciation is determined from the database and the electrical imbalance was calculated. Figure 67 shows the evolution as a function of time of the electrical imbalance normalized by the ionic strength of the solution.

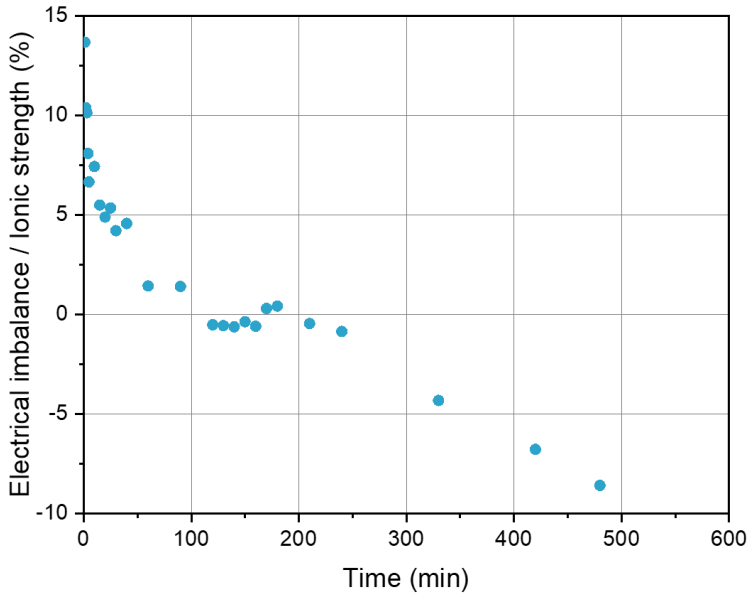


**Figure 67: Evolution of the electrical imbalance normalized by the ionic strength for the simulations carried out with CHESS and the CEMDATA2018 database as a function of the hydration time.**

The normalized electrical imbalance ranged from -10 % up to 15 %. Such a difference with electroneutrality could not be explained by titration uncertainty. The reason for such a discrepancy was likely due to the fact that CEMDATA2018 database was not able to properly reflect the speciation of aluminate-containing solutions and in particular the measured pH values. Such an observation was also recently reported by Maach *et al.* [40].

### *2.2.3.2.Second approach: the solubility diagram*

To circumvent this electroneutrality issue and its consequence on saturation index values, the hydration path was plotted in the plane defined by the Ca and Al aqueous concentrations. With this representation, the [$OH^-$] concentration becomes an implicit variable. The invariant points and solubility lines were calculated and replotted in this system by using the CEMDATA2018 thermodynamic database (Appendix A.9). The resulting diagram (Figure 23) was consistent with that already reported by Matschei *et al.* [41] when considering gibbsite, $C_3AH_6$, $CAH_{10}$, $C_2AH_8$, $C_4AH_{13}$ and CH. In the diagram replotted in this work, $CA_2$, $C_2AH_{7.5}$, microcrystalline aluminium hydroxide and amorphous aluminium hydroxide were further taken into account. Solution compositions at invariant points are reported in Appendix A.10 (Table 47). The aqueous Ca and Al concentrations determined experimentally after increasing periods of hydration were plotted in this diagram (Figure 68).

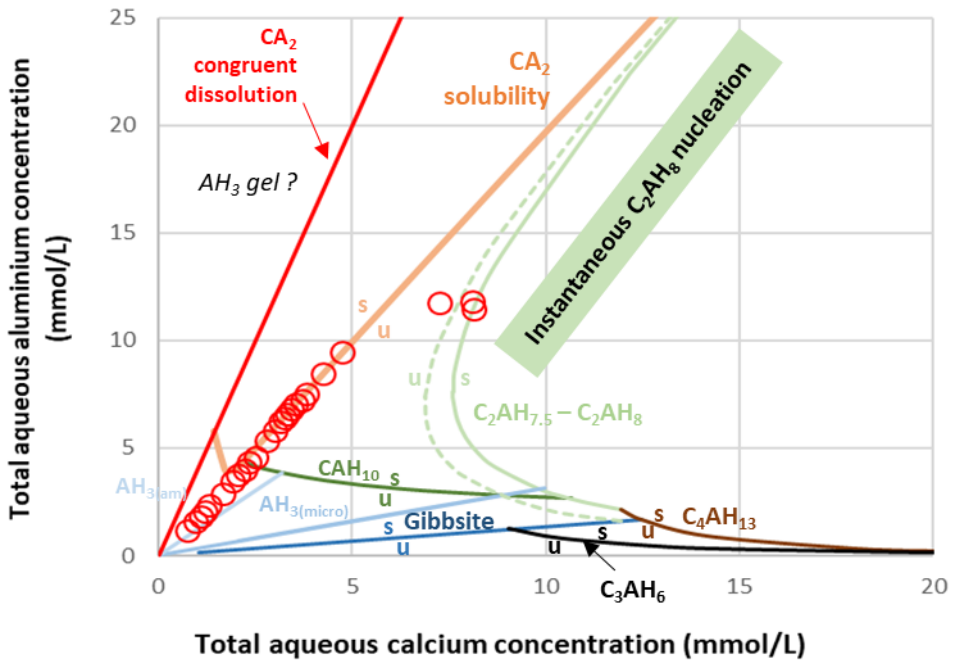


**Figure 68 : Total calcium and aluminium concentrations measured in the liquid fraction during $CA_2$ hydration (w/c = 25 – T = 25 °C) plotted in the {$CaO$-$Al_2O_3$-$H_2O$} diagram. Note that the red line is not a solubility curve. It simply shows the expected concentrations if the system is driven by congruent dissolution of $CA_2$. Abbreviations: u–undersaturation, s–supersaturation.**

First of all, it appeared that the $CA_2$ solubility curve stood below the line which would be followed by the aqueous aluminium and calcium concentrations if congruent dissolution of $CA_2$ occurred. During the first period, from 1 min to 4 h, the aqueous calcium and aluminium concentrations were located on the $CA_2$ solubility line. During this period and using this representation, it could be concluded that the Ca and Al concentrations were defined by the solubility product of $CA_2$ hydration. Dissolution of $CA_2$ thus did not limit the kinetics since its solubility limit was reached over the whole period. The total aqueous concentrations of calcium and aluminium remained in a zone located above the solubility curve of $CAH_{10}$ from 25 min, but its precipitation seems to be strongly limited: only traces of this hydrate were evidenced by mineralogical analysis at 4 h. In his PhD thesis, Maach N. reported the difficulty for $CAH_{10}$ to nucleate, which seems consistent with our results. Complementary investigations would be needed however to support this point. Assuming that $CAH_{10}$ nucleates following classical nucleation theory, measurements of $CAH_{10}$ interfacial energy might be of interest. During this first period, the total aluminium aqueous concentration remained in a zone of the {$CaO$-$Al_2O_3$-$H_2O$} diagram located far above the solubility curves of the aluminium hydroxide solid polymorphs. In this zone, formation of an aluminium hydroxide gel has already been reported [42, 43]. Experimentally, precipitated aluminium hydroxide was evidenced by $^{27}$Al MAS-NMR in the 30 min- and 4 h-old samples. Nevertheless, there remains an uncertainty about its origin: impurity from the reactant, or precipitation with ongoing hydration.

After this first period, the hydration path followed by calcium and aluminate ions diverged from the $CA_2$ solubility curve to reach that of $C_2AH_{7.5}$ – $C_2AH_8$. During this stage, $AH_3$ was the main

product observed experimentally, together with traces of $CAH_{10}$, but the presence of $C_2AH_8$ was not clearly evidenced until 24 h. At this sampling time, $C_2AH_{7.5}$ – $C_2AH_8$ was clearly detected, without any $CAH_{10}$.

The reason for the switch of the system from the solubility curve of $CA_2$ to that of $C_2AH_8$ still needs to be elucidated. A hypothesis may be the accelerated precipitation of $AH_3$, evidenced by TGA from 4 h. This reaction consumes aluminate ions and releases $OH^-$ ions ($Al(OH)_4^- \rightleftharpoons Al(OH)_3 + OH^-$) which are necessary for the nucleation of $C_2AH_8$ according to Maach N. [44].

The last stage of hydration could be described by further $CA_2$ dissolution, aluminium hydroxide precipitation and $C_2AH_8$ precipitation, yielding the mineralogical assemblage observed 24 hours after mixing. The limiting step during this stage could be assumed as being the dissolution of $CA_2$, the nucleation of aluminium hydroxide or both. $C_2AH_8$ precipitation was not likely a limiting step, since its nucleation has already been reported as being easy. Manninger T. *et al.* [42] described indeed the zone of the diagram located above the $C_2AH_{7.5}$ – $C_2AH_8$ solubility lines as a zone where nucleation of $C_2AH_{7.5}$ – $C_2AH_8$ was instantaneous.

## 3. Summary and discussion

In this chapter, the hydration study of a pure synthetic $CA_2$ phase has been presented.

Firstly, is has been observed that the higher the w/c ratio, the higher the heat released. An estimation of the hydration degree as a function of time has been made by assuming that $CA_2$ dissolution and precipitation of hydrates contribute to the release of heat. Such an assumption appeared to be consistent when compared to progress of hydration quantified by NMR.

After 7 days of hydration and for a paste elaborated with a w/c ratio of 0.5, the hydration degree, defined here as the amount of dissolved $CA_2$ and estimated by using isothermal calorimetry, was found to be equal to 75 % while the remaining amount of $CA_2$ was quantified by NMR to be equal to about 28.5 %. Thus, a hydration degree of 71.5 % would be achieved 7 days after mixing pure water and the studied $CA_2$ synthetic phase. The two approaches used to assess the hydration degree of $CA_2$ were thus consistent. Regarding the hydrates and for a paste elaborated with a w/c ratio of 0.5, the mineralogical assemblage was composed of about 63 % of aluminium hydroxide and less than 9 % of calcium aluminate phases ($CAH_{10}$ and $C_2AH_8$). There was no evidence to indicate the presence of stable $C_3AH_6$ at this stage based on the XRD, TGA and NMR results. As expected, the rate of hydration of $CA_2$ was low since notable heat release started after 80 hours only. Nevertheless, about 75 % of $CA_2$ had dissolved after 7 days of hydration.

From the monitoring of hydration as a function of time carried out in suspension, three main stages were identified during the course of hydration.

During the first stage, ionic concentrations slowly increased. Replotting the {$CaO$-$Al_2O_3$-$H_2O$} diagram including $CA_2$ solubility line and comparing this diagram to the measured total calcium and aluminium ions concentrations show that the kinetics is not limited by the dissolution of $CA_2$ but rather by the precipitation of the hydrates (likely $CAH_{10}$). The aqueous calcium and aluminate concentrations were governed by the solubility of $CA_2$. They increased during this stage and moved in the direction of the solubility lines of $C_2AH_{7.5}$-$C_2AH_8$.

The second stage was characterized by an increase in the total calcium, aluminate and hydroxide ions concentrations which followed the solubility curve of $C_2AH_{7.5}$-$C_2AH_8$ in the {$CaO$-$Al_2O_3$-$H_2O$} diagram. The trigger for starting this period might have been the accelerated precipitation of an aluminium hydroxide phase. At this stage, about 20 wt. % of $CA_2$ had dissolved.

The third step was characterized by a conductivity plateau, suggesting an unchanged solution composition located on the $C_2AH_8$ solubility curve. During this stage, dissolution of $CA_2$ was going on and reached a degree of 75 % 7 days after mixing. $CA_2$ dissolution and/or aluminium hydroxide precipitation could be assumed to be limiting steps during this stage, while $C_2AH_x$ precipitation was reported to be almost instantaneous in the literature.

The reason for aluminium hydroxide precipitation for the specific measured chemical concentrations is not elucidated yet. However, it must be noted that a better description of species speciation in solution has to be achieved since the thermodynamic database used in this study did not allow reproducing the measured compositions, especially in terms of pH. This point will be further discussed in the last chapter of this manuscript.

## 4. References

[1] D. Sorrentino, F. Sorrentino, and M. George, "Mechanisms of hydration of calcium aluminate cement," in *Materials Science of Concrete IV*, vol. 4, J. Skalny and S. Mindess, Eds. Westerville: American Ceramic Society, 1995, pp. 41-90.

[2] A. Negro, L. Montanaro, and A. Bachiorrini, "On the reactivity of the cement clinkers components by means of Laser Granulometer," *Cement and Concrete Research,* vol. 15, no. 2, pp. 315-319, 1985/03/01/ 1985.

[3] B. Singh and A. J. Majumdar, "The hydration of calcium dialuminate and its mixtures containing slag," *Cement and Concrete Research,* vol. 22, no. 6, pp. 1019-1026, 1992/11/01/ 1992.

[4] S. Klaus, "Quantification of CA hydration and influence of its particle fineness during early hydration of calcium aluminate cement," Friedrich-Alexander-Universität Erlangen-Nürnberg, 2015.

[5] F. Hüller, "Hydration mechanisms of CA2 and alumina-rich calcium aluminate cements: Effects of mechanical activation, critical CA contents and crystallinity of AH3," PhD, Geographie und Geowissenschaften, Friedrich-Alexander-Universität Erlangen-Nürnberg (FAU), 2019.

[6] S. K. Das and P. K. Daspoddar, "Dehydration kinetics of hydrated calcium dialuminate," *Thermochimica Acta,* vol. 293, no. 1, pp. 125-128, 1997/06/01/ 1997.

[7] P. Lura, F. Winnefeld, and X. Fang, "A simple method for determining the total amount of physically and chemically bound water of different cements," *Journal of Thermal Analysis and Calorimetry,* vol. 130, no. 2, pp. 653-660, 2017/11/01 2017.

[8] J. Justs, M. Wyrzykowski, F. Winnefeld, D. Bajare, and P. Lura, "Influence of superabsorbent polymers on hydration of cement pastes with low water-to-binder ratio," *Journal of Thermal Analysis and Calorimetry,* vol. 115, no. 1, pp. 425-432, 2014/01/01 2014.

[9] S. Klaus, A. Buhr, D. Schmidtmeier, S. Kuiper, and F. Goetz-Neunhoeffer, "Hydration of calcium aluminate cement phase CA and $CA_2$ in refractory applications," presented at the UNITECR 2015 - 14th Biennial Worldwide Congress, Vienna, 2015.

[10] S. R. Klaus, J. Neubauer, and F. Goetz-Neunhoeffer, "Hydration kinetics of CA2 and CA—Investigations performed on a synthetic calcium aluminate cement," *Cement and Concrete Research,* vol. 43, pp. 62-69, 2013/01/01/ 2013.

[11] V. Antonovič, J. Kerienė, R. Boris, and M. Aleknevičius, "The Effect of Temperature on the Formation of the Hydrated Calcium Aluminate Cement Structure," *Procedia Engineering,* vol. 57, pp. 99-106, 2013/01/01/ 2013.

[12] F. Guirado, S. Galí, and J. S. Chinchón, "Thermal Decomposition of Hydrated Alumina Cement (CAH10)," *Cement and Concrete Research,* vol. 28, no. 3, pp. 381-390, 1998/03/01/ 1998.

[13] T. Dos Santos *et al.*, "Gluconate action in the hydration of calcium aluminate cements: Theoretical study, processing of aqueous suspensions and hydration reactivation," *Journal of the European Ceramic Society,* vol. 39, no. 8, pp. 2748-2759, 2019/07/01/ 2019.

[14] J. Szczerba, D. Madej, E. Śnieżek, and R. Prorok, "The application of DTA and TG methods to investigate the non-crystalline hydration products of CaAl2O4 and

Ca7ZrAl6O18 compounds," *Thermochimica Acta,* vol. 567, pp. 40-45, 2013/09/10/ 2013.

[15] S. Kumar, A. Bandopadhyay, T. C. Alex, and R. Kumar, "Influence of mechanical activation on the synthesis and hydraulic activity of calcium dialuminate," *Ceramics International,* vol. 32, no. 5, pp. 555-560, 2006/01/01/ 2006.

[16] N. Ukrainczyk, T. Matusinovic, S. Kurajica, B. Zimmermann, and J. Sipusic, "Dehydration of a layered double hydroxide—$C_2AH_8$," *Thermochimica Acta,* vol. 464, no. 1, pp. 7-15, 2007/11/25 2007.

[17] C. S. Gosselin, K.L., "Microstructure development of calcium aluminate cements accelerated by lithium sulfate," presented at the Proceedings of the Calcium Aluminate Cements the Centenary Conference, Avignon, France, 30 June–2 July, 2008, 2008.

[18] K. Irisawa, I. Garcia-Lodeiro, and H. Kinoshita, "Influence of mixing solution on characteristics of calcium aluminate cement modified with sodium polyphosphate," *Cement and Concrete Research,* vol. 128, p. 105951, 2020/02/01/ 2020.

[19] J. H. Skibsted, E.; Jakobsen, H.J., "Characterization of Calcium Aluminate Phases in Cements by 27Al MAS NMR Spectroscopy," *Inorg. Chem.,* vol. 32, pp. 1013-1027, 1993.

[20] P. Faucon, T. Charpentier, D. Bertrandie, A. Nonat, J. Virlet, and J. C. Petit, "Characterization of Calcium Aluminate Hydrates and Related Hydrates of Cement Pastes by 27Al MQ-MAS NMR," *Inorganic Chemistry,* vol. 37, no. 15, pp. 3726-3733, 1998/07/01 1998.

[21] W. Gessner, D. Müller, H.-J. Behrens, and G. Scheler, "Zur Koordination des Aluminiums in den Calciumaluminathydraten $2CaO{\cdot}Al_2O_3{\cdot}8H_2O$ und $CaO{\cdot}Al_2O_3{\cdot}10H_2O$," *Zeitschrift für anorganische und allgemeine Chemie,* https://doi.org/10.1002/zaac.19824860122 vol. 486, no. 1, pp. 193-199, 1982/03/01 1982.

[22] R. A. Kinsey, R. J. Kirkpatrick, J. Hower, K. A. Smith, and E. Oldfield, "High resolution aluminum-27 and silicon-29 nuclear magnetic resonance spectroscopic study of layer silicates, including clay minerals," *American Mineralogist,* vol. 70, no. 5-6, pp. 537-548, 1985.

[23] X. Cong and R. J. Kirkpatrick, "Hydration of Calcium Aluminate Cements: A Solid-State $^{27}$Al NMR Study," *Journal of the American Ceramic Society,* vol. 76, no. 2, pp. 409-416, 1993/02/01 1993.

[24] Y. Zhang, J. Chang, J. Zhao, and Y. Fang, "Nanostructural characterization of Al(OH)3 formed during the hydration of calcium sulfoaluminate cement," *Journal of the American Ceramic Society,* vol. 101, no. 9, pp. 4262-4274, 2018/09/01 2018.

[25] G. B. S. Ng, "Interactions of Polycarboxylate based Superplasticizers with Montmorillonite Clay in Portland Cement and with Calcium Aluminate Cement," Dissertation Fakultät für Chemie Technische Universität München, 2013.

[26] N. Collier, "Transition and Decomposition Temperatures of Cement Phases – a Collection of Thermal Analysis Data," *Ceramics Silikaty,* vol. 60, 10/01 2016.

[27] J. Bensted and P. Barnes, *Structure and performance of cements*, (2nd Edition) ed. London; New York: Spon Press, 2002.

[28] K. Gdowska *et al.*, *Selected Aspects of Modern Engineering*. Krakow: AGH University of Science and Technology Press, 2013.

[29] S. M. Bushnell-Watson and J. H. Sharp, "The application of thermal analysis to the hydration and conversión Reactions of calcium alumínate Cements," *Materiales de Construcción; Vol 42, No 228 (1992)*, 1992.

[30] M. R. Nilforoushan and N. Talebiaan, "The hydration products of a refractory calcium aluminate cement at low temperatures," (in English), *Iranian Journal of Chemistry and Chemical Engineering (IJCCE),* Article vol. 26, no. 2, pp. 71-76, 2007.

[31] P. T. Durdziński, "Hydration of multi-component cements containing cement clinker, slag, calcareous fly ash and limestone," PhD, Faculté Sciences et Techniques de l'Ingénieur, EPFL, Suisse, 6834, 2016.

[32] V. S. Ramachandran, R. M. Paroli, J. J. Beaudoin, and A. H. Delgado, "10 - Non-Portland Rapid Setting Cements," in *Handbook of Thermal Analysis of Construction Materials*, V. S. Ramachandran, R. M. Paroli, J. J. Beaudoin, and A. H. Delgado, Eds. Norwich, NY: William Andrew Publishing, 2002, pp. 403-448.

[33] H. Lahalle *et al.*, "Influence of the w/c ratio on the hydration process of a magnesium phosphate cement and on its retardation by boric acid," *Cement and Concrete Research,* vol. 109, pp. 159-174, 2018/07/01/ 2018.

[34] D. Damidot, A. Nonat, and P. Barret, "Kinetics of Tricalcium Silicate Hydration in Diluted Suspensions by Microcalorimetric Measurements," *Journal of the American Ceramic Society,* vol. 73, no. 11, pp. 3319-3322, 1990.

[35] K. Scrivener, R. Snellings, and B. Lothenbach, *A Practical Guide to Microstructural Analysis of Cementitious Materials*. Boca Raton: CRC Press, Taylor & Francis Group, 2016.

[36] F. Šoukal *et al.*, "The influence of pH buffers on hydration of hydraulic phases in system CaO–Al2O3," *Journal of Thermal Analysis and Calorimetry,* Article vol. 124, no. 2, pp. 629-638, 2016.

[37] L. Nicoleau and A. Nonat, "A new view on the kinetics of tricalcium silicate hydration," *Cement and Concrete Research,* vol. 86, pp. 1-11, 2016/08/01/ 2016.

[38] J. van der Lee, "Thermodynamic and mathematical concepts of CHESS," in "Technical Report Nr. LHM/RD/98/39," École des Mines de Paris, Fontainebleau, France, École des Mines de Paris, Fontainebleau, France1998.

[39] B. Lothenbach *et al.*, "Cemdata18: A chemical thermodynamic database for hydrated Portland cements and alkali-activated materials," *Cement and Concrete Research,* vol. 115, pp. 472-506, 2019/01/01/ 2019.

[40] N. Maach, J. F. Georgin, S. Berger, and J. Pommay, "Chemical mechanisms and kinetic modeling of calcium aluminate cements hydration in diluted systems: Role of aluminium hydroxide formation," *Cement and Concrete Research,* vol. 143, p. 106380, 2021/05/01/ 2021.

[41] T. Matschei, B. Lothenbach, and F. P. Glasser, "Thermodynamic properties of Portland cement hydrates in the system CaO–Al2O3–SiO2–CaSO4–CaCO3–H2O," *Cement and Concrete Research,* vol. 37, no. 10, pp. 1379-1410, 2007/10/01/ 2007.

[42] T. Manninger, D. Jansen, J. Neubauer, and F. Goetz-Neunhoeffer, "The retarding effect of phosphoric acid during CAC hydration," *Cement and Concrete Research*, vol. 122, pp. 83-92, 2019/08/01/ 2019.

[43] P. Barret, D. Bertrandie, and D. Beau, "Calcium hydrocarboaluminate, carbonate, alumina gel and hydrated aluminates solubility diagram calculated in equilibrium with CO2g and with Naaq+ ions," *Cement and Concrete Research*, vol. 13, no. 6, pp. 789-800, 1983/11/01/ 1983.

[44] N. Maach, "Kinetic modeling of the early age hydration of calcium aluminate cements : From chemical mechanism to the modeling by the Population Balance Equations," Thèse de doctorat, Mécanique, Energétique, Génie Civil, Acoustique (MEGA), l'INSA de Lyon, 2019LYSEI127, 2019.

# Chapter 4: Investigation of pure CA hydration at early age

# **Chapitre 4** : Étude de l'hydratation au jeune âge de CA pur

**Résumé:** Ce chapitre est dédié à l'étude de l'hydratation au jeune âge de CA pur à 25°C. La même méthodologie que pour l'étude du $CA_2$ a été adoptée. Dans un premier temps, la vitesse d'hydratation des pâtes avec différents rapports massiques eau/ciment (e/c) a été étudiée par calorimétrie isotherme. Il a été observé que plus le rapport e/c est élevé, plus la chaleur libérée est importante comme déjà constaté dans le cas de $CA_2$. Les pâtes résultantes ont ensuite été caractérisées afin de définir leurs assemblages minéralogiques 7 jours après le mélange. Une estimation du degré d'hydratation en fonction du temps a été faite en supposant que la dissolution de CA contribue principalement à la libération de chaleur. Un degré d'hydratation de 70 % a été estimé 7 jours après le mélange du CA anhydre avec de l'eau (e/c=0.5). Néanmoins, à partir de la quantification par RMN de l'assemblage minéralogique de la même pâte à l'échéance de 7 jours, un degré d'hydratation de 89 % a été estimé. Cet écart pourrait provenir des incertitudes de mesure et de calcul, sachant que l'identification par RMN des phases d'aluminate de calcium s'est révélée compliquée à cause de la multiplicité des résonances qui se chevauchent. Du point de vue des hydrates et pour une pâte élaborée avec un rapport e/c de 0.5, l'assemblage minéralogique est composé principalement de gibbsite (53 % en masse) et de $C_3AH_6$ (31 % en masse).

Dans un second temps, l'étude du suivi de l'hydratation par la conductimétrie a été menée en suspension diluée à 25°C avec un rapport massique e/c fixé à 25. L'évolution de la composition de la solution interstitielle et de la minéralogie a été étudiée en fonction du temps. Les résultats suggèrent qu'un hydroxyde d'aluminium soit la principale phase hydratée dans une pâte de CA avec un rapport e/c de 0.5 pendant les 7 premières heures d'hydratation. Dans cet intervalle de temps, une période d'induction a été observée par calorimétrie isotherme et a été mise en évidence dans l'étude des suspensions également. Selon les expériences réalisées en suspension, la dissolution du CA n'est pas cinétiquement limitante car l'équilibre de solubilité est atteint. La fin de la période d'induction est caractérisée par la précipitation de la gibbsite et du $C_2AH_8$. Selon Maach [1], et en accord avec notre travail, l'étape limitante durant cette période pourrait être la précipitation de la gibbsite qui apporte au milieu réactif les ions hydroxyde nécessaires à la précipitation du $C_2AH_8$. Un tel mécanisme est soutenu par ce travail puisqu'aucune sursaturation par rapport au $C_2AH_8$ n'est observée pendant la période étudiée.

# Introduction

The previous chapter was dedicated to the study of $CA_2$ hydration. In this chapter, the hydration of monocalcium aluminate ($CaAl_2O_4$ or CA), the main hydraulic constituent of calcium aluminate cements leading to early strength development, is investigated with the same experimental procedure.

Hydration reactions of calcium aluminate phases depend on various parameters (temperature, relative humidity, fineness of particles, availability of $H_2O$ …) [2-4]. In particular, hydration of CA highly depends on the temperature and on the reaction time. At temperatures below 15 °C, the metastable $CAH_{10}$ phase forms together with amorphous $AH_3$. With time, these phases convert into crystalline phases such as $C_2AH_{7.5\text{-}8}$ and $AH_3$ [5]. Between 15 °C and 27 °C, the co-existence of metastable $CAH_{10}$ and $C_2AH_8$ phases with $AH_3$ is reported [6]. For temperatures ranging between 27 and 50 °C, $C_2AH_8$ is formed, together with $AH_3$. Eventually, it is expected that the metastable hydrates will all convert into the thermodynamically stable hydrogarnet phase ($C_3AH_6$). Lothenbach B. *et al.* [7] report that at ambient temperature, the kinetics of the conversion reactions slows down and that, consequently, the co-existence of metastable and stable phases can be observed for long periods of time. The results concerning the products formed during hydration of CACs with a C/A ratio around 1 are sometimes contradictory. According to Lothenbach *et al.* [8], $CAH_{10}$ was detected at 20 °C and below, together with $AH_3$ . On the other hand, it was reported that during the hydration of CA, metastable $C_2AH_8$ forms first (together with $AH_3$) and then converts with time into $C_2AH_{7.5}$, and finally into $C_3AH_6$ [8]. The presence of monocarboaluminate among the CA hydration products was also observed because of accidental carbonation during drying and grinding of the samples [8].

The kinetics of CA hydration was studied by Klaus S.R. *et al.* [5]. After the initial period (directly measured after the mixing process of the anhydrous phase with water), the induction period lasts for 1.8 h. It is followed by a sharp heat flow event after 2.4 h of hydration. No significant heat occurs after 14 h of hydration. Unreacted CA remains after 22 h of hydration, possibly because of a lack of water to get full hydration

Recently, Manninger T. reexamined the early hydration of CA by calorimetry [3]. Three explanations were proposed for the presence of the induction period. The first explanation postulates the existence of an inert layer around the CA grains. The second explanation is based on a slow nucleation process during the induction period. In the third explanation, the induction period is associated with the precipitation of $AH_3$ with a very low crystallinity. Most interestingly, Maach N. investigated the formation of $AH_3$ in different CA suspensions at 20 °C and its influence on the kinetics of hydration [1]. A transient state caused by the formation of $AH_3$ is observed. Precipitation of $AH_3$, which consumes aluminate ions in excess, is accompanied by a new flux of hydroxide ions. In addition, the amount of precipitated $AH_3$ phase decreases when the concentration of the CA suspension increased from 3 g/L to 50 g/L.

In summary, the hydration process of CA is complex, involving conversion between metastable and stable phases. Among them, $AH_3$, amorphous or crystalline, seems to play an important

role on the induction period. Considering these open questions, this fourth chapter is therefore devoted to the study of the hydration of pure CA at early age.

# 1. Hydration study of CA pastes at early age

## 1.1. Investigation of the influence of w/c ratio on the early age hydration of CA pastes

### 1.1.1. Heat flow monitoring

The influence of the w/c ratio on the course of CA hydration was studied by varying its value from 0.375 up to 0.60 and by monitoring the hydration by using isothermal calorimetry at 25 °C. The heat flow released during hydration was measured during 7 days after ex-situ mixing (Figure 69).

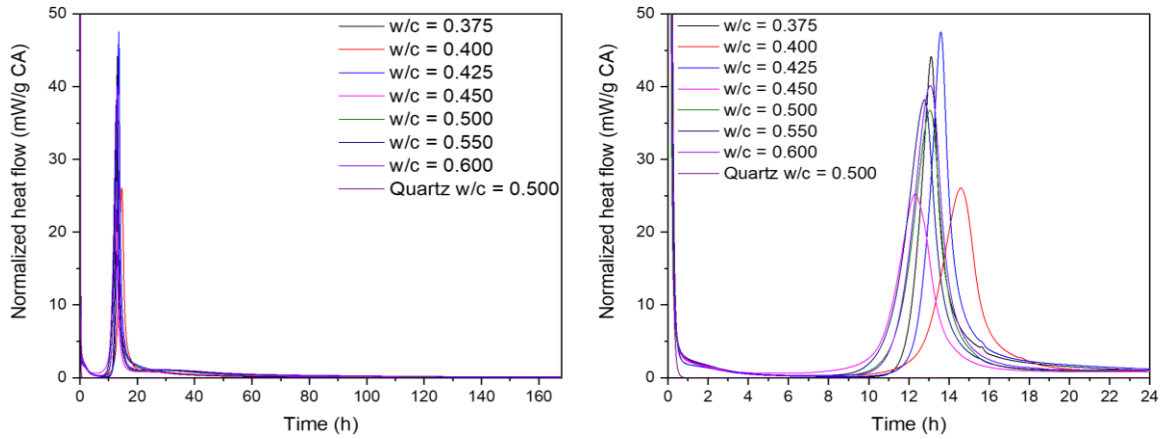


**Figure 69 : Heat flow measurement of pure CA pastes with different w/c ratios at 25 °C for 7 days of hydration. On the right, zoom on the first 24 hours of hydration.**

As shown in Figure 69, the heat flow profiles can be divided into three main periods:

- An induction period of low thermal activity lasting 7.5 h to 10 h depending on the w/c ratio of the paste.
- An acceleration period with a pronounced ascending heat flow up to the maximum of a single main exothermic peak reached after about 12 to 15 h of hydration depending on the w/c ratio.
- A deceleration period during which the heat flow decreased and reached a low heat flow value close to the baseline.

From these results, no clear relationship between the w/c ratio and the length of each period could be clearly established (see Table 18).

The cumulative heat released during the first seven days after mixing, expressed in J per g of calcium aluminate anhydrous phase, is plotted as a function of time in Figure 70 for each studied w/c ratio. As described in chapter 2, cumulative heat values were considered as being relevant when comparing the heat released by the studied samples with an inert sample. This was further

confirmed by comparing calorimetry measurements carried out with the *in-situ* and *ex-situ* mixing procedures, which led to the same results.

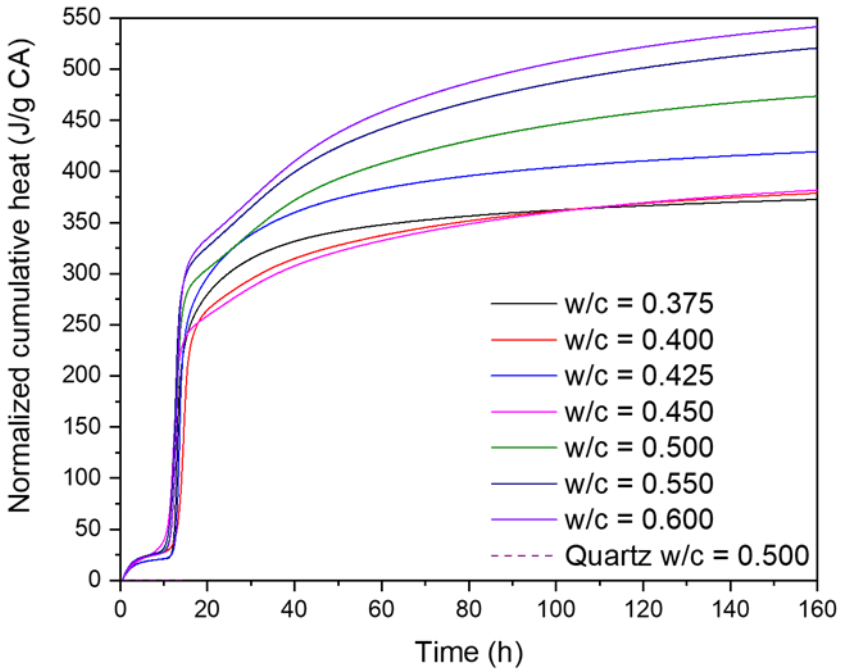


**Figure 70 : Normalized cumulative heat of CA pastes prepared with different w/c ratios during seven days of hydration at 25 °C.**

**Table 18 : Summary of the heat flow and cumulative heat measurements of pure CA pastes with different w/c ratios at 25 °C.**

| w/c | End of the induction period (h) | Time of maximum heat flow (h) | Maximum heat flow (mW/$g_{CA}$) | Cumulative heat at 7 days of hydration (J/$g_{CA}$) |
|---|---|---|---|---|
| **0.375** | 10.5 | 13 | 44 | 373 |
| **0.400** | 9.5 | 15 | 26 | 381 |
| **0.425** | 9 | 13.5 | 47 | 420 |
| **0.450** | 7.5 | 12.5 | 25 | 385 |
| **0.500** | 8.5 | 13 | 36 | 477 |
| **0.550** | 8 | 13 | 38 | 525 |
| **0.600** | 8.5 | 13 | 40 | 546 |

As already observed in the heat flow profiles, the w/c ratio did not affect in a straightforward manner neither the beginning nor the end of the acceleration period. However, the increase in w/c ratio resulted, to one exception, in a monotonous increase in cumulative heat. After 7 days of hydration, cumulative heats tended to stabilize at a plateau value. The relationship between the cumulative heat released 7 days after mixing and the initial w/c ratio is shown in Figure 71. Increasing the w/c ratio from 0.40 up to 0.60 yielded an increase of about 45 %.

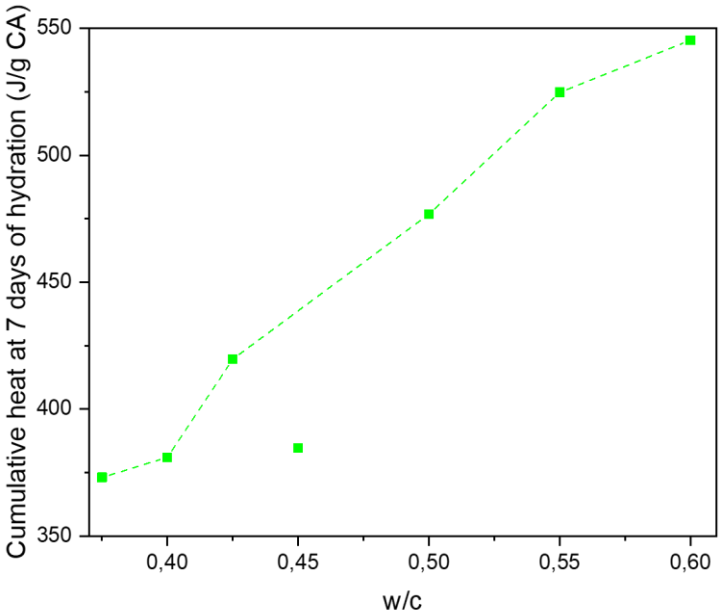


**Figure 71 : Cumulative heat values measured after 7 days of CA hydration as a function of w/c ratio (at 25 °C).**

An almost linear relationship (excluding the 0.450 w/c ratio) could be observed between the cumulative heat measured 7 days after mixing and the w/c ratio in the range 0.375 - 0.550. Since no clear plateau was observed in this range of w/c ratio, the water demand, defined as the minimum w/c ratio leading to the highest hydration degree of the considered anhydrous cementitious phase, could not be clearly identified.

By assuming that only the dissolution of CA contributes to the heat release (reaction equation (15)), and thus neglecting the heat that could be released by hydrated phases precipitation, a hydration degree of CA can be estimated by normalizing the cumulative heat Q by the CA dissolution enthalpy $\Delta_{diss}H$ (Figure 72).

$$CaAl_2O_4 + 4\,H_2O \rightleftharpoons Ca^{2+} + 2\,Al(OH)_4^- \qquad \Delta_{diss}H = -466.6\ J/g \qquad (15)$$

When only the dissolution of anhydrous CA was considered to be contributing to the heat release, hydration degrees exceeding 100 % were obtained. Therefore, the enthalpy of reaction ($\Delta_rH$) of CA as reported by Klaus *et al.* was applied to estimate the hydration degree in this

section. Indeed, Klaus *et al.* calculated an enthalpy of reaction by assuming a simultaneous hydration of the anhydrous CA and precipitation of hydrates. The resulting $\Delta_r H$ for the hydration of CA was found to be equal to -693 J/g.

The plots in Figure 72 shows that increasing the w/c ratio from 0.375 to 0.600 would raise the hydration degree of CA 7 days after mixing from 54 % up to 79 %.

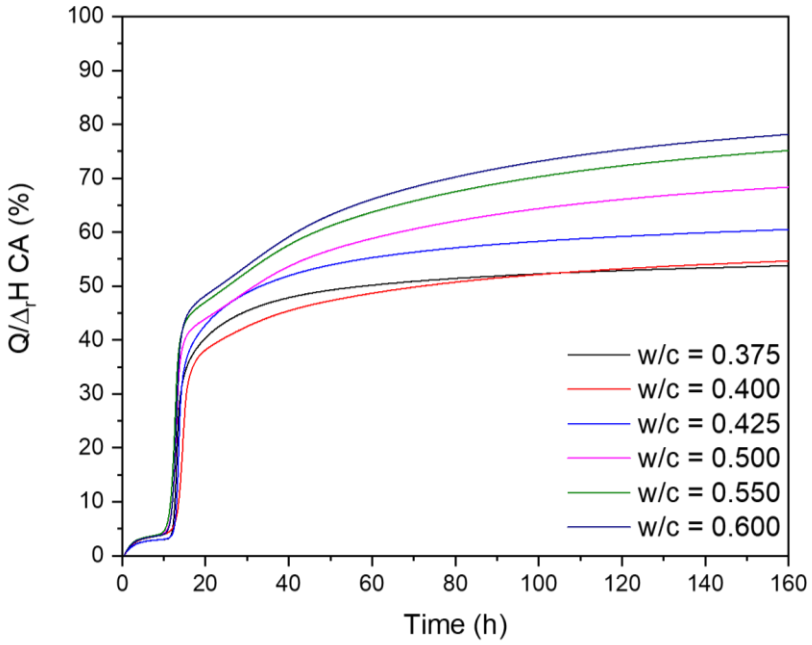


**Figure 72 : Influence of the w/c ratio on the degree of hydration of the pastes at 7 d, assuming that the heat release is due to the dissolution of anhydrous CA and precipitation of hydrates – 25 °C.**

To assess the relevance of such a hypothesis, mineralogical assemblages of pastes 7 days after mixing were characterized by using TGA and XRD in order to quantify the amount of bound water and identify the crystalline phases in presence. The mineralogical composition of a sample elaborated with a w/c ratio of 0.50 was further investigated by $^{27}$Al NMR spectroscopy.

### 1.1.2. Influence of w/c ratio on mineralogical assemblages after 7 days of hydration

The pastes prepared with different w/c ratios were analyzed 7 days after initial mixing by using XRD analysis, TGA and $^{27}$Al-NMR analysis in order to identify the hydration products and to quantify bound water and mineralogical composition.

Figure 73 shows the XRD patterns of the hydrated CA pastes at 25 °C for 7 days. Whatever the w/c ratio used, $CAH_{10}$, $C_2AH_{7.5}$, $AH_3$ (gibbsite) and $C_3AH_6$ were identified. In addition, in all of the pastes, unreacted CA was detected.

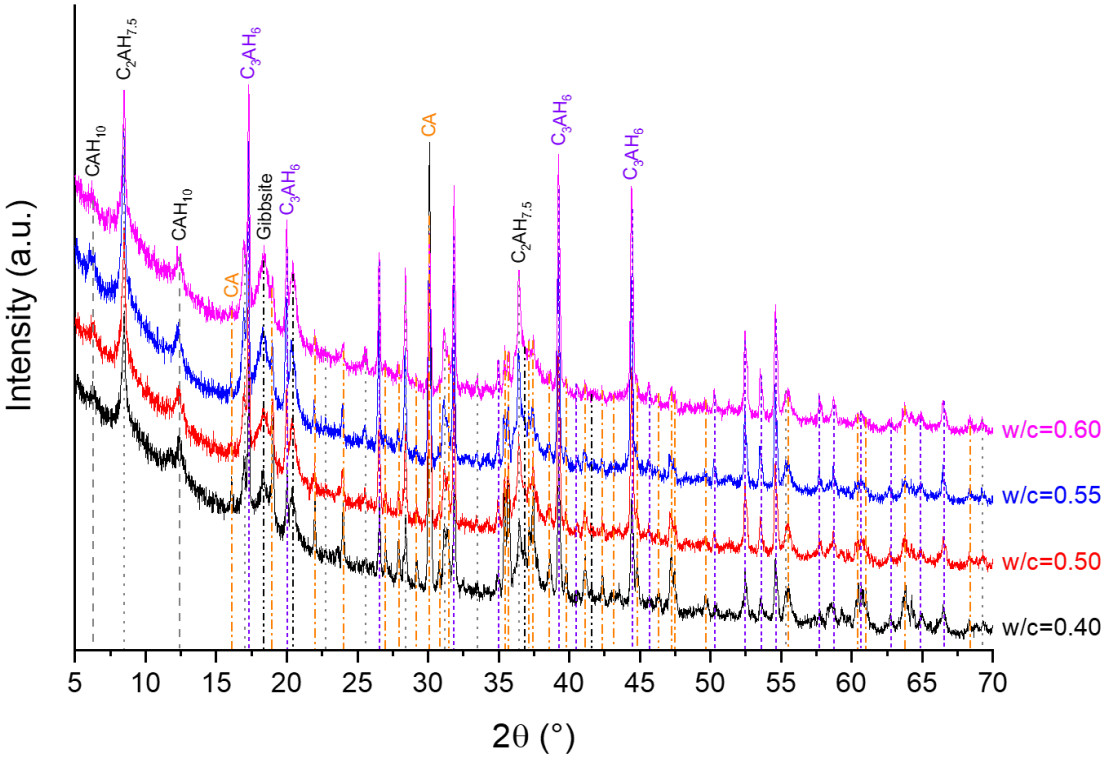


**Figure 73 : XRD patterns representing hydration products after hydrating CA with w/c ratios ranging from 0.4 to 0.6 at 25 °C for 7 days.**

Figure 74 shows the TGA and DTG curves of these systems.

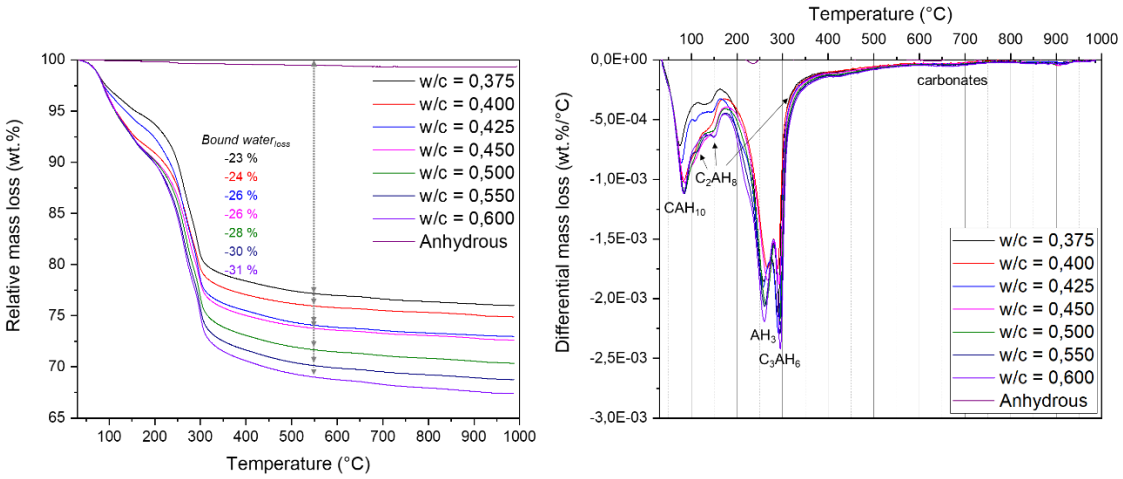


**Figure 74 : TGA and DTG curves obtained from hydrated CA pastes with different w/c ratios at 25 °C for 7 days. On the TGA curves, the arrow shows the mass loss in the range of temperatures between 30 and 550 °C.**

Several thermal events were observed on the thermograms of the pastes and assigned based on XRD results as follows:

- Below 120 °C: decomposition of metastable $CAH_{10}$ and/or amorphous $AH_3$ hydrates [9-11],
- At 110, 170 and 300 °C: decomposition of metastable $C_2AH_8$ proceeding in three main steps [12],
- Close to 250 °C : a main DTG peak related to the decomposition of $AH_3$ [11, 13, 14],
- At the temperature ranges of 300 – 330 °C: decomposition of stable $C_3AH_6$ [6, 15, 16].

From TG analysis, the amount of bound water after 7 days was defined as being equal to the weight loss measured from 30 up to 550 °C. This parameter is plotted as a function of the w/c ratio in Figure 75.

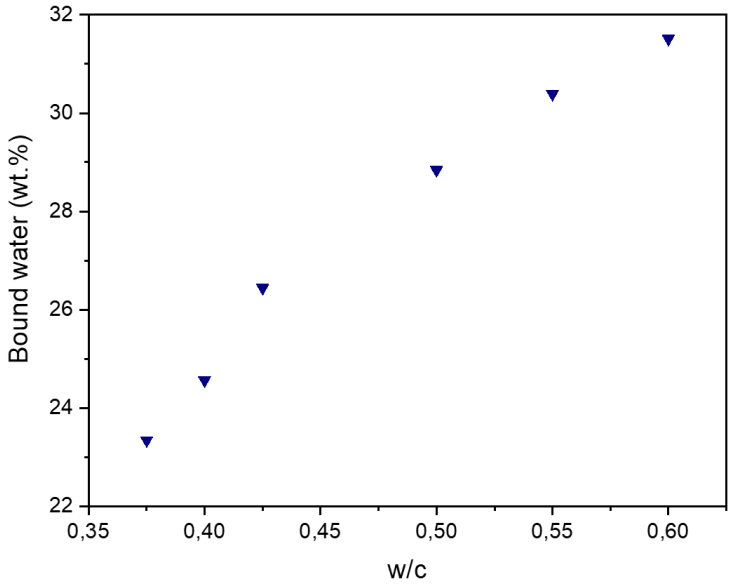


**Figure 75 : Bound water amount of CA pastes with different w/c ratios hydrated at 25 °C for 7 days.**

As the w/c ratio increased, the amount of bound water also increased progressively. The bound water amounts varied between 23 to 31 % for w/c ratios from 0.375 to 0.600. Noticeably, there was a linear relationship between the bound water content and the cumulative heat measured after 7 days of hydration, as illustrated in Figure 76. Also, a similar mineralogical assemblage, whatever the w/c ratios, was evidenced by using XRD analysis.

Based on the calculation of the theoretical amounts of hydrates in the pastes after complete hydration of CA reported by Hueller [4], the theoretical amount of stable $C_3AH_6$ and $AH_3$ phases from a total hydration of 1 g anhydrous CA phase was found to be equal to 0.80 g and 0.66 g respectively, with a $C_3AH_6/AH_3$ molar ratio of 0.5. Also, the corresponding water amount to reach a complete hydration of anhydrous CA was calculated as 0.46 g (46 %) by using reaction equation (16):

$$3\,CA + 12\,H \rightleftharpoons C_3AH_6 + 2\,AH_3 \qquad (16)$$

According to the bound water contents shown in Figure 52, it was suspected that none of the pastes was completely hydrated as confirmed by the presence of unreacted CA and of metastable phases evidenced by XRD.

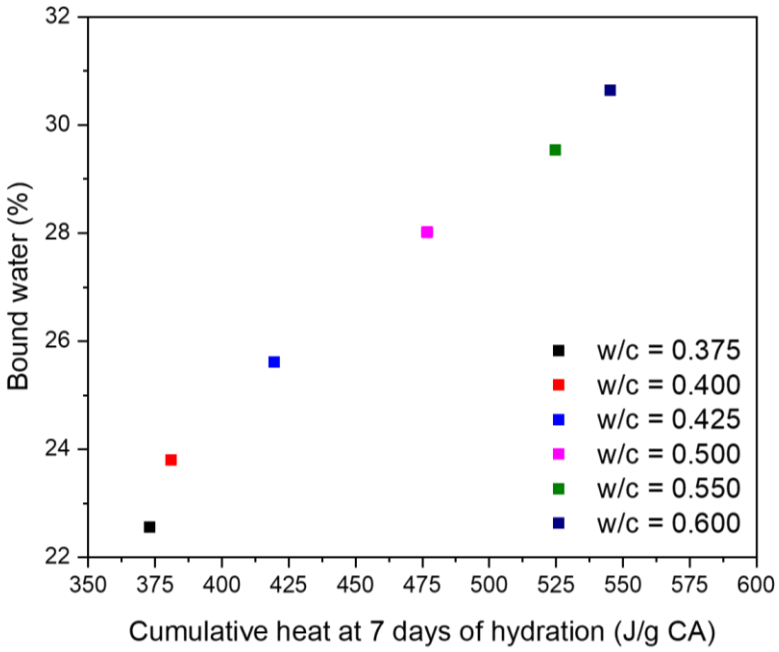


**Figure 76 : Bound water content of CA pastes from TGA results as a function of the maximum cumulative heat after reaching a plateau.**

Following TGA and powder XRD analysis, $^{27}$Al MAS-NMR spectrometry was performed on a 7 day-old CA sample prepared with a w/c ratio of 0.50 in order to determine as quantitatively as possible its mineralogical composition. The collected spectrum and its corresponding decomposition are shown in Figure 77 and Figure 78.

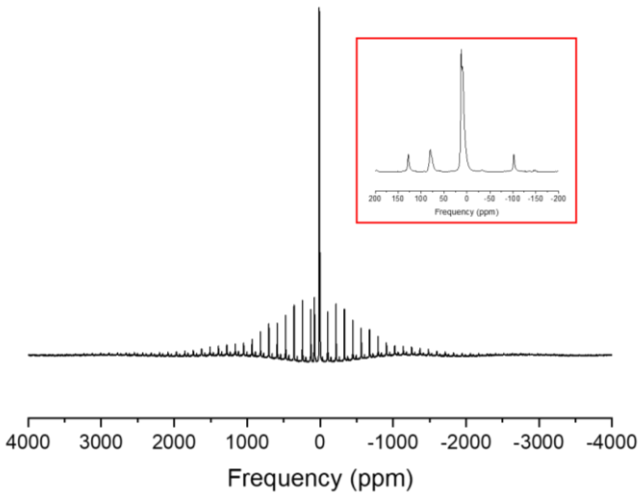


**Figure 77 : $^{27}$Al MAS-NMR spectrum of the 7 d-old CA paste (w/c = 0.50).**

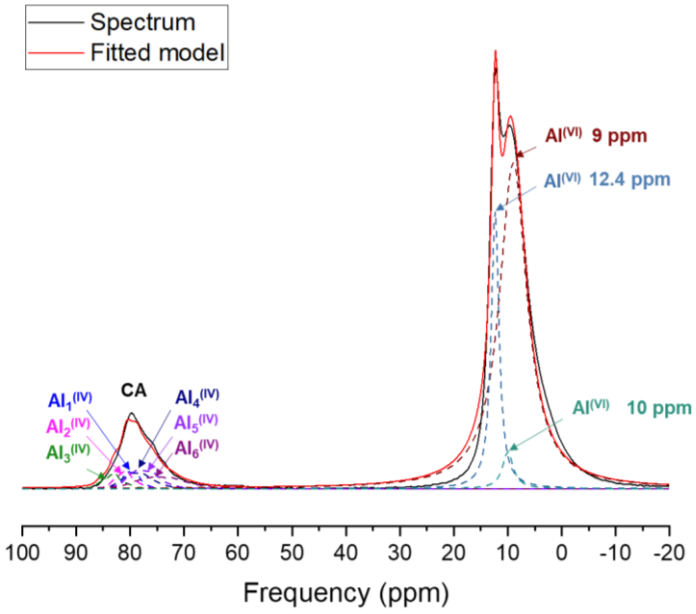


**Figure 78 : Decomposition of the $^{27}$Al MAS-NMR spectrum central bands of the 7 d-old CA paste (w/c = 0.5).**

According to the literature, the six tetrahedral Al sites in CA occur at 81.9, 83.8, 86.3, 82.8, 81.6 and 81.2 ppm (the precision was about ±0.2 ppm on the last number of each given value) for $Al_1^{(IV)}$, $Al_2^{(IV)}$, $Al_3^{(IV)}$, $Al_4^{(IV)}$, $Al_5^{(IV)}$ and $Al_6^{(IV)}$ respectively [17]. The fitted model resulting from these six Al sites was in agreement with the experimental spectrum attributed to CA phase in this study (Chapter 2, Figure 39b). From the decomposition of the $^{27}$Al NMR spectrum of the 7 d-old CA paste (w/c = 0.5), the following hydrates were identified with the data obtained from literature as summarized in Table 19:

- $CAH_{10}$
- $AH_3$
- $C_2AH_8$
- $C_3AH_6$

In the fitted model (Figure 78), chemical shifts at 9 ppm were attributed to the octahedrally coordinated Al site in gibbsite and $C_2AH_8$, while chemical shifts at 10 ppm and 12.4 ppm were assigned to $CAH_{10}$ and $C_3AH_6$ respectively. An attempt to quantify the amount of $C_2AH_8$ phase using the peaks with chemical shifts at 10.3 ppm and 66 ppm [12, 18, 19] was not successful for two reasons. *(i)* It was hard to distinguish the octahedral resonances of the different hydrates from each other because of their very close chemical shifts. *(ii)* The tetrahedrally coordinated Al site of $C_2AH_8$ phase at 66 ppm could not be observed because of insufficient resolution of the spectra. By taking into account these limitations, the peak at 9 ppm was attributed to gibbsite and $C_2AH_8$ phases without distinguishing one from the other. While the tetrahedral resonances of well-crystallized CA were modelled considering a second-order powder spectrum for the

central transition, the resonances of the hydrates were modelled with Lorentzian dipolar broadening because of the weak quadrupolar coupling.

**Table 19 : Summary of chemical shifts, intensities and quadrupolar parameters corresponding to the identified hydrates from the decomposition of the $^{27}$Al MAS-NMR spectrum of the 7 d-old CA paste (w/c = 0.5).**

| Phase | Site | $\delta_{iso}$ (ppm) | Model | Peak intensity | Quadrupole coupling constant, $C_Q$ (MHz) | Asymmetry parameter, η | Width | Reference |
|---|---|---|---|---|---|---|---|---|
| CA | $Al_1^{(IV)}$ | 82 | Q mas 1/2 | 3897 | 2.5 | 0.20 | - | [17] |
| | $Al_2^{(IV)}$ | 84 | Q mas 1/2 | 3971 | 2.6 | 0.75 | - | |
| | $Al_3^{(IV)}$ | 86 | Q mas 1/2 | 3500 | 2.6 | 0.95 | - | |
| | $Al_4^{(IV)}$ | 83 | Q mas 1/2 | 3652 | 3.3 | 0.53 | - | |
| | $Al_5^{(IV)}$ | 82 | Q mas 1/2 | 4300 | 3.4 | 0.39 | - | |
| | $Al_6^{(IV)}$ | 81 | Q mas 1/2 | 2686 | 4.3 | 0.47 | - | |
| $CAH_{10}$ | $Al^{(VI)}$ | 10 | Lorentzian | 2515 | - | - | 2.3 | [17] |
| $AH_3$ | $Al^{(VI)}$ | 9 | Lorentzian | 21820 | - | - | 6.2 | [20, 21] |
| $C_3AH_6$ | $Al^{(VI)}$ | 12.4 | Lorentzian | 18653 | - | - | 1.8 | [22] |

Such a decomposition of the spectrum yields the mineralogical composition described in Table 20.

**Table 20 : Quantification of Al-containing phases in the 7 d-old CA paste (w/c = 0.5).**

| Phase | Chemical shift (ppm) | Al atomic fraction (%) | Phase weight fraction (wt. %) | Corresponding bound water content (wt. %) |
|---|---|---|---|---|
| **CA** | 81.9/83.8/86.3/82.8/81.6/81.2 | 14 | 11 | - |
| **$CAH_{10}$** | 10 | 3 | 5 | 3 |
| **$AH_3$** | 9 | 67 | 53 | 18 |
| **$C_3AH_6$** | 12.4 | 16 | 31 | 9 |

Most of the CA anhydrous phase (86 %) was hydrated after 7 days of hydration. In hydrated compounds, the $AH_3$ phase content represented 53 wt. % of the sample. Small amounts (below

the margin of error of the decomposition) of a transient $CAH_{10}$ phase were detected. As a second main hydrate, the stable hydrogarnet $C_3AH_6$ with an amount of 31 wt. % was evidenced by the spectrum decomposition. Moreover, this mineralogical composition yielded a bound water content of about 30 wt. %. Such a value was consistent with the 28 wt. % measured by TGA, giving confidence to the NMR mineralogical analysis.

Still according to this mineralogical composition, the remaining anhydrous CA content was equal to 14 %. A hydration degree of 86 % would thus be achieved 7 days after mixing pure water and the studied CA synthetic phase. Based on calorimetric data and assuming that only dissolution was contributing to the heat release, a hydration degree of 70 % was estimated in the previous section. Such a difference could result from the uncertainty on both measurements but was nevertheless significant. It could result from the fact that the spinning side band pattern was not considered in the NMR fit thus underestimating the amount of anhydrous phases (i.e. CA).

Moreover and despite the relative consistency of the results obtained and presented in the above section, the mineralogical assemblage estimated by using $^{27}Al$ NMR spectrum could be seen as surprising. The $C_3AH_6/AH_3$ molar ratio was found be equal to 0.24. This value was significantly lower than that expected assuming the formation of $C_3AH_6$ according to reaction (2) (0.5). Again, either this resulted in errors in decomposition of the NMR spectrum, or this suggested that balance equation (2) was not adapted to describe the early stages of hydration of CA. To get more information on the CA hydration process, the sequence of precipitation of the hydrates was investigated for a CA paste at w/c) 0.5 during the first 7 hours of hydration, corresponding to the induction period of hydration.

## 1.2. Evolution of mineralogical assemblages during the first seven hours of CA paste with a w/c ratio of 0.5

Hydration stoppages were performed on a paste with a w/c ratio of 0.5 after the following periods of hydration: 30, 60, 90, 120, 150, 180, 240, 300 and 420 min.

The powder XRD patterns corresponding to the different characterization times are shown in Figure 79.

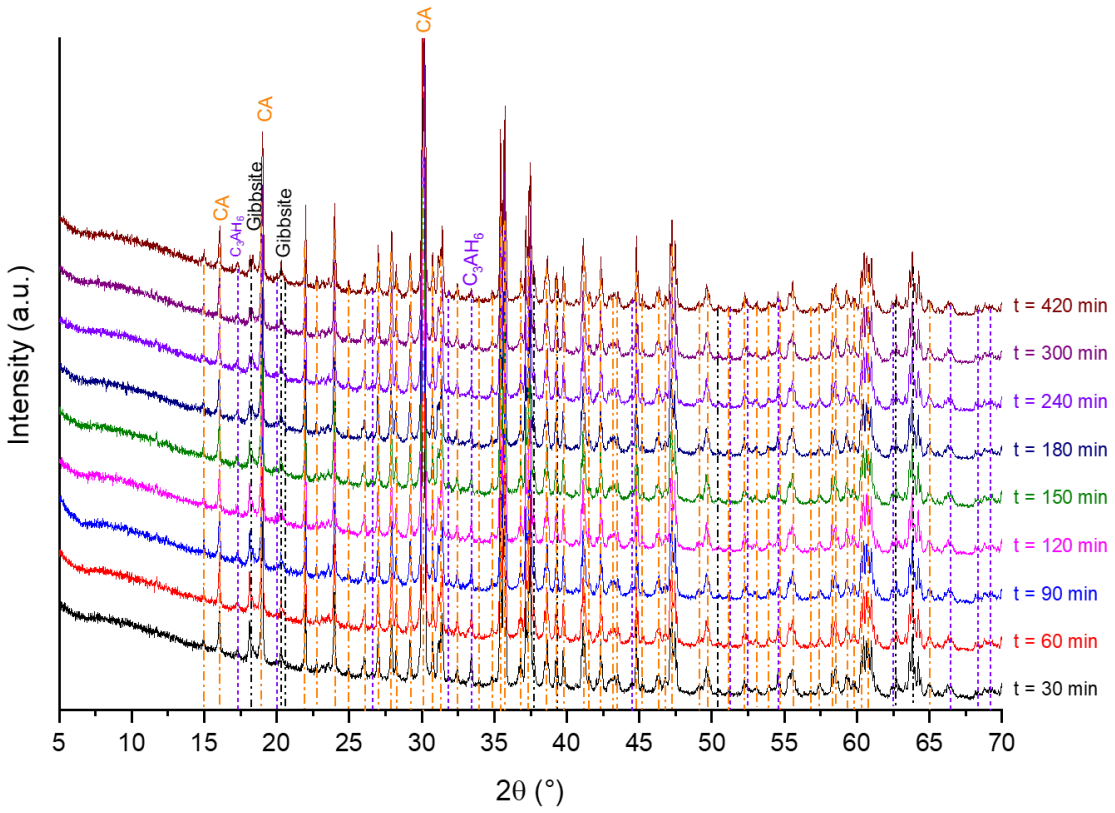


**Figure 79 : XRD patterns of the CA paste with a w/c ratio of 0.5 after increasing periods of hydration.**

During the induction period studied in these experiments, precipitation of hydrated phases could not be clearly evidenced by XRD. Small amounts of gibbsite and of $C_3AH_6$ could be evidenced on the XRD patterns, but probably resulted from the fact that the CA sample used for the experiments was slightly hydrated, as shown in chapter 2 (see Figure 35).

From the TGA analysis (Figure 80) of samples stopped during the induction period, an increasing mass loss was observed in the temperature range from 50 up to 150 °C. Such a range of decomposition could correspond to the presence of an amorphous aluminium hydroxide phase [9, 23] or of poorly crystallized $CAH_{10}$ [10, 24].

The presence of $AH_3$ was clearly evidenced by the weight loss at 250 °C for all the characterization times, but its amount remained almost constant.

The asterisk in the DTG curves of Figure 80 represents a questioned compound with a main thermal decomposition at 430 °C. In the literature, the decomposition of portlandite ($Ca(OH)_2$) was reported around 450 °C [25] and Kumar *et al.* [26] cited a decomposition of aluminium hydroxide with an endothermic peak at 360-430 °C. According to the TGA results, the bound water content evolved from 2 % to 3 % as shown in Figure 80.

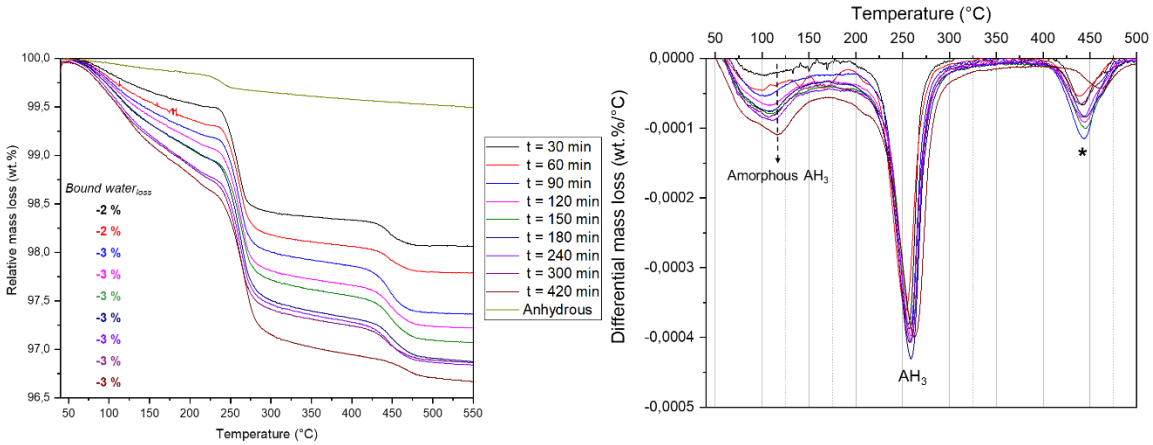


**Figure 80 : TGA and DTG curves obtained from hydrated CA paste with a w/c of 0.5 at 25 °C after increasing periods of hydration. On the TGA curves, the arrow shows the mass loss in the range of temperatures between 33 and 550 °C.**

The $^{27}$Al MAS-NMR spectra of the pastes with a w/c ratio of 0.5 hydrated at 25 °C for different periods of time but still during the induction period, are shown in Figure 81. Based on the phase assignment by XRD, the contents of unreacted CA, gibbsite and hydrogarnet were estimated by decomposing the spectra (Table 21). The amount of unreacted CA, 95 wt. % at 0.5 h, decreased to 91 wt. % after 7 h of hydration. The amount of gibbsite slightly increased over time from 3 to 5 wt. %. The presence of $C_3AH_6$, previously evidenced by XRD, was suspected as a minor phase from the NMR analysis.

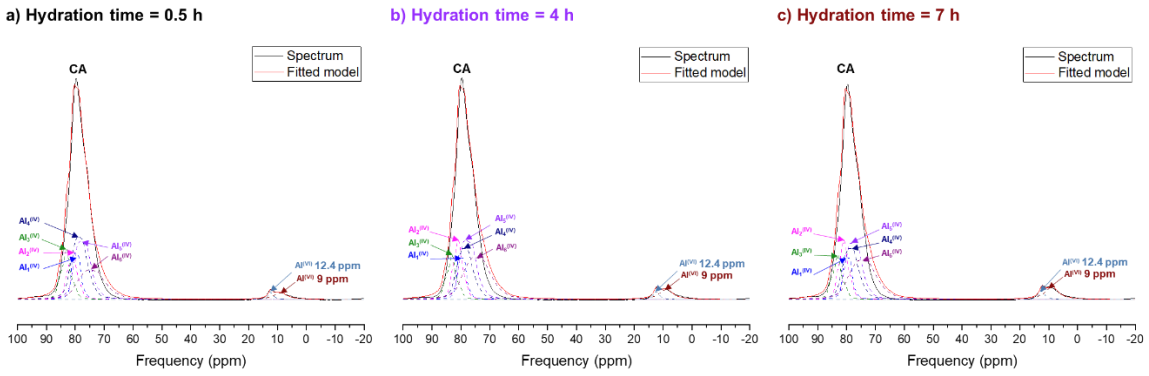


**Figure 81 : $^{27}$Al solid-state NMR spectra decomposed into the identified phases for the CA paste (w/c = 0.5) at different characterization times: a) 0.5 h, b) 4 h and c) 7 h.**

**Table 21 : Quantification by $^{27}$Al NMR of Al phases present in the CA paste (w/c = 0.5) at three different characterization times.**

| Hydration stoppage time (h) | Phases | Chemical shift (ppm) | Al atomic fraction (%) | Phase weight fraction (wt. %) | Corresponding bound water content (wt. %) |
|---|---|---|---|---|---|
| **0.5** | CA | 81.9/83.8/86.3/82.8/81.6/81.2 | 96 | 95 | - |
| | $AH_3$ | 9 | 3 | 3 | 1 |
| | $C_3AH_6$ | 12.4 | 1 | 2 | 1 |
| **4** | CA | 81.9/83.8/86.3/82.8/81.6/81.2 | 95 | 94 | - |
| | $AH_3$ | 9 | 4 | 4 | 1 |
| | $C_3AH_6$ | 12.4 | 1 | 2 | 1 |
| **7** | CA | 81.9/83.8/86.3/82.8/81.6/81.2 | 94 | 93 | - |
| | $AH_3$ | 9 | 5 | 5 | 2 |
| | $C_3AH_6$ | 12.4 | 1 | 2 | 1 |

From TGA, XRD and NMR results, it can be concluded that from 0.5 h to 7 h of hydration, the mineralogical assemblage was mainly composed of unreacted CA. Small amounts of $AH_3$ and $C_3AH_6$, probably resulting from the fact that the reactant (CA) was slightly hydrated prior to the experiment were detected. A compound that decomposes at 430 °C was also evidenced. Its content seemed to increase slightly in the investigated period of time.

The corresponding total bound water amount for these hydrates was calculated to be equal to 2 wt. % after 0.5 h and 4 h of hydration, and to 3 wt. % after 7 h of hydration. These results were also consistent with TGA results where the increase in bound water was associated to the presence of small amounts of hydrates.

**To sum up:**

From TGA, XRD and NMR results, it was concluded that after 7 days of hydration at 25 °C, the mineralogical assemblage was mainly composed of $C_3AH_6$ and $AH_3$, with the presence of smaller amounts of unreacted CA, $CAH_{10}$ and $C_2AH_8$.

The heat profiles of CA hydration showed an induction period before the massive precipitation of hydrates in agreement with data from the literature. The hydration degree reached after 7 days of hydration was assessed to increase from 54 % to 79 % when the w/c ratio of the paste increased from 0.375 to 0.6.

Additional experiments were performed using CA suspensions in order to investigate the evolution of the aqueous phase composition with ongoing hydration.

## 2. Hydration study of CA suspensions at early age

As for $CA_2$, the hydration of CA was studied under diluted conditions by using a w/c ratio ranging from 12.5 up to 75 in order to collect the liquid fraction and measure its composition evolution as a function of time. The influence of the w/c ratio on the course of CA hydration was firstly evaluated by using electrical conductivity monitoring and by comparing the mineralogical assemblages obtained 24 hours after mixing. The composition of the solution was then measured as a function of time for a w/c ratio of 25.

### 2.1. Influence of the w/c ratio on the early age hydration of CA elaborated in suspensions

#### 2.1.1. Electrical conductivity monitoring

Suspensions containing CA were prepared with decarbonated Milli-Q water (18.2 MΩ.cm) using different w/c ratios, namely, 12.5, 25, 50 and 75. The evolution of the electrical conductivity with ongoing hydration was measured at 25 °C using a special conductivity cell with an acquisition time of 5 min (Figure 82).

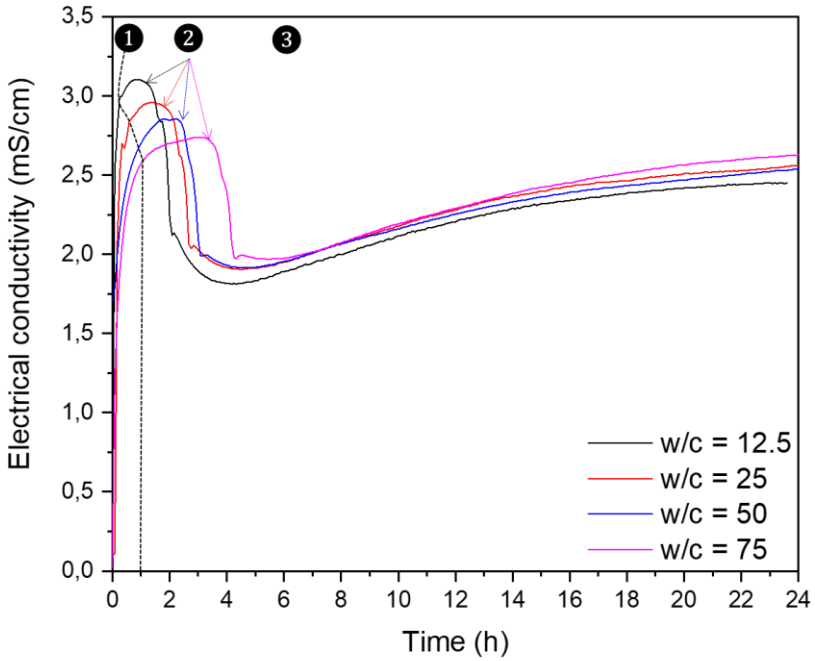


**Figure 82 : Electrical conductivity monitoring of CA suspensions prepared with different w/c ratios at 25 °C. The arrows show the end of the assigned period.**

The evolution of the electrical conductivity can be described by a succession of three stages in all cases:

- 1st stage: the ionic conductivity increases rapidly, likely because of the dissolution of anhydrous CA;
- 2nd stage: After reaching a maximum, the conductivity stabilizes for a short time before decreasing sharply;
- 3rd stage: After a drop, the conductivity increases over time.

Characteristic times and conductivity values corresponding to these three periods are summarized in Table 22.

**Table 22 : Summary of characteristic parameters defined on the electrical conductivity curves of CA suspensions.**

| Water-to-solid ratio | Time of maximum conductivity (h) | Maximum conductivity value (mS/cm) | Start of the plateau (h) | End of the plateau (h) | Conductivity value at the end of monitoring (mS/cm) |
|---|---|---|---|---|---|
| **12.5** | 1 | 3.10 | 0.4 | 1.5 | 2.45 |
| **25** | 1.5 | 2.96 | 0.6 | 2 | 2.56 |
| **50** | 2 | 2.85 | 1 | 2.5 | 2.55 |
| **75** | 3 | 2.74 | 1.2 | 3.6 | 2.63 |

Comparing the electrical conductivity of the different diluted suspensions revealed different rates of hydration, even though the curve profiles were very similar. As the w/c ratio increased, the following points were noticed:

- increase in the period of time needed to reach the maximal conductivity value during the 1st stage,
- decrease of the maximal conductivity value,
- longer plateau associated to the stable electrical conductivity values during the 2nd stage,
- higher conductivity values for the beginning of the 3rd stage
- higher conductivity values after 24 h of hydration.

Mineralogical assemblages of the solid fractions of suspensions collected 24 hours after mixing were compared for each of the studied w/c ratio.

### 2.1.2. Characterization of the solid fraction of suspensions

According to the XRD patterns of the solid fraction of suspensions hydrated for 24 h at 25 °C, the following products were identified in solid fractions whatever the w/c ratio (Figure 83):

- Small amounts of $CAH_{10}$,

- $C_2AH_{7.5-8}$,
- $AH_3$ indexed as gibbsite,
- hemicarboaluminate $C_4A\check{C}_{0.5}H_{12}$,
- monocarboaluminate $C_4A\check{C}H_{11}$,
- Calcite $CaCO_3$,
- Unreacted CA.

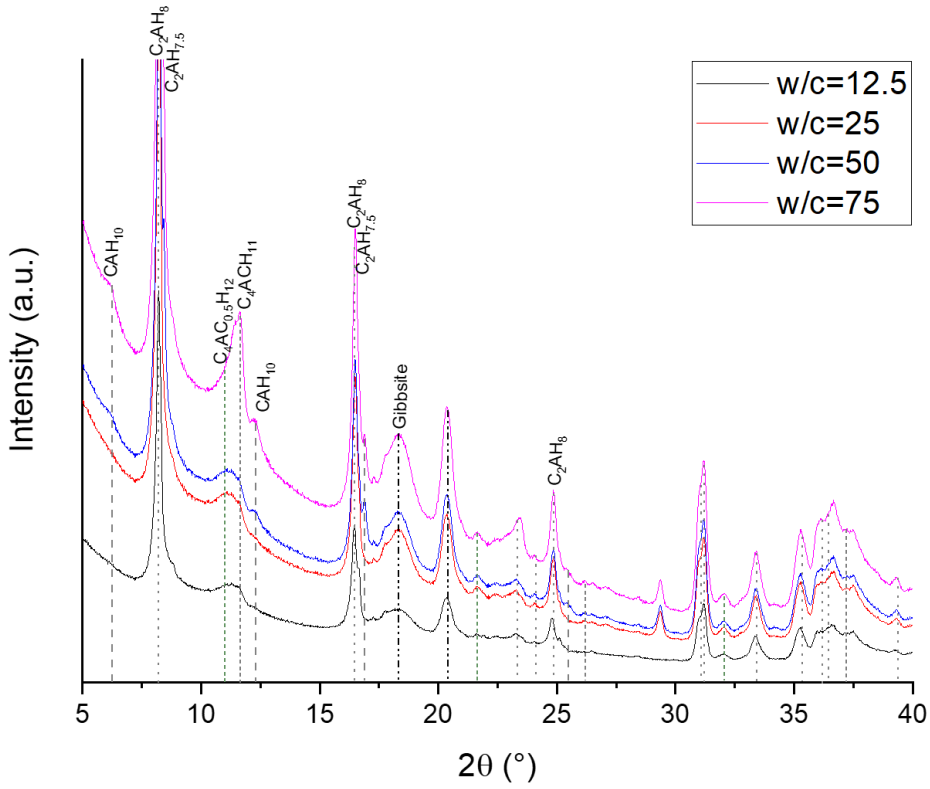


**Figure 83 : XRD patterns representing mineralogical assemblages of CA suspensions after 24 hours of hydration at 25 °C.**

The TGA results are presented in Figure 84. Several thermal events were observed and interpreted as follows.

The first endothermic peak was due to the decomposition of $CAH_{10}$ and probably amorphous aluminium hydroxide at around 120 °C [27]. In all of the DTG curves, it was seen that there was a progressive weight loss at around 110, 170 and close to 300 °C due to the dehydration of $C_2AH_{7.5-8}$ [12]. The decomposition of $AH_3$ at 250 °C followed a shoulder at around 210 °C attributed to monocarboaluminate $C_4A\check{C}H_{11}$ in all of the samples [27-29]. The thermal decomposition of hemicarboaluminate was observed near 450 °C [30]. The last peaks at around 700 °C were due to the release of $CO_2$ during the thermal decomposition of carbonated phases. Also, the presence of calcite, which was previously evidenced by XRD was pointed out with

mass losses in the temperature range 700–850 °C [30]. Note that it was difficult to distinguish the hydration products due to their overlapping decomposition intervals.

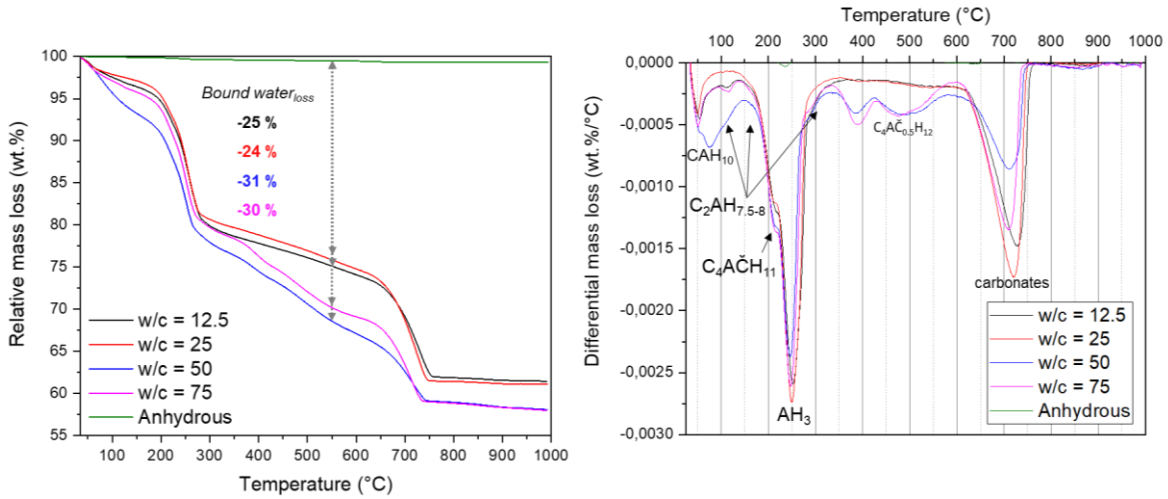


**Figure 84 : TGA and derivative TGA results obtained from CA suspensions with various w/c ratios after 24 hours of hydration at 25 °C.**

Figure 84 shows the mass loss content determined experimentally using TG on the solid fraction of the suspensions with different w/c ratios. Here, the calculated bound water content was related to the mass loss below 550 °C. The results for the suspensions with a w/c of 12.5, 25, 50 and 75 were 25, 24, 31 and 30 % respectively.

## 2.2. Course of CA hydration during the first 24 hours – w/c = 25

In order to investigate the early age hydration of CA phase, a suspension with a w/c of 25 was monitored by using an electrical conductivity probe during the first 7 hours at 25 °C. The chemical evolution of the liquid fraction composition and mineralogical assemblages were characterized after fixed periods of hydration time as follows: 30, 60, 90, 120, 150, 180, 240, 300 and 420 min. The fixed periods of time to characterize the mineralogical assemblage evolution are symbolized on the corresponding ionic conductivity curve in Figure 85.

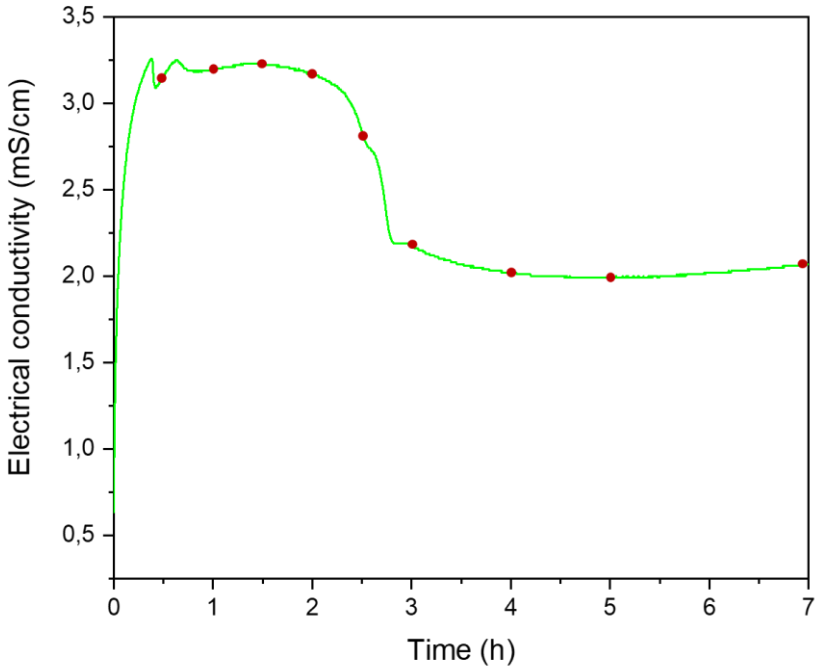


**Figure 85 : Definition of characterization times (red dots) based on the variation of the electrical conductivity during CA hydration with a w/c = 25.**

### 2.2.1. Characterization of the solid fraction of suspensions

After each of the described periods, a hydration stoppage was carried out and the collected solid fraction was characterized by XRD analysis, TGA and $^{27}$Al MAS-NMR spectroscopy.

Diffractograms of the collected solid fractions are plotted in Figure 86. XRD patterns remained unchanged until 150 min. From 180 min, the precipitation of $C_2AH_{7.5}$ and of aluminium hydroxide was observed and accompanied by a decrease in the CA peak intensity.

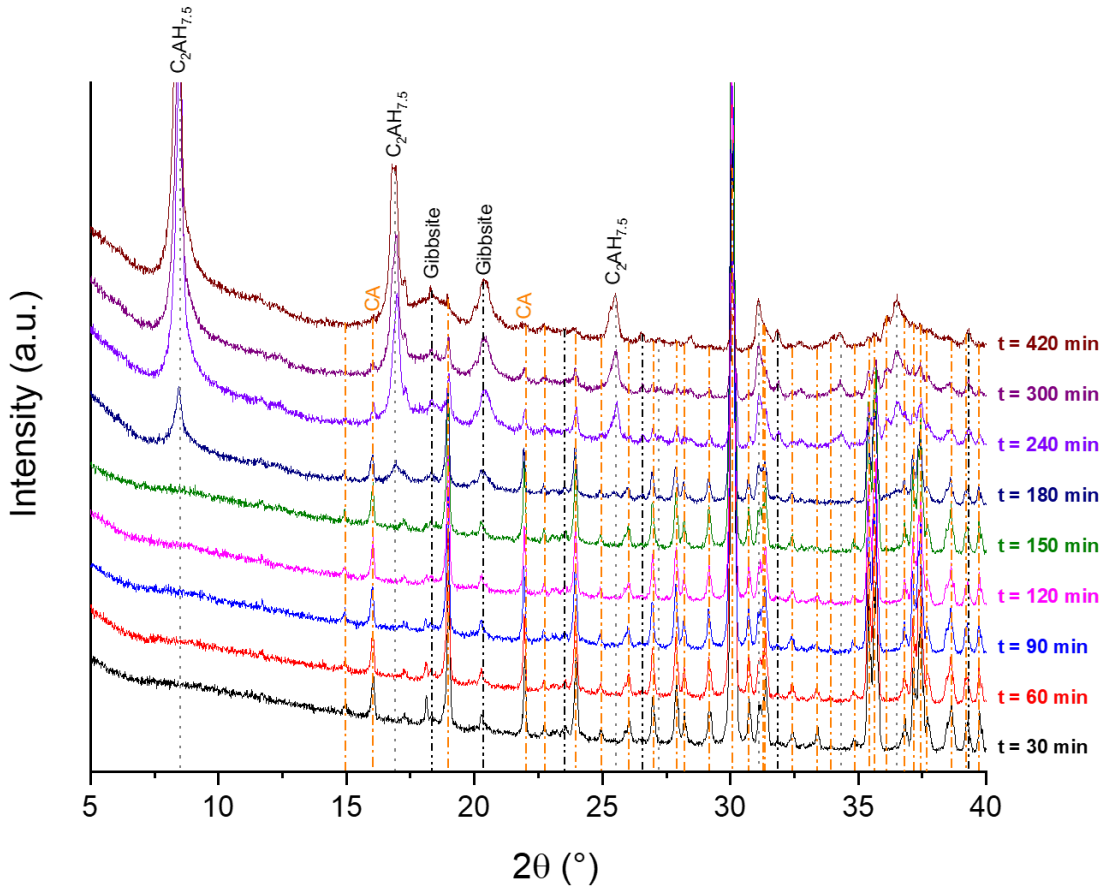


**Figure 86 : XRD patterns of the solid fractions of CA suspension with a w/c ratio of 25 after increasing periods of hydration at 25 °C.**

Figure 87 shows the DTG curves at the selected characterization times for the CA suspension with a w/c ratio of 25. An increasing mass loss was observed in the temperature range from 50 up to 150 °C. Such a range of decomposition could correspond to the presence of an amorphous aluminium hydroxide phase [9, 23] or of poorly crystallized $CAH_{10}$ [10, 24]. After 3 h of hydration, the decomposition of metastable $C_2AH_8$ was revealed by three mass losses first around 110 °C, around 170 and 300 °C. It must be noted that $C_2AH_8$ dehydrates to $C_2AH_{7.5}$ within a few hours of hydration [12]. The presence of both hydrates in the solid phase increased steadily with time after 3 h of hydration. From the mass loss in the temperature range of 250–280 °C, the presence of $AH_3$ was identified from 0.5 h of hydration [6]. In samples hydrated more than 2.5 h, the broadening of the derivative curves indicated the dehydration of $C_2AH_8$ and/or formation of $C_2AH_{7.5}$ and monocarboaluminate with mass losses in the temperature range 160–210 °C. On the other hand, the overlapping of peaks of $C_2AH_{7.5}$ and monocarboaluminate could be the reason for the presence of the two peaks in the range 215–270 °C, instead of one peak centered at 250 °C for $AH_3$.

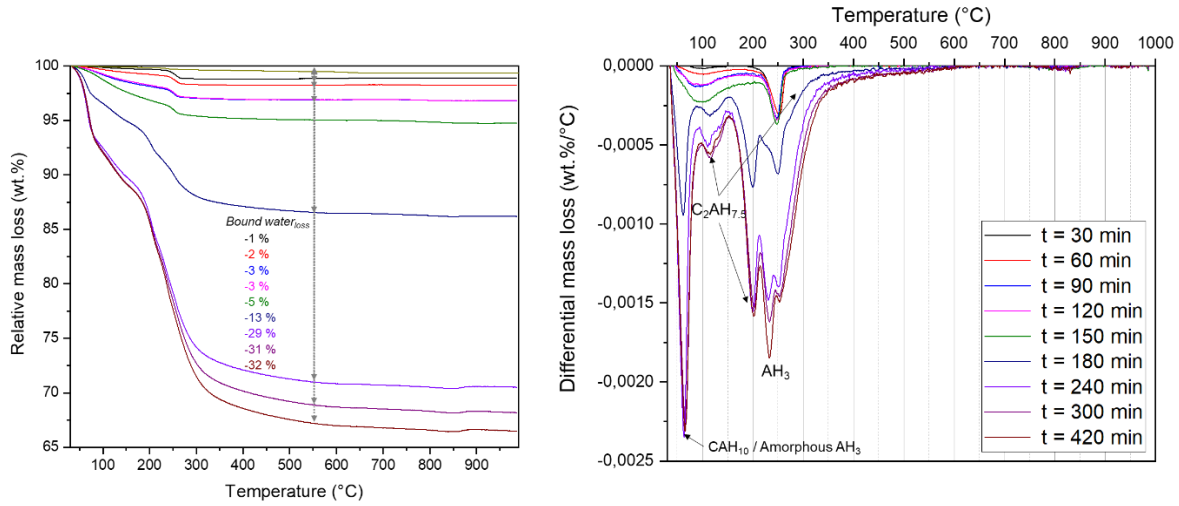


**Figure 87 : TGA and DTG curves obtained from CA suspension with a w/c ratio of 25 after increasing periods of hydration at 25 °C.**

The decomposition of hydrates occurred below 500 °C. Thus, the bound water content was calculated using the weight loss between 30 °C and 550 °C. Figure 88 shows its evolution with time. The rise at 3 h of hydration reflected the beginning of massive precipitation of hydrates.

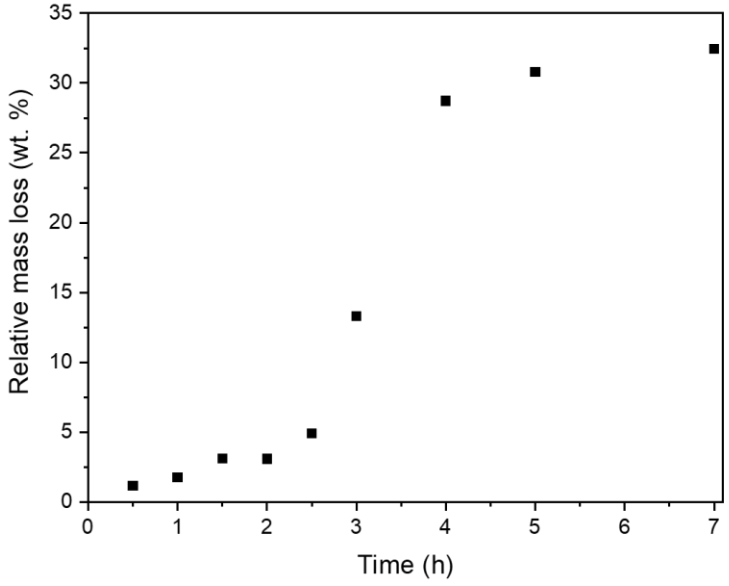


**Figure 88 : Mass loss between 30 and 550 °C of the solid fraction of the CA suspension with a w/c of 25.**

Some of the collected solid fractions were also characterized by $^{27}$Al MAS-NMR spectroscopy in order to estimate their phase composition. The collected spectra and their corresponding decompositions are shown in Figure 89.

The six tetrahedral Al sites in CA occurred as discussed previously between 86.6 and 81.3 ppm [17]. The fitted model resulting from these six Al sites was in agreement with the experimental spectrum attributed to CA in this study. In addition, three hydrates were evidenced regardless of the hydration stoppage time (Table 23):

- $C_2AH_{7.5}$
- $AH_3$
- $C_4AČH_{11}$

The presence of $C_3AH_6$ was also suspected in the 0.5 h-, 1.5 h- and 2 h-old samples. It likely originated from the impurities initially present in the reactant (see Figure 35 for the XRD pattern of CA phase) and not from the hydration process.

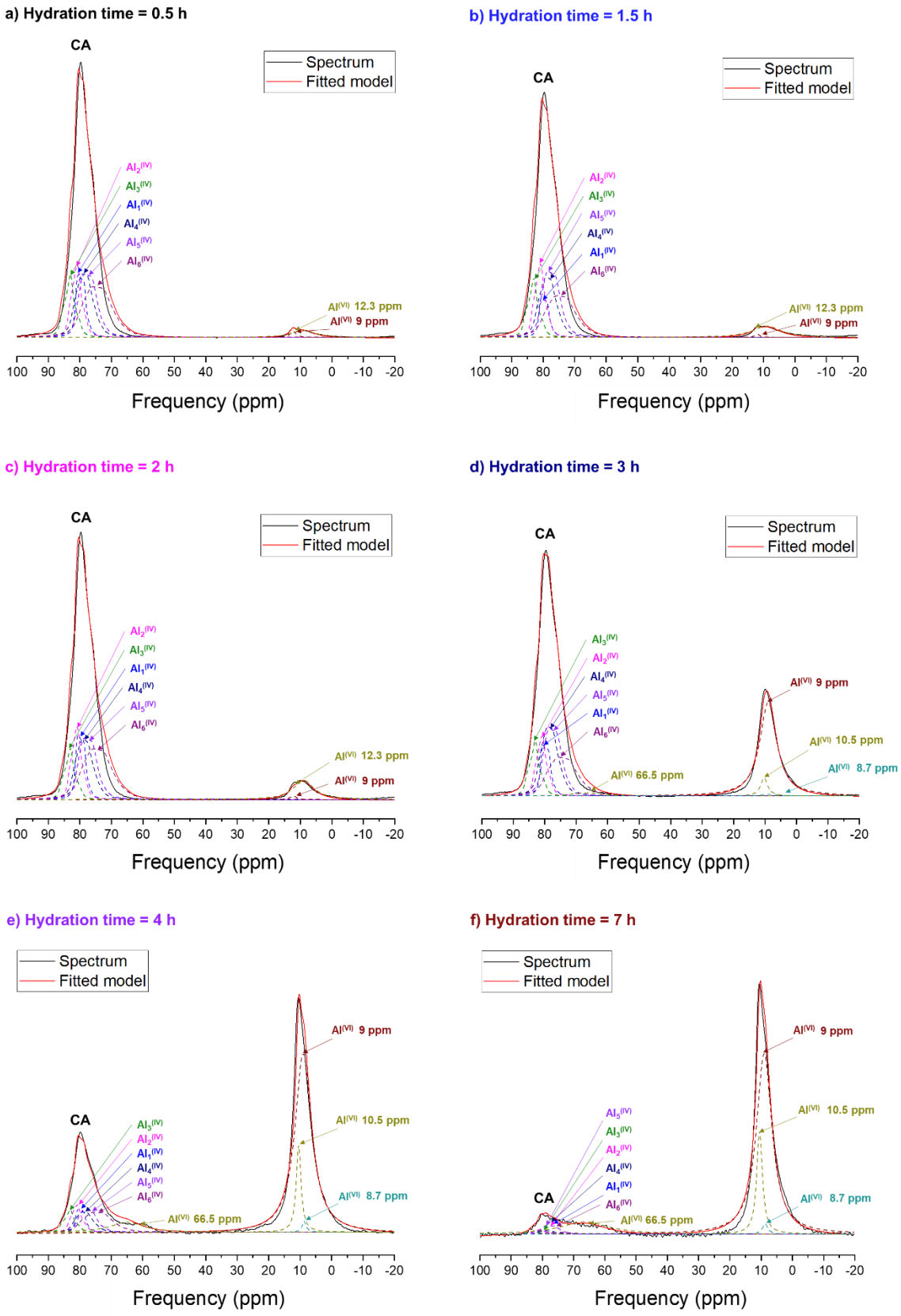


**Figure 89 : $^{27}$Al NMR spectra of CA suspension with a w/c of 25 at different hydration times : a) 0.5 h, b) 1.5 h, c) 2 h, d) 3 h, e) 4 h and f) 7 h.**

**Table 23 : Summary of chemical shifts, intensities and quadrupolar parameters corresponding to the identified hydrates from the decomposition of the $^{27}$Al MAS-NMR spectrum of the CA suspension at different characterization times (w/c = 25).**

| Phase | Site | $\delta_{iso}$ (ppm) | Model | Peak intensity | Quadrupolar coupling constant, $C_Q$ (MHz) | Asymmetry parameter, η | Width | Reference |
|---|---|---|---|---|---|---|---|---|
| CA | $Al_1^{(IV)}$ | 82 | Q mas 1/2 | 266 | 2.5 | 0.20 | - | [17] |
| | $Al_2^{(IV)}$ | 84 | Q mas 1/2 | 307 | 2.6 | 0.75 | - | |
| | $Al_3^{(IV)}$ | 86 | Q mas 1/2 | 210 | 2.6 | 0.95 | - | |
| | $Al_4^{(IV)}$ | 83 | Q mas 1/2 | 230 | 3.3 | 0.53 | - | |
| | $Al_5^{(IV)}$ | 82 | Q mas 1/2 | 584 | 3.4 | 0.39 | - | |
| | $Al_6^{(IV)}$ | 81 | Q mas 1/2 | 115 | 4.3 | 0.47 | - | |
| $C_4AČH_{11}$ | $Al^{(VI)}$ | 8.7 | Lorentzian | 1080 | - | - | 1.9 | [17] |
| $C_2AH_{7.5}$ | $Al^{(IV)}$ | 10.5 | Lorentzian | 2000 | - | - | 2.2 | [12, 18, 19, 31] |
| | $Al^{(IV)}$ | 66.5 | Lorentzian | 241 | - | - | 18.3 | |
| $AH_3$ | $Al^{(VI)}$ | 9 | Lorentzian | 200 | - | - | 2.0 | [20, 21] |
| $C_3AH_6$ | $Al^{(VI)}$ | 12.3 | Lorentzian | 400 | - | - | 2.15 | [22] |

Table 24 summarizes the phase assemblages derived from the decomposition of the spectra.

**Table 24 : Quantification by $^{27}$Al NMR of Al phases present in the CA suspension (w/c = 25) after increasing periods of hydration.**

| Hydration stoppage time (h) | Phase | Chemical shift (ppm) | Al atomic fraction (%) | Phase weight fraction (wt. %) | Corresponding bound water content (wt. %) |
|---|---|---|---|---|---|
| **0.5** | CA | 81.9/83.8/86.3/82.8/81.6/81.2 | 95.7 | 95 | - |
| | $AH_3$ | 9 | 3.6 | 4 | 1 |
| | *$C_3AH_6$* | *12.3* | *0.7* | *2* | *0.5* |
| **1.5** | CA | 81.9/83.8/86.3/82.8/81.6/81.2 | 92.9 | 92 | - |
| | $AH_3$ | 9 | 6.8 | 7 | 2 |
| | *$C_3AH_6$* | *12.3* | *0.3* | *1* | *0.2* |
| **2** | CA | 81.9/83.8/86.3/82.8/81.6/81.2 | 90.5 | 90 | - |
| | $AH_3$ | 9 | 8 | 8 | 3 |
| | *$C_3AH_6$* | *12.3* | *0.5* | *1* | *0.3* |
| **3** | CA | 81.9/83.8/86.3/82.8/81.6/81.2 | 68.5 | 64 | - |
| | $AH_3$ | 9 | 27 | 25 | 9 |
| | $C_2AH_{7.5}$ | 10.5/66.5 | 4 | 9 | 3 |
| | $C_4A\check{C}H_{11}$ | 8.7 | 0.5 | 2 | 0.6 |
| **4** | CA | 81.9/83.8/86.3/82.8/81.6/81.2 | 29 | 24 | - |
| | $AH_3$ | 9 | 56 | 46 | 16 |
| | $C_2AH_{7.5}$ | 10.5/66.5 | 14 | 27 | 11 |
| | $C_4A\check{C}H_{11}$ | 8.7 | 1 | 3 | 1 |
| **7** | CA | 81.9/83.8/86.3/82.8/81.6/81.2 | 7 | 5 | - |
| | $AH_3$ | 9 | 65 | 47 | 16 |
| | $C_2AH_{7.5}$ | 10.5/66.5 | 27 | 45 | 18 |
| | $C_4A\check{C}H_{11}$ | 8.7 | 1 | 3 | 0.9 |

Based on these mineralogical compositions, the bound water amount was calculated and found equal to 1.5 wt. %, 2 wt. %, 3 wt. %, 13 wt. %, 28 wt. % and 35 wt. % for the solid fractions of 0.5 h-, 1.5 h-, 2 h-, 3 h-, 4 h- and 7 h-old CA mixtures, respectively. The bound water content derived from TGA was (1, 3, 3, 13, 29 and 32 wt. % respectively) was found to be in rather good agreement with those obtained from NMR analysis.

The measured bound water content and the mineralogical composition obtained from NMR are superimposed on the conductivity curve in Figure 90.

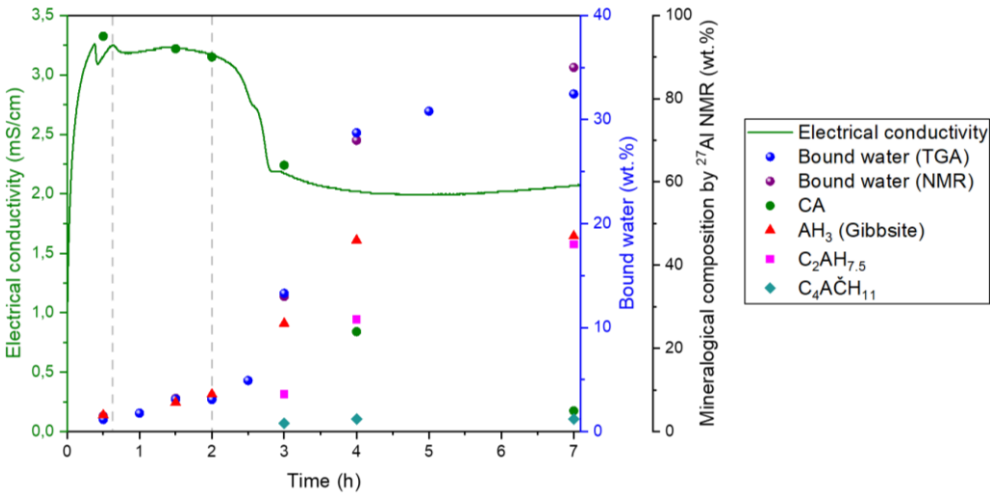


**Figure 90 : Measured mass loss of the solid fraction of CA suspension with a w/c of 25 at different temperature ranges.**

Based on this figure, the massive precipitation of hydrated phases started 2 hours after mixing, which was showed by the sharp decrease in conductivity and the increase in the amount of bound water. After 7 h of hydration, the analyzed sample contained approximately 45 wt. % of $C_2AH_8$, 47 wt. % of aluminium hydroxide, 3 wt. % of monocarboaluminate and 5 wt. % of anhydrous CA.

As already noticed previously, the $C_2AH_8/AH_3$ molar ratio determined experimentally from the NMR results was always smaller than the ratio expected from mass balance equation (17) on the investigated period of time (Table 25). This means that aluminium hydroxide precipitates prior to $C_2AH_8$.

$$2\ CA + 11\ H \rightleftharpoons C_2AH_8\ + AH_3 \qquad (17)$$

**Table 25 : Experimental $C_2AH_8/AH_3$ molar ratio compared to theoretical ratio assuming hydration of CA following equation (17).**

| molar ratio | $C_2AH_8/AH_3$ |
|---|---|
| Measured composition at 0.5 h | 0 |
| Measured composition at 1.5 h | 0 |
| Measured composition at 2 h | 0 |
| Measured composition at 3 h | 0.15 |
| Measured composition at 4 h | 0.22 |
| Measured composition at 7 h | 0.42 |
| Considering equation (17) | 1 |

### 2.2.2. Characterization of the liquid fraction of suspensions

The evolution of the liquid fraction composition during the hydration was characterized by ICP-AES analysis and pH-metry. The results are plotted in Figure 91.

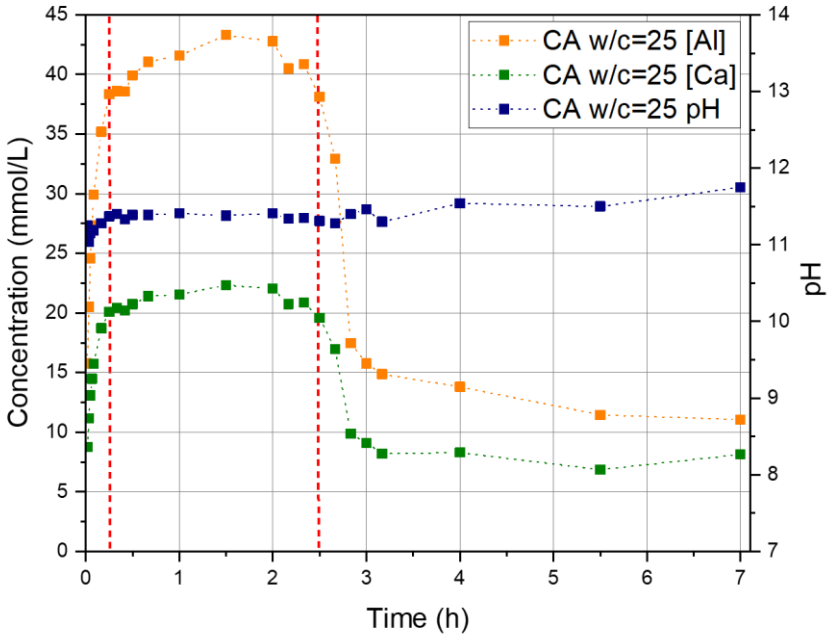


**Figure 91 : Characterization of the liquid fractions of CA suspension (w/c ratio = 25, T = 25 °C) during the first seven hours of hydration: evolution of pH and chemical composition.**

As soon as CA was mixed with water, calcium, aluminate and hydroxide ions were released in solution. As observed on the conductivity profile, the aqueous Ca and Al concentrations remained approximately constant during the second stage before a concentration drop that correspond to the third period of hydration. During the third period, the Ca concentration remained constant, the Al concentration decreased slightly whereas the pH tended to increase. This third stage starts simultaneously with the massive precipitation of hydrates, as evidenced by the solid fraction characterization.

From these raw results, the ratio between the Ca and Al aqueous concentrations was plotted as a function time (Figure 92). This [Ca]/[Al] ratio was decreasing from the beginning of hydration down to a value of 0.50 and was kept constant at this value from 0.5 h up to 2.6 h. Such a ratio was consistent with a congruent dissolution of CA (equation (15)):

$$CA + 4\,H_2O \rightleftharpoons Ca^{2+} + 2\,Al(OH)_4^- \qquad (15)$$

During the third stage of hydration, after 2.5 h of hydration, the [Ca]/[Al] ratio increased and thus diverged from the 0.5 value (corresponding to the congruent dissolution of CA).

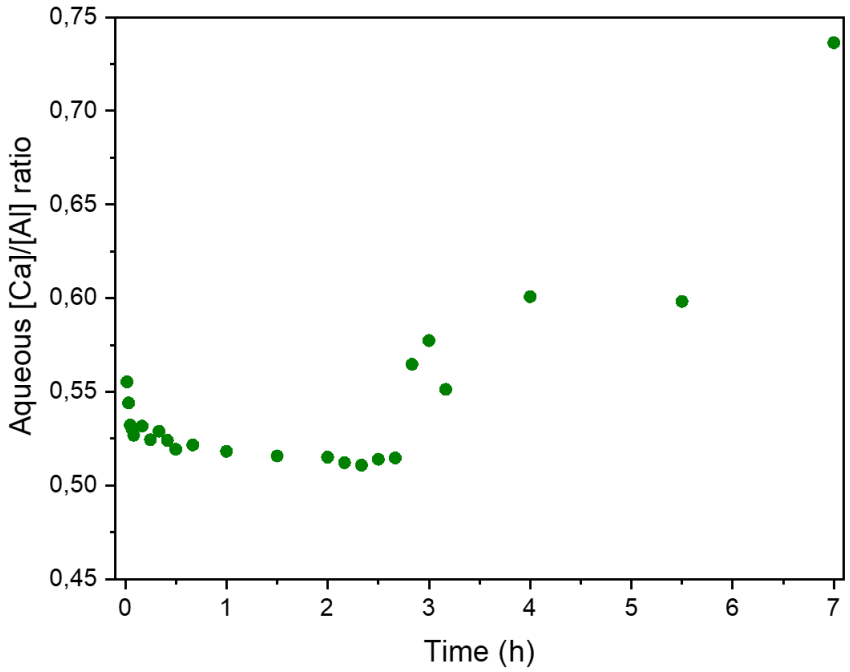


**Figure 92 : Evolution of [Ca]/[Al] ratio in the liquid fraction as a function of time during CA hydration in suspension (w/c = 25 – T = 25 °C).**

### 2.2.3. Calculation of saturation indexes and identification of the hydration path

Based on the previous solution compositions, saturation indexes in the $CaO\text{-}Al_2O_3\text{-}H_2O$ systems were calculated by using CEMDATA2018 and CHESS software. Evolution of the saturation index over time of some phases of interest is presented in Figure 93.

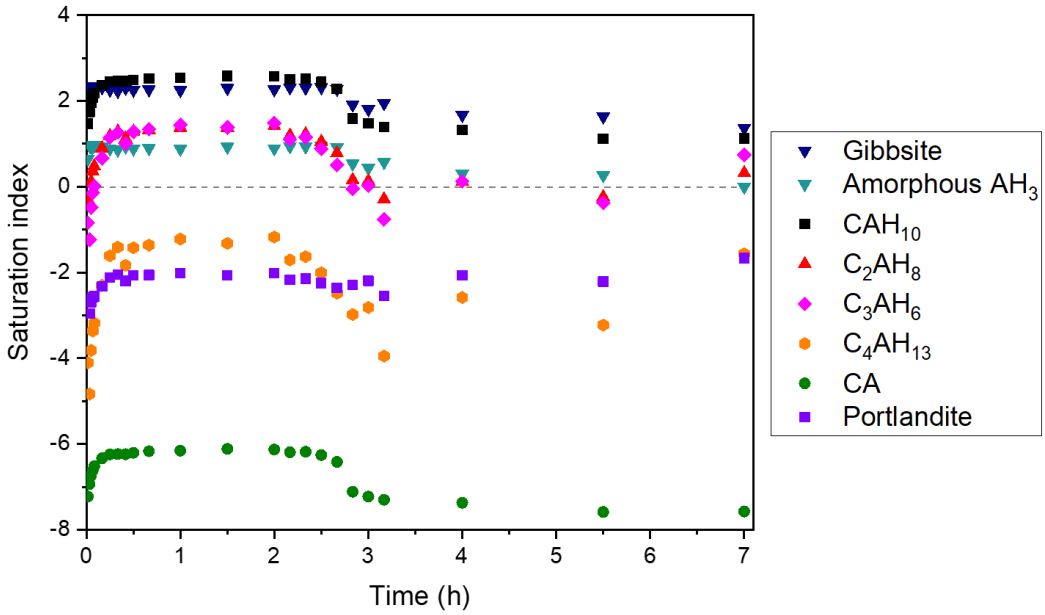


**Figure 93 : Evolution of saturation indexes in the $CaO-Al_2O_3-H_2O$ system as a function of time during the hydration of CA in suspension (w/c = 25 – T = 25 °C).**

From mixing and up to 3 hours of hydration:

- The saturation index of $C_2AH_8$ and $C_3AH_6$ remained negative for the first 2 minutes, and then increased above 0, meaning that the precipitation of these hydrates could be expected.
- The $CAH_{10}$ saturation index was positive from the beginning of hydration, making the precipitation of this phase possible at very early age.
- The CA saturation index increased right from the beginning of hydration and remained approximately constant up to 2.5 hours. Its profile was similar to the concentration variations illustrated in Figure 91.
- The saturation index of aluminium hydroxide polymorphs showed a similar trend than that of CA, but at positive values.

As already observed and mentioned previously when studying the $CA_2$ hydration in suspension, the saturation index values presented above were questionable since the electroneutrality of the solutions was not respected when performing the speciation calculations using CHESS and CEMDATA2018 database. The electrical imbalance of the solutions, normalized by their ionic strength, is reported as a function of time in Figure 94.

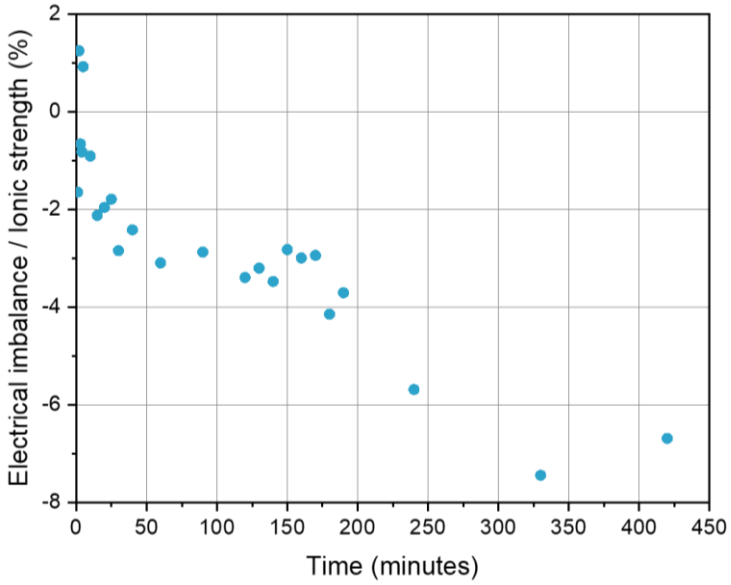


**Figure 94: Evolution of the electrical imbalance normalized by the ionic strength for the simulations carried out with CHESS and the CEMDATA2018 database as a function of the hydration time.**

The normalized electrical imbalance ranged from -8 % up to 1 % during the whole studied period. Identification of the limiting step in the hydration process was thus hard to discuss based only on the saturation index evolution. As mentioned in the previous chapter, this discrepancy was likely due to the irrelevance of CEMDATA2018 thermodynamic database to describe aluminium speciation under these experimental conditions, as already reported by Maach [1].

### 2.2.4 Investigations in the {$CaO$-$Al_2O_3$-$H_2O$} phase diagram

To circumvent the electrical balance issue, the aqueous Ca and Al concentrations measured experimentally after increasing periods of hydration were plotted in the {$CaO$-$Al_2O_3$-$H_2O$} phase diagram (Figure 95).

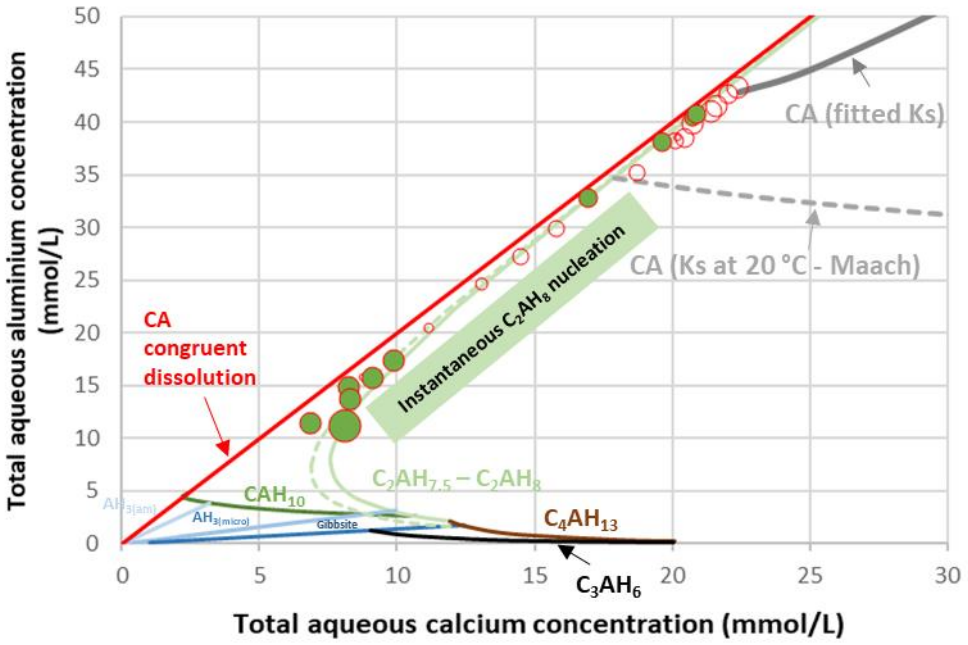


**Figure 95 : Total calcium and aluminium concentrations measured in the liquid fraction during CA hydration (w/c = 25 – T = 25 °C) plotted in the {CaO-$Al_2O_3$-$H_2O$} phase diagram. Note that the red line is not a solubility curve. It simply shows the expected concentrations if the system is driven by congruent dissolution of CA.**

On this diagram, empty dots correspond to the hydration stage during which calcium and aluminate ions concentrations were increasing up to a maximum. Filled dots correspond to the hydration stage during which these concentrations were decreasing. The dots getting larger depict the concentration evolution of the solution through hydration time. From this representation, several observations can be made.

First of all, the hydration path followed by the Ca and Al aqueous concentrations was very close to concentrations corresponding to a CA congruent dissolution and to $C_2AH_{7.5}$ – $C_2AH_8$ solubility lines during the whole studied hydration period.

In his PhD thesis, Maach N. [1] reported that during the first period of hydration, when the Ca and Al concentrations increased, these concentrations were governed by the solubility of CA, meaning that dissolution of CA was not limiting from a kinetic point of view since the solubility limit could be reached. Maach also showed that the apparent solubility product of CA was much lower than that reported in CEMDATA2018 thermodynamic database. Using the CA solubility product value reported in CEMDATA2018 database, a CA solubility of 1.3 mol/L at 20 °C was obtained versus a solubility of 18.0 ± 2 mmol/L measured by Maach at 20 °C. The CA solubility line was plotted in Figure 27 using the solubility product value at 20 °C reported by Maach, expressed using the CHESS software formalism. However, all the experiments were carried out at 25 °C in this work. Thus, the CA solubility product was fitted in order to be consistent with the calcium and aluminate concentrations measured experimentally. A -40.80 value, associated with reaction equation (18), was obtained at 25 °C, in comparison to the -40.57 value reported by Maach at 20 °C.

$$Ca^{2+} + 2\,Al^{3+} + 4\,H_2O \rightleftharpoons CaAl_2O_4 + 8\,H^{+} \qquad \text{K = -40.80} \qquad (18)$$

During this first period of hydration, from 1 min to 2 h, the hydration path followed by aqueous calcium and aluminium concentration increased on the line corresponding to CA congruent dissolution until reaching the solubility curve of CA. Al concentration stood in a zone far above the solubility curve of aluminium hydroxide regardless of the solid form considered. Experimentally, the phase characterization performed during this period showed a content increase for only one mineral exhibiting a weight loss between 50 °C and 150 °C on the thermograms. Such a weight loss might be assigned to the formation of small amounts of aluminium hydroxide gel.

The beginning of the second period of hydration, from 140 min to 7 h, was characterized by a decrease in the calcium and aluminate concentrations and by the precipitations of gibbsite and $C_2AH_8$. During this second period, the aqueous aluminium and calcium concentrations followed the $C_2AH_{7.5}$-$C_2AH_8$ solubility lines, without any oversaturation phenomenon. In the literature, the zone located above these solubility lines was reported as being a zone where instantaneous precipitation of $C_2AH_8$ occurred [32-34]. In agreement with the analysis and interpretations proposed by Maach, the trigger for this hydrate formation could be the precipitation of aluminium hydroxide that brings to the reacting medium hydroxide ions needed for $C_2AH_8$ precipitation. The trigger for aluminium hydroxide precipitation after a given period located at high oversaturation with respect to amorphous or microcrystalline aluminium hydroxide or gibbsite was not clearly elucidated. Further investigations would be needed to describe more extensively the mechanisms involved, as discussed in the last part of this manuscript.

## 3. Summary and discussion

In this chapter, the hydration study of synthetic CA was presented.

At first, the studies on pastes showed that the higher the w/c ratio, the higher the heat released. Based on these results and knowing the enthalpy of reaction of CA hydration, a hydration degree was estimated by assuming that CA dissolution and precipitation of hydrates contribute to heat release. A hydration degree of 70 % was estimated after 7 days when CA was mixed with water at a w/c ratio of 0.5. The phase assemblage of such a paste was also determined using $^{27}$Al MAS-NMR spectroscopy and yielded a hydration degree of 86 % at 7 d. Although the trends were similar, differences were noted concerning the progress of hydration derived from calorimetry and NMR results. They could arise from uncertainties on both kinds of measurements, knowing that the assignment of calcium aluminate phases on NMR spectra was complex due to by the multiplicity of overlapping resonances. Furthermore, the intense spinning side band pattern probably led to an underestimation of the anhydrous content and thus an overestimation of the hydration degree. Regarding the hydrated phases, mainly gibbsite (67 %) and $C_3AH_6$ (16 %) were observed in the pastes characterized 7 days after mixing.

An aluminium hydroxide was suspected as being the main hydrated phase in the CA paste with a w/c ratio of 0.5 during the first 7 hours of hydration. In this time interval, an induction period was observed by isothermal calorimetry and was further evidenced by the hydration study in suspension. From experiments performed in suspensions, CA solubility was shown to be the process governing the aqueous calcium and aluminate concentrations.

The end of the induction period was characterized by the precipitations of gibbsite and of $C_2AH_8$. According to Maach, the limiting step during this period could be the precipitation of gibbsite that brought to the reacting medium the hydroxide ions that were needed for $C_2AH_8$ precipitation. Such a mechanism was supported by this work since the hydration path followed by the Ca and Al aqueous concentrations did not exceed the $C_2AH_8$ solubility curve during the studied period. The trigger for gibbsite precipitation was not clearly elucidated yet. It should be noted that the aluminium concentration always stood far above the displayed aluminium hydroxide solubility lines. The role of $AH_3$ precipitation will be further discussed in the last chapter of this manuscript.

## 4. References

[1] N. Maach, "Kinetic modeling of the early age hydration of calcium aluminate cements : From chemical mechanism to the modeling by the Population Balance Equations," Thèse de doctorat, Mécanique, Energétique, Génie Civil, Acoustique (MEGA), l'INSA de Lyon, 2019LYSEI127, 2019.

[2] S. Klaus, "Quantification of CA hydration and influence of its particle fineness during early hydration of calcium aluminate cement," Friedrich-Alexander-Universität Erlangen-Nürnberg, 2015.

[3] T. Manninger, "Early hydration of CA and CA-cement in interaction with calcite and additives," PhD, Naturwissenschaftliche Fakultät, Friedrich-Alexander-Universität Erlangen-Nürnberg, Friedrich-Alexander-Universität Erlangen-Nürnberg, 2020.

[4] F. Hüller, "Hydration mechanisms of CA2 and alumina-rich calcium aluminate cements: Effects of mechanical activation, critical CA contents and crystallinity of AH3," PhD, Geographie und Geowissenschaften, Friedrich-Alexander-Universität Erlangen-Nürnberg (FAU), 2019.

[5] S. R. Klaus, J. Neubauer, and F. Goetz-Neunhoeffer, "Hydration kinetics of CA2 and CA—Investigations performed on a synthetic calcium aluminate cement," *Cement and Concrete Research*, vol. 43, pp. 62-69, 2013/01/01/ 2013.

[6] J. Bizzozero, "Hydration and dimensional stability of calcium aluminate cement based systems," Theses 2014 2014, Art. no. 6336.

[7] B. Lothenbach, L. Pelletier-Chaignat, and F. Winnefeld, "Stability in the system CaO–$Al_2O_3$–$H_2O$," *Cement and Concrete Research*, vol. 42, no. 12, pp. 1621-1634, 2012/12/01/ 2012.

[8] B. Lothenbach *et al.*, "Cemdata18: A chemical thermodynamic database for hydrated Portland cements and alkali-activated materials," *Cement and Concrete Research*, vol. 115, pp. 472-506, 2019/01/01/ 2019.

[9] V. Antonovič, J. Kerienė, R. Boris, and M. Aleknevičius, "The Effect of Temperature on the Formation of the Hydrated Calcium Aluminate Cement Structure," *Procedia Engineering*, vol. 57, pp. 99-106, 2013/01/01/ 2013.

[10] F. Guirado, S. Galí, and J. S. Chinchón, "Thermal Decomposition of Hydrated Alumina Cement (CAH10)," *Cement and Concrete Research*, vol. 28, no. 3, pp. 381-390, 1998/03/01/ 1998.

[11] T. Dos Santos *et al.*, "Gluconate action in the hydration of calcium aluminate cements: Theoretical study, processing of aqueous suspensions and hydration reactivation," *Journal of the European Ceramic Society*, vol. 39, no. 8, pp. 2748-2759, 2019/07/01/ 2019.

[12] N. Ukrainczyk, T. Matusinovic, S. Kurajica, B. Zimmermann, and J. Sipusic, "Dehydration of a layered double hydroxide—$C_2AH_8$," *Thermochimica Acta*, vol. 464, no. 1, pp. 7-15, 2007/11/25 2007.

[13] K. Irisawa, I. Garcia-Lodeiro, and H. Kinoshita, "Influence of mixing solution on characteristics of calcium aluminate cement modified with sodium polyphosphate," *Cement and Concrete Research*, vol. 128, p. 105951, 2020/02/01/ 2020.

[14] P. Lura, F. Winnefeld, and X. Fang, "A simple method for determining the total amount of physically and chemically bound water of different cements," *Journal of Thermal Analysis and Calorimetry*, vol. 130, no. 2, pp. 653-660, 2017/11/01 2017.

[15] E. Litwinek and D. Madej, "Structure, microstructure and thermal stability characterizations of C3AH6 synthesized from different precursors through hydration," *Journal of Thermal Analysis and Calorimetry*, vol. 139, no. 3, pp. 1693-1706, 2020/02/01 2020.

[16] T. Durán, P. Pena, S. De Aza, J. Gómez-Millán, M. Alvarez, and A. H. De Aza, "Interactions in Calcium Aluminate Cement (CAC)-Based Castables Containing Magnesia—Part II: Hydration–Dehydration Behavior of CAC and their Mixtures with Dead-Burned and Reactive-Grade MgO," *Journal of the American Ceramic Society*, vol. 94, no. 3, pp. 909-917, 2011/03/01 2011.

[17] J. H. Skibsted, E.; Jakobsen, H.J., "Characterization of Calcium Aluminate Phases in Cements by 27Al MAS NMR Spectroscopy," *Inorg. Chem.*, vol. 32, pp. 1013-1027, 1993.

[18] P. Faucon, T. Charpentier, D. Bertrandie, A. Nonat, J. Virlet, and J. C. Petit, "Characterization of Calcium Aluminate Hydrates and Related Hydrates of Cement Pastes by 27Al MQ-MAS NMR," *Inorganic Chemistry*, vol. 37, no. 15, pp. 3726-3733, 1998/07/01 1998.

[19] W. Gessner, D. Müller, H.-J. Behrens, and G. Scheler, "Zur Koordination des Aluminiums in den Calciumaluminathydraten $2CaO{\cdot}Al_2O_3{\cdot}8H_2O$ und $CaO{\cdot}Al_2O_3{\cdot}10H_2O$," *Zeitschrift für anorganische und allgemeine Chemie*, https://doi.org/10.1002/zaac.19824860122 vol. 486, no. 1, pp. 193-199, 1982/03/01 1982.

[20] R. A. Kinsey, R. J. Kirkpatrick, J. Hower, K. A. Smith, and E. Oldfield, "High resolution aluminum-27 and silicon-29 nuclear magnetic resonance spectroscopic study of layer silicates, including clay minerals," *American Mineralogist*, vol. 70, no. 5-6, pp. 537-548, 1985.

[21] X. Cong and R. J. Kirkpatrick, "Hydration of Calcium Aluminate Cements: A Solid-State $^{27}Al$ NMR Study," *Journal of the American Ceramic Society*, vol. 76, no. 2, pp. 409-416, 1993/02/01 1993.

[22] P. Pena, J. M. Rivas Mercury, A. H. de Aza, X. Turrillas, I. Sobrados, and J. Sanz, "Solid-state 27Al and 29Si NMR characterization of hydrates formed in calcium aluminate–silica fume mixtures," *Journal of Solid State Chemistry*, vol. 181, no. 8, pp. 1744-1752, 2008/08/01/ 2008.

[23] J. Bensted and P. Barnes, *Structure and performance of cements*, (2nd Edition) ed. London; New York: Spon Press, 2002.

[24] F. Šoukal *et al.*, "The influence of pH buffers on hydration of hydraulic phases in system CaO–Al2O3," *Journal of Thermal Analysis and Calorimetry*, Article vol. 124, no. 2, pp. 629-638, 2016.

[25] P. Hlaváček, R. Šulc, V. Šmilauer, C. Rößler, and R. Snop, "Ternary binder made of CFBC fly ash, conventional fly ash, and calcium hydroxide: Phase and strength evolution," *Cement and Concrete Composites*, vol. 90, pp. 100-107, 2018/07/01/ 2018.

[26] V. Kumar, V. K. Singh, A. Srivastava, and G. N. Agrawal, "Low Temperature Synthesis of High Alumina Cements by Gel-Trapped Co-Precipitation Process and Their Implementation as Castables," *Journal of the American Ceramic Society*, https://doi.org/10.1111/j.1551-2916.2012.05453.x vol. 95, no. 12, pp. 3769-3775, 2012/12/01 2012.

[27] M. R. Nilforoushan and N. Talebiaan, "The hydration products of a refractory calcium aluminate cement at low temperatures," (in English), *Iranian Journal of Chemistry and Chemical Engineering (IJCCE)*, Article vol. 26, no. 2, pp. 71-76, 2007.

[28] P. T. Durdziński, "Hydration of multi-component cements containing cement clinker, slag, calcareous fly ash and limestone," PhD, Faculté Sciences et Techniques de l'Ingénieur, EPFL, Suisse, 6834, 2016.

[29] V. S. Ramachandran, R. M. Paroli, J. J. Beaudoin, and A. H. Delgado, "10 - Non-Portland Rapid Setting Cements," in *Handbook of Thermal Analysis of Construction Materials*, V. S. Ramachandran, R. M. Paroli, J. J. Beaudoin, and A. H. Delgado, Eds. Norwich, NY: William Andrew Publishing, 2002, pp. 403-448.

[30] O. Chowaniec, "Limestone Addition in Cement," PhD, Faculté des sciences et techniques de l'ingénieur, EPFL, Lausanne, EPFL, N°5335, 2012.

[31] N. Richard, N. Lequeux, and P. Boch, "EXAFS Study of Refractory Cement Phases: $CaAl_2O_{14}H_{20}$, $Ca_2Al_2O_{13}H_{16}$, and $Ca_3Al_2O_{12}H_{12}$," *Journal de Physique III France*, vol. 5, no. 11, pp. 1849-1864, 1995 1995.

[32] G. Le Saout, "Phase Assemblage in Calcium Aluminate Cements: A Review," (in English), *ALITinform*, vol. 2, no. 51, pp. 12-20, 2018.

[33] W. Kurdowski, *Cement and Concrete Chemistry*. Krakow, Poland: Springer, Netherlands, New York, 2014, p. 705.

[34] M. Zajac, J. Skocek, F. Bullerjahn, B. Lothenbach, K. Scrivener, and M. Ben Haha, "Early hydration of ye'elimite: Insights from thermodynamic modelling," *Cement and Concrete Research*, vol. 120, pp. 152-163, 2019/06/01/ 2019.

# Chapter 5: Investigation of pure $C_{12}A_7$ hydration at early age

# **Chapitre 5** : Étude de l'hydratation au jeune âge de $C_{12}A_7$ pur

**Résumé:** Ce chapitre est dédié à l'étude de l'hydratation au jeune âge de $C_{12}A_7$ pur à 25°C. Dans un premier temps, la vitesse d'hydratation des pâtes de $C_{12}A_7$ avec différents rapports e/c massiques a été étudiée par calorimétrie isotherme. Il a été observé que plus le rapport e/c est bas, plus la fin de la période de décélération est tardive. Malgré des profils de flux thermique différents, c'est-à-dire la présence de deux ou trois pics exothermiques lorsque le rapport e/c varie, l'assemblage minéralogique des systèmes étudiés est constitué des mêmes produits d'hydratation après 7 jours d'hydratation. Une estimation du degré d'hydratation en fonction du temps a été faite pour une pâte élaborée avec un rapport e/c de 0.5 et a conduit à un avancement de 79 % après 7 jours d'hydratation. En ce qui concerne les hydrates de la pâte (e/c=0.5), les résultats de l'ATG, de la DRX et de la RMN ont permis de conclure qu'après 7 jours d'hydratation à 25°C, l'assemblage minéralogique est composé majoritairement de $C_3AH_6$ et d'$AH_3$. D'autres résultats importants découlent de ces analyses. Premièrement, l'anhydre $C_{12}A_7$ a réagi rapidement, la période d'accélération ayant commencé juste après le mélange avec l'eau, ce qui est en accord avec la littérature qui fait état d'une forte réactivité de $C_{12}A_7$. Deuxièmement, le début de la réaction de conversion a également été observé rapidement après le mélange, puisqu'une augmentation de la quantité de $C_3AH_6$ aux dépens de $C_2AH_8$ a été observée entre 5 et 7 heures d'hydratation. Cette étape est concomitante avec la deuxième période d'accélération observée par calorimétrie isotherme. Dans un second temps, l'étude de l'hydratation par conductimétrie a été menée en suspension diluée avec un rapport massique e/c fixé à 25 à 25°C. L'évolution de la composition de la solution et de la minéralogie a été étudiée en fonction du temps, ce qui a permis de définir trois étapes principales du mécanisme d'hydratation. D'abord, une dissolution rapide de $C_{12}A_7$, accompagnée par la précipitation d'hydroxyde d'aluminium et de $C_2AH_8$ a été observée dès la sursaturation du système par rapport à $C_2AH_8$. Une deuxième étape de faible vitesse d'hydratation est ensuite caractérisée par une solution dont les concentrations en calcium et aluminium sont gouvernées par la solubilité de $C_2AH_8$. La précipitation de l'hydroxyde d'aluminium pourrait être limitante au cours de cette étape, alors que cela ne semblait pas être le cas lors de la première étape d'hydratation. Enfin, une dernière étape est caractérisée par une diminution des concentrations en ions aluminium et calcium, suivant les courbes de solubilité de $C_2AH_{7.5}$-$C_2AH_8$, ce jusqu'à la conversion de $C_2AH_{7.5\text{-}8}$ en phase stable $C_3AH_6$.

# Introduction

Dodecacalcium heptaluminate $C_{12}A_7$ (mayenite, $Ca_{12}Al_{14}O_{33}$ or $12CaO{\cdot}7Al_2O_3$) is an important phase in calcium aluminate cements. Commercial calcium aluminate cements such as Ciment Fondu contain varying amounts of $C_{12}A_7$ [1]. The amount of $C_{12}A_7$ has an influence on the mechanical properties of cement-based materials, but it can also strongly accelerate their setting [2]. That is the reason why $C_{12}A_7$ is one of the mineral-based accelerators used in the cement industry [3]. A commercial calcium aluminate cement from IMERYS containing high amount of $C_{12}A_7$ is currently produced for applications requiring rapid drying and hardening [4].

Negro *et al.* [5] reported a faster dissolution of CA and $C_{12}A_7$ phases compared to $CA_2$ within 1 hour of hydration using a w/c ratio of 1200. Capmas *et al.* [6] monitored the conductivity of $C_{12}A_7$ in suspensions (w/c=10) at different temperatures ranging initially from 15 to 35 °C to predict the dissolution and precipitation processes. The conductivity reached higher values when the temperature was increased, and precipitation of hydrates occurred faster. Then, the experiments were conducted for different w/c ratios ranging from 10 to 200. The resulting C/A ratios from the suspensions with a w/c ratio of 50, 100 and 150 showed a congruent dissolution of $C_{12}A_7$ and the almost instantaneous precipitation of calcium aluminate hydrates ($C_2AH_8$ and $C_4AH_x$). Ukrainczyk N. [7] reported the presence of $CAH_{10}$ with traces of poorly crystalline $AH_3$ and $C_2AH_8$ during the hydration of $C_{12}A_7$ at 15 °C. Moreover, as the temperature of hydration was increased to 55 °C, the conversion of metastable phases to katoite was evidenced.

Furthermore, the precipitation of $AH_3$ from the early beginning of $C_{12}A_7$ hydration was observed by Damidot D. et Rettel A. in their study about the effect of gypsum on CA and $C_{12}A_7$ hydration [8]. In addition, these authors showed that the induction period was primarily governed by the nucleation and growth of $AH_3$. Damidot D. *et al.* [9] reported basic rules followed by $C_{12}A_7$ hydration at 20 °C. The experiments were performed with Ciment Fondu with a w/c ratio of 10 and the nucleation experiments were performed on supersaturated solution obtained by the filtration of the suspension after 70 minutes of hydration and the addition of $C_{12}A_7$ solids. According to their study, first the kinetic path followed the regions richest in aluminate concentration. Afterwards, due to the reduction of the concentrations in solution, the kinetic path was bounded by the critical supersaturation regions of both $C_2AH_8$ and $AH_3$. Meanwhile, a low reaction rate was observed until the growth rate of $AH_3$ reached a level high enough.

This fifth chapter is devoted to the study of the hydration of pure $C_{12}A_7$ at early age to determine the influence of w/c ratio on the course of pure $C_{12}A_7$ hydration, degree of hydration and also to investigate the hydration path.

# 1. Hydration study of $C_{12}A_7$ pastes at early age

## 1.1. Investigation of the influence of the w/c ratio on the early age hydration of $C_{12}A_7$ pastes

### 1.1.1. Heat flow monitoring

The influence of a w/c ratio ranging from 0.40 to 0.60 on the early age hydration of $C_{12}A_7$ was monitored during 7 days by isothermal calorimetry at 25 °C. Figure 96 shows the measured heat flows, normalized by the initial mass of $C_{12}A_7$ in the sample with a more detailed view of the first 24 hours of hydration on the right of the figure.

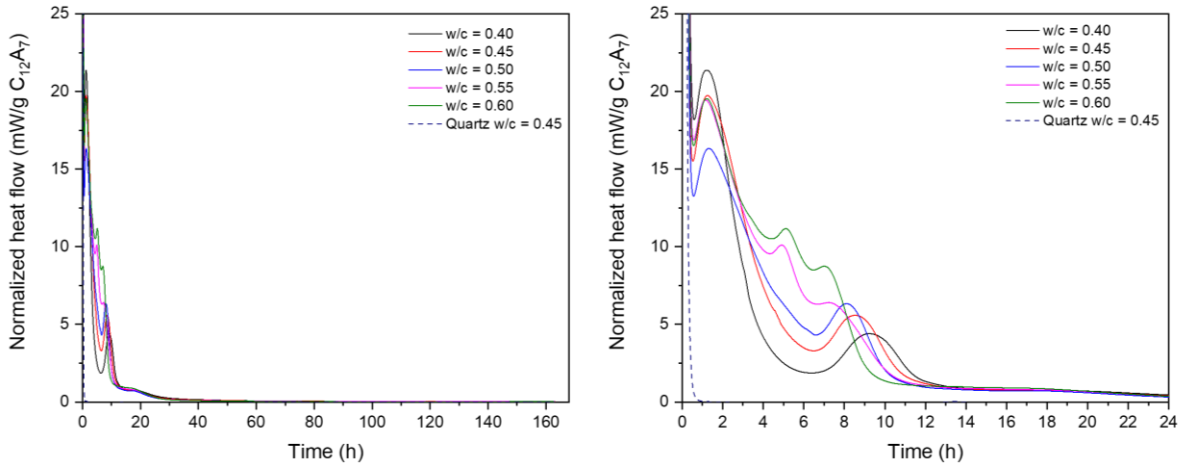


**Figure 96 : Heat flow measurement of pure $C_{12}A_7$ pastes with different w/c ratios at 25 °C for 7 days. On the right, zoom on the first 24 hours of hydration.**

As already reported in the literature, $C_{12}A_7$ reacts quickly with water. Indeed, whatever the w/c ratio, measured heat flows did not return to the baseline immediately after the introduction of the samples into the calorimeter, something that was evidenced by comparison with an inert sample composed of quartz.

The first heat flow peak reached its maximum value 1.2 +/- 0.1 hour after mixing. Afterwards, two exothermic heat flow peaks appeared for pastes prepared with w/c ratios of 0.55 and 0.60, whereas one only was evidenced at lower w/c ratio (0.4 or 0.5). The lower the w/c ratio, the later the end of the deceleration period. Such heat flow profiles are already reported in the literature [10]. Moreover, He Z. and Li Y. stated that the second peak following the first peak as a shoulder is controlled by the nucleation process of amorphous $AH_3$ [11]. Characteristic parameters derived from the heat flow profiles are reported in Table 26.

**Table 26 : Characteristic parameters derived from heat flow measurements.**

| w/c | Time of maximum heat flow (h) | Maximum heat flow (mW/$g_{C12A7}$) | Time of second heat flow maximum (h) | Time of third heat flow maximum (h) |
|---|---|---|---|---|
| **0.40** | 1.2 | 21.4 | 9.3 | - |
| **0.45** | 1.2 | 19.7 | 8.5 | - |
| **0.50** | 1.3 | 16.4 | 8.1 | - |
| **0.55** | 1.1 | 19.4 | 4.9 | 7.2 |
| **0.60** | 1.2 | 19.5 | 5.1 | 7 |

The cumulative heat of hydration over the first week of hydration, expressed in J/g relative to the initial weight of anhydrous $C_{12}A_7$, is shown in Figure 97. Such cumulative curves were obtained by starting the integration of the heat flow profiles 30 minutes after the sample introduction into the calorimeter. This procedure underestimated the cumulative heat release by at least 30 % 7 days after mixing, when compared to an in situ mixing procedure (see chapter 2).

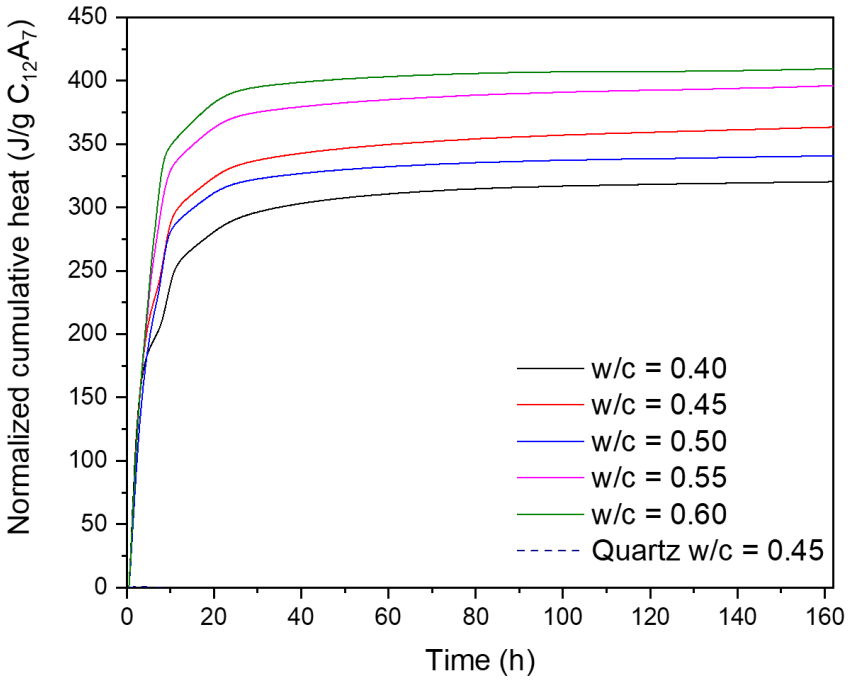


**Figure 97 : Normalized cumulative heat of $C_{12}A_7$ pastes prepared with different w/c ratios during seven days of hydration at 25 °C.**

In Figure 98, the measured heat released after 7 days of hydration is plotted as a function of w/c ratio. The lower the w/c ratio, the lower the cumulative heat measured after 7 days of hydration. This was because as the w/c ratio decreased, the hydration was initially faster (heat flow measurements were higher). More heat was released during the first 30 minutes, which was not accounted with this ex-situ mixing method. In addition, plotting the maximum cumulative heat versus the w/c ratio did not make it possible to assess the chemical water demand following the method proposed by Lura *et al.* [12] : the plot in Figure 98 did not show any plateau.

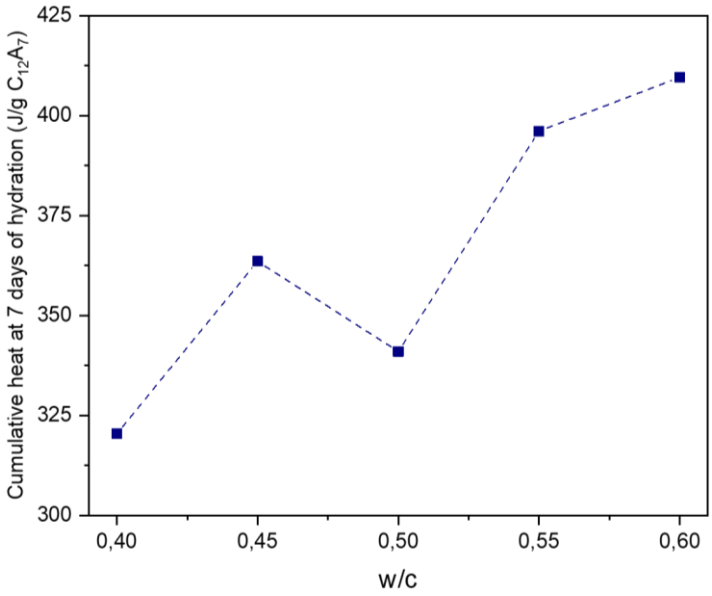


**Figure 98 : Cumulative heat values measured after 7 days of $C_{12}A_7$ hydration as a function of the w/c ratio (at 25 °C).**

As previously done for $CA_2$ and CA, a hydration degree of $C_{12}A_7$ was assessed at first order by formulating a rough hypothesis. By assuming that only the dissolution of anhydrous $C_{12}A_7$ phase contributes to the heat release (reaction equation (19)) and thus neglecting the heat that could be released by hydrated phases precipitation, the hydration degree of $C_{12}A_7$ was estimated by normalizing cumulative heat Q by the $C_{12}A_7$ dissolution enthalpy $\Delta_{diss}H$ as described by equation (19).

$$C_{12}A_7 + 33\ H_2O \rightleftharpoons 12\ Ca^{2+} + 14\ Al(OH)_4^- + 10\ OH^- \qquad \Delta_{diss}H = -703\ \text{J/g [4]} \qquad (19)$$

Such an approach was carried out on the heat release measured by using an in-situ mixing procedure, in order to limit the underestimation resulting from the previous ex-situ mixing procedure. The resulting curve is presented in Figure 99. For a paste prepared with a w/c ratio of 0.50, a hydration degree of about 53 % would be achieved 7 days after mixing.

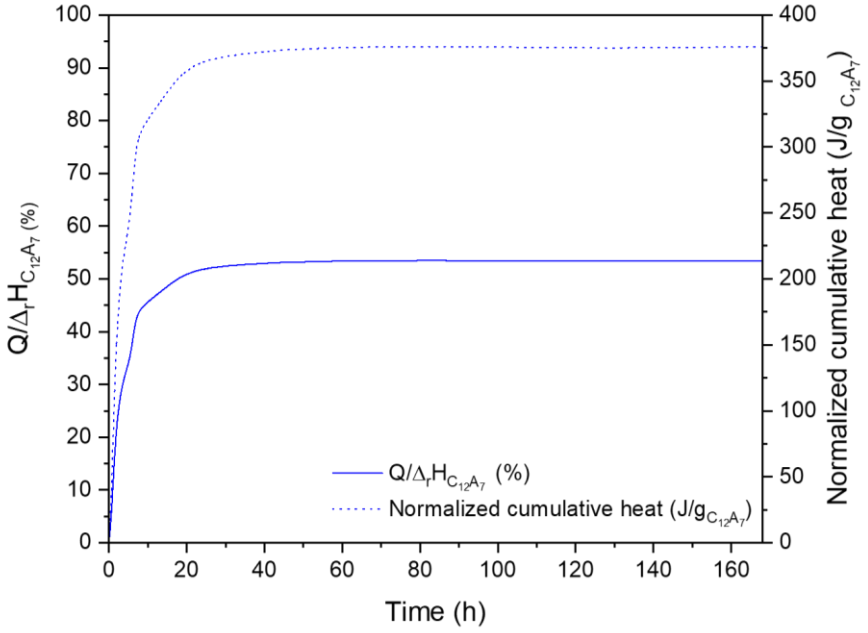


**Figure 99 : Cumulative heat profile and estimated degree of hydration of the 7 d-old $C_{12}A_7$ paste (w/c = 0.5), assuming that the heat release is only due to the dissolution of anhydrous $C_{12}A_7$ – 25 °C.**

To complement this calorimetric study, mineralogy of the 7 d-old pastes was characterized by XRD, TGA and $^{27}$Al NMR spectroscopy.

### 1.1.2. Influence of w/c ratio on mineralogical assemblages after 7 days of hydration

Figure 100 shows the powder XRD patterns of the hydrated $C_{12}A_7$ pastes at 25 °C for 7 days. The presence of $C_2AH_{7.5}$, $AH_3$ (gibbsite), $C_4AČH_{11}$ and stable $C_3AH_6$ is evidenced, in addition to unreacted $C_{12}A_7$.

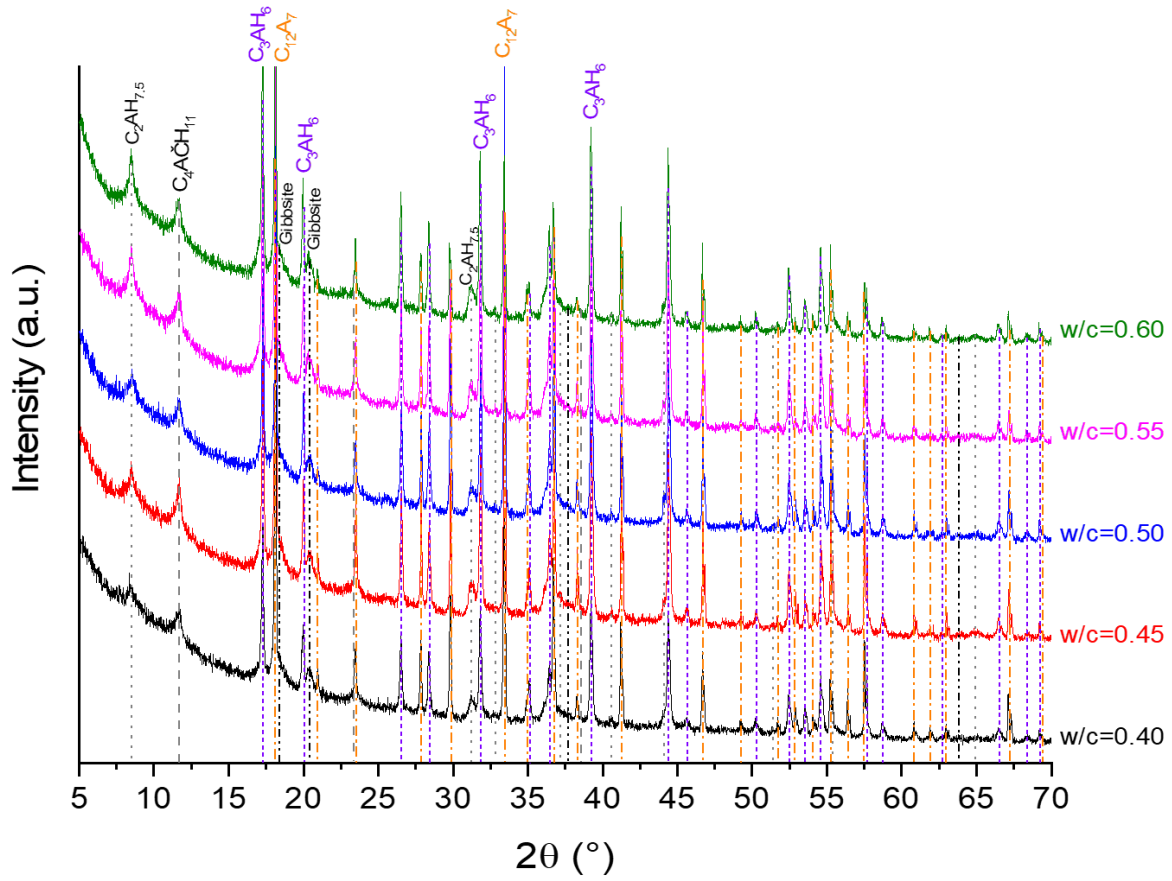


**Figure 100 : XRD patterns representing hydration products after hydrating $C_{12}A_7$ with w/c ratios ranging from 0.4 to 0.6 at 25 °C for 7 days.**

The $C_{12}A_7$ pastes were also analyzed by TGA in order to point out non-crystalline hydration products and determine the bound water content after hydration stoppage at 7 days. Figure 101 shows the TGA and DTG curves of these systems.

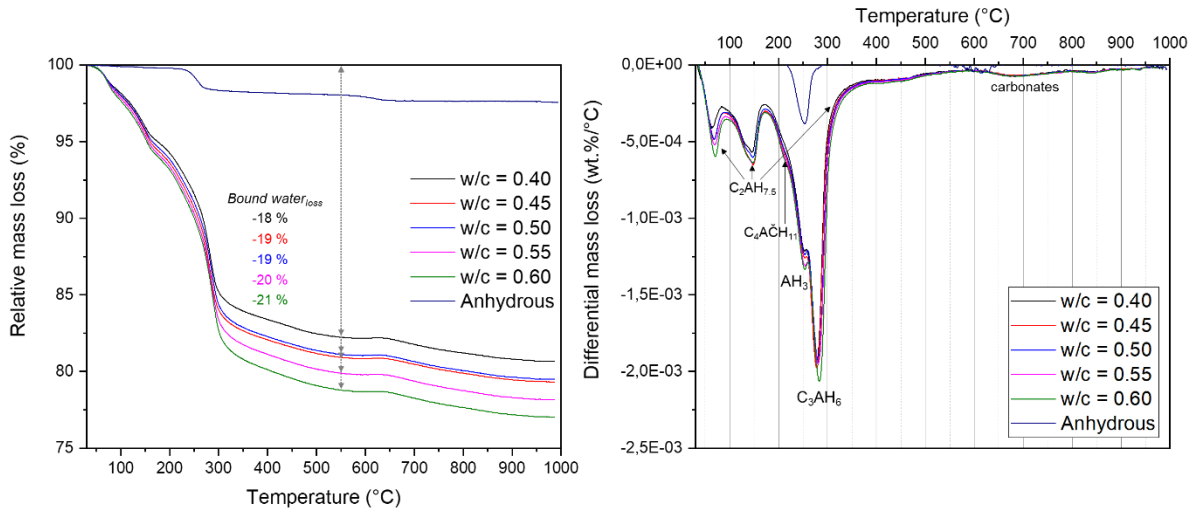


**Figure 101 : TGA and DTG curves obtained from hydrated $C_{12}A_7$ pastes with different w/c ratios at 25 °C for 7 days. On the TGA curves, the arrow shows the mass loss in the range of temperatures between 25 and 550 °C.**

According to TG and DTG curves presented in Figure 101, thermal events for all the samples were assigned as follows:

- At 110, 170 and 300 °C : decomposition of metastable $C_2AH_8$ proceeding in three main steps [13]; $C_2AH_8$ is also responsible for the shoulder at 230 °C on the left side of the peak corresponding to dehydration of $AH_3$ [14],
- At the temperature ranges of 60 – 200, 200 – 300 and up to 650 °C: decomposition of monocarboaluminate $C_4A\check{C}H_{11}$ [15-17],
- Close to 250 °C : a DTG peak related to the decomposition of $AH_3$ [12, 14, 18],
- Between 300 and 430 °C : overlapping DTG peaks due to the decomposition of $AH_3$ and $C_3AH_6$ [19, 20].

This phase assemblage is in good agreement with that derived from XRD, and also consistent with data from the literature [21-23].

The mass change above 550 °C, related to the decomposition of carbonates and was close to 2 wt. % for all the samples. The bound water content, assessed from the weight loss within the temperature range 30-550 °C, slightly increased with the w/c ratio of pastes, as indicated in Figure 102.

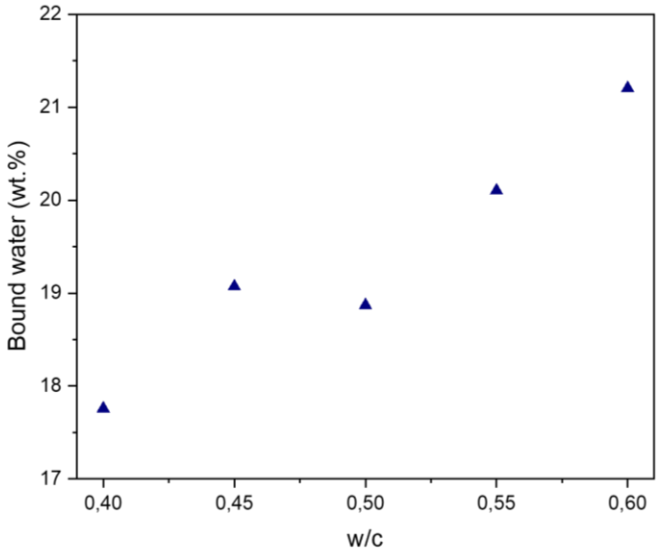


**Figure 102 : Bound water amount of $C_{12}A_7$ pastes with different w/c ratios hydrated at 25 °C for 7 days.**

In Figure 103, the cumulative heat is shown to increase with the to the bound water content after 7 days of hydration.

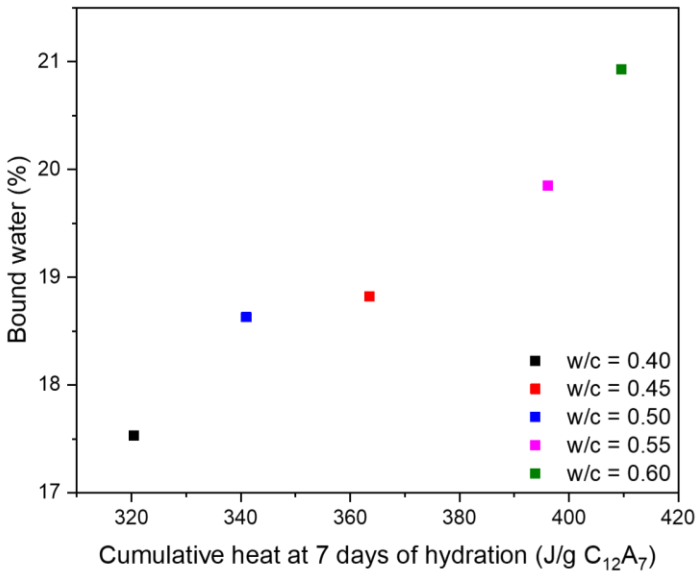


**Figure 103 : Bound water content of $C_{12}A_7$ pastes from TGA results as a function of maximum cumulative heat values after reaching a plateau.**

The linear relationship between cumulative heat and bound water after 7 days suggests that similar mineralogical assemblages precipitated in the different pastes, as already reported by

Raab B. and Poellmann H. [22], and Edmonds R.N. and Majumdar A.J. [21]. This was also evidenced by our XRD and TGA results.

Following TGA and XRD analyses, $^{27}$Al MAS-NMR spectrometry was performed on a 7 day-old $C_{12}A_7$ sample elaborated with a w/c ratio of 0.50 in order to quantitatively determine its mineralogical composition. The collected spectrum (Figure 104) and its corresponding decomposition are presented in Figure 105.

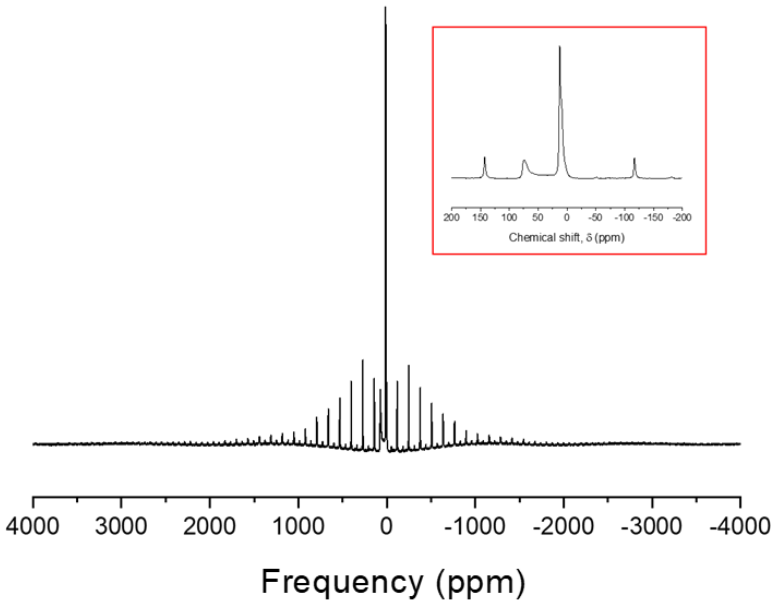


**Figure 104 : $^{27}$Al MAS-NMR spectrum of the 7 d-old $C_{12}A_7$ paste (w/c = 0.50).**

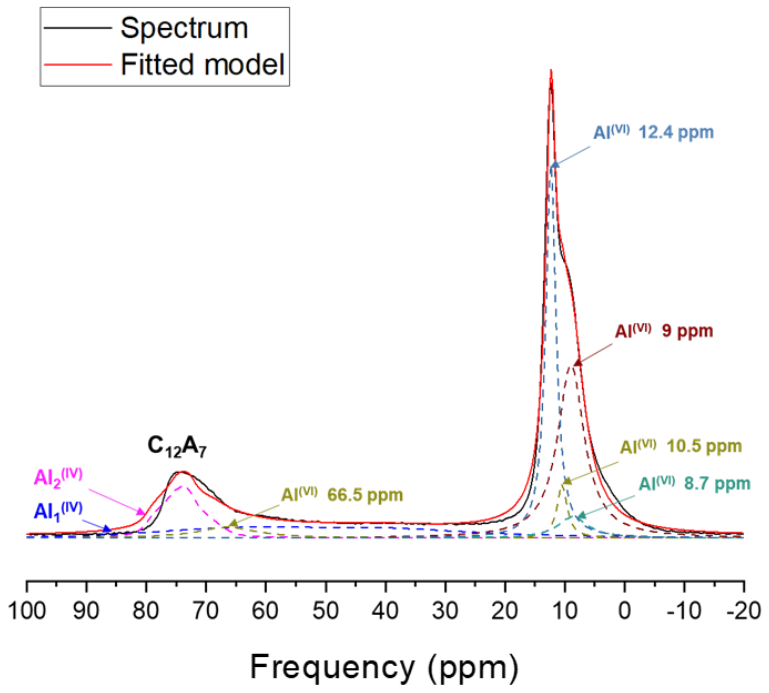


**Figure 105 : Decomposition of the $^{27}$Al MAS-NMR spectrum central bands of the 7 d-old $C_{12}A_7$ paste (w/c = 0.5).**

According to the literature, the two tetrahedral Al sites in $C_{12}A_7$ occur at 86 ppm for $Al_1^{(IV)}$ and 80 ppm for $Al_2^{(IV)}$ [24]. The fitted model resulting from these two tetrahedrally coordinated sites is in agreement with the experimental spectrum attributed to $C_{12}A_7$. From the decomposition of the $^{27}$Al NMR spectrum of the 7 d-old $C_{12}A_7$ paste (w/c = 0.5), the following hydrates were assigned using the data obtained from literature as summarized in Table 27:

- $C_{12}A_7$
- $C_4AČH_{11}$
- $AH_3$
- $C_2AH_8$
- $C_3AH_6$

Besides $C_{12}A_7$, the spectrum was fitted considering four hydrates (Figure 105):

- $C_4AČH_{11}$ (δ = 8.7 ppm corresponding to an octahedrally coordinated Al site),
- $C_2AH_8$ (a sharp octahedral peak at 10.5 ppm and broader tetrahedral one at 66.5 ppm),
- Gibbsite (δ = 9 ppm corresponding to an octahedrally coordinated Al site),
- $C_3AH_6$ (δ = 12.3 ppm corresponding to an octahedrally coordinated Al site).

**Table 27 : Summary of chemical shifts, intensities and quadrupolar parameters corresponding to the identified hydrates from the decomposition of the $^{27}$Al MAS-NMR spectrum of the 7 d-old $C_{12}A_7$ paste (w/c = 0.5).**

| Phase | Site | $\delta_{iso}$ (ppm) | Model | Peak intensity | Quadrupole coupling constant, $C_Q$ (MHz) | Asymmetry parameter, η | Width | Reference |
|---|---|---|---|---|---|---|---|---|
| $C_{12}A_7$ | $Al_1^{(IV)}$ | 86 | Q mas 1/2 | 1800 | 9.7 | 0.4 | - | [24] |
| | $Al_2^{(IV)}$ | 80 | Q mas 1/2 | 8100 | 3.8 | 0.7 | - | |
| $C_2AH_8$ | $Al^{(IV)}$ | 10.5 | Lorentzian | 2495 | - | - | 2 | [13, 25, 26] |
| | $Al^{(VI)}$ | 66.5 | Lorentzian | 507 | - | - | 12 | |
| $C_4AČH_{11}$ | $Al^{(VI)}$ | 8.7 | Lorentzian | 1000 | - | - | 6 | [25] |
| $AH_3$ | $Al^{(VI)}$ | 9 | Lorentzian | 8065 | - | - | 5.4 | [24, 27, 28] |
| $C_3AH_6$ | $Al^{(VI)}$ | 12.4 | Lorentzian | 17439 | - | - | 2.1 | [29] |

Such a decomposition of the spectrum yields the mineralogical composition described in Table 28.

**Table 28 : Quantification of Al-containing phases in the 7 d-old $C_{12}A_7$ paste (w/c = 0.5).**

| Phase | Chemical shift (ppm) | Al atomic fraction (%) | Phase weight fraction (wt. %) | Corresponding bound water content (wt. %) |
|---|---|---|---|---|
| $C_{12}A_7$ | 86/80 | 28 | 21 | - |
| $C_4AČH_{11}$ | 8.7 | 4 | 9 | 3 |
| $AH_3$ | 9 | 32 | 19 | 7 |
| $C_2AH_8$ | 10.5/66.5 | 8 | 11 | 4 |
| $C_3AH_6$ | 12.4 | 28 | 40 | 12 |

The results obtained from the decomposition of the NMR spectrum indicated a remaining amount of $C_{12}A_7$ equal to 21 wt. %. The hydration degree, defined as the amount of reacted anhydrous phases, would thus be equal to 72 % after 7 days of hydration (w/c = 0.5, T = 25°C). It has to be noted that such a value is higher than the hydration degree of 53 % estimated by calorimetry with an in-situ mixing protocol. The use of calorimetric data with the assumption

that dissolution of anhydrous $C_{12}A_7$ phase was the only process contributing to heat release thus seemed irrelevant for the evaluation of the hydration degree.

Regarding the hydrated phases, the agreement between the total bound water contents assessed by $^{27}$Al-NMR spectroscopy (26 wt. %) and TGA was acceptable given the uncertainties of the two techniques.

However and despite the whole consistency of the results obtained and presented in the above section, the mineralogical assemblage estimated by using $^{27}$Al NMR spectrum could be seen as surprising. First, the theoretical fraction of $AH_3$ expected by the stoichiometry of equations (20) and (21) [11] was calculated by taking into account the Al molar fractions of $C_2AH_8$ and $C_3AH_6$ measured from the NMR results. Afterwards, the total fraction of $AH_3$ obtained by the sum of the molar $AH_3$ fractions resulted from these reaction equations was compared to the one measured from the NMR results. The theoretical molar fraction of $AH_3$ (22 %) was found to be smaller than the measured one (32 %).

$$C_{12}A_7 + 51\,H \rightarrow 6\,C_2AH_8 + AH_3 \quad (20)$$

$$C_{12}A_7 + 33\,H \rightarrow 4\,C_3AH_6 + 3\,AH_3 \quad (21)$$

On the other hand, this approach can be applied for the Ca molar fractions. From the NMR results, a 72 % of anhydrous $C_{12}A_7$ was found to be consumed 7 days after hydration. When the Ca molar fractions of calcium-containing hydrates were considered to be formed by the depleted calcium amount of anhydrous phase, a difference was observed. The calcium amount consumed was higher than the sum of the calcium fraction present in calcium aluminate hydrates. As the presence of another calcium-containing phase such as CH and/or CČ was not identified in the solid fraction, one can be concluded on the interest in a further study to determine the Ca concentration evolution in the aqueous phase.

Overall, from TGA, XRD and NMR, it could be concluded that after 7 days of hydration, the mineralogical assemblages was mainly composed of unreacted $C_{12}A_7$, $AH_3$ and $C_3AH_6$, with the presence of much smaller amounts of metastable $C_2AH_8$ and $C_4AČH_{11}$ phases. The evolution of the mineralogical assemblage during the first week of hydration is presented in the following section.

### 1.2. Phase evolution in a $C_{12}A_7$ paste with a w/c ratio of 0.5 over the first week of hydration

Hydration stoppages at 60, 300, 420 min and 7 days were performed on the $C_{12}A_7$ paste (w/c=0.5) in order to describe its mineralogical evolution. The collected solid fractions were characterized by XRD, TGA and $^{27}$Al MAS-NMR spectroscopy.

On the XRD patterns in Figure 106, reflections around 8.4° 2θ and 16.9° 2θ were attributed to $C_2AH_{7.5}$ and around 20° 2θ, 26.5° 2θ and 28.4° 2θ to $C_3AH_6$,. Furthermore, gibbsite was detected in all samples with a small peak at 18.3° 2θ. Meanwhile, unreacted $C_{12}A_7$ was also detected in all samples. Note the additional presence of $C_4AČH_{11}$ in the 7 d-old sample.

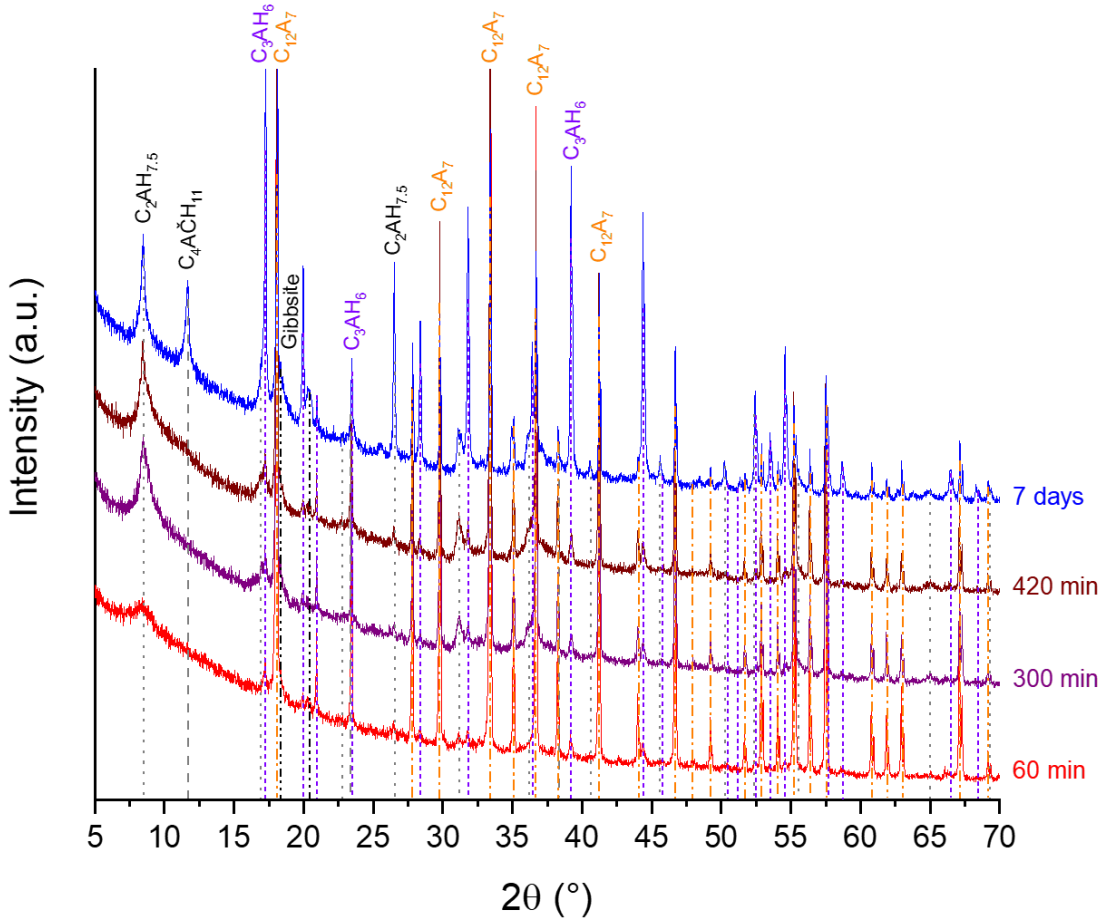


**Figure 106 : XRD patterns of the $C_{12}A_7$ paste with a w/c ratio of 0.5 after increasing periods of hydration.**

Figure 107 shows the TGA and DTG curves of these systems. The thermal events could be assigned as follows as follows based on the dehydration temperatures of hydrates reported in the literature (Table 16):

- $AH_3$
- $C_2AH_{7.5-8}$
- $C_4AČH_{11}$
- $C_3AH_6$

In addition, traces of carbonates were indicated on DTG curves by thermal decompositions above 600 °C for all of the samples. TGA revealed more sensitive than XRD analysis, since with this latter technique, $C_4AČH_{11}$ phase was only detected in the 7-d old $C_{12}A_7$ paste.

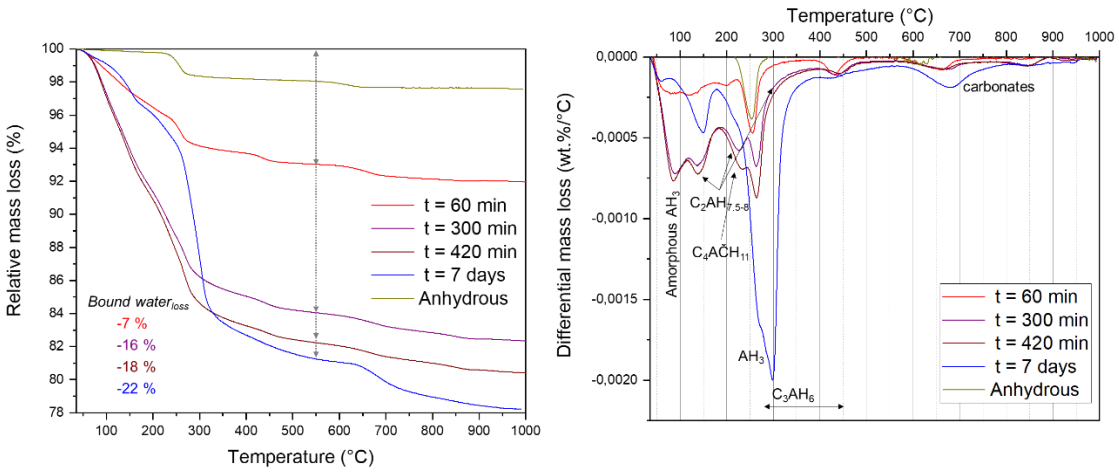


**Figure 107 : TGA and DTG curves obtained from hydrated $C_{12}A_7$ paste with a w/c ratio of 0.5 at 25 °C after increasing periods of hydration. On the TGA curves, the arrow shows the mass loss in the range of temperatures between 30 and 550 °C.**

The bound water content was calculated from the weight loss between 30 °C and 550 °C. Values of 7, 16, 18 and 22 % were achieved after 60 min, 300 min, 420 min and 7 days of hydration respectively. It is interesting to note in Figure 107 that the DTG peak assigned to $C_2AH_{7.5-8}$ increased from 60 min to 300 min, but decreased at later age, whereas the peak assigned to $C_3AH_6$ increased strongly. This result shows that conversion of $C_2AH_{7.5-8}$ into $C_3AH_6$ started after 300 min.

As a complement to XRD and TGA analysis, $^{27}$Al MAS-NMR spectroscopy was carried out to characterize and more importantly quantify the hydration products found in the solid fractions of the paste samples.

Mineralogical assemblages of the solid fractions were obtained from the decomposition of the $^{27}$Al NMR spectrum. The distinction between tetrahedrally and octahedrally coordinated Al sites in hydrated $C_{12}A_7$ paste is shown in Figure 108. Two overlapping centerbands were observed at 86 ppm and 80 ppm due to the two tetrahedrally coordinated Al sites of unreacted $C_{12}A_7$ [24].

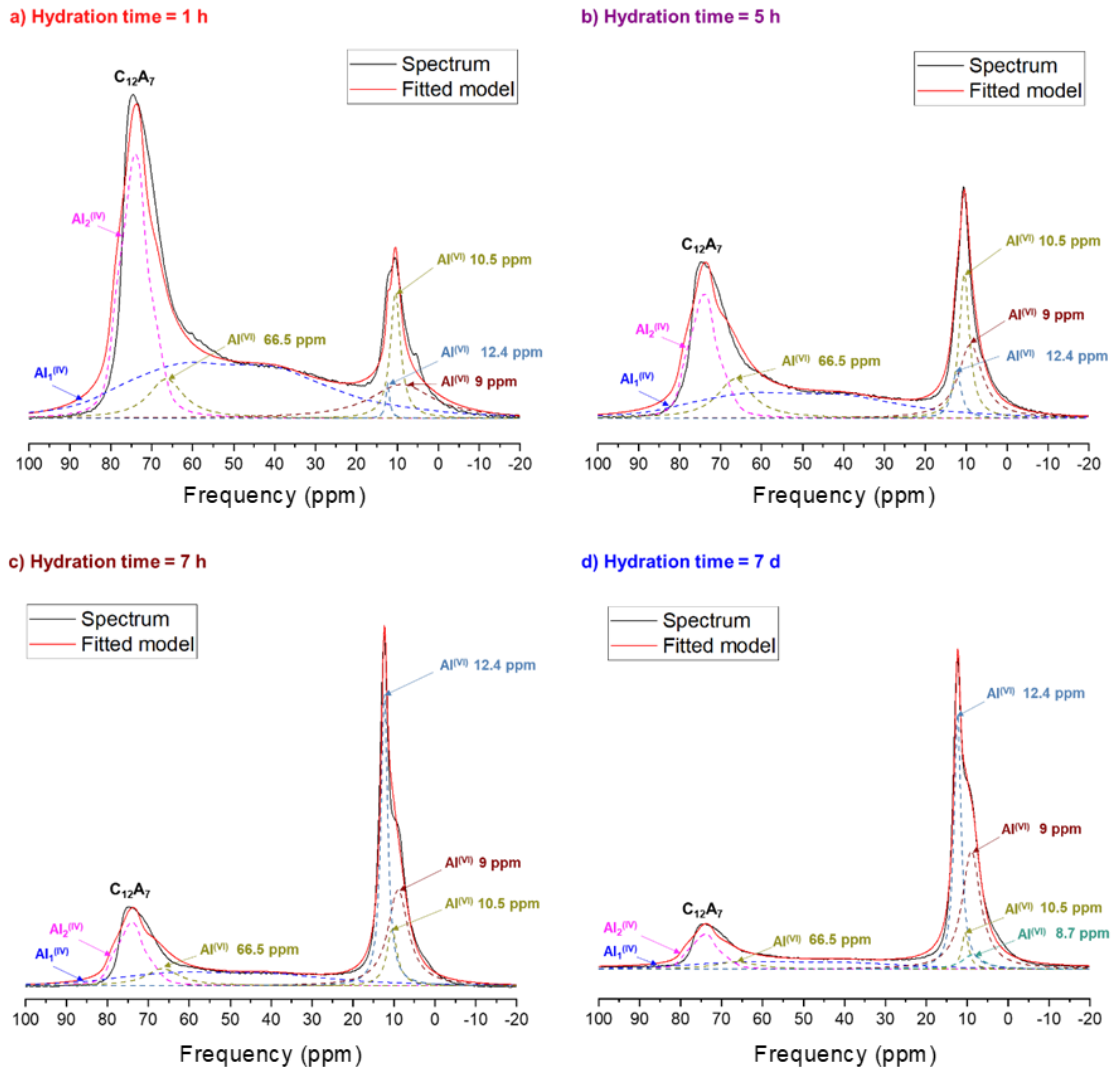


**Figure 108 : $^{27}$Al solid-state NMR spectra of $C_{12}A_7$ paste with a w/c ratio of 0.5 at different characterization times: a) 1 h, b) 5 h, c) 7 h and d) 7 days.**

In agreement with the XRD and TGA results, the presence of $AH_3$ (gibbsite), $C_2AH_8$ and $C_3AH_6$ was confirmed from the decomposition of the spectra for all solid fractions at 9 ppm [24, 27, 28], 10.5/66.5 ppm [13, 25, 26] and 12.4 ppm [24], respectively. Besides, the presence of a carbonated phase such as monocarboaluminate was only identified from the spectrum of the 7-d old paste at 8.7 ppm [25]. Table 29 summarizes the quantification results of Al-containing phases in the different $C_{12}A_7$ paste samples.

**Table 29 : Quantification by $^{27}$Al NMR of Al-containing phases in the $C_{12}A_7$ paste (w/c = 0.5) at four different characterization times.**

| Hydration stoppage time | Phases | Chemical shift (ppm) | Al atomic fraction (%) | Phase weight fraction (wt. %) | Corresponding bound water content (wt. %) |
|---|---|---|---|---|---|
| **1 h** | $C_{12}A_7$ | 86/80 | 74 | 67 | - |
| | $AH_3$ | 9 | 11 | 8 | 3 |
| | $C_2AH_8$ | 10.5/66.5 | 14 | 23 | 9 |
| | $C_3AH_6$ | 12.4 | 1 | 2 | 0.5 |
| **5 h** | $C_{12}A_7$ | 86/80 | 55 | 46 | - |
| | $AH_3$ | 9 | 16 | 10 | 4 |
| | $C_2AH_8$ | 10.5/66.5 | 25 | 38 | 15 |
| | $C_3AH_6$ | 12.4 | 4 | 6 | 2 |
| **7 h** | $C_{12}A_7$ | 86/80 | 39 | 30 | - |
| | $AH_3$ | 9 | 23 | 14 | 5 |
| | $C_2AH_8$ | 10.5/66.5 | 14 | 20 | 8 |
| | $C_3AH_6$ | 12.4 | 24 | 36 | 10 |
| **7 days** | $C_{12}A_7$ | 86/80 | 28 | 21 | - |
| | $C_4AČH_{11}$ | 8.7 | 4 | 9 | 3 |
| | $AH_3$ | 9 | 32 | 19 | 7 |
| | $C_2AH_8$ | 10.5/66.5 | 8 | 11 | 4 |
| | $C_3AH_6$ | 12.4 | 28 | 40 | 12 |

Based on these mineralogical compositions, the bound water content was calculated and found equal to 12 wt. %, 21 wt. %, 23 wt. % and 26 wt. % after 1 h, 5 h, 7 h and 7 d of hydration, respectively, which could be regarded as consistent with the data derived from TGA (7, 16, 18 and 26 wt. % respectively) given the uncertainties associated to the NMR spectra decomposition.

In Figure 109, the mineralogical evolution and heat flow profile of the $C_{12}A_7$ paste (w/c=0.5) were superimposed. It can be observed that the second heat flow peak occurred simultaneously with a decrease in the content of $C_2AH_{7.5\text{-}8}$, and an increase in those of $C_3AH_6$ and $AH_3$. The second thermal event thus seemed linked with the start of the conversion process.

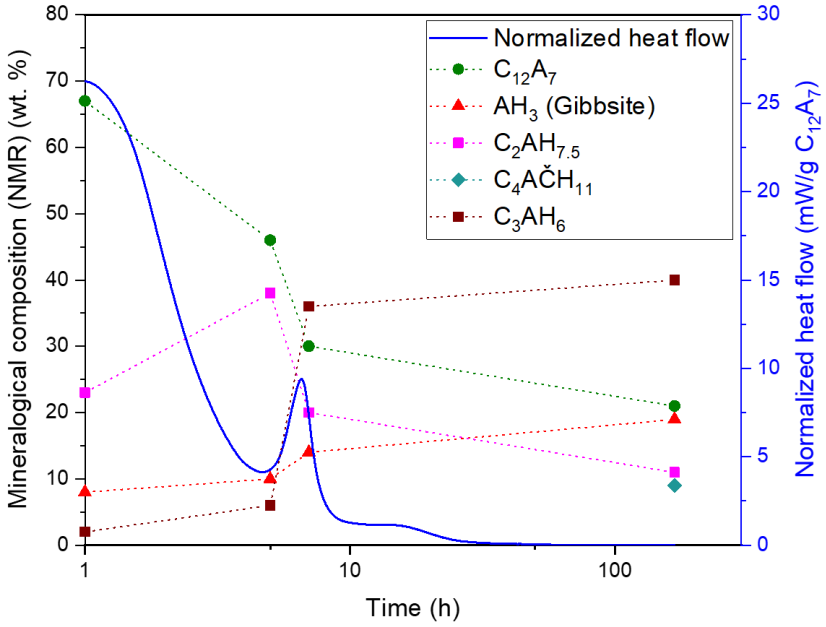


**Figure 109 : Investigation of $C_{12}A_7$ hydration for 7 days: heat flow and phase evolution.**

From these results, it can be concluded that $C_{12}A_7$ hydration occurred quickly after mixing and was accompanied by the precipitation of metastable $C_2AH_8$ which started to convert into stable $C_3AH_6$ was after 5 hours of hydration.

**To sum up:**

From TGA, XRD and NMR results, it was concluded that after 7 days of hydration at 25 °C, the mineralogical assemblage of $C_{12}A_7$ pastes with w/c ratio ranging from 0.4 to 0.6 was composed of $C_{12}A_7$, $C_3AH_6$ and $AH_3$, with smaller amounts of calcium aluminate hydrates $C_4AČH_{11}$ (caused by $CO_2$ uptake from air) and metastable $C_2AH_{7.5}$. Despite different heat flow profiles, with the presence of two or three exothermic peaks as the w/c ratio was increased, similar mineralogical assemblages were achieved after 7 days of hydration.

As expected from the literature, $C_{12}A_7$ reacted rapidly, the acceleration period starting right after the contact with water. Under our experimental conditions, 72 % of initially introduced $C_{12}A_7$ was consumed after 7 hours when the w/c ratio was set to 0.5. The beginning of the conversion reaction also occurred quickly after mixing, since the $C_3AH_6$ amount started to increase at the expense of $C_2AH_8$ 7 hours only after mixing. The starting of this stage seemed to be concomitant with the heat flow peak observed by isothermal calorimetry.

Complementary investigation of $C_{12}A_7$ hydration in suspensions at 25 °C is presented in the next section in order to point out the limiting steps.

## 2. Hydration study of $C_{12}A_7$ suspensions at early age

### 2.1. Course of $C_{12}A_7$ hydration during the first 24 hours – w/c = 25

In order to describe more precisely the course of $C_{12}A_7$ hydration is suspension at w/c = 25, as detailed in Chapter 2.3 (Figure 44), the chemical composition of the liquid fraction and the mineralogy of the solid fraction were characterized after increasing hydration times as follows: 30, 60, 90, 120, 180, 240, 300, 330, 360, 390 and 420 min. The characterization times are shown on the conductivity curve in Figure 110. Note that the pointedness of the drop at 5.5 hours is an artefact caused by the sampling of the mixture at this period of time.

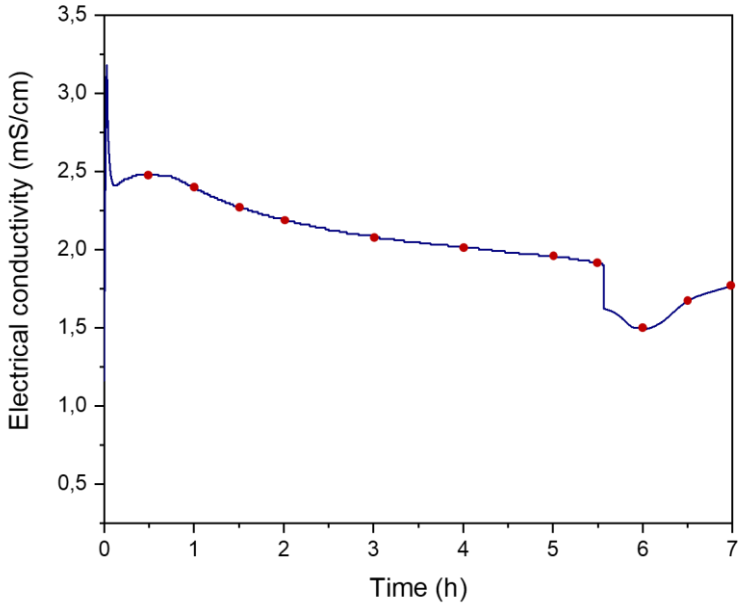


**Figure 110 : Definition of characterization times (red dots) based on the variation of the electrical conductivity during $C_{12}A_7$ hydration with a w/c = 25.**

#### 2.1.1. Characterization of the solid fraction of suspensions

In Figure 111, the XRD patterns of the samples taken during the first 7 hours of hydration indicated the presence of unreacted $C_{12}A_7$ and $C_2AH_{7.5}$. The decrease in the $C_{12}A_7$ amount could be qualitatively observed from these patterns whereas the area of $C_2AH_{7.5}$ phase peaks increased as hydration progressed. Meanwhile, the $AH_3$ (gibbsite) peak area also increased. The presence of monocarboaluminate $C_4A\check{C}H_{11}$ was observed in the analyzed sample 7 hours after mixing. The precipitation of this hydrate could result from carbonation occurring during hydration stoppage and/or drying prior to XRD analysis. In addition, the presence of small amounts of poorly crystalline $CAH_{10}$ was suspected with small peaks close to 6.2° 2θ and 12.4° 2θ in the

sample hydrated for 7 hours. In brief, according to the XRD patterns of the solid fraction of suspensions hydrated for 7 h at 25 °C, the following products were identified:

- $CAH_{10}$ (possibly at 7 h of hydration),
- $C_2AH_{7.5}$,
- $AH_3$ indexed as gibbsite,
- monocarboaluminate $C_4A\check{C}H_{11}$,
- unreacted $C_{12}A_7$.

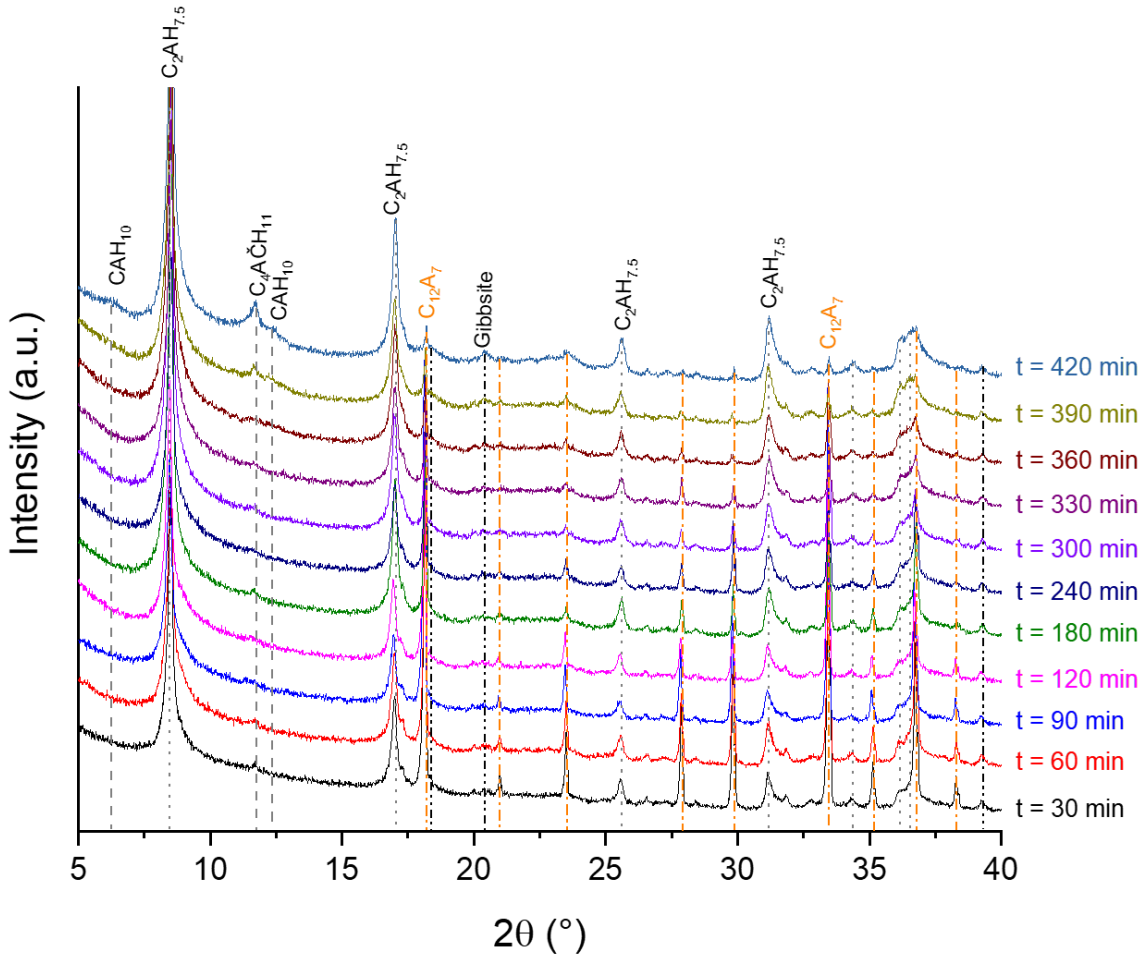


**Figure 111 : XRD patterns of the solid fractions of $C_{12}A_7$ suspension with a w/c of 25 after increasing periods of hydration at 25 °C.**

The thermograms of the studied samples and their derivatives are plotted in Figure 112. As expected, the mass loss from 35 to 550 °C, corresponding to bound water, increased with time; At all characterization times, the plots showed the presence of:

- amorphous $AH_3$ (mass loss around 60 °C [30])
- gibbsite (mass loss in the temperature range 220-280 °C with a main peak close to 250 °C),
- $C_2AH_8$ (mass loss below 100 °C [31] and at 110, 170 and approximately 300 °C [13]).

The shoulder on the left side of the DTG peak corresponding to the decomposition of $AH_3$ at around 200 °C was assigned to $C_4A\check{C}H_{11}$ in the samples hydrated more than 6.5 hours.

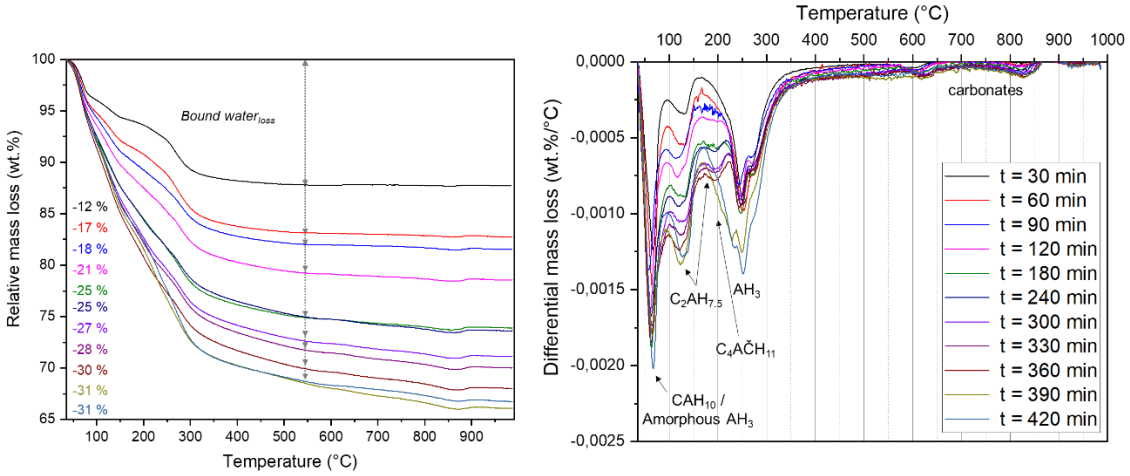


**Figure 112 : TGA and DTG curves obtained from $C_{12}A_7$ suspension with a w/c ratio of 25 after increasing periods of hydration at 25 °C.**

As a complement to XRD and TGA studies, $^{27}Al$ NMR spectroscopy was carried out to quantify the hydration products formed in the solid fractions of the suspension. Both tetrahedrally and octahedrally coordinated Al sites were observed on the spectra (Figure 113). However, the identification of hydrates was complex. $C_2AH_8$, $C_4A\check{C}H_{11}$ and aluminium hydroxide all contained Al atoms in octahedral environments with close chemical shifts [32]. The crystallinity of the aluminium hydroxide was another concern. The chemical shift of this phase varies with its crystallinity (higher crystallinity resulting in higher chemical shift). Consequently, in this study, a chemical shift at 9 ppm was attributed to $AH_3$. Considering the phases detected by XRD and TGA, a model was fitted to the spectra in order to quantify the hydration products.

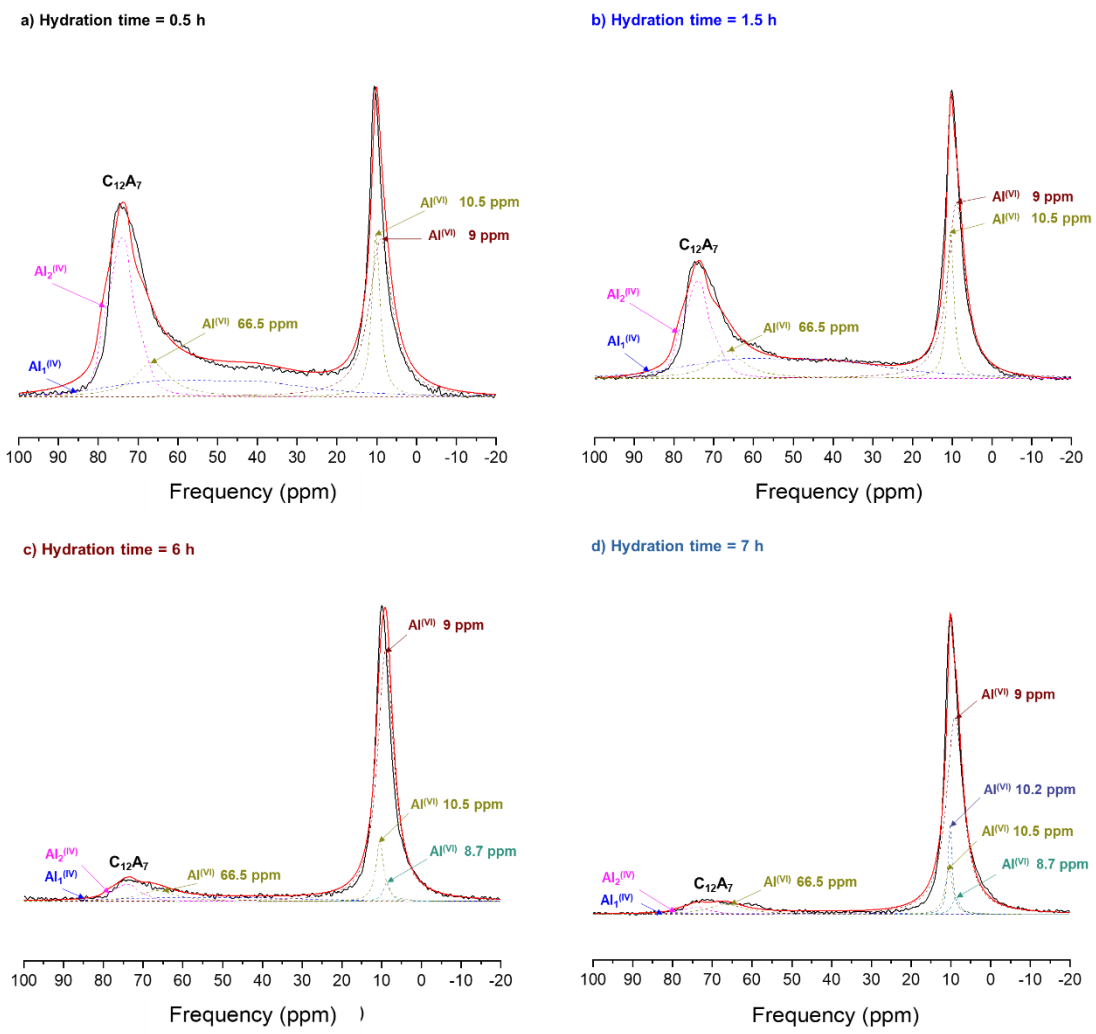


**Figure 113 : $^{27}$Al NMR spectra of $C_{12}A_7$ suspension with a w/c of 25 at different hydration times: a) 0.5 h, b) 1.5 h, c) 6 h and d) 7 h.**

For each of the solid fractions, two overlapping centerbands of unreacted $C_{12}A_7$ related to the two tetrahedrally coordinated Al sites of this phase appeared as shown in Figure 113. In the fitted model, the intensity ratio of 4:3 imposed by the $C_{12}A_7$ structure [24] for the $Al_1$(IV) and $Al_2$(IV) sites was respected. From 0.5 h to 7 h of hydration, the content of unreacted $C_{12}A_7$ decreased from 51 to 7 wt. % (Table 30).

After 30 minutes, the depleted fraction of $C_{12}A_7$ was 44% based on the NMR atomic fractions of Al sites and the amount of aluminium hydroxide and of metastable $C_2AH_{7.5}$ were calculated as 19 wt. % and 30 wt. % respectively.

After 7 hours of hydration, the analyzed sample were constituted of approximately 59 wt. % of aluminium hydroxide, 9 wt. % of monocarboaluminate, 25 wt. % $C_2AH_{7.5}$ and 7 wt. % anhydrous $C_{12}A_7$.

**Table 30 : Quantification of Al-containing phases in $C_{12}A_7$ suspensions (w/c = 25) at 0.5 h, 1.5 h, 6 h and 7 h by $^{27}$Al NMR.**

| Hydration stoppage time (h) | Phase | Chemical shift (ppm) | Al atomic fraction (%) | Phase weight fraction (wt. %) | Corresponding bound water content (wt. %) |
|---|---|---|---|---|---|
| **0.5** | $C_{12}A_7$ | 86/80 | 56 | 51 | - |
| | $AH_3$ | 9 | 26 | 19 | 7 |
| | $C_2AH_{7.5}$ | 10.5/66.5 | 18 | 30 | 12 |
| **1.5** | $C_{12}A_7$ | 86/80 | 49 | 45 | - |
| | $AH_3$ | 9 | 32 | 23 | 8 |
| | $C_2AH_{7.5}$ | 10.5/66.5 | 19 | 32 | 13 |
| **6** | $C_{12}A_7$ | 86/80 | 14 | 14 | - |
| | $C_4AČH_{11}$ | 8.7 | 2 | 6 | 2 |
| | $AH_3$ | 9 | 69 | 54 | 19 |
| | $C_2AH_{7.5}$ | 10.5/66.5 | 15 | 27 | 11 |
| **7** | $C_{12}A_7$ | 86/80 | 7 | 7 | - |
| | $C_4AČH_{11}$ | 8.7 | 3 | 9 | 3 |
| | $AH_3$ | 9 | 76 | 59 | 21 |
| | $C_2AH_{7.5}$ | 10.5/66.5 | 14 | 25 | 10 |

Based on these mineralogical compositions, the calculated bound water content was equal to 19 wt. %, 21 wt. %, 32 wt. % and 34 wt. % after 0.5 h, 1.5 h, 6 h and 7 h, respectively. This was reasonably consistent with the set of data obtained by TGA (12 wt. %, 18 wt. %, 30 wt. % and 31 wt. % respectively), given the uncertainties of NMR spectra decomposition.

The theoretical fraction of $AH_3$ expected by the stoichiometry of equations (20) was calculated by taking into account the Al molar fractions of $C_2AH_8$ measured from the NMR results for 0.5 h-old and 1.5 h-old solid fractions. Afterwards, the resulting theoretical fraction of $AH_3$ was compared to the one measured from the NMR results. The theoretical molar fractions of $AH_3$ (3 % for both of the samples) was found to be smaller than the measured ones. Such a difference might highlight that the precipitation of $AH_3$ had already begun before the precipitation of $C_2AH_8$ according to the stoichiometry of equations (20).

The bound water content from TGA and NMR, as well as the mineralogical composition obtained from NMR, are superimposed on the conductivity curve in Figure 114.

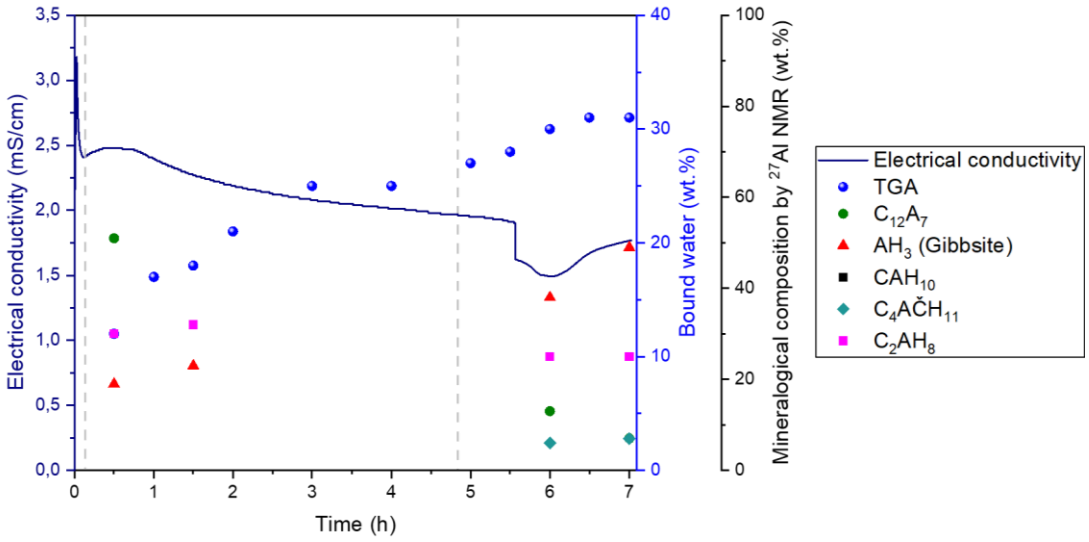


**Figure 114 : Investigation of $C_{12}A_7$ hydration at early age: electrical conductivity and phase evolution.**

The increase in aluminium hydroxide content was not concomitant with an increase in the reflection peak areas gibbsite on the XRD patterns (cf Figure 111). Such an observation suggested that the aluminium hydroxide precipitating in the system was an amorphous or a microcrystalline form of the aluminium hydroxide. That was also supported by the weight loss increase slightly below 100 °C on the DTG curves, without any increase of the weight loss measured at 250 °C until 6 h.

### 2.1.2. Characterization of the liquid fraction of suspensions

Figure 115 shows the evolution of the pH and chemical composition of the aqueous fraction of the $C_{12}A_7$ suspension (w/c = 25).

The Ca and Al concentrations increased rapidly within the first minutes of hydration and reached a maximum after 1.5 h of hydration. Then they decreased slowly until 5 h of hydration. Afterwards, the concentrations decreased rapidly until the end of the monitoring. Meanwhile, the pH showed little change over the period.

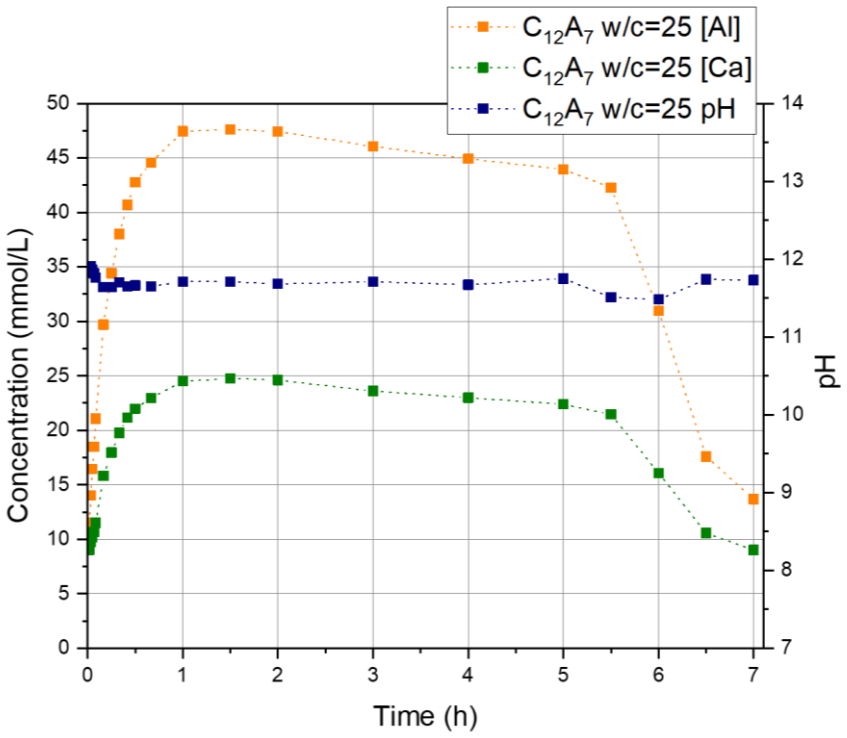


**Figure 115 : Characterization of the liquid fractions of $C_{12}A_7$ suspension (w/c ratio = 25, T = 25 °C) during the first seven hours of hydration: evolution of pH and chemical composition.**

From these raw results, the ratio between calcium and aluminate ions was plotted as a function of time (Figure 116). This $[Ca^{2+}]/[Al_{tot}]$ ratio decreased within the first 15 minutes of hydration to a value of around 0.50 and remained constant until 6 h. Noticeably, this ratio was smaller than the Ca/Al ratio of 0.86 expected if the sole process is the congruent dissolution of $C_{12}A_7$ phase following equation (19):

$$C_{12}A_7 + 33\ H_2O \rightleftharpoons 12\ Ca^{2+} + 14\ Al(OH)_4^- + 10\ OH^- \qquad (19)$$

Damidot *et al.* [33] investigated the hydration of $C_{12}A_7$ with a w/c of 10 at 20 °C. As $C_2AH_8$ precipitated, the Ca/Al ratio in solution decreased within 10 minutes under their experimental conditions. This was explained by the fact that the Ca/Al ratio of precipitating $C_2AH_8$ (1) was higher than that of dissolving $C_{12}A_7$ (0.86). Then, the Ca and Al concentrations decreased slowly from 24 to 21 mmol/l and from 45 to 42 mmol/l respectively, which is in fairly good agreement with our observations. In their work, this period was attributed to nucleation of $AH_3$. Also, it was claimed that the $AH_3$ formed in this period was not crystalline and thus could not be detected by XRD.

After 6 h of hydration, the Ca/Al ratio increased again. This was supported by increased precipitation of $AH_3$ evidenced by the weight loss increase measured at 250 °C on DTG curve.

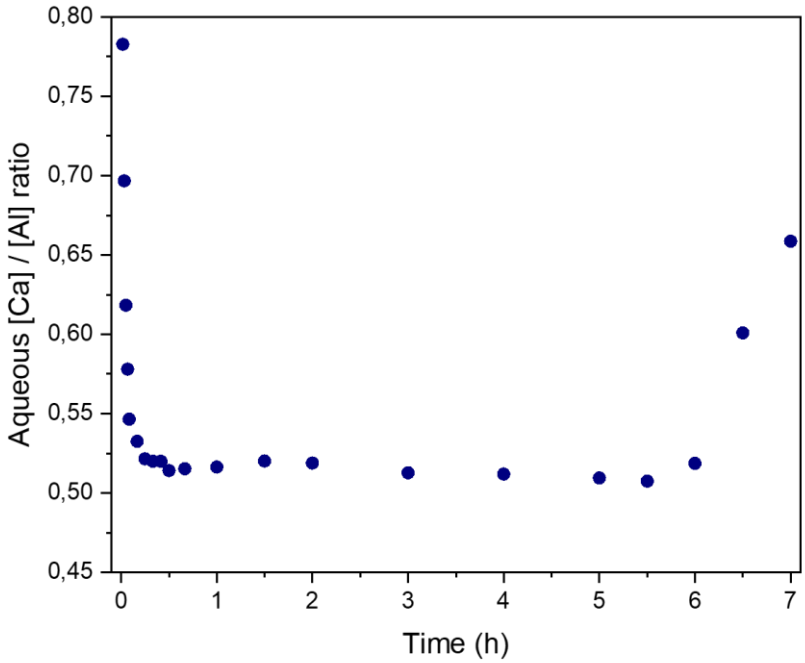


**Figure 116 : Evolution of Ca/Al ratio in the liquid fraction as a function of time during $C_{12}A_7$ hydration in suspension (w/c = 25 – T = 25 °C).**

In the following section, the hydration path followed by aluminium and calcium ions was plotted in order to identify the limiting steps during hydration.

### 2.1.3. Investigation of the hydration pathway

#### *2.1.3.1 First approach: calculation of the saturation indexes*

Figure 117 shows the evolution over time of the saturation indexes of the main phases involved in $C_{12}A_7$ hydration.

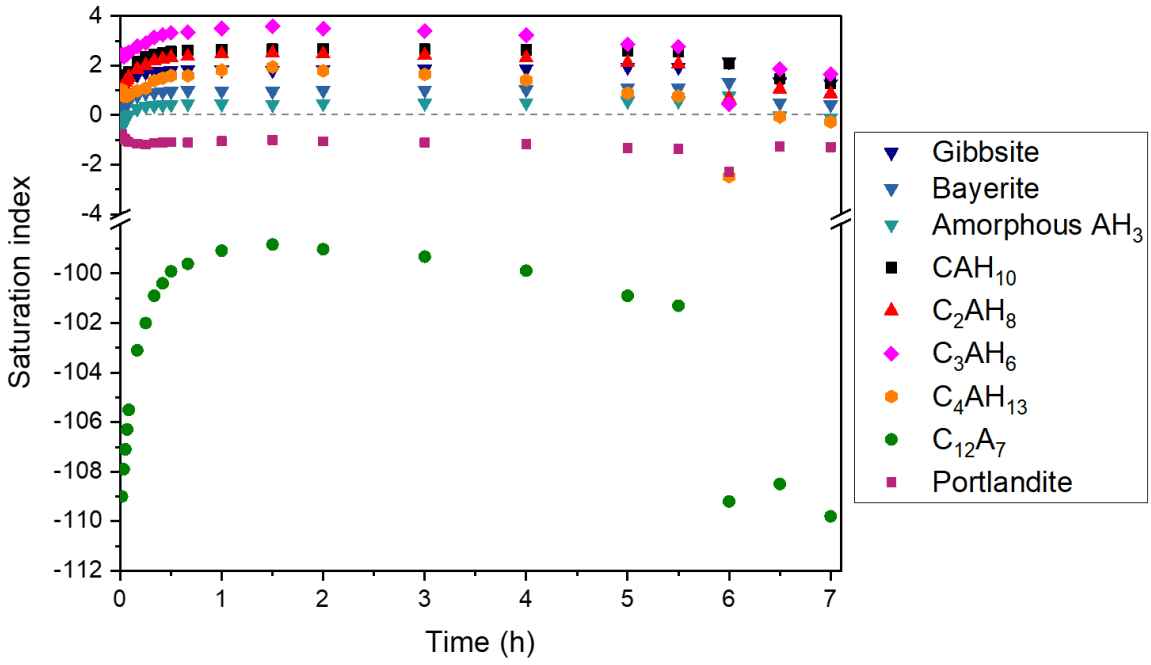


**Figure 117 : Evolution of saturation indexes in the $CaO$-$Al_2O_3$-$H_2O$ system as a function of time during the hydration of $C_{12}A_7$ in suspension (w/c = 25 – T = 25 °C).**

The saturation index of $C_{12}A_7$ was always negative, and exhibited a significant drop after 5.5 h of hydration. The saturation index of $CAH_{10}$, $C_2AH_8$ and $C_3AH_6$ remained positive, meaning that precipitation of these phases was possible from a thermodynamic point of view. The saturation index of aluminium hydroxide polymorphs was positive excepting amorphous $AH_3$.

Just as for the phases investigated in the previous chapters, the relevance of the calculated saturation index values discussed above is questionable since the electroneutrality of the solution was not reached from speciation calculations. Figure 118 shows the evolution as a function of time of the electrical imbalance normalized by the ionic strength of the solution.

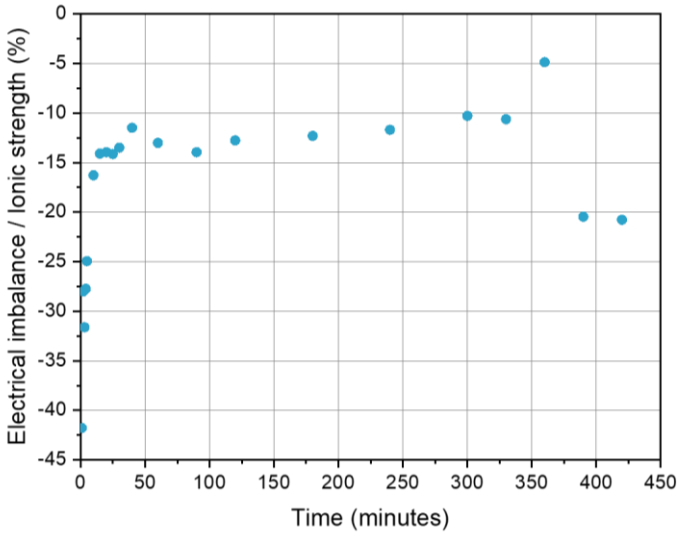


**Figure 118 : Evolution of the electrical imbalance normalized by the ionic strength for the simulations carried out with CHESS and the CEMDATA2018 database as a function of the hydration time.**

### *2.1.3.2 Second approach: the solubility diagram*

To circumvent this electroneutrality issue, the hydration path followed by aqueous calcium and aluminium concentrations was plotted in the {$CaO$-$Al_2O_3$-$H_2O$} phase diagram (Figure 119). In this diagram, empty dots correspond to the hydration stage during which Ca and Al aqueous concentrations increased up to a maximum. Filled dots correspond to the hydration stage during which these concentrations decreased slightly. From this diagram, several comments can be made.

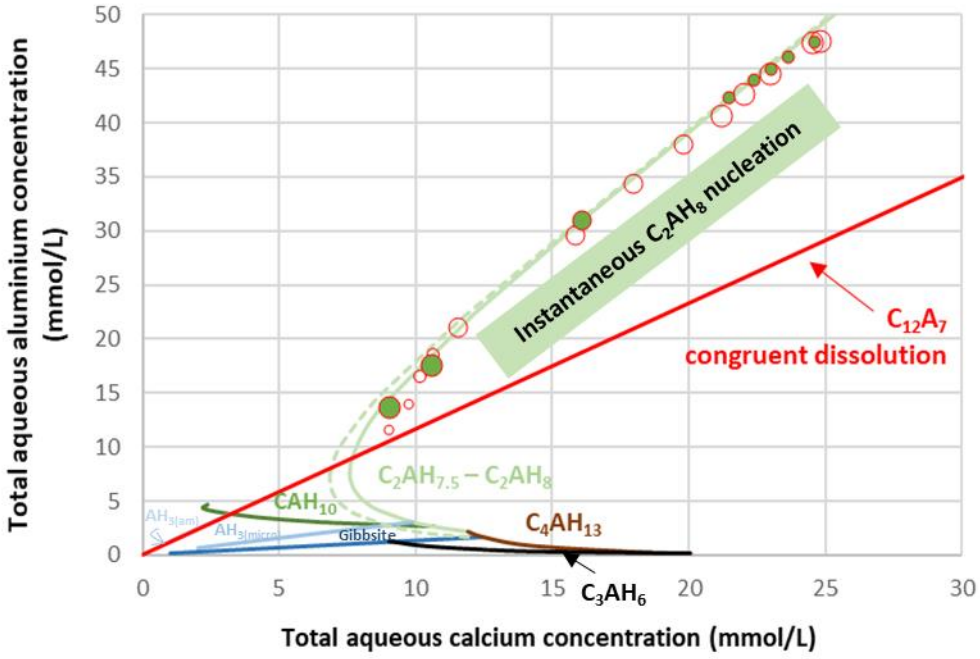


**Figure 119 : Total calcium and aluminium concentrations measured in the liquid fraction during $C_{12}A_7$ hydration (w/c = 25 – T = 25 °C) plotted in the {$CaO$-$Al_2O_3$-$H_2O$} phase diagram. Note that the red line is not a solubility curve. It simply shows the expected concentrations if the system is driven by congruent dissolution of $C_{12}A_7$.**

On this diagram, empty dots correspond to the hydration stage during which calcium and aluminate ions concentrations were increasing up to a maximum. Filled dots correspond to the hydration stage during which these concentrations were decreasing. The dots getting larger depict the concentration evolution of the solution through hydration time.

It appeared that 30 minutes after mixing, the Ca and Al aqueous concentrations were located close to the intersection between the $C_2AH_8$ solubility line and the $C_{12}A_7$ congruent dissolution line. The system was also strongly supersaturated with respect to aluminium hydroxide. At this moment, depletion of $C_{12}A_7$ as well as precipitation of $C_2AH_{7.5\text{-}8}$ and aluminium hydroxide were observed experimentally in the solid fraction. It can thus be assumed that $C_{12}A_7$ started to dissolve readily after mixing. The Ca and Al concentrations increased following the congruent dissolution line of $C_{12}A_7$, with possible precipitation of $AH_3$, until crossing the solubility curve of $C_2AH_8$ which started to precipitate. At this point, the pore solution composition was controlled by the $C_2AH_8$ solubility.

After this first period, the aqueous calcium and aluminium concentrations diverged from $C_{12}A_7$ congruent dissolution line, but remained located on the $C_2AH_8$ solubility line as $C_{12}A_7$ dissolution progressed. The second stage of hydration was characterized by a solution composition governed by the solubility of $C_2AH_{7.5\text{-}8}$. During this period, the mineralogical assemblages did not evolve drastically and a slow $C_{12}A_7$ dissolution occurred. Since the precipitation of $C_2AH_8$ is reported as instantaneous after crossing the zone above its solubility curve [34], one might assume that the limiting step during this period was the precipitation of

aluminium hydroxide bringing hydroxide ions for further $C_2AH_8$ precipitation. Such an assumption is consistent with the fact that the amount of $C_2AH_8$ remained approximately constant whereas the amount of aluminium hydroxide quantified by $^{27}$Al-NMR analysis increased. The trigger for concentration decrease and further precipitation of hydrates might be produced by the increased precipitation of aluminium hydroxide.

## 3. Summary and discussion

In this chapter, the hydration of synthetic $C_{12}A_7$ was investigated.

After 7 days of hydration and for a paste elaborated with a w/c ratio of 0.5, the hydration degree, defined here as the amount of dissolved $C_{12}A_7$ and estimated by using isothermal calorimetry, was found to be equal to 53 % while a hydration degree of 72 %, obtained from the quantification of the reacted anhydrous phase by NMR, would be achieved 7 days after mixing pure water and the studied $C_{12}A_7$ synthetic phase. Regarding the hydrates and for a paste elaborated with a w/c ratio of 0.5, the mineralogical assemblage was composed of 32 % of aluminium hydroxide and 40 % of calcium aluminate phases ($C_2AH_8$, $C_4AČH_{11}$ and $C_3AH_6$).

The beginning of hydration was characterized by a fast dissolution of $C_{12}A_7$, accompanied by the precipitation of aluminium hydroxide and then $C_2AH_8$ as soon as the aqueous calcium and aluminium concentrations exceeded the solubility curve of $C_2AH_8$ in the {$CaO$-$Al_2O_3$-$H_2O$} diagram. A second period of hydration was then characterized by a solution composition governed by the solubility of $C_2AH_8$. During this stage, precipitation of aluminium hydroxide could be assumed as the hydration-limiting step, although its precipitation did not seem to be hindered in the first stage of hydration. Finally, a last period was characterized by a decrease in the concentrations of aluminium and calcium ions, which still followed the solubility curves of $C_2AH_{7.5}$-$C_2AH_8$ until its conversion to $C_3AH_6$.

## 4. References

[1] P. F. G. Banfill, "Superplasticizers for Ciment Fondu. Part 2: Effects of temperature on the hydration reactions," *Advances in Cement Research,* vol. 7, no. 28, pp. 151-157, 1995.

[2] W. Kurdowski, *Cement and Concrete Chemistry*. Krakow, Poland: Springer, Netherlands, New York, 2014, p. 705.

[3] H.-G. Park, S.-K. Sung, C.-G. Park, and J.-P. Won, "Influence of a C12A7 mineral-based accelerator on the strength and durability of shotcrete," *Cement and Concrete Research,* vol. 38, no. 3, pp. 379-385, 2008/03/01/ 2008.

[4] H. T. Nguyen, "Transfert hydrique dans le milieu poreux réactif : Application à l'étude de séchage d'une pâte pure ettringitique au jeune âge," Doctorat, Mécanique, Energétique, Génie Civil, Acoustique, INSA Lyon, Ecole Doctorale ED162, INSA Lyon, 2018LYSEI124, 2018.

[5] A. Negro, L. Montanaro, and A. Bachiorrini, "On the reactivity of the cement clinkers components by means of Laser Granulometer," *Cement and Concrete Research,* vol. 15, no. 2, pp. 315-319, 1985/03/01/ 1985.

[6] A. Capmas, D. Sorrentino, and D. Damidot, "The effect of temperature on the setting time of calcium aluminate cements," in *Calcium Aluminate Cements: Proceedings of a Symposium*, R. J. Mangabhai, Ed. London: Taylor&Francis, CRC Press, 1990, pp. 65-80.

[7] N. Ukrainczyk, "Chemical Shrinkage During Hydration Reactions of Calcium Aluminate Cement," *Austin Journal of Chemical Engineering,* vol. 1, no. 3, pp. 1-7, 2014.

[8] D. D. a. A. Rettel, "Effect of Gypsum on CA and $C_{12}A_7$ Hydration at Room Temperature," in *Cement's Contribution to the Development in the 21st Century*, Durban, South Africa, 2003, pp. 1855-1866: Proceedings of the 11th International Congress on the Chemistry of Cement (ICCC).

[9] D. Damidot, D. Sorrentino, and D. Guinot, "Factors influencing the nucleation and growth of the hydrates in cementitious systems : an experimental approach," presented at the 2nd International RILEM symposium on hydration and setting : why does cement set? an interdisciplinary approach Dijon, 1997 Available: https://www.researchgate.net/profile/Denis_Damidot/publication/269707339_Factors_influencing_the_nucleation_and_growth_of_the_hydrates_in_cementitious_systems_an_experimental_approach/links/54944c910cf2de21bb561b7f.pdf

[10] A. J. Majumbar, B. Singh, and R. N. Edmonds, "Hydration of mixtures of C12A7 and granulated blastfurnace slag," *Cement and Concrete Research,* vol. 19, no. 6, pp. 848-856, 1989/11/01/ 1989.

[11] Z. He and Y. Li, "The Influence of Mayenite Employed as a Functional Component on Hydration Properties of Ordinary Portland Cement," *Materials,* vol. 11, no. 10, 2018.

[12] P. Lura, F. Winnefeld, and X. Fang, "A simple method for determining the total amount of physically and chemically bound water of different cements," *Journal of Thermal Analysis and Calorimetry*, vol. 130, no. 2, pp. 653-660, 2017/11/01 2017.

[13] N. Ukrainczyk, T. Matusinovic, S. Kurajica, B. Zimmermann, and J. Sipusic, "Dehydration of a layered double hydroxide—$C_2AH_8$," *Thermochimica Acta,* vol. 464, no. 1, pp. 7-15, 2007/11/25 2007.

[14] T. Dos Santos *et al.*, "Gluconate action in the hydration of calcium aluminate cements: Theoretical study, processing of aqueous suspensions and hydration reactivation," *Journal of the European Ceramic Society,* vol. 39, no. 8, pp. 2748-2759, 2019/07/01/ 2019.

[15] U. M. Ukrainczyk N, Šipušić J, Matusinović T., "XRD and TGA investigation of hardened cement paste," presented at the 11th conference on materials, processes, friction and wear, Vela Luka, Croatia, 2006.

[16] J. Kaufmann, R. Loser, F. Winnefeld, and A. Leemann, "Sulfate resistance and phase composition of shotcrete," *Tunnelling and Underground Space Technology,* vol. 109, p. 103760, 2021/03/01/ 2021.

[17] X. Jing, Y. Zhang, H. Liu, J. Liu, and S. Kong, "Effect of Aluminum Sulfate on the Hydration of Tricalcium Aluminate," *IOP Conference Series: Earth and Environmental Science,* vol. 719, no. 2, p. 022079, 2021/04/01 2021.

[18] K. Irisawa, I. Garcia-Lodeiro, and H. Kinoshita, "Influence of mixing solution on characteristics of calcium aluminate cement modified with sodium polyphosphate," *Cement and Concrete Research,* vol. 128, p. 105951, 2020/02/01/ 2020.

[19] N. Collier, "Transition and Decomposition Temperatures of Cement Phases – a Collection of Thermal Analysis Data," *Ceramics Silikaty,* vol. 60, 10/01 2016.

[20] S. Joseph, J. Skibsted, and Ö. Cizer, "A quantitative study of the C3A hydration," *Cement and Concrete Research,* vol. 115, pp. 145-159, 2019/01/01/ 2019.

[21] R. N. Edmonds and A. J. Majumdar, "The hydration of 12CaO.7A12O3 at different temperatures," *Cement and Concrete Research,* vol. 18, no. 3, pp. 473-478, 1988/05/01/ 1988.

[22] B. Raab and H. Poellmann, "Heat flow calorimetry and SEM investigations to characterize the hydration at different temperatures of different 12CaO·Al2O3 (C12A7) samples synthesized by solid state reaction, polymer precursor process and glycine nitrate process," *Thermochimica Acta,* vol. 513, no. 1, pp. 106-111, 2011/01/20/ 2011.

[23] S. K. S.K. Das, P.K. Das Poddar, "Crystal morphology of calcium aluminates hydrated for 14 days," *J. Mater. Sci. Lett.,* vol. 16, pp. 735-736, 1997.

[24] J. H. Skibsted, E.; Jakobsen, H.J., "Characterization of Calcium Aluminate Phases in Cements by 27Al MAS NMR Spectroscopy," *Inorg. Chem.,* vol. 32, pp. 1013-1027, 1993.

[25] P. Faucon, T. Charpentier, D. Bertrandie, A. Nonat, J. Virlet, and J. C. Petit, "Characterization of Calcium Aluminate Hydrates and Related Hydrates of Cement Pastes by 27Al MQ-MAS NMR," *Inorganic Chemistry,* vol. 37, no. 15, pp. 3726-3733, 1998/07/01 1998.

[26] W. Gessner, D. Müller, H.-J. Behrens, and G. Scheler, "Zur Koordination des Aluminiums in den Calciumaluminathydraten $2CaO·Al_2O_3·8H_2O$ und $CaO·Al_2O_3·10H_2O$," *Zeitschrift für anorganische und allgemeine Chemie,* https://doi.org/10.1002/zaac.19824860122 vol. 486, no. 1, pp. 193-199, 1982/03/01 1982.

[27] X. Cong and R. J. Kirkpatrick, "Hydration of Calcium Aluminate Cements: A Solid-State $^{27}$Al NMR Study," *Journal of the American Ceramic Society*, vol. 76, no. 2, pp. 409-416, 1993/02/01 1993.

[28] Y. Zhang and J. Chang, "Microstructural evolution of aluminum hydroxide gel during the hydration of calcium sulfoaluminate under different alkali concentrations," *Construction and Building Materials*, vol. 180, pp. 655-664, 2018/08/20/ 2018.

[29] P. Pena, J. M. Rivas Mercury, A. H. de Aza, X. Turrillas, I. Sobrados, and J. Sanz, "Solid-state 27Al and 29Si NMR characterization of hydrates formed in calcium aluminate–silica fume mixtures," *Journal of Solid State Chemistry*, vol. 181, no. 8, pp. 1744-1752, 2008/08/01/ 2008.

[30] M. Zhang *et al.*, "Understanding the binding and leaching of Cr(VI) in calcium aluminate cement based solidified/stabilized pastes," *Construction and Building Materials*, vol. 262, p. 120040, 2020/11/30/ 2020.

[31] F. Šoukal *et al.*, "The influence of pH buffers on hydration of hydraulic phases in system CaO–Al2O3," *Journal of Thermal Analysis and Calorimetry*, Article vol. 124, no. 2, pp. 629-638, 2016.

[32] P. Padilla-Encinas, A. Palomo, M. T. Blanco-Varela, and A. Fernández-Jiménez, "Calcium sulfoaluminate clinker hydration at different alkali concentrations," *Cement and Concrete Research*, vol. 138, p. 106251, 2020/12/01/ 2020.

[33] D. Damidot and F. Sorrentino, "Modification of the hydration process from $C_{12}A_7$ to $C_3A$ at 20 °C," in *10$^{th}$ International Congress on the Chemistry of Cement*, Göteborg, Sweden, 1997.

[34] G. Le Saout, "Phase Assemblage in Calcium Aluminate Cements: A Review," (in English), *ALITinform*, vol. 2, no. 51, pp. 12-20, 2018.

# Chapter 6: Investigation of pure cubic-$C_3A$ hydration at early age

# **Chapitre 6** : Étude de l'hydratation au jeune âge de $C_3A$ cubique pur

**Résumé:** Ce chapitre est dédié à l'étude de l'hydratation au jeune âge de $C_3A$ cubique pur à 25°C. Dans un premier temps, la vitesse d'hydratation des pâtes de $C_3A$ cubique avec différents rapports e/c massiques a été étudiée par calorimétrie isotherme. Dans le cas d'un mélange ex situ du $C_3A$ et de l'eau, l a été observé que seule la période de décélération pouvait être suivie par calorimétrie isotherme en raison des réactions d'hydratation très rapides. Une quantité significative de chaleur est en effet perdue pendant le mélange et la mise en place de l'échantillon dans le calorimètre. Par conséquent, c'est un protocole de mélange in situ qui a dû être mis en place pour estimer le degré d'hydratation à partir de la chaleur cumulée produite par la pâte. Des degrés d'hydratation de 40 %, 54 % et 66.5 % ont été atteints après respectivement 0.5 h, 4 h et 7 h d'hydratation d'une pâte de rapport e/c 0.5. A cette dernière échéance, deux hydrates ont été mis en évidence : la katoite (69 % en masse) ainsi que le monocarboaluminate (5%). Cette composition s'est avérée proche de celle prédites à partir du bilan massique des équations de réaction d'hydratation. La variation du rapport e/c de la pâte dans l'intervalle 0.375 – 0.6 n'a pas modifié la nature des hydrates précipités à 7 jours. Dans un second temps, l'étude de l'hydratation par conductimétrie a été menée en suspension diluée avec des rapports massiques e/c augmentant de 12 à 75 à 25°C. Après 24 heures d'hydratation, des assemblages minéralogiques similaires, composés principalement de $C_3AH_6$, ont été obtenus. D'un point de vue thermodynamique, les concentrations en ions calcium et aluminate mesurées par ICP se sont révélées proches de celles observées par la limite de solubilité de $C_2AH_8$ pendant la période étudiée, sans pour autant que cet hydrate métastable soit observé cet hydrate dans l'assemblage minéralogique.

# Introduction

One of the important hydraulic constituents of cement powders, most commonly of Portland cement clinkers, is tricalcium aluminate ($C_3A$) [1]. It should be noted that in general $C_3A$ exists in cubic form (cubic-$C_3A$) [2]. $C_3A$ has a significant influence on the early hydration reactions and thus on the overall hydration kinetics. These early hydration reactions occur with no induction period due to the rapid dissolution of $C_3A$ grains in contact with water inducing rapid initial precipitation of calcium aluminate hydrates as well as aluminium hydroxide [3]. If nothing is done, this leads to a loss of workability and a rapid stiffening (referred as "flash-set") of the pastes. With the addition of calcium sulphates in the form of gypsum, hemihydrate or anhydrite, the $C_3A$ hydration reactions are retarded and the cement workability is controlled [3-5].

Minard H. [6] has shown that hydration rate of $C_3A$ is very rapid, albeit continuously decreasing with time. Within 30 minutes, 50 % of $C_3A$ was hydrated when this time represented only 10 % of the full hydration time. The slowing down of the hydration process was explained by two phenomena consisting firstly in a decrease in surface area as the $C_3A$ is consumed, and secondly in a limitation of $C_3A$ dissolution related to the precipitation of calcium aluminate hydrates. Furthermore, according to the conductivity experiments of $C_3A$ hydration in pure water and in water saturated with respect to $Ca(OH)_2$, the formed hydrates in both systems always have a C/A ratio ranging between 2 and 4 [6].

Precipitated hydrates are metastable $AF_m$-like phases such as $C_2AH_8$, $C_4AH_{13}$ or $C_4AH_{19}$, which later convert into stable $C_3AH_6$ at ordinary temperatures [7-10]. Synchrotron X-ray diffraction of $C_3A$ pastes shows that the most stable calcium aluminate hydrate $C_3AH_6$ was formed only after a few minutes following contact with water at room temperature. Intermediate $AF_m$ phase $C_2AH_8$, possibly mixed with $C_4AH_{19}$ [9, 11], precipitated transiently. The factors influencing the conversion of intermediate hydrates to stable phase were summarized by Gmira A. [7] as being temperature, w/s ratio, particle size of anhydrous phase and $CO_2$ concentration. For instance, increasing the w/c ratio of $C_3A$ pastes increases the overall degree of hydration reached after 7 days.

Previous studies conducted to monitor the hydration of $C_3A$ by isothermal calorimetry show that a single peak releasing great amount of heat during the first minutes is associated to the precipitation of $C_3AH_6$ [12-14]. Furthermore, Myers R.J. *et al*. [13] have established that $C_3AH_6$ is the main solid hydration product immediately after the beginning of cubic-$C_3A$ dissolution in water (w/s = 10) at ambient temperature. In addition, microcrystalline aluminium hydroxide forms at 4 min, together with small amounts of $C_4AČH_{11}$ due to the superficial carbonation of the sample during storage, preparation and analysis.

This sixth chapter is devoted to the study of the hydration of pure cubic-$C_3A$ at early age to determine the hydration rate, degree of hydration and influence of w/c ratio on the course of pure cubic-$C_3A$ hydration.

# 1. Hydration study of cubic-$C_3A$ pastes at early age

## 1.1. Investigation of the influence of the w/c ratio on the early age hydration of $C_3A$ pastes

### 1.1.1. Heat flow monitoring

Using the *in-situ* mixing procedure heat profile, a hydration degree of cubic-$C_3A$ was evaluated as already done in the previous chapters for the other studied calcium aluminate phases by assuming that only the dissolution of cubic-$C_3A$ contributes to the heat release (reaction equation (22) [15]). The hydration degree was thus estimated by normalizing the cumulative heat Q by the cubic-$C_3A$ dissolution enthalpy $\Delta_{diss}H$ as described by equation (22).

$$C_3A + 6\,H_2O \rightleftharpoons 3\,Ca^{+2} + 2\,Al(OH)_4^- + 4\,OH^- \qquad \Delta_{diss}H = -868 \text{ J/g [16]} \qquad (22)$$

The evolution of this calculated hydration degree and the cumulative heat profile are plotted as a function of time in Figure 120 for a $C_3A$ sample hydrated by using a w/c ratio of 0.50 at 25 °C. A hydration degree of 36 % was estimated at 24 h.

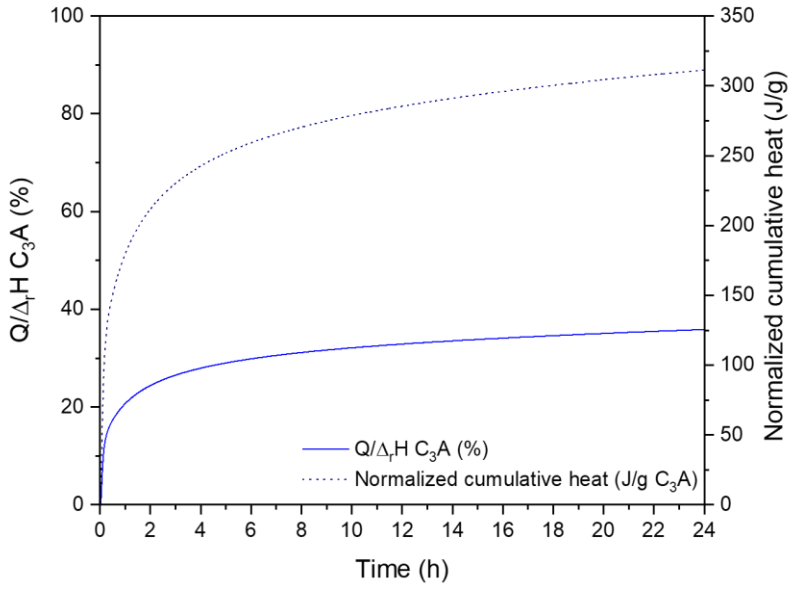


**Figure 120 : Cumulative heat profile and estimated degree of hydration of the 24 h-old cubic-$C_3A$ paste (w/c = 0.5), assuming that the heat release is only due to the dissolution of anhydrous cubic-$C_3A$ – 25 °C.**

To assess the relevance of such a hypothesis on the degree of hydration, mineralogical assemblages of pastes 7 days after mixing were characterized by TGA and XRD in order to quantify the amount of bound water and identify the crystalline phases in presence. The mineralogical composition of a sample elaborated with a w/c ratio of 0.50 was further investigated by $^{27}$Al MAS-NMR spectroscopy.

### 1.1.2. Influence of w/c ratio on mineralogical assemblages after 7 days of hydration

Comparing the bound water in the mineralogical assemblages of pastes with the hydration degree calculated from calorimetry allows to discuss the consistency of the quantification methods at play.

Figure 121 shows the powder XRD patterns of the hydrated cubic-$C_3A$ pastes at 25 °C for 7 days. In cubic-$C_3A$ pastes, unreacted $C_3A$, $C_4AČH_{11}$ and $C_3AH_6$ were identified.

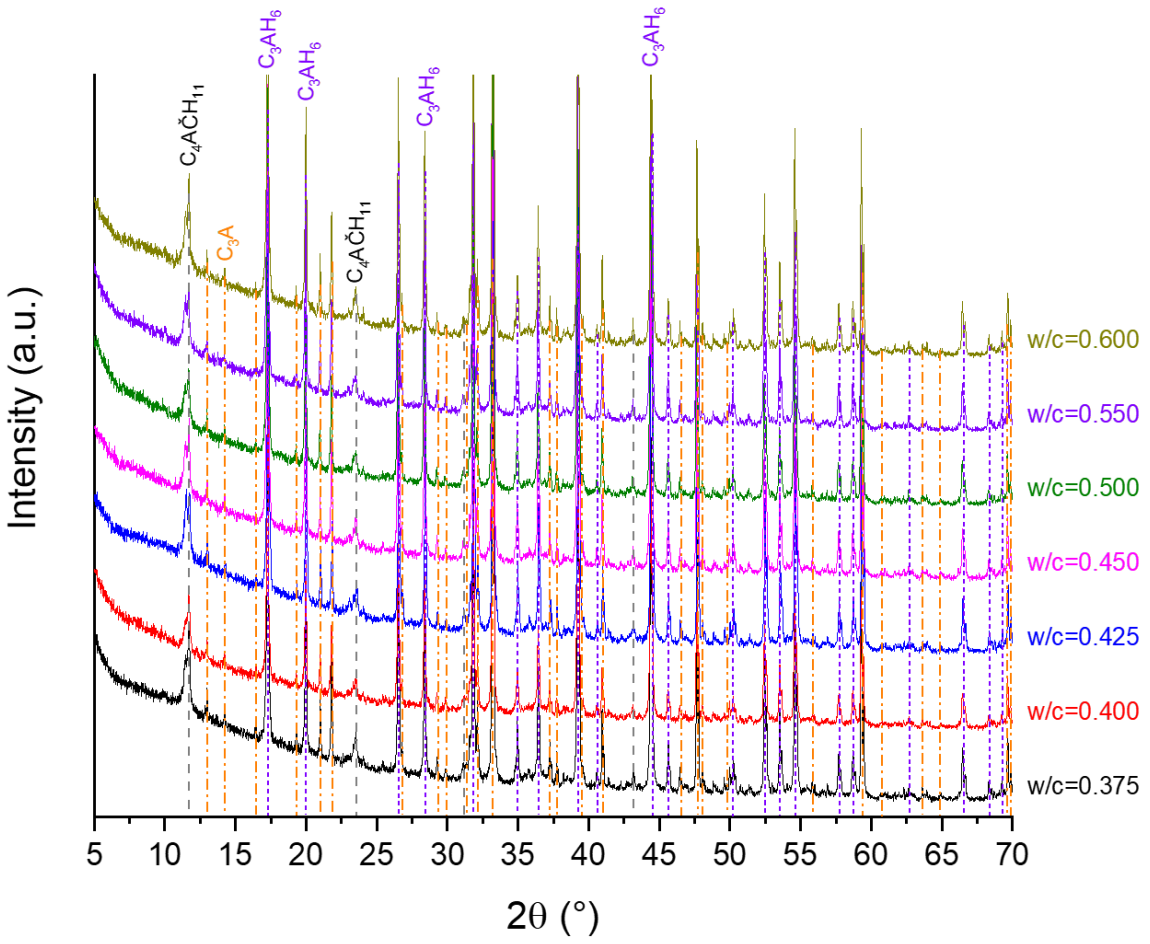


**Figure 121 : XRD patterns representing hydration products after hydrating cubic-$C_3A$ with w/c ratios ranging from 0.4 to 0.6 at 25 °C for 7 days.**

The reflections located at 11.5° 2θ and 11.7° 2θ indicated the presence of $C_4AČH_{11}$ (PDF file numbers #41-0219 and #82-3612, respectively). The hydration reactions of $C_3A$ are described by equations (23) and (24) [17]. Thus, the identified phases in Figure 121 seemed to belong a stable mineralogical assemblage after 7 days of hydration.

$$2\,C_3A + 21\,H \rightleftharpoons C_2AH_8 + C_4AH_{13} \qquad (23)$$

$$C_2AH_8 + C_4AH_{13} \rightleftharpoons 2\ C_3AH_6 + 9\ H \quad (24)$$

The pastes prepared with different w/c ratios were then analyzed by TGA in order to quantify the hydration products and thus determine the bound water content after hydration stoppage at 7 days. Figure 122 shows the TGA and DTG curves of these systems.

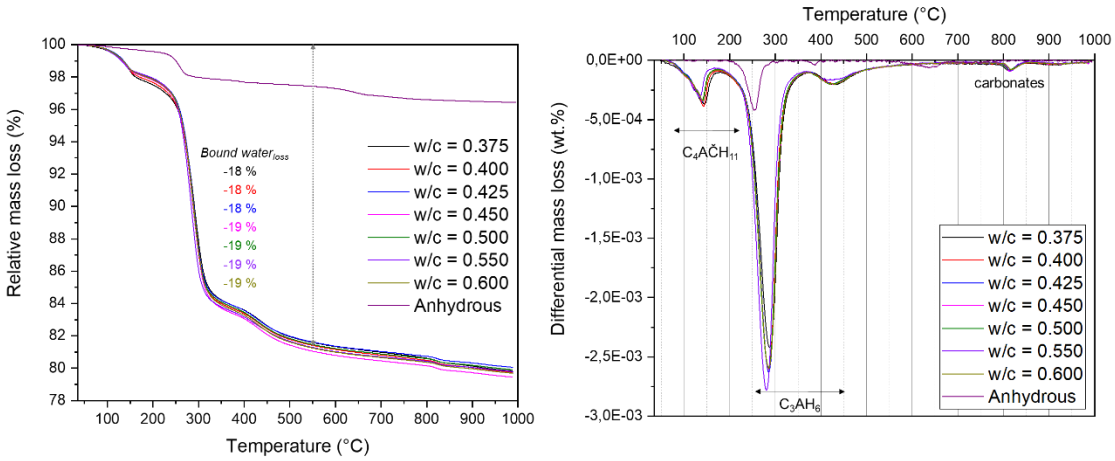


**Figure 122 : TGA and DTG curves obtained from hydrated cubic-$C_3A$ pastes with different w/c ratios at 25 °C for 7 days. On the TGA curves, the arrow shows the mass loss in the range of temperatures between 25 and 550 °C.**

The thermal events were assigned as follows:

- At the temperature range of 30 and 220 °C: dehydroxylation of $C_4A\check{C}H_{11}$ phase [18],
- At the temperature range of 300 and 430 °C: dehydroxylation of $C_3AH_6$ phase [19, 20],
- Around 800 °C: decomposition of the carbonates [21, 22].

It should be noted that the mass loss obtained around 800 °C revealed the presence of carbonates in the samples most likely due to the carbonation of $C_4AH_{19}$ during drying or grinding stages [1, 23].

The bound water amount of the samples was taken as the mass loss between 33 and 550 °C normalized to the initial weight of sample. The measured bound water after 7 days of hydration is plotted as a function of the w/c ratio in Figure 123. The amount of bound water followed no clear trend, ranging between 18.5 and 19 wt. %.

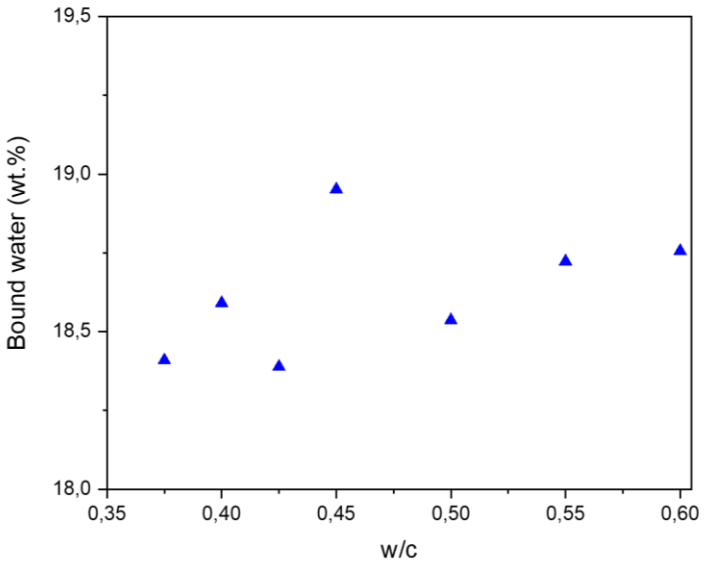


**Figure 123 : Bound water amount of cubic-$C_3A$ pastes with different w/c ratios hydrated at 25 °C for 7 days.**

Considering a complete hydration of cubic-$C_3A$ up to a thermodynamically stable mineralogical assemblage, a theoretical amount of water that would be bound to hydrates was determined using reaction equation (25) and found to be equal to 40 wt. %. This theoretical value was higher than the measured bound water amounts, which was consistent with the presence of unreacted $C_3A$ observed by XRD analysis.

$$C_3A + 6\,H \rightleftharpoons C_3AH_6 \tag{25}$$

Following TGA and powder XRD analysis, $^{27}$Al MAS-NMR spectrometry was performed on a 7 day-old cubic-$C_3A$ paste prepared with a w/c ratio of 0.50 in order to determine as quantitatively as possible its mineralogical composition. The collected spectrum (Figure 124) and its corresponding decomposition are shown in Figure 125.

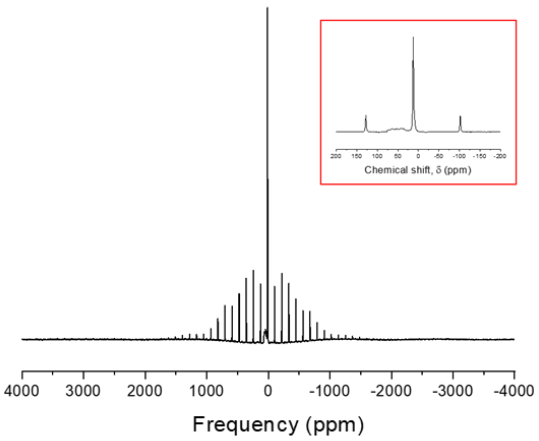


**Figure 124 : $^{27}$Al MAS-NMR spectrum of the 7 d-old cubic-$C_3A$ paste (w/c = 0.50).**

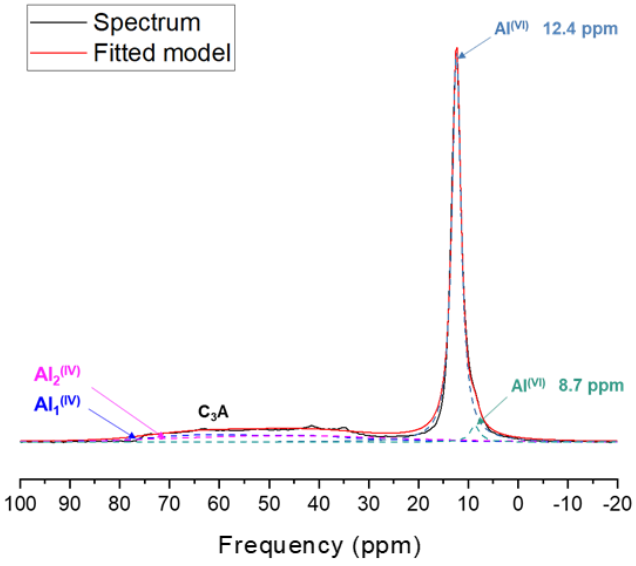


**Figure 125 : Decomposition of the $^{27}$Al MAS-NMR spectrum central bands of the 7 d-old cubic-$C_3A$ paste (w/c = 0.5).**

The tetrahedral resonance was modelled by the two Al sites at 79 and 78 ppm of anhydrous $C_3A$ phase, in agreement with the spectra of $C_3A$ modelled in Figure 40 [24, 25]. Octahedral Al sites revealed the presence of hydrates in the hydration products in the range of 20 ppm to -5 ppm. From the decomposition of the $^{27}$Al NMR spectrum of the 7 d-old cubic-$C_3A$ paste (w/c = 0.5), the following hydrates, identified by XRD, were quantified as summarized in Table 19:

- $C_4AČH_{11}$
- $C_3AH_6$

The fitted model (Figure 125) comprised two peaks assigned to:

- $C_4A\check{C}H_{11}$ ($\delta$ = 8.7 ppm),
- $C_3AH_6$ ($\delta$ = 12.4 ppm).

**Table 31 : Summary of chemical shifts, intensities and quadrupolar parameters corresponding to the identified hydrates from the decomposition of the $^{27}$Al MAS-NMR spectrum of the 7 d-old cubic-$C_3A$ paste (w/c = 0.5), according to the hydrates identified by XRD.**

| Phase | Site | $\delta_{iso}$ (ppm) | Model | Peak intensity | Quadrupole coupling constant, $C_Q$ (MHz) | Asymmetry parameter, $\eta$ | Width | Reference |
|---|---|---|---|---|---|---|---|---|
| $C_3A$ | $Al_1^{(IV)}$ | 80 | Q mas 1/2 | 1670 | 8.7 | 0.32 | - | [24] |
| | $Al_2^{(IV)}$ | 78.7 | Q mas 1/2 | 711 | 9.3 | 0.54 | - | |
| $C_4A\check{C}H_{11}$ | $Al^{(VI)}$ | 8.7 | Lorentzian | 1380 | - | - | 2.5 | [26] |
| $C_3AH_6$ | $Al^{(VI)}$ | 12.4 | Lorentzian | 26665 | - | - | 2.2 | [24] |

Such a decomposition of the spectrum yields the mineralogical composition described in Table 32.

**Table 32 : Quantification of Al-containing phases in the 7 d-old cubic-$C_3A$ paste (w/c = 0.5).**

| Phase | Chemical shift (ppm) | Al atomic fraction (%) | Phase weight fraction (wt. %) | Corresponding bound water content (wt. %) |
|---|---|---|---|---|
| $C_3A$ | 80/79 | 34 | 26 | - |
| $C_4A\check{C}H_{11}$ | 8.7 | 3 | 5 | 2 |
| $C_3AH_6$ | 12.4 | 63 | 69 | 20 |

The results obtained from the decomposition of the NMR spectrum are consistent with the TG results. It could be concluded that the mineralogical phase assemblage after 7 days of hydration were constituted of $C_3AH_6$ as a major hydrate with a small amount of $C_4A\check{C}H_{11}$ and unreacted cubic-$C_3A$. In addition, from the molar fraction of Al present in different hydration products of a 7 d-old cubic-$C_3A$ paste with a w/c ratio of 0.5, the bound water content of these hydrates was calculated. For each Al present in $C_3AH_6$, quantified by MAS-NMR, six water molecules are present and the corresponding water mass was obtained. The same calculation was performed for the other identified hydrate, monocarboaluminate. The amount of bound water inferred from

NMR data was thus equal to 22 wt. % while a weight loss of 19 wt. % was measured by TGA and assigned to bound water.

From mass balance of Ca and Al, considering the formation of $C_3AH_6$ (equation (25)) and assuming that 69 wt. % of $C_3AH_6$ has been formed, the amount of anhydrous $C_3A$ after 7 days of hydration was found to be in agreement with the $^{27}$Al NMR result (Table 33).

$$C_3A + 6\,H \rightleftharpoons C_3AH_6 \tag{25}$$

**Table 33 : Calculation of the weight fraction of the Al-containing $C_3AH_6$ phase identified by $^{27}$Al NMR (69 wt. % of $C_3AH_6$) based on the corresponding mass balance equation from the hydration reaction of anhydrous cubic-$C_3A$ with water.**

| **Wt. %** | **Cubic-$C_3A$** | **$C_3AH_6$** |
|---|---|---|
| Measured composition | 26 | 69 |
| Considering equation (25) | 24 | 69 |

The cubic-$C_3A$ phase is highly reactive with water [6]. Thus after 7 days of hydration, one can expect that the mineralogical assemblage would have already reached a stable mineralogy. In the following section, a focus on the hydration of cubic-$C_3A$ was decided to monitor the mineralogical assemblage evolution during the first 7 hours of hydration of a cubic-$C_3A$ paste with a w/c ratio of 0.5.

## 1.2. Evolution of mineralogical assemblages during the first seven hours of cubic-$C_3A$ paste with a w/c ratio of 0.5

This section focusses on the study of the hydration of a paste elaborated with a w/c of 0.5 at 25 °C. Hydration stoppages were performed on the paste in order to describe the mineralogical evolution with time. Hydration stoppage and corresponding mineralogical analysis were performed 30, 60, 90, 120, 150, 180, 240, 300 and 420 min after mixing.

XRD patterns obtained for different periods of time are compared in Figure 126.

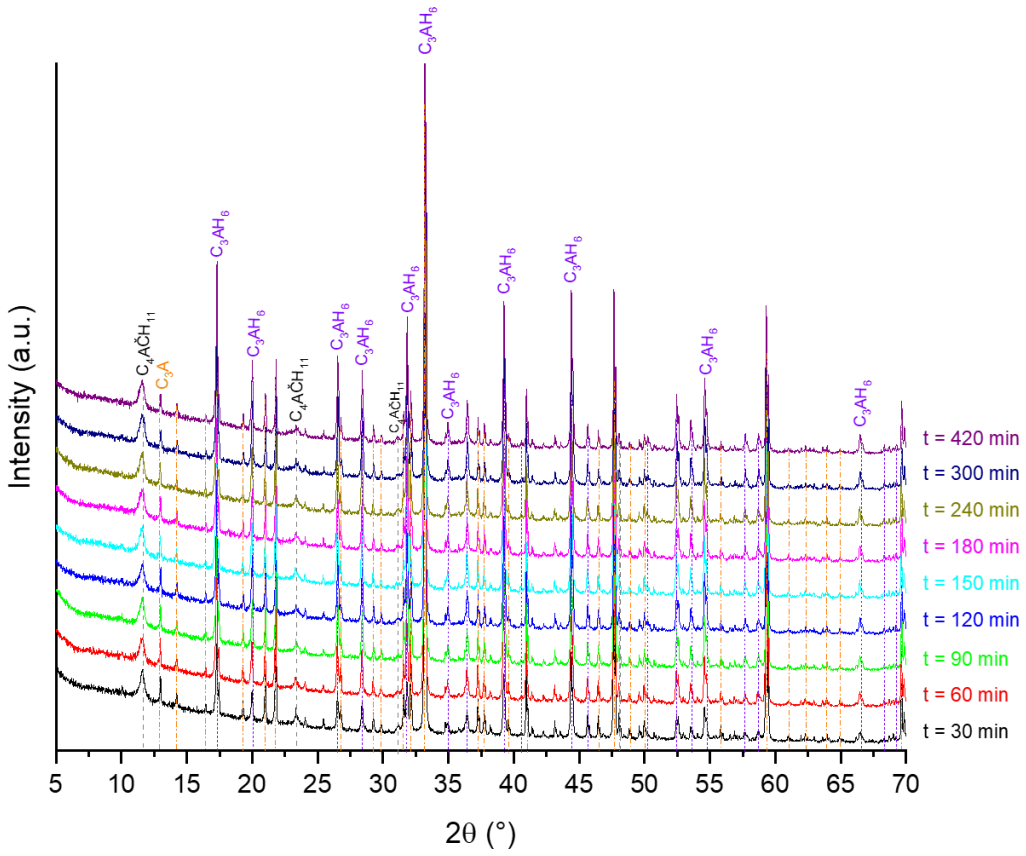


**Figure 126 : XRD patterns of the cubic-$C_3A$ paste with a w/c ratio of 0.5 after increasing periods of hydration.**

According to the XRD patterns, unreacted cubic-$C_3A$ (13° 2θ, 21.8° 2θ and 33.2 °2θ), $C_4AČH_{11}$ (11.7° 2θ and 23.4° 2θ) and $C_3AH_6$ (20° 2θ, 26.5° 2θ and 28.4° 2θ) phases were identified. Qualitatively, the peaks indexed to unreacted cubic-$C_3A$ phase decreased with time concurrently to an increase of the $C_3AH_6$ peaks, reflecting the ongoing hydration.

Figure 127 shows the TGA and DTG curves of these systems. The thermal events were assigned as follows:

- At the temperature ranges of 60 – 200, 200 – 300 and up to 650 °C, decomposition of monocarboaluminate $C_4AČH_{11}$ [18, 21, 22],
- At the temperature range of 300 – 430 °C, decomposition of $C_3AH_6$ [19, 20].

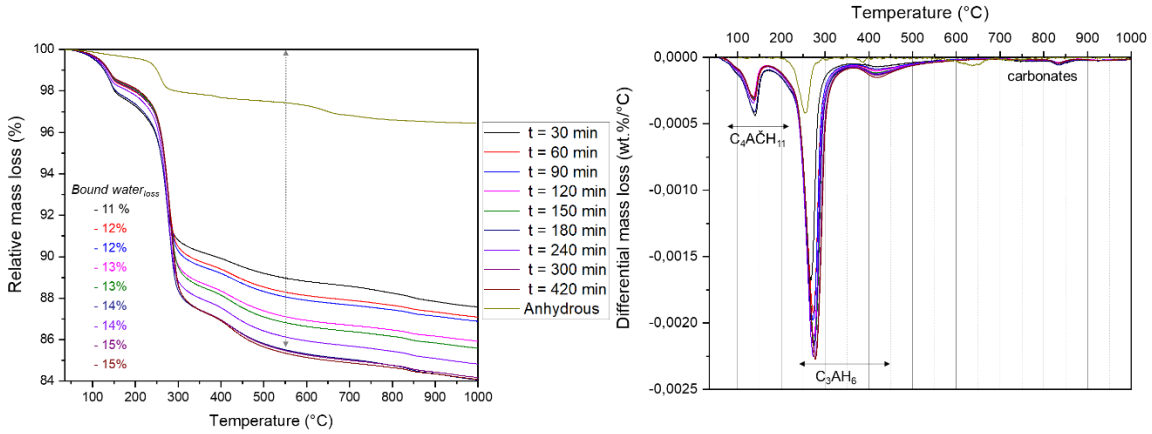


**Figure 127 : TGA and DTG curves obtained from hydrated cubic-$C_3A$ paste with a w/c of 0.5 at 25 °C after increasing periods of hydration. On the TGA curves, the arrow shows the mass loss in the range of temperatures between 33 and 550 °C.**

The bound water amount of the samples was taken to correspond to the mass loss between 33 and 550 °C normalized to the initial weight of sample. Based on these TG results, the bound water content evolved from 11 to 14 wt. % during the first 2.5 h of hydration. Afterwards the mass loss stabilized at 15 wt. %.

As a complement to XRD and TGA studies, $^{27}$Al MAS-NMR spectroscopy was carried out to characterize and more importantly quantify the hydration products found in the solid fractions of the paste at three different sampling times. The distinction between tetrahedrally and octahedrally coordinated Al sites was observed in Figure 128.

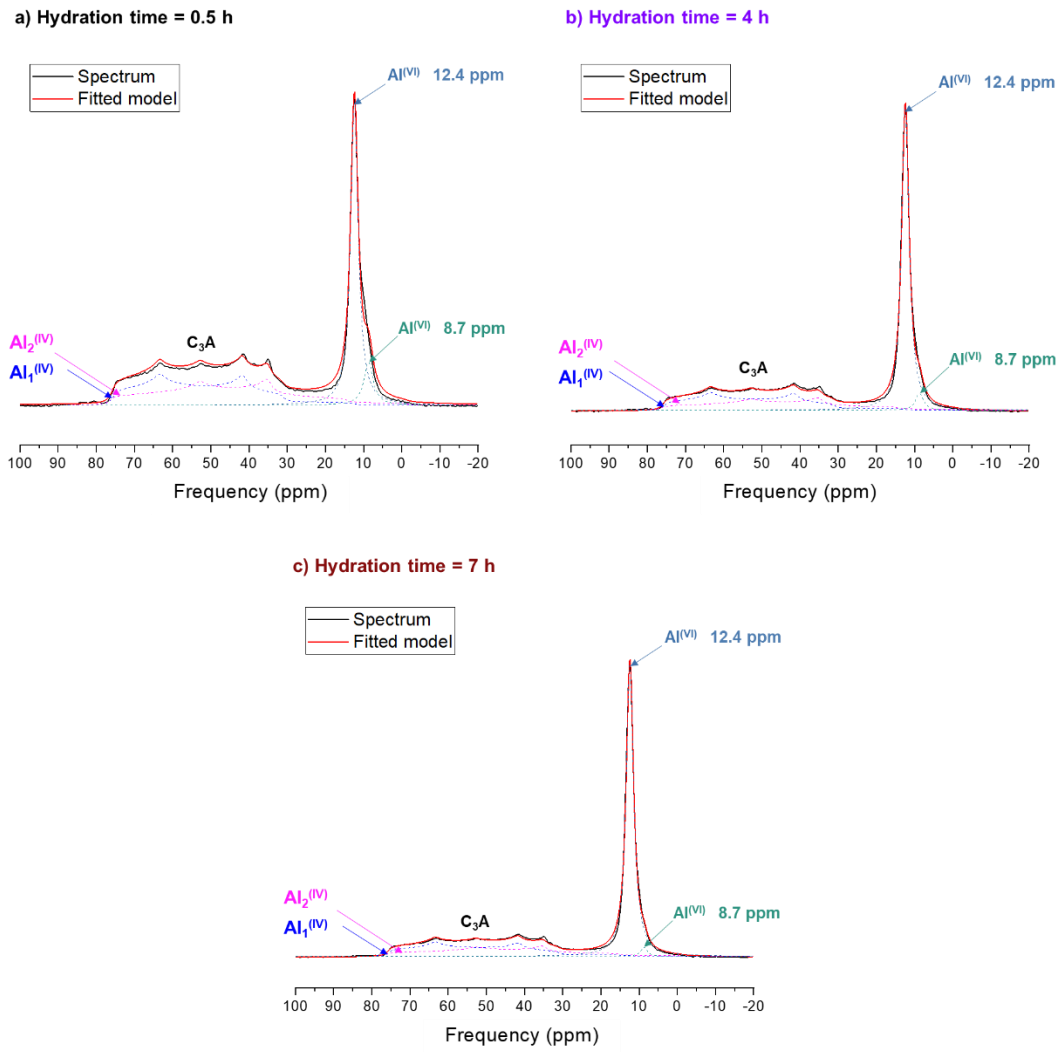


**Figure 128 : $^{27}$Al solid-state NMR spectra of cubic-$C_3A$ paste with a w/c ratio of 0.5 at different characterization times: a) 0.5 h, b) 4 h and c) 7 h.**

For each of the solid fractions, two overlapping centerbands of unreacted cubic-$C_3A$ related to their two tetrahedrally coordinated Al sites at 80 ppm and 78.7 ppm were observed as shown in Figure 128. As identified by XRD and TGA studies, the presence of monocarboaluminate $C_4A\check{C}H_{11}$ and $C_3AH_6$ phases was confirmed from the decomposition of the spectrum for all solid fractions at 8.7 ppm [26] and 12.4 ppm [24], respectively. The results obtained from the decomposition of the NMR spectrum with ongoing hydration are summarized in Table 34.

**Table 34 : Quantification of Al-containing phases in the cubic-$C_3A$ paste after hydrating with a w/c of 0.5 as a function of the hydration time.**

| Hydration stoppage time (h) | Phases | Chemical shift (ppm) | Al atomic fraction (%) | Phase weight fraction (wt. %) | Corresponding bound water content (wt. %) |
|---|---|---|---|---|---|
| **0.5** | $C_3A$ | 80/79 | 60 | 50 | - |
| | $C_4AČH_{11}$ | 8.7 | 6 | 10 | 4 |
| | $C_3AH_6$ | 12.4 | 34 | 40 | 11 |
| **4** | $C_3A$ | 80/79 | 46 | 37 | - |
| | $C_4AČH_{11}$ | 8.7 | 3 | 5 | 2 |
| | $C_3AH_6$ | 12.4 | 51 | 58 | 16 |
| **7** | $C_3A$ | 80/79 | 43.5 | 35 | - |
| | $C_4AČH_{11}$ | 8.7 | 1.5 | 3 | 1 |
| | $C_3AH_6$ | 12.4 | 55 | 62 | 18 |

Based on these mineralogical compositions, the bound water amount was calculated and found equal to 15, 18 and 19 wt. % for the solid fractions of the 0.5 h-, 4 h- and 7 h-old cubic-$C_3A$ mixtures, respectively. The bound water contents derived from TGA, 11, 14 and 14 wt. % respectively, were a bit smaller than those calculated from NMR analysis. Approximately half of anhydrous $C_3A$ was hydrated within the first 0.5 h. Overall, these results were found to be also consistent with TGA results where the increase in bound water was associated to the presence of $C_3AH_6$ and carbonated phase around similar values.

From TGA, XRD and NMR results, it was concluded that, from 0.5 h of hydration on, the mineralogical assemblage was mainly composed of unreacted cubic-$C_3A$ and $C_3AH_6$, with the presence of smaller amounts of $C_4AČH_{11}$. The amount of unreacted cubic-$C_3A$ decreased from 50 wt. % to 35 wt. % during the first 7 h of hydration while the amount of stable $C_3AH_6$ phase increased with a small amount of carbonated phase as qualitatively observed by XRD analysis. Accordingly, the hydration degrees were estimated on the basis of the depleted $C_3A$ phase over time. These hydration degrees estimated by NMR increased from 40 % to 57 % up to 7 hours of hydration.

In brief, rapid hydration reactions made the monitoring on pastes difficult. Hydration of cubic-$C_3A$ phase was thus studied as a function of time in suspensions in order increase the different hydration stages. Evolution of the aqueous concentrations was determined in order to identify the hydration path followed.

**To sum up:**

From TGA, XRD and NMR results, it was concluded that after 7 days of hydration at 25 °C, the mineralogical assemblage was mainly composed of $C_3AH_6$, with the presence of smaller amounts of unreacted cubic-$C_3A$ and $C_4A\check{C}H_{11}$. A hydration degree of 66 % was obtained for the paste elaborated with a w/c of 0.5 after 7 days of hydration by NMR analysis.

The cubic-$C_3A$ phase reacted rapidly in agreement with literature since no induction period was observed under the studied conditions. From the mineralogical point of view, 40 % of $C_3A$ was depleted within 30 minutes, yielding mainly $C_3AH_6$ and traces of monocarboaluminate. 43 % of $C_3A$ remained 7 hours after mixing.

## 2. Hydration study of cubic-$C_3A$ suspensions at early age

As a first step, the influence of an increase in the w/c ratio from 12.5 up to 75.0 on the hydration progress and on mineralogy was evaluated to investigate the w/c ratio influence on the course of hydration. Then, the composition evolution of a suspension with a w/c ratio of 25 was measured as a function of time at 25 °C.

### 2.1. Influence of the w/c ratio on the early age hydration of $C_3A$ elaborated in suspensions

#### 2.1.1. Electrical conductivity monitoring

Due to the fast hydration reactions of calcium aluminate phases particularly cubic-$C_3A$, the hydration studies are performed in diluted media with higher water-to-solid ratios in order to define both chemical and mineralogical evolution of the systems. Furthermore, the reaction mechanisms aimed at identifying the hydration path followed by calcium and aluminate ions. First, suspensions containing cubic-$C_3A$ phase were prepared with decarbonated Milli-Q water (18.2 MΩ.cm) using different w/c ratios, namely, 12.5, 25, 50 and 75. The evolution of the electrical conductivity of the suspensions at 25 °C is shown in Figure 129. Measurements were performed every 5 min.

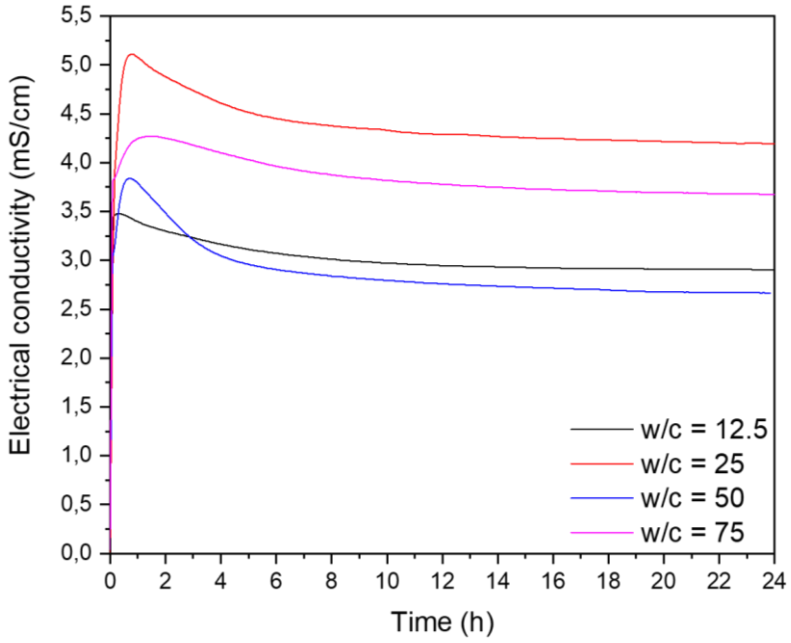


**Figure 129 : Electrical conductivity monitoring of cubic-$C_3A$ suspensions prepared with different w/c ratios at 25 °C.**

Electrical conductivity profiles were divided into two main periods. During the first period, when the anhydrous cubic-$C_3A$ grains came in contact with water, dissolution of particles bringing $Ca^{2+}$, $Al(OH)_4^-$ and $OH^-$ ions into solution took place within 10 min of hydration with a sharp increase in conductivity. After reaching a maximum, the conductivity then decreased in a same manner for all cubic-$C_3A$ mixtures.

For cubic-$C_3A$ mixtures with a w/c of 12.5, 25 and 50, the conductivity reached their maximum within the first hour of hydration. Briefly, the maximum conductivity values of the studied suspensions were shifted to longer hydration times as the w/c ratio of the suspensions was increased from 12.5 to 75. Such a behaviour could be explained by the fact that higher amount of anhydrous phase has to dissolve to reach a saturation index that might enable hydrates precipitation.

### 2.1.2. Characterization of the solid fraction of suspensions

In order to define the mineralogical phase assemblage, the solid fractions were characterized by XRD and TGA after 24 h of hydration. First, XRD patterns are presented in Figure 130. According to the XRD patterns of the solid fractions of suspensions hydrated for 24 h at 25 °C, the following mineralogical phases were identified (Figure 130) regardless of the w/c ratio:

- $C_2AH_{7.5}$,
- Hemicarboaluminate $C_4A\check{C}_{0.5}H_{12}$,
- Monocarboaluminate $C_4A\check{C}H_{11}$,
- $C_3AH_6$,
- unreacted cubic-$C_3A$.

The mineralogical assemblage was not significantly modified by a variation in the w/c ratio. The only difference was a small peak attributable to $C_2AH_{7.5}$ observed in the solid issued from the suspension with a w/c of 25.

The XRD patterns revealed the formation of $C_4A\check{C}H_{11}$ (11.7° 2θ and 23.4° 2θ) and $C_3AH_6$ (20° 2θ, 26.5° 2θ and 28.4° 2θ). The presence of unreacted cubic-$C_3A$ (13° 2θ, 21.8° 2θ and 33.2 °2θ) was also identified in all samples. For the solid fraction of cubic-$C_3A$ suspension with a w/c ratio of 25, the peaks at 8.4° 2θ and 16.9° 2θ were attributed to the presence of $C_2AH_{7.5}$. Indeed, several studies reported this hexagonal phase as an hydration product of $C_3A$ hydrated at 25 °C according to fast hydration reactions at very early age [13, 23, 27]. Moreover, carbonated hemicarboaluminate ($C_4A\check{C}_{0.5}H_{12}$, abbreviation: cHc) [28] was identified in all samples with the peaks at 11.5° 2θ, 23° 2θ and 31° 2θ. The latter phase was likely formed from the carbonation of OH-$AF_m$ phases such as $C_4AH_X$ (X = 13 or 19 depending on relative humidity) [13, 29, 30].

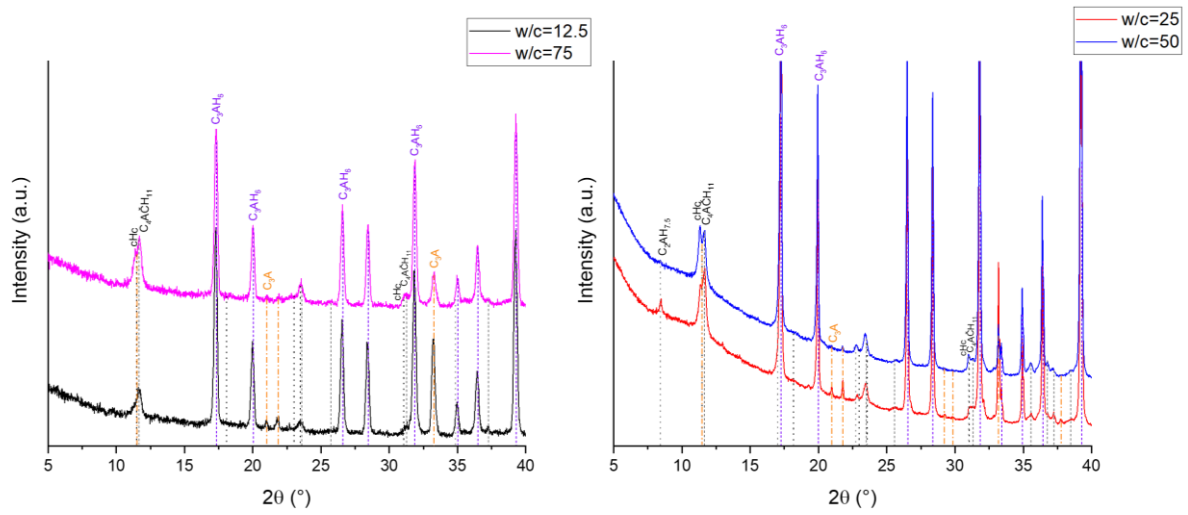


**Figure 130 : XRD patterns representing mineralogical assemblages of cubic-$C_3A$ suspensions after 24 hours of hydration at 25 °C (two different XRD detectors were used; therefore the results are divided in two figures).**

TGA results are presented in Figure 131. The thermal decomposition of the solid fractions occurred in several steps as described in Table 35.

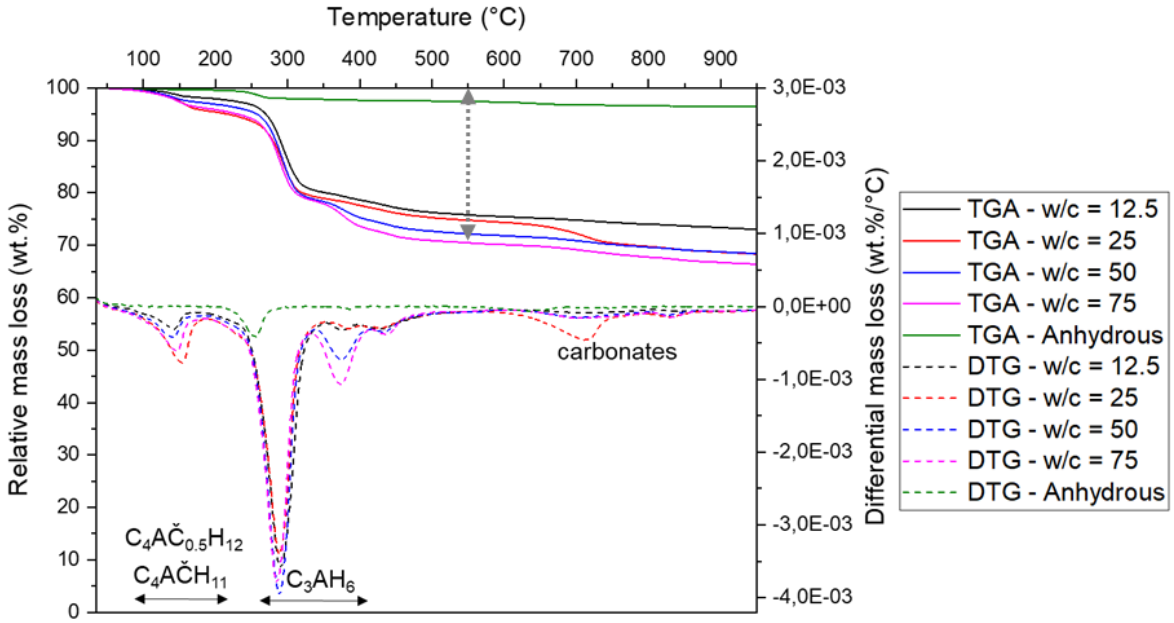


**Figure 131 : TGA and derivative TGA results obtained from cubic-$C_3A$ suspensions with various w/c ratios after 24 hours of hydration at 25 °C.**

Based on Figure 131, two main thermal events at around 150 °C and 300 °C were assigned to the thermal decompositions of $C_4A\check{C}H_{11}$, $C_4A\check{C}_{0.5}H_{12}$ and $C_3AH_6$ respectively. In the literature, the decomposition of $C_2AH_8$ is reported to proceed in three main steps as shown in Table 35. However, these steps could not observed with certainty in Figure 131, possibly because of the very small content of this phase.

**Table 35 : Decomposition temperatures of anhydrous calcium aluminate phase hydration products.**

| Temperature (°C) | Phase composition | Nomenclature | Reference |
|---|---|---|---|
| 110 – 170 – 300 | $Ca_2Al_2O_5 \cdot 8H_2O$ | $C_2AH_8$ | [31, 32] |
| 150 – 180 | $4CaO \cdot Al_2O_3 \cdot 0.5CO_2 \cdot 12H_2O$ | $C_4A\check{C}_{0.5}H_{12}$ | [33] |
| 700-800 | | | |
| 60 – 200 | $4CaO \cdot Al_2O_3 \cdot CO_3 \cdot 11H_2O$ | $C_4A\check{C}H_{11}$ | [34-37] |
| 200 – 300 | | | |
| 650 | | | |
| 300 – 430 | $Ca_3Al_2O_6 \cdot 6H_2O$ | $C_3AH_6$ | [19, 20] |

Knowing that the decomposition of hydrates mostly occurs below 550 °C, the bound water can be calculated. The mass loss up to 550 °C was 24, 25, 28 and 30 % for the suspensions with a w/c of 12.5, 25, 50 and 75 respectively. Mass losses around 4 % were obtained above 550 °C, showing the presence of carbonates in all of the samples.

## 2.2. Course of cubic-$C_3A$ hydration during the first 24 hours – w/c = 25

In order to investigate the early age hydration of cubic-$C_3A$, a suspension with a w/c of 25 was monitored with an electrical conductivity probe during the first 7 hours at 25 °C, as detailed in Chapter 2.3 (Figure 44). The w/c ratio of 25 was chosen in view of preliminary tests on the values of electrical conductivity in order to allow a good monitoring of the dissolution and precipitation steps within a feasible testing time (≤ 7 hours), while allowing sufficient sample quantities to be characterized.

The chemical evolution of the liquid fraction composition and mineralogical assemblages were characterized after fixed times of hydration. These times are figured by red dots on the conductivity plot of Figure 132.

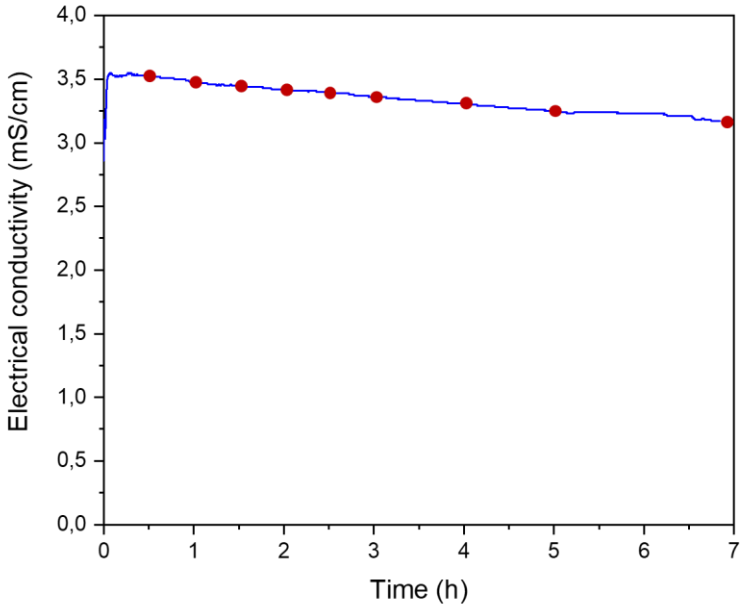


**Figure 132 : Definition of characterization times (red dots) based on the variation of the electrical conductivity during cubic-$C_3A$ hydration with a w/c = 25.**

### 2.2.1. Characterization of the solid fraction of suspensions

After each of the described periods, a hydration stoppage was carried out and the collected solid fraction was characterized by XRD, TGA and $^{27}$Al MAS-NMR spectroscopy.

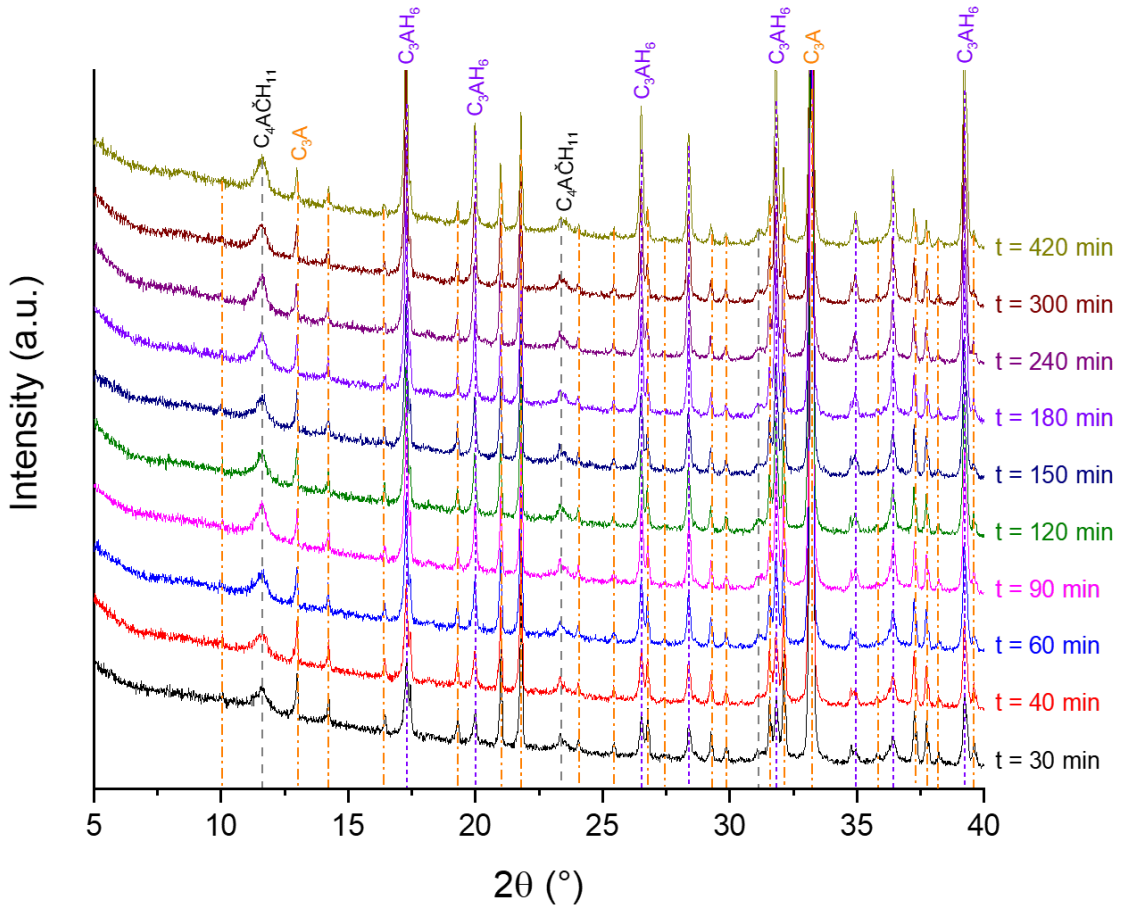


**Figure 133 : XRD patterns of the solid fractions of cubic-$C_3A$ suspension with a w/c of 25 after increasing periods of hydration at 25 °C.**

In Figure 133, the XRD patterns show the presence of three crystalline phases, unreacted cubic-$C_3A$ (13° 2θ, 21.8° 2θ and 33.2° 2θ), $C_3AH_6$ (20° 2θ, 26.5° 2θ and 28.4° 2θ) and monocarboaluminate (11.7° 2θ and 23.4° 2θ). This latter phase was evidenced on all of the patterns and might result from carbonation occurring during the stoppage procedure and/or the drying performed prior to XRD analysis.

The thermograms of the studied samples and their derivatives are plotted in Figure 87. The thermal events evidenced the presence of precipitated crystalline phases that had been also identified by XRD analysis. The formation of $C_4AČH_{11}$ phase from the first 0.5 h of hydration was confirmed by three thermal decompositions (see Table 35). The part of DTG curve between 300 and 430 °C showed the weight loss resulting from the dehydroxylation of $C_3AH_6$.

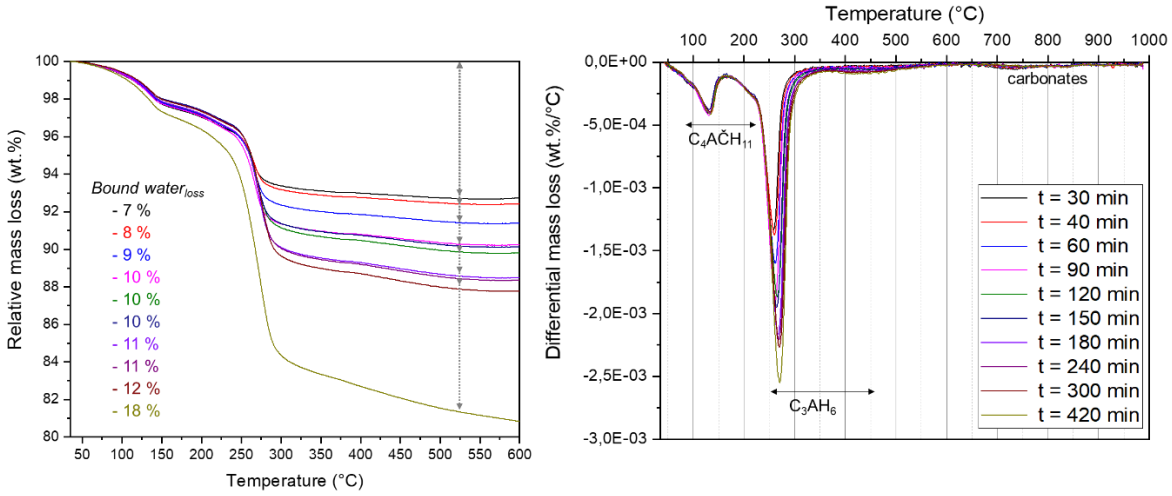


**Figure 134 : TGA and DTG curves obtained from cubic-$C_3A$ suspension with a w/c ratio of 25 after increasing periods of hydration at 25 °C.**

The measured bound water content is superimposed on the conductivity curve in Figure 135.

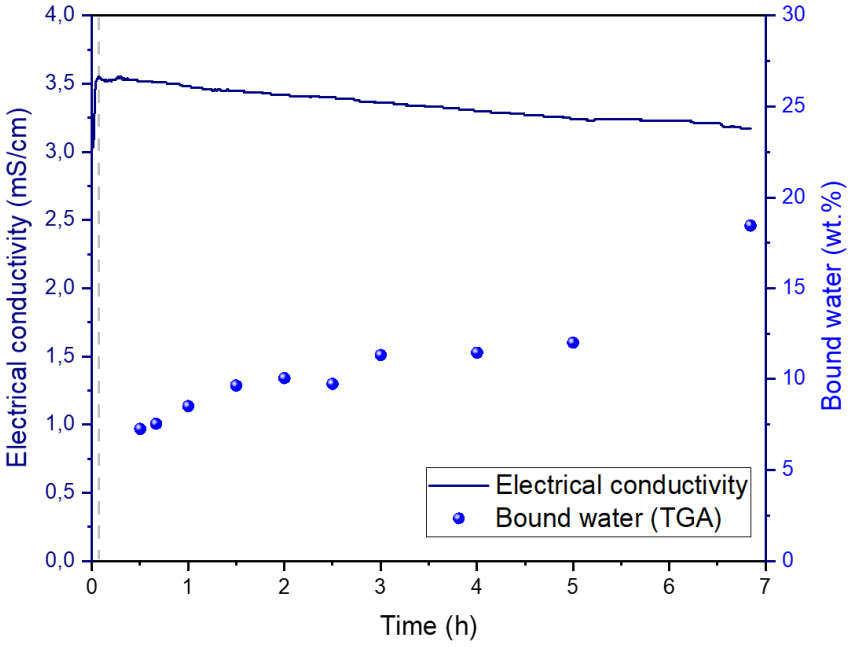


**Figure 135 : Investigation of cubic-$C_3A$ hydration at early age: electrical conductivity and bound water evolution.**

As a complement to XRD and TGA studies, $^{27}$Al MAS-NMR spectroscopy was carried out to characterize and more importantly quantify the hydration products found in the solid fraction

of the suspension. For practical reasons, only one of the solid fraction of the cubic-$C_3A$ suspensions hydrated for 7 h was studied. This time was chosen knowing that the mineralogical assemblage did not vary significantly for the first 5 h of hydration. However, an acceleration of hydrate precipitation was suspected between 5 and 7 h of hydration (Figure 135).

First, a centerband was observed for anhydrous cubic-$C_3A$ corresponding to overlapping chemical shifts at 79 ppm and 78 ppm [24]. A narrower resonance in the spectrum was observed for the chemical shifts corresponding to the hydrates in the range 20 ppm to -10 ppm.

The distinction between tetrahedrally and octahedrally coordinated Al sites is clear in Figure 136. However, the chemical shifts of $^{27}Al$ in hydrates are all very close since they contain Al in relatively similar octahedral environments, thus leading to ambiguous overlapping resonances for these phases if only based on $^{27}Al$ NMR results. Nevertheless, the XRD observations allowed to limit the number of hydrates to consider and a tentative quantitative fitting of the MAS-NMR octahedral resonances is provided in Figure 136.

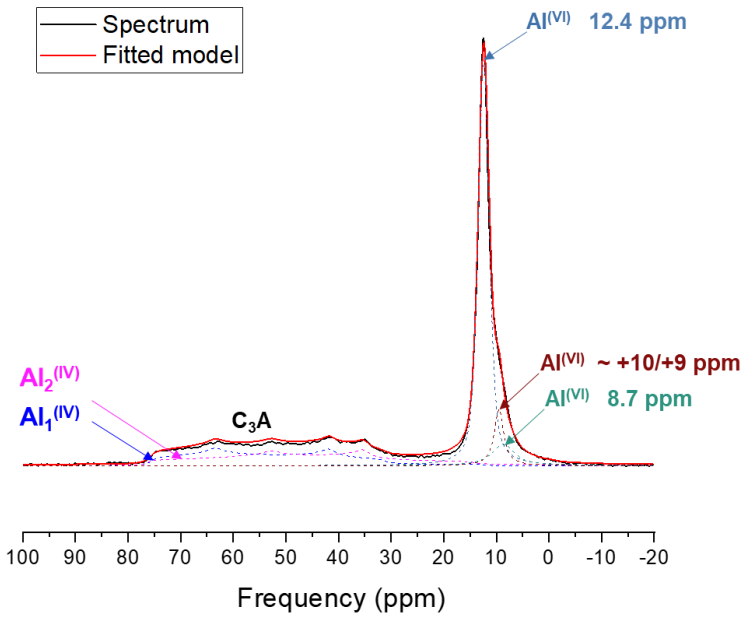


**Figure 136 : $^{27}Al$ NMR spectrum of the cubic-$C_3A$ suspension with a w/c of 25 after 7 h of hydration.**

Table 36 summarizes the parameters used for the decomposition of the $^{27}Al$ NMR spectrum of the 7 h-old cubic-$C_3A$ suspension. Quantification of Al-containing phases present in the cubic-$C_3A$ suspension with a w/c of 25 after 7 h of hydration is shown in Table 37.

**Table 36 : Summary of chemical shifts, intensities and quadrupolar parameters corresponding to the identified hydrates from the decomposition of the $^{27}$Al MAS-NMR spectrum of the 7 h-old cubic-$C_3A$ suspension (w/c = 25).**

| Phase | Site | $\delta_{iso}$ (ppm) | Model | Peak intensity | Quadrupole coupling constant, $C_Q$ (MHz) | Asymmetry parameter, η | Width | Reference |
|---|---|---|---|---|---|---|---|---|
| $C_3A$ | $Al_1^{(IV)}$ | 80 | Q mas 1/2 | 1100 | 8.7 | 0.32 | - | [24] |
| | $Al_2^{(IV)}$ | 78.7 | Q mas 1/2 | 1000 | 9.3 | 0.54 | - | |
| $C_4AČH_{11}$ | $Al^{(VI)}$ | 8.7 | Lorentzian | 650 | - | - | 5.0 | [26] |
| $C_3AH_6$ | $Al^{(VI)}$ | 12.4 | Lorentzian | 12200 | - | - | 2.5 | [24] |
| AFm* | $Al^{(VI)}$ | 9.5 | Lorentzian | 1692 | - | - | 2.1 | [38] |

The presence of stable $C_3AH_6$ phase, already identified by TGA and XRD, was distinguished with the chemical shift at 12.4 ppm [20, 24]. There is a significant shoulder around 8-10 ppm $^{27}$Al chemical shift range confirming the formation of AFm-type phases [26]. The $^{27}$Al MAS-NMR octahedral resonances not being resolved, it was not possible to determine their exact nature but for the sake of illustration and to be able to quantify the bound water content, a decomposition in two peaks was attempted, possibly showing the simultaneous occurrence of two different forms of AFm phases at 8.7 and 9.5 ppm. From XRD results, the second hydrate present in the solid fraction of the suspension after 7 h of hydration was identified as $C_4AČH_{11}$ and the resonance at 8.7 ppm was attributed to this AFm phase.

**Table 37 : Quantification of Al-containing phases present in the 7 h-old cubic-$C_3A$ suspension (w/c = 25) by $^{27}$Al NMR.**

| Phase | Site | Chemical shift (ppm) | Al atomic fraction (%) | Phase weight fraction (wt. %) | Corresponding bound water content (wt. %) |
|---|---|---|---|---|---|
| $C_3A$ | $Al_1^{(IV)}$ | 80 | 40.5 | 31 | - |
| | $Al_2^{(IV)}$ | 78.7 | | | |
| $C_4AČH_{11}$ | $Al^{(VI)}$ | 8.7 | 6 | 10 | 3 |
| $C_3AH_6$ | $Al^{(VI)}$ | 12.4 | 47 | 51 | 14 |
| AFm* | $Al^{(VI)}$ | 9.5 | 6.5 | 8 | 2 – 3 |

Based on these mineralogical compositions, the bound water content at 7 h was calculated to be equal to 19-20 wt. % of the solid fraction, which was in good agreement with the value derived from TGA (18 wt.%). After 7 h of hydration, the analyzed sample contained

approximately 51 wt. % of $C_3AH_6$, 8 wt. % of $AF_m$*, 10 wt. % of $C_4A\check{C}H_{11}$ and 31 wt. % anhydrous cubic-$C_3A$.

### 2.2.2. Characterization of the liquid fraction of suspensions

Evolution of the liquid fraction composition during hydration was measured by ICP-AES. pH values were measured and corresponding $OH^-$ concentrations were calculated. Results are plotted in Figure 137. Dissolution of $C_3A$ grains released $Ca^{2+}$, $Al(OH)_4^-$ and $OH^-$ ions. Consequently, the Ca and Al concentrations increased rapidly and reached their maximum value after 4 min of hydration. Afterwards, the concentration values decreased until 40 min, levelled-off, and increased again slowly after 3 h. Meanwhile, the pH values remained at a constant level around 12.2 over the investigated period.

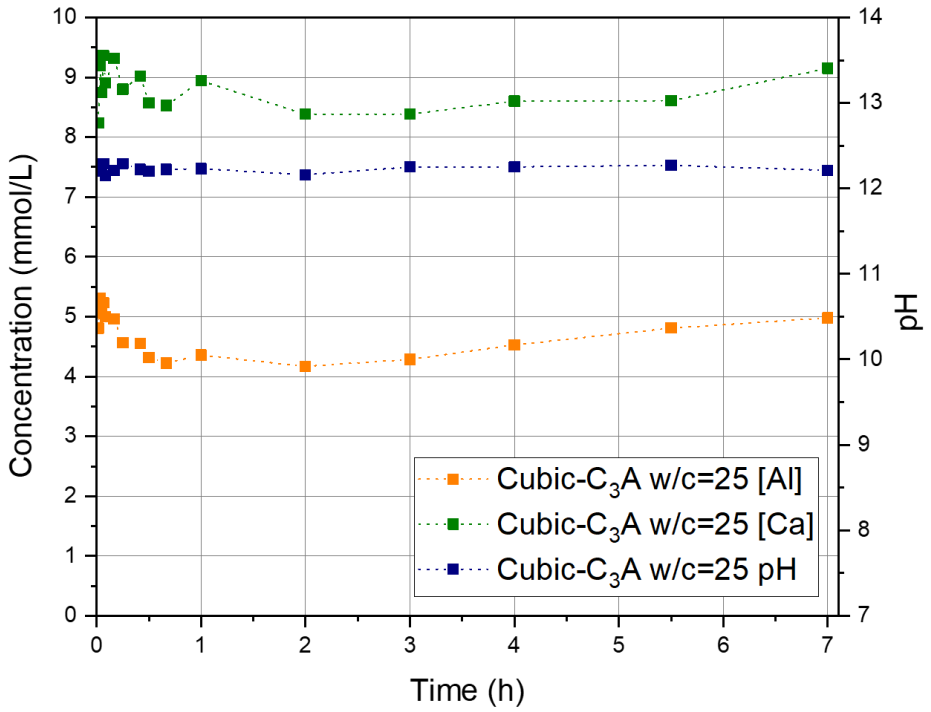


**Figure 137 : Characterization of the liquid fractions of cubic-$C_3A$ suspension (w/c ratio = 25, T = 25 °C) during the first seven hours of hydration: evolution of pH and chemical composition.**

The hydration path followed by calcium and aluminium concentrations was reported in the plotted {$CaO$-$Al_2O_3$-$H_2O$} solubility diagram (Figure 138).

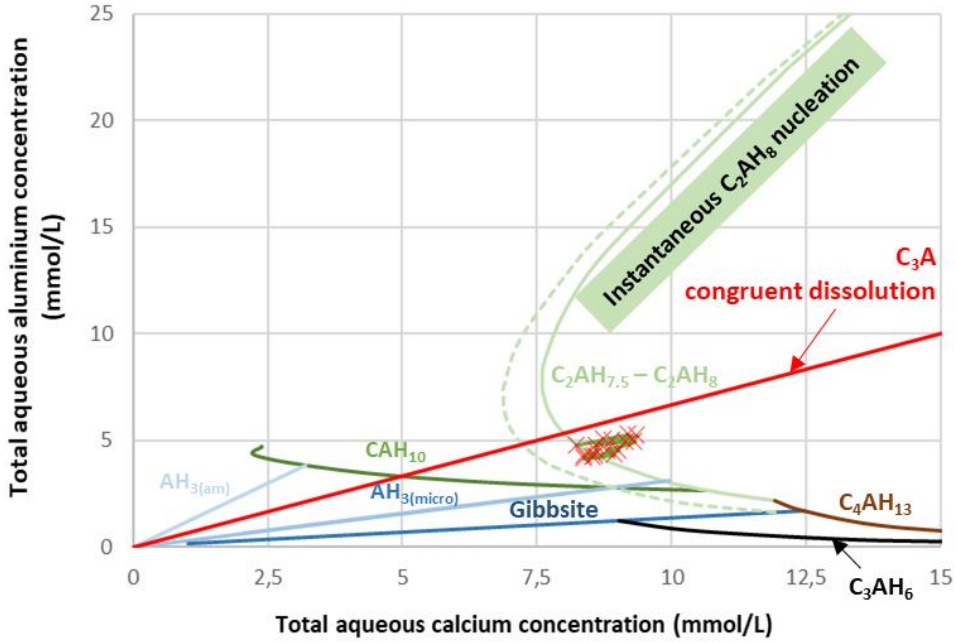


**Figure 138 : Total calcium and aluminium concentrations measured in the liquid fraction during cubic-$C_3A$ hydration (w/c = 25 – T = 25 °C) plotted in the {$CaO$-$Al_2O_3$-$H_2O$} solubility diagram. Note that the red line is not a solubility curve. It simply shows the expected concentrations if the system is driven by congruent dissolution of $C_3A$.**

The system remained strongly undersaturated with respect to $C_3A$ (solubility curve not visible in the range of Ca and Al concentrations plotted in Figure 138). The Al and Ca concentrations showed little evolution over the investigated period, with a ratio slightly below the expected value of 2/3 for a pore solution composition determined by congruent dissolution of $C_3A$.

The pore solution composition remained in a region supersaturated with respect to $C_3AH_6$, close to the intersection of $C_3A$ congruent dissolution line and $C_2AH_8$ solubility curve. Note that several authors reported the transient precipitation of this latter hydrate, possibly mixed with $C_4AH_{19}$ [9, 11], during the very first stages of $C_3A$ hydration. In our study, the first analysis of the phases precipitating was performed after 30 minutes of hydration, which was too late to have a chance to evidence $C_2AH_8$ formation. Nevertheless, this initial precipitation, which still needs to be confirmed in our study, might continue to influence the pore solution composition during later stages of hydration, when $C_3AH_6$ is the main hydrate formed. It would be interesting to continue to characterize the solution composition after 7 h, when higher degrees of hydration are reached, to determine whether it drifts in the direction of the solubility curve of $C_3AH_6$.

## 3. Summary and discussion

In this chapter, the hydration study of a pure synthetic cubic-$C_3A$ phase was presented.

First, it was observed that only the deceleration period could be monitored by isothermal calorimetry due to the very quick hydration reactions. Also, significant amount of heat was lost during ex-situ mixing and placing the sample in the isothermal calorimetry. Therefore, estimation of the hydration degree, by assuming that only heat release contributed to the dissolution of cubic-$C_3A$, was based on the results obtained from in-situ mixing procedure. From the point of view of mineralogical assemblage, all pastes, regardless of their w/c ratios (within the range 0.375-0.6), mainly comprised $C_3AH_6$ 7 days after mixing, together with small amounts of $C_4A\check{C}H_{11}$.

After 0.5 h, 4 h and 7 h of hydration of a paste elaborated with a w/c ratio of 0.5, hydration degrees of 40 %, 54 % and 56.5 % were achieved based on $^{27}$Al NMR results. From the point of view of hydrates and for a paste elaborated with a w/c ratio of 0.5, the mineralogical assemblage derived from $^{27}$Al NMR spectroscopy was composed of about 63 % of stable $C_3AH_6$ and 3 % of $C_4A\check{C}H_{11}$ which were also identified by XRD and TGA. This measured composition was found to be close to that expected from mass balance hydration equations for cubic-$C_3A$.

The hydration studies of cubic-$C_3A$ in diluted media with w/c ratios increasing from 12 to 75 resulted in similar mineralogical assemblages mainly composed of $C_3AH_6$ after 24 h of hydration. The increase in bound water for higher w/c ratios calculated from TGA was related to the increase in $C_3AH_6$ content. From a thermodynamic view and during the studied period, calcium and aluminate ions concentrations were located close to the intersection of $C_3A$ congruent dissolution line and $C_2AH_8$ solubility curve.

## 4. References

[1] L. B. Black, C.; Yarwood, J.; Deng, C.-S.; Phipps, J.; Maitland, G., "Hydration of tricalcium aluminate (C3A) in the presence and absence of gypsum—studied by Raman spectroscopy and X-ray diffraction," *J. Mater. Chem.*, vol. 16, pp. 1263-1272, 2006.

[2] A. S. Brand and J. W. Bullard, "Dissolution Kinetics of Cubic Tricalcium Aluminate Measured by Digital Holographic Microscopy," *Langmuir*, vol. 33, no. 38, pp. 9645-9656, 2017/09/26 2017.

[3] J. W. Bullard *et al.*, "Mechanisms of cement hydration," *Cement and Concrete Research*, vol. 41, no. 12, pp. 1208-1223, 2011.

[4] A. P. Kirchheim, V. Fernàndez-Altable, P. J. M. Monteiro, D. C. C. Dal Molin, and I. J. J. o. M. S. Casanova, "Analysis of cubic and orthorhombic C3A hydration in presence of gypsum and lime," journal article vol. 44, no. 8, pp. 2038-2045, April 01 2009.

[5] K. L. Scrivener and A. Nonat, "Hydration of cementitious materials, present and future," *Cement and Concrete Research*, vol. 41, no. 7, pp. 651-665, 2011/07/01/ 2011.

[6] H. Minard, "Etude intégrée des processus d'hydratation, de coagulation, de rigidification et de prise pour un système C3S-C3A - sulfates - alcalins," 2003.

[7] A. Gmira, "Structural and thermodynamical study of hydartes cement model," Université d'Orléans, 2003.

[8] J. Pommersheim and J. Chang, "Kinetics of hydration of tricalcium aluminate," *Cement and Concrete Research*, vol. 16, no. 3, pp. 440-450, 1986/05/01/ 1986.

[9] P. Meredith, A. M. Donald, N. Meller, and C. Hall, "Tricalcium aluminate hydration: Microstructural observations by in-situ electron microscopy," *Journal of Materials Science*, vol. 39, no. 3, pp. 997-1005, 2004/02/01 2004.

[10] A. Quennoz, "Hydration of C3A with Calcium Sulfate Alone and in the Presence of Calcium Silicate," PhD, Faculté Sciences et Techniques de l'Ingénieur, École de Polytechnique Fédérale de Lausanne, Suisse, 5035, 2011.

[11] A. C. Jupe *et al.*, "Fast in situ x-ray-diffraction studies of chemical reactions: A synchrotron view of the hydration of tricalcium aluminate," *Physical Review B*, vol. 53, no. 22, pp. R14697-R14700, 06/01/ 1996.

[12] M. Collepardi, G. Baldini, M. Pauri, and M. Corradi, "Tricalcium aluminate hydration in the presence of lime, gypsum or sodium sulfate," *Cement and Concrete Research*, vol. 8, no. 5, pp. 571-580, 1978/09/01/ 1978.

[13] R. J. Myers, G. Geng, E. D. Rodriguez, P. da Rosa, A. P. Kirchheim, and P. J. M. Monteiro, "Solution chemistry of cubic and orthorhombic tricalcium aluminate hydration," *Cement and Concrete Research*, vol. 100, pp. 176-185, 2017/10/01/ 2017.

[14] W. Han, T. Sun, X. Li, Z. Shui, Y. Chen, and M. Sun, "Influence of Lithium Carbonate on $C_3A$ Hydration," *Advances in Materials Science and Engineering*, vol. 2018, p. 6120269, 2018/02/25 2018.

[15] N. Maach, "Kinetic modeling of the early age hydration of calcium aluminate cements : From chemical mechanism to the modeling by the Population Balance Equations," Thèse de doctorat, Mécanique, Energétique, Génie Civil, Acoustique (MEGA), l'INSA de Lyon, 2019LYSEI127, 2019.

[16] D. Jansen, F. Goetz-Neunhoeffer, B. Lothenbach, and J. Neubauer, "The early hydration of Ordinary Portland Cement (OPC): An approach comparing measured heat flow with calculated heat flow from QXRD," *Cement and Concrete Research,* vol. 42, no. 1, pp. 134-138, 2012/01/01/ 2012.

[17] E. Nicolas, "Compatibilités et incompatibilités liants cimentaires/superplastifiants," PhD Thèse de Doctorat, Université Henri Poincaré, Luxembourg, 2010.

[18] X. Jing, Y. Zhang, H. Liu, J. Liu, and S. Kong, "Effect of Aluminum Sulfate on the Hydration of Tricalcium Aluminate," *IOP Conference Series: Earth and Environmental Science,* vol. 719, no. 2, p. 022079, 2021/04/01 2021.

[19] N. Collier, "Transition and Decomposition Temperatures of Cement Phases – a Collection of Thermal Analysis Data," *Ceramics Silikaty,* vol. 60, 10/01 2016.

[20] S. Joseph, J. Skibsted, and Ö. Cizer, "A quantitative study of the C3A hydration," *Cement and Concrete Research,* vol. 115, pp. 145-159, 2019/01/01/ 2019.

[21] U. M. Ukrainczyk N, Šipušić J, Matusinović T., "XRD and TGA investigation of hardened cement paste," presented at the 11th conference on materials, processes, friction and wear, Vela Luka, Croatia, 2006.

[22] J. Kaufmann, R. Loser, F. Winnefeld, and A. Leemann, "Sulfate resistance and phase composition of shotcrete," *Tunnelling and Underground Space Technology,* vol. 109, p. 103760, 2021/03/01/ 2021.

[23] J. Plank, M. Zhang-Preße, N. P. Ivleva, and R. Niessner, "Stability of single phase C3A hydrates against pressurized CO2," *Construction and Building Materials,* vol. 122, pp. 426-434, 2016/09/30/ 2016.

[24] J. H. Skibsted, E.; Jakobsen, H.J., "Characterization of Calcium Aluminate Phases in Cements by 27Al MAS NMR Spectroscopy," *Inorg. Chem.,* vol. 32, pp. 1013-1027, 1993.

[25] J. Skibsted, H. Bildsøe, and H. J. Jakobsen, "High-speed spinning versus high magnetic field in MAS NMR of quadrupolar nuclei. 27Al MAS NMR of 3CaO·Al2O3," *Journal of Magnetic Resonance (1969),* vol. 92, no. 3, pp. 669-676, 1991/05/01/ 1991.

[26] S. Ferreiro, T. Blasco, M. I. Sánchez de Rojas, and M. Frías, "Influence of Activated Art Paper Sludge-Lime Ratio on Hydration Kinetics and Mechanical Behavior in Mixtures Cured at 20°C," *Journal of the American Ceramic Society,* https://doi.org/10.1111/j.1551-2916.2009.03334.x vol. 92, no. 12, pp. 3014-3021, 2009/12/01 2009.

[27] J. V. Jr. Bothe and P. W. Brown, "Kinetics of Tricalcium Aluminate Hydration in the Presence of Boric Acid and Calcium Hydroxide," *Journal of the American Ceramic Society,* https://doi.org/10.1111/j.1151-2916.1999.tb02012.x vol. 82, no. 7, pp. 1882-1888, 1999/07/01 1999.

[28] T. Runcevski, R. E. Dinnebier, O. V. Magdysyuk, and H. Pollmann, "Crystal structures of calcium hemicarboaluminate and carbonated calcium hemicarboaluminate from synchrotron powder diffraction data," *Acta Crystallographica Section B,* vol. 68, no. 5, pp. 493-500, 2012.

[29] C. B. Leon Black, Jack Yarwood, C.-S. Deng, Jonathan Phipps and Geoff Maitland, "Hydration of tricalcium aluminate ($C_3A$) in the presence and absence of gypsum—

studied by Raman spectroscopy and X-ray diffraction," *J. Mater. Chem.*, vol. 16, pp. 1263-1272, 2006.

[30] A. P. Kirchheim *et al.*, "Effect of Gypsum on the Early Hydration of Cubic and Na-Doped Orthorhombic Tricalcium Aluminate," *Materials*, vol. 11, no. 4, 2018.

[31] N. Ukrainczyk, T. Matusinovic, S. Kurajica, B. Zimmermann, and J. Sipusic, "Dehydration of a layered double hydroxide—$C_2AH_8$," *Thermochimica Acta*, vol. 464, no. 1, pp. 7-15, 2007/11/25 2007.

[32] F. Šoukal *et al.*, "The influence of pH buffers on hydration of hydraulic phases in system CaO–Al2O3," *Journal of Thermal Analysis and Calorimetry*, Article vol. 124, no. 2, pp. 629-638, 2016.

[33] J. Bizzozero, "Hydration and dimensional stability of calcium aluminate cement based systems," Theses 2014 2014, Art. no. 6336.

[34] M. R. Nilforoushan and N. Talebiaan, "The hydration products of a refractory calcium aluminate cement at low temperatures," (in English), *Iranian Journal of Chemistry and Chemical Engineering (IJCCE)*, Article vol. 26, no. 2, pp. 71-76, 2007.

[35] P. T. Durdziński, "Hydration of multi-component cements containing cement clinker, slag, calcareous fly ash and limestone," PhD, Faculté Sciences et Techniques de l'Ingénieur, EPFL, Suisse, 6834, 2016.

[36] V. S. Ramachandran, R. M. Paroli, J. J. Beaudoin, and A. H. Delgado, "10 - Non-Portland Rapid Setting Cements," in *Handbook of Thermal Analysis of Construction Materials*, V. S. Ramachandran, R. M. Paroli, J. J. Beaudoin, and A. H. Delgado, Eds. Norwich, NY: William Andrew Publishing, 2002, pp. 403-448.

[37] P. Padilla-Encinas, A. Palomo, M. T. Blanco-Varela, and A. Fernández-Jiménez, "Calcium sulfoaluminate clinker hydration at different alkali concentrations," *Cement and Concrete Research*, vol. 138, p. 106251, 2020/12/01/ 2020.

[38] M. D. Andersen, H. J. Jakobsen, and J. Skibsted, "A new aluminium-hydrate species in hydrated Portland cements characterized by 27Al and 29Si MAS NMR spectroscopy," *Cement and Concrete Research*, vol. 36, no. 1, pp. 3-17, 2006/01/01/ 2006.

# Chapter 7: Conclusions and perspectives

# **Chapitre 7** : Conclusions et perspectives

**Résumé** : Ce dernier chapitre est constitué de la comparaison des systèmes en pates et en suspensions, les conclusions retirées en mettant l'accent sur les perspectives.

Acher *et al.* [1] ont constaté que le rendement de production radiolytique en dihydrogène ($G(H_2)$) est beaucoup plus faible pour les hydrates des ciment alumineux que pour les hydrates de ciment Portland. Parmi ces hydrates, l'hydroxyde d'aluminium présente les plus faibles valeurs de $G(H_2)$, par rapport au $C_3AH_6$. Ces résultats, qui relancent l'intérêt de l'utilisation des ciments alumineux pour l'immobilisation de déchets nucléaires irradiants, ont été le point de départ de cette étude. L'objectif à terme sera de concevoir un mortier à base de ciments alumineux présentant un rendement radiolytique en dihydrogène minimisé et respectant également les spécifications du procédé de cimentation, notamment en terme de temps de prise. De nombreuses questions se sont posées sur l'assemblage minéralogique pouvant être obtenu en fonction de la composition des ciments alumineux considérés, mais aussi sur le contrôle de leur vitesse d'hydratation.

Dans un premier temps, une recherche fondamentale a donc été entreprise afin de recueillir des informations sur les vitesses d'hydratation et les assemblages minéralogiques, en étudiant l'hydratation de quatre aluminates de calcium anhydres synthétiques, se distinguant les uns des autres par leur rapport C/A. Conformément à la littérature, la réactivité au jeune âge de ces phases anhydres peut être classée de la manière suivante : $CA_2 < CA < C_{12}A_7 < C_3A$. Les courbes de chaleur cumulée montrent que le vitesse d'hydratation pendant la période d'accélération augmente avec le rapport C/A.

Dans un second temps, l'assemblage minéralogique des pâtes à sept jours a été déterminé par DRX, ATG et RMN du solide de l'$^{27}$Al. Nous avons pu constater qu'environ 75 % de la phase d'aluminate de calcium anhydre a été consommée, quelle que soit l'anhydre considéré. En revanche, la nature de l'anhydre considéré influe fortement l'assemblage minéralogique obtenu sept jours après le début de l'hydratation. Lors de l'hydratation de $CA_2$, l'hydroxyde d'aluminium était le principal produit sept jours après le mélange, avec moins de 4 % de $CAH_{10}$, tandis que la pâte préparée avec $C_3A$ était composée principalement de $C_3AH_6$. De manière générale, nous avons pu constater que plus le rapport C/A de la phase anhydre est faible, plus la quantité d'hydroxyde d'aluminium est élevée. Toujours dans le cadre du conditionnement des déchets nucléaires et dans le but de minimiser la production d'hydrogène due à la radiolyse, des quantités élevées d'$AH_3$ seraient préférables si l'on considère uniquement les rendements de production d'hydrogène radiolytique des hydrates.

Au cours de la deuxième partie de l'étude systématique menée dans ce travail, l'hydratation de chaque phase anhydre a été étudiée en suspension afin de collecter et de caractériser la fraction liquide. Ces expériences visaient à identifier les chemins d'hydratation suivis par les ions calcium et aluminate lors de l'hydratation de chacune des phases anhydres étudiées. Basée sur l'évolution temporelle de la composition de la fraction liquide, la première approche adoptée a

consisté à tracer la concentration aqueuse d'aluminium en fonction de la concentration aqueuse de calcium sur le diagramme de phase {$CaO$-$Al_2O_3$-$H_2O$}. Pour chacune des phases anhydres, le chemin de réaction est décrit.

Une autre approche pour identifier les voies d'hydratation a consisté à prêter attention à l'évolution de l'indice de saturation dans le temps. L'indice de saturation des phases d'intérêt a été calculé en effectuant des calculs de spéciation à l'aide du logiciel CHESS et de la base de données thermodynamiques CEMDATA2018 convertie dans le formalisme CHESS. Il est apparu tout d'abord que les calculs effectués avec la base de données thermodynamiques CEMDATA2018 ne permettaient pas de reproduire les valeurs expérimentales de pH. Ceci était indiqué par une balance électronique loin de l'électroneutralité. Une telle divergence entre les données expérimentales et modélisées a été observée dans un système plus simple au cours de ce travail. Des quantités croissantes d'aluminate de sodium $NaAlO_2$ ont été dissoutes dans de l'eau pure. Les valeurs de pH calculées étaient systématiquement inférieures aux valeurs expérimentales, d'environ 2 unités de pH pour une solution contenant 100 mmol/L de $NaAlO_2$ à 25 °C. Une autre perspective de ce travail de thèse consisterait à améliorer la compréhension de la spéciation de l'aluminium et à mettre en évidence les raisons de cette divergence. L'étape suivante consisterait à étudier en détail la voie de précipitation de l'hydroxyde d'aluminium à partir de ces solutions d'aluminate de sodium et de solutions représentatives des solutions interstitielles des ciments alumineux.

# Conclusions and perspectives

Acher *et al.* [2] have reported that the radiolytic yield in dihydrogen ($G(H_2)$) is much lower for Calcium Aluminate Cements hydrates than for Portland cement hydrates (Figure 139). Among these hydration products, aluminium hydroxide presents the lowest $G(H_2)$ values, when compared to $C_3AH_6$. These results, which revive interest in using CACs for nuclear waste immobilization, were the starting point of this study. The end-objective is to design a CAC-based grout mortar presenting a minimized radiolytic hydrogen production yield that also complies with cementation process specifications, especially in term of setting time.

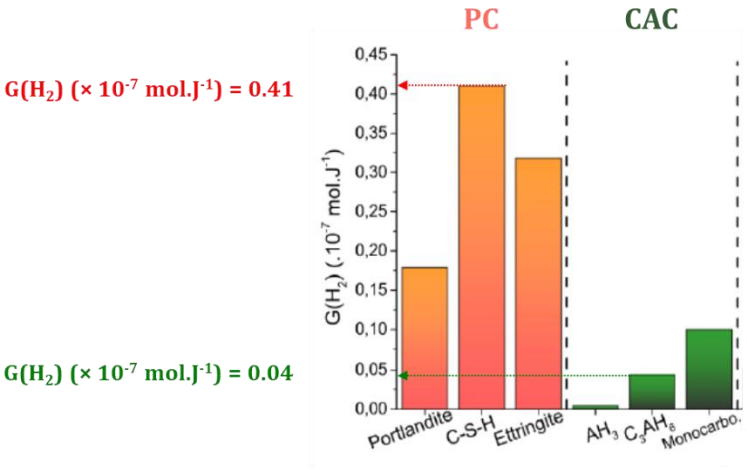


**Figure 139 : $G(H_2)$ values determined from Portland and Ciment Fondu® pastes, adapted from [1].**

From this point of view, many questions arose on the mineralogical assemblage that could be achieved depending on the composition of the considered CAC, but also on the control of their hydration rate. A fundamental research was thus undertaken in order to collect information on these hydration rates and mineralogical assemblages, by studying the hydration of four different synthetic calcium aluminate anhydrous phases varying from each other by their C/A ratio:

- $CA_2$,
- CA,
- $C_{12}A_7$,
- $C_3A$.

A systematic methodology was firstly applied to characterize pastes elaborated with each of these anhydrous phases and cured at 25 °C.

First, reactivity at early age was evaluated by using isothermal conduction calorimetry (Figure 140). In this work, the reactivity of each anhydrous phases was defined as the time needed for each pastes, elaborated by using a w/c ratio of 0.5, to release 100 and 250 J/g of anhydrous

phase (Table 38). In accordance with literature, the early age reactivity of these calcium aluminate anhydrous phases can be ranked as follows:

$$CA_2 < CA < C_{12}A_7 < C_3A$$

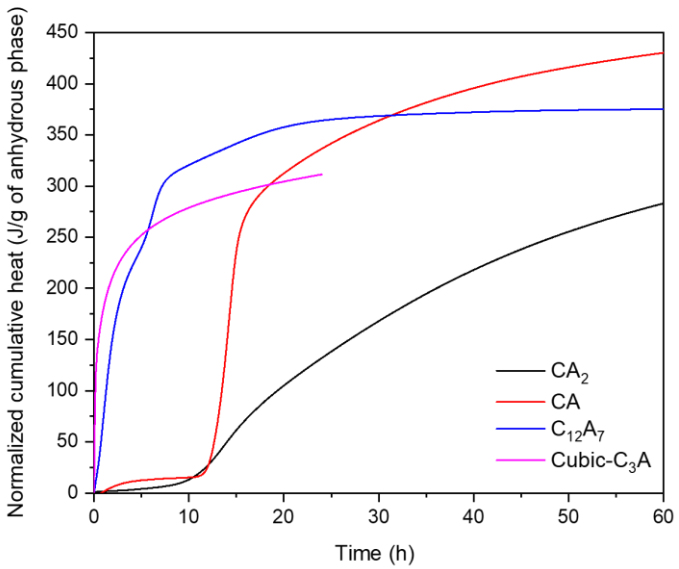


**Figure 140 : Hydration monitoring of $CA_2$, CA, $C_{12}A_7$ and $C_3A$ pastes elaborated with a w/c of 0.5 by using isothermal conduction calorimetry at 25 °C.**

**Table 38 : Time to reach the cumulative heat values of 100 J/g and 250 J/g.**

| Phase | Time at 100 J/g (h) | Time at 250 J/g (h) |
|---|---|---|
| $CA_2$ | 19.3 | 48.3 |
| CA | 13.5 | 15.3 |
| $C_{12}A_7$ | 1.3 | 5.5 |
| $C_3A$ | 0.2 | 4.8 |

In the framework of nuclear waste immobilization where organic admixtures should be avoided to control the setting, a calcium aluminate cement with a low C/A ratio would be recommended to design a grout mortar for two main reasons. First, a cement with an induction period longer than 4 hours is needed to comply with nuclear waste cementation process specifications. Secondly, self-heating of elaborated mortars has to be as low as possible given the large volumes usually cast in canisters. This latter specification can be achieved by reducing the heat resulting from cement hydration or by lengthening the period over which heat is liberated. Klaus *et al.* [3] studied the hydration of $CA_2$/CA mixes and reported that a slower rate of hydration

can be achieved for 50:50 (wt. %) mixes. The first prospect of this PhD thesis would consist in evaluating the early age reactivity of $CA_2$/CA blends containing more than 50 wt. % of $CA_2$. The resulting mechanical properties of elaborated mortars should also be determined to evaluate the relevance of such blends for nuclear waste immobilization.

Second, mineralogical compositions of paste samples were determined by XRD, TGA and $^{27}$Al-NMR. When comparing mineralogical assemblages achieved seven days after mixing (at a w/c ratio of 0.5) with a curing temperature of 25 °C, it can first be observed on Figure 141 that about 75 % of the anhydrous calcium aluminate phase was consumed, regardless of its composition. However, the precipitated hydrates differed strongly for each of the four anhydrous phase. When hydrating $CA_2$, aluminium hydroxide was the main product, together with less than 4 % of $CAH_{10}$ whereas the paste prepared with $C_3A$ mainly comprised $C_3AH_6$. Broadly speaking, it appears that the lower C/A ratio of the anhydrous phase, the higher the amount of aluminium hydroxide. Still in the framework of nuclear waste conditioning and with the objective of minimizing the hydrogen production due to radiolysis, high amounts of $AH_3$ would be preferable if only the radiolytic hydrogen production yields of hydrates are considered. Therefore, the second prospect of this study would consist in measuring the radiolytic hydrogen production yield of pastes elaborated by using a CAC still presenting a low C/A ratio. It would also be interesting to compare the $H_2$ production resulting from the hydrates and from residual "free" water present in the pore solution of these materials. It has to be noted that a stable hydrates assemblage was not reached within the studied period and the role of the conversion of hydrates should deserve deeper investigation.

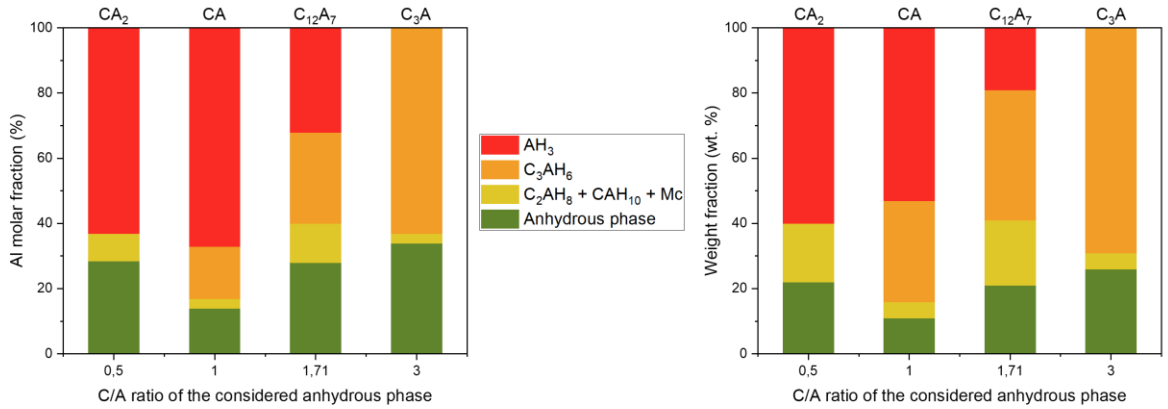


**Figure 141 : Comparison between mineralogical assemblages achieved after seven days for each of the studied anhydrous phases – w/c = 0.5 – T = 25 °C. Estimation from $^{27}$Al MAS NMR.**

During the second part of the systematic study carried out in this work, the hydration of each anhydrous phase was studied in suspension in order to collect and characterize the liquid fraction. These experiments aimed at identifying hydration paths followed by calcium and aluminate ions during the hydration of each of the studied anhydrous phase. Based on the time

evolution of the liquid fraction composition, one approach consisted in plotting the aqueous aluminium concentration as a function of the aqueous calcium concentration on the {CaO-$Al_2O_3$-$H_2O$} phase diagram. All the results are collected in Figure 142.

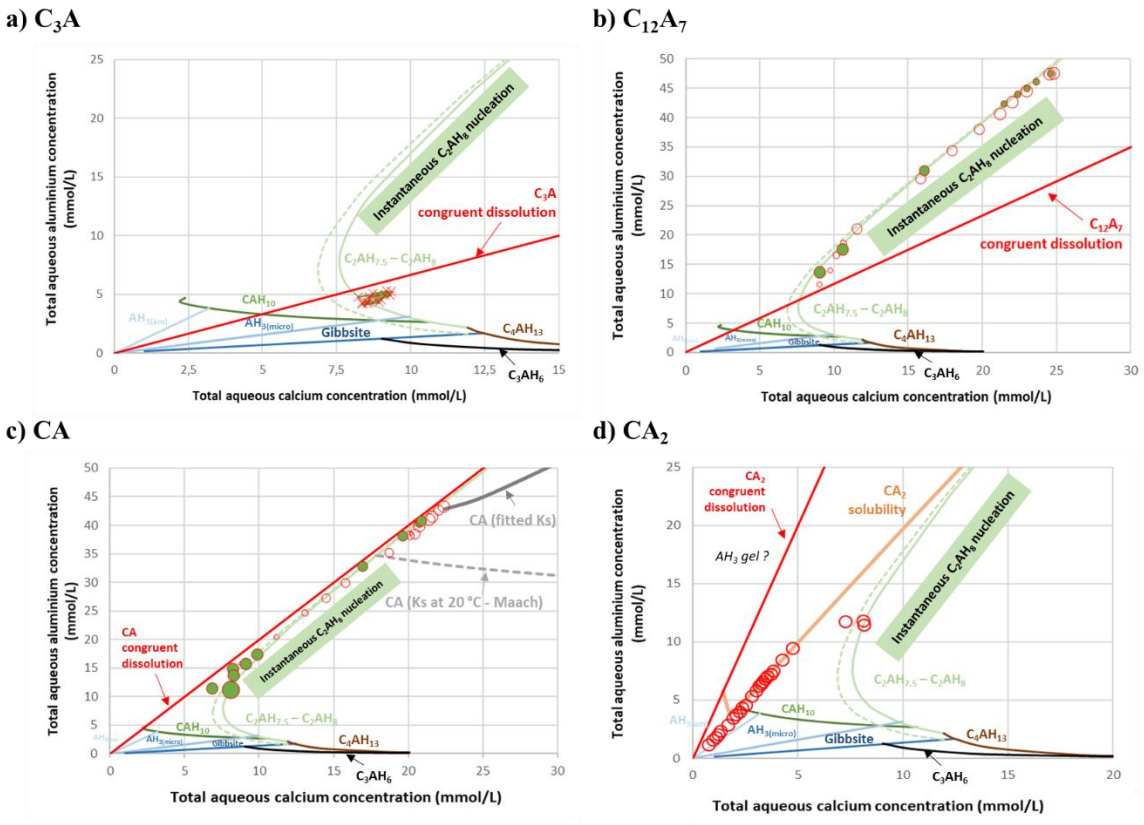


**Figure 142 : Hydration path followed by aqueous aluminium and calcium concentrations during the hydration of a) $C_3A$, b) $C_{12}A_7$, c) CA and d) $CA_2$ in the {CaO-$Al_2O_3$-$H_2O$} diagram – w/c = 25 – T = 25 °C.**

The reaction path followed by each phase can be described as follows.

When $C_3A$ was mixed with pure water, its dissolution occurred very quickly. This is consistent with its high solubility. From the results collected during the period studied, from 1 minute to 7 hours, no drastic change of the liquid fraction composition occurred. The composition of this liquid fraction remained close to the intersection of the $C_2AH_8$ solubility curve with $C_3A$ congruent dissolution line. From the mineralogical point of view, $C_3AH_6$ was mainly observed in the collected solid fractions, from 30 minutes to 7 hours after mixing by XRD and TGA. Further investigations would be needed *(i)* to check whether $C_2AH_8$ is observed under our experimental conditions at very early age as reported in literature, and *(ii)* to determine if the liquid fraction composition drifts towards the $C_3AH_6$ solubility curve at later stages of hydration.

Concerning $C_{12}A_7$, its dissolution also occurred very quickly during the first period of its hydration but led to the precipitation of $C_2AH_8$. This hydrate was observed in the first collected

solid fraction, 30 minutes after mixing, by XRD, TGA and $^{27}$Al MAS-NMR. At this stage, the composition of the liquid fraction was located at the intersection between the $C_2AH_8$ solubility curve and the $C_{12}A_7$ congruent dissolution line. With ongoing hydration, it appeared that $C_{12}A_7$ continued to dissolve while the amounts of $AH_3$ and $C_2AH_8$ increased in the solid fractions, evidenced by TGA and $^{27}$Al MAS-NMR. The hydration path followed by the liquid fraction diverged from the $C_{12}A_7$ congruent dissolution line and followed the $C_2AH_8$ solubility line with the calcium and aluminate concentrations first increasing before decreasing. Such a behaviour showed that the hydration was of $C_{12}A_7$ was driven by competition between its dissolution and $C_2AH_8$ precipitation. The bound water content increased almost linearly, meaning that the precipitation rate of hydrates showed little change over the investigated period. The accumulation of ions in solution observed initially indicated that the dissolution rate first predominated over the precipitation rates. The situation reversed with dissolution slowing down, and precipitation dominating the process as the aqueous calcium and aluminate concentrations started to decrease.

Interestingly, CA exhibited a different hydration process. Although the Ca and Al concentrations followed a similar trajectories, the kinetics were very different from had been observed for $C_{12}A_7$. When CA was mixed with pure water, the aqueous calcium and aluminium concentrations increased but much smaller amounts of hydrates precipitated compared to $C_{12}A_7$. Both Ca and Al concentrations reached a maximum and the composition remained stable for a given period. Maach [4] suggested in his work that the liquid fraction composition is governed at this point by the CA solubility product. During this first period, from 1 minute to 2 hours, the liquid fraction composition thus followed the CA congruent dissolution line up to a maximum corresponding to the CA solubility. The end of this period was accompanied by a sudden precipitation of hydrated phases (mainly $AH_3$ and minor amounts of $C_2AH_8$), which resulted in a second increase in the dissolution rate. During this period, from 140 minutes to 7 hours, the aqueous calcium and aluminium concentrations decreased following the $C_2AH_8$ solubility curve. The trigger for this hydrates precipitation was not elucidated during this work but according to literature, the precipitation of aluminium hydroxide could be the limiting step [5-7].

As for $CA_2$, it is significant that in the {$CaO$-$Al_2O_3$-$H_2O$} diagram its solubility curve appears below the $CA_2$ congruent dissolution line. Initially, when mixing $CA_2$ with water, the liquid fraction composition followed the $CA_2$ solubility and was thus controlled by this process. From the solid fraction point of view, small amounts of hydrated phases precipitated during this period, as illustrated by the evolution of the bound water amount measured by TGA from 30 minutes to 4 hours of hydration. DTG curves evidence a peak close to 100 °C, suggesting the precipitation of an amorphous aluminium hydroxide. From the liquid fraction composition, the end of the first period was characterized by the shift of the aqueous calcium and aluminate concentrations from the solubility curve of $CA_2$ to that of $C_2AH_8$. The nature of this trigger is not known. However, this trigger might again be the precipitation of aluminium hydroxide, observed by using XRD, TGA and $^{27}$Al MAS-NMR, that would bring enough hydroxide ions to allow $C_2AH_8$ or $CAH_{10}$ precipitation. Only traces of $CAH_{10}$ were evidenced by $^{27}$Al MAS-NMR at 4 hours.

Another approach to identify hydration paths consisted in paying attention to saturation index evolution over time. Saturation index for relevant phases were calculated by carrying out speciation calculations using CHESS software and CEMDATA2018 thermodynamic database converted in CHESS formalism.

However, it appeared that the calculations made with CEMDATA2018 thermodynamic database were not able to reproduce the experimental pH values. This was established by a significant electrical balance. Maach [4] previously reported such an observation. An incomplete description of the aluminium-containing species seems to be the most plausible reason for this bias. Such a discrepancy between experimental and modelled data was further observed in a simpler system during this work. Increasing amounts of sodium aluminate $NaAlO_2$ were dissolved in pure water. The calculated pH values were systematically lower than the experimental ones, by about 2 pH units for a solution containing 100 mmol/L of $NaAlO_2$ at 25 °C (Figure 143). Another prospect of this PhD work would therefore consist in improving the understanding of aluminium speciation in calcium aluminate hydration solutions. First, one could try to identify the reasons for the discrepancy between the calculated and measured sodium aluminate solutions. The following step would consist in studying in detail the route for aluminium hydroxide precipitation first from these sodium aluminate solutions, and then from solutions representative of CAC interstitial solutions.

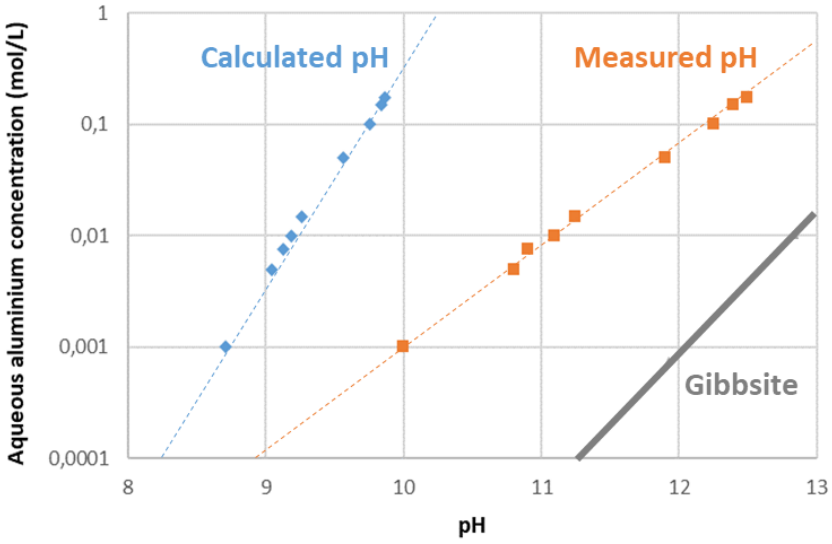


**Figure 143 : Comparison between measured and calculated pH values of $NaAlO_2$ solutions of increasing concentration in pure water – 25 °C.**

## References

[1] L. Acher, "Etude du comportement sous irradiation γ et électronique de matrices cimentaires et de leurs hydrates constitutifs," Doctorat École doctorale n°573 Interfaces Université Paris-Saclay, NNT : 2017SACLX045, 2017.

[2] L. Acher *et al.*, "H2 production under gamma irradiation of a calcium aluminate cement: An experimental study on both cement pastes and its stable hydrates," *Radiation Physics and Chemistry*, vol. 189, p. 109689, 2021/12/01/ 2021.

[3] S. R. Klaus, J. Neubauer, and F. Goetz-Neunhoeffer, "Hydration kinetics of CA2 and CA—Investigations performed on a synthetic calcium aluminate cement," *Cement and Concrete Research*, vol. 43, pp. 62-69, 2013/01/01/ 2013.

[4] N. Maach, "Kinetic modeling of the early age hydration of calcium aluminate cements : From chemical mechanism to the modeling by the Population Balance Equations," Thèse de doctorat, Mécanique, Energétique, Génie Civil, Acoustique (MEGA), l'INSA de Lyon, 2019LYSEI127, 2019.

[5] S. R. Klaus, J. Neubauer, and F. Goetz-Neunhoeffer, "How to increase the hydration degree of CA — The influence of CA particle fineness," *Cement and Concrete Research*, vol. 67, pp. 11-20, 2015/01/01/ 2015.

[6] F. Hüller, "Hydration mechanisms of CA2 and alumina-rich calcium aluminate cements: Effects of mechanical activation, critical CA contents and crystallinity of AH3," PhD, Geographie und Geowissenschaften, Friedrich-Alexander-Universität Erlangen-Nürnberg (FAU), 2019.

[7] M. T. Gaztañaga, S. Goñi, and J. L. Sagrera, "Reactivity of high-alumina cement in water: pore-solution and solid phase characterization," *Solid State Ionics*, vol. 63-65, pp. 797-802, 1993/09/01/ 1993.

# Appendix

# Appendix A.1 Analytical procedures

**Laser granulometry**

Particle size distributions of the studied anhydrous calcium aluminate phases were measured using laser granulometry with a Malvern Master Sizer 3000 analyzer, which uses a laser diffraction technique to measure particles sizes ranging from 10 nm to 2 mm. Powders were dispersed in ethanol (0.1 g of powder in 1 L of ethanol) rather than water because of the reactive nature of cement in water.

**Specific surface area measurement**

The specific surfaces areas were determined by nitrogen adsorption following the Brunauer Emmett and Teller (BET) method, with a Micromeritics ASAP2020 instrument. Prior to all measurements, the samples (~0.5 g) were degassed at 625 K for 17 h under vacuum and finally outgassed to 20 Torr.

**Helium pycnometry**

The absolute densities of the anhydrous cement phases were measured with a Micromeritics AccuPyc II 1340 Helium Pycnometer.

# Appendix A.2 XRD analysis

X-ray diffraction is a powerful technique for the study of crystalline materials. The interaction of the incident rays with the sample produces constructive interference (and a diffracted ray) when conditions satisfy Bragg's Law:

$$n\lambda = 2d.\sin\theta$$

where n is an integer, $\lambda$ is the wavelength of the radiation used, d the spacing of the crystal planes, and $\theta$ the diffraction peak angle.

This law relates the wavelength of electromagnetic radiation to the diffraction angle and the lattice spacing in a crystalline sample. These diffracted X-rays are then detected, processed and counted. By scanning the sample through a range of $2\theta$ angles, all possible diffraction directions of the lattice should be attained due to the random orientation of the powdered material. Conversion of the diffraction peaks to d-spacings allows identification of the mineral because each mineral has a set of unique d-spacings. Typically, this is achieved by comparison of d-spacings with standard reference patterns.

The samples were ground to a fine powder prior to the XRD measurement and put in the sample holder. Afterwards, they were packed with a metallic cylinder to obtain a very flat upper surface and the excess on the edges were removed with a brush. For the low sample amount, zero diffraction plate with cavity (Si Crystal) was used, especially for the solid fractions obtained from suspension experiments.

XRD powder patterns of each anhydrous calcium aluminate phase were collected using a Bragg Brentano geometry (PanAlytical X'pert Pro, copper anode, $\lambda_{K\alpha 1}$=1.5418 Å, scanning from 2θ = 5° to 70° in 0.013° steps, for a total counting time of 3 h).

For routine XRD analysis, the acquisition was performed over a range of scanning from 2θ = 5° to 70° in 0.017° steps, for a total counting time of 42 min.

Additionally, the evolution of the amounts of hydration products was qualitatively assessed from XRD patterns by comparing the areas of characteristic peaks using the EVA analysis software.

## Appendix A.3 Thermogravimetric analysis

Thermogravimetric analysis is a destructive measuring technique. It makes it possible to measure the mass variation of a sample relative to a reference by means of a thermo-balance. as a function of the temperature in an inert medium. The TGA apparatus is composed of a total enclosure, an oven, a microbalance and a thermocouple. The TGA enables the analyst to observe the effects of thermal decomposition and evaporation.

Thermogravimetric analyses were carried out in alumina 70 µL crucibles under a 50 mL/min $N_2$ gas flow using a METTLER TOLEDO TGA/DSC 3+ instrument at 10 °C/min up to 1000 °C. A systematic error related to the buoyancy or instrument effects can be corrected by performing a blank measurement. Thus, a blank crucible was also analysed at the beginning of each series of samples. Afterwards, the calculations were realized by subtracting the blank from each experimental result. From TGA results, the relative mass loss was calculated as the ratio of the time dependent mass to the initial mass of the sample. First, the evolution of the relative mass percentage was plotted as a function of temperature. The effect of different sample masses is discarded by using the relative mass loss instead of the absolute mass loss and it provides an adequate comparison between results. The first derivative of the relative mass loss curve was also plotted in order to depict more precisely the different thermal events.

## Appendix A.4 $^{27}$Al solid-state NMR analysis

Solid-state $^{27}$Al MAS-NMR spectra were acquired on a Bruker Avance500 (11.7 T) spectrometer operating at 130.3 MHz for $^{27}$Al. A commercial Bruket MAS probe (4 mm Zirconia rotors) was used, with a spinning speed of about 15 kHz for all the spectra. The one-pulse $^{27}$Al (I = 5/2) NMR spectra were acquired following a short pulse length of 1 µs corresponding to a pulse angle of π/6, a recycle delay time of 20 s, and 80 scans were collected per spectrum. The frequency shifts were referenced to a 0.1 M $Al(NO_3)_3$ aqueous solution.

The decomposition of the $^{27}$Al NMR spectra of the samples was performed using the DMFIT program [1]. While the tetrahedral center band resonances of well-crystallized anhydrous phases were modelled considering a second-order powder spectrum for the central transition,

the resonances of the hydrates were modelled with Lorentzian dipolar broadening because of the weak quadrupolar coupling expected in the hydrates. The spinning sidebands were not modelled and their contributions to the spectral intensity neglected.

The calculation of the bound water amount from $^{27}Al$ NMR results is explained below with an example (Table 39):

**Table 39 : Calculation of the bound water amount of 7 h-old $C_3A$ paste.**

| Phase | Integrated peak intensity (% of Al site) | Phase amount fraction (a.u.) | Molar mass (g/mol) | Weight fraction of the phase (wt. %) | Bound water (wt. %) |
|---|---|---|---|---|---|
| $Ca_3Al_2O_6$ | 43.5 | 21.75 | 270 | 35 | - |
| $Ca_3Al_2(OH)_{12}$ | 55 | 27.5 | 378 | 62 | 18 |
| $Ca_4Al_2O_6CO_3{\cdot}11H_2O$ | 1.5 | 0.75 | 568 | 3 | 1 |

$$Weight\ fraction\ of\ phase\ i = \frac{Phase\ fraction_i * M_i}{\sum_0^i Phase\ fraction * M_i}$$

$$Bound\ water_{phase} = \frac{Weight\ fraction_i * n(H_2O) * M_{H_2O}}{M_{phase}}$$

With $M_i$ molar mass of phase i. Table 40 summarizes the molar mass of the species of interest in this study

**Table 40 : Molar mass of the species.**

| Species | M (g/mol) |
|---|---|
| $CA_2$ | 260 |
| CA | 158 |
| $C_{12}A_7$ | 1386.68 |
| $C_3A$ | 270 |
| $CAH_{10}$ | 338.24 |
| $C_2AH_8$ | 358 |
| $C_2AH_{7.5}$ | 341 |
| $C_4AH_{19}$ | 668 |
| $C_4AH_{13}$ | 560 |
| $C_4AčH_{11}$ | 568 |
| Katoite – $C_3AH_6$ | 378.32 |
| Gibbsite – $AH_3$ | 156.02 |

# Appendix A.5 Isothermal conduction calorimetry

Isothermal calorimetry measures the difference in heat flow between a sample of hydrating cement paste and an inert sample (of the same heat capacity as the sample, an ampoule containing water was used as a reference). The measurements are performed on a few grams of paste introduced in a glass tube immediately after the mixing then sealed with a metal cap and introduced into a TA Instruments 8-channel TAM Air isothermal conduction calorimeter. The temperature of the isotherm is fixed at 25 °C. For in-situ mixing method, a special commercial apparatus (Admix Ampoule Stirrer, TA Instruments) combined with two syringes of 1 ml was used. The mixing is directly performed inside the calorimeter. Regarding the uncertainty of measurements when ex-situ mixing is realized. Table 41 shows the normalized cumulative heat results of CA pastes hydrated for one day at 25°C with a w/c of 0.5 and the calculated standard deviation on the four measurements.

**Table 41: Estimation of uncertainty based on the standard deviation calculated from isothermal calorimetry results of 24 h-old CA pastes (w/c=0.6. 25 °C).**

| CA paste (w/c=0.6) | Normalized cumulative heat ($J/g_{CA}$) |
|---|---|
| 1 | 352.3 |
| 2 | 352.5 |
| 3 | 318.1 |
| 4 | 342.7 |
| 5 | 349.9 |
| *Standard deviation* | *10 $J/g_{CA}$* |
| ***Uncertainty*** | *5 %* |

# Appendix A.6 ICP-AES analysis

The elemental concentrations of solutions were quantified with ICP-AES (Thermo Scientific iCAP 6000 Series). All reagents and stock standard solutions used were purchased from Sigma-Aldrich. Before the analysis, the sample uptake tubing and torch glassware were rinsed with diluted nitric acid and demineralized water. In addition, during the analysis, it was necessary to rinse the tubes before/after sample analysis.

The pH and temperature of the collected aqueous fractions were immediately measured after sampling with a pH electrode (Mettler Toledo, InLab Expert Pt1000 pH 0-14T 0-100°C) calibrated using two IUPAC pH buffers at 12.45 (25 °C) and 9.18 (25 °C). After pH measurements, the liquid fractions of the suspensions were acidified with 2 wt. % nitric acid ($HNO_3$) solution to prevent their carbonation. The dilution resulting from $HNO_3$ addition was

recorded and used afterwards to exploit the ICP-AES analysis results. The stock standard solutions (at a concentration of 1000 mg/L) of each cation were used for the preparation of aqueous standard and diluted with the prepared $HNO_3$ solution at concentrations ranging from 0.5 to 10 ppm for aluminium and from 2.5 to 30 ppm for calcium (see Table 42). The dilution factors used to analyze aluminium and calcium of the samples were 10, 20 and 100. The standard error of measurement was approximately 10 %.

**Table 42 : Calibration range of the elements analyzed during ICP-AES measurements.**

| | Standard solution | | | | | |
|---|---|---|---|---|---|---|
| **Element** | 1 | 2 | 3 | 4 | 5 | 6 |
| **Al (mg/L)** | 0 | 0.5 | 1 | 2.5 | 5 | 10 |
| **Ca (mg/L)** | 0 | 2.5 | 5 | 10 | 25 | 30 |

# Appendix A.7 **Characterization of hydration products**

In order to characterize the evolution of mineralogical phase assemblages as a function of the hydration time, hydration stoppage is performed by using the solvent displacement method [2, 3]. Hydration reactions were stopped in the pastes and suspensions by rinsing with isopropanol.

For both pastes and suspensions samples, solid fractions were collected and crushed manually into fine powders in isopropanol (IPA or propan-2-ol. Technical. *VWR. France*). Afterward, the powders were rinsed three times with isopropanol by filtration under vacuum using a polyethersulfone (PES) membrane with a 0.45 µm pore size. Successively, the samples were stored and dried at room temperature in a controlled humidity chamber (with a relative humidity of 20 % at 22±2 °C) for several days.

All of the powders were further ground by hand below 100 µm. The mineralogical assemblage of the hydration products were characterized by TGA, XRD and certain samples by $^{27}Al$ solid-state NMR.

Qualitative phase analyses of the phases of powder diffraction patterns were performed by XRD. As mentioned in literature review section, the common hydrates formed in $CaO\text{-}Al_2O_3\text{-}H_2O$ systems are $CAH_{10}$, $C_2AH_{7.5\text{-}8}$, $C_4AH_x$ (here x=13 or 19 depending on the relative humidity), aluminium hydroxide and $C_3AH_6$ [4-6]. Table 43 lists the Powder Diffraction File™ (PDF®) numbers used to identify the different hydrated phases in this study.

**Table 43 : Identity numbers of crystalline hydration products from the Powder Diffraction File.**

| PDF number | Phase |
|---|---|
| 00-061-0217 | $CaAl_2O_4 \cdot 10H_2O$ |
| 00-062-0851 | $Ca_2Al_2O_5 \cdot 7.5H_2O$ |
| 00-045-0564 | $Ca_2Al_2O_5 \cdot 8H_2O$ |
| 01-087-0493 | $Ca_4Al_2(OH)_{12}(CO_3)(H_2O)_5$ |
| 00-041-0219 | $Ca_4Al_2O_6CO_3 \cdot 11H_2O$ |
| 00-036-0377 | $Ca_4Al_2(OH)_{12}(OH)(CO_3)_{0.5}(H_2O)_4$ |
| 00-042-0487 | $Ca_4Al_2O_7 \cdot 19H_2O$ |
| 00-024-0217 | $Ca_3Al_2(OH)_{12}$ |
| 01-080-6432 | $Al(OH)_3$ (Gibbsite) |

# Appendix A.8 Summary of enthalpy values

The enthalpies of dissolution of $CA_2$ and CA are calculated from their corresponding enthalpies of formation [7] as follows:

$$\Delta_r H = \Sigma \Delta_f H(\text{products}) - \Sigma \Delta_f H(\text{reactants})$$

The enthalpy of dissolution of $CA_2$:

$$CA_2 + 2\ OH^- + 7\ H_2O \rightleftharpoons Ca^{2+} + 4\ Al(OH)_4^-$$

$$-4000 - 2x230 - 7x286 \rightleftharpoons -543 - 4x1500.85$$

$\Delta_{diss}H$ = -80.6 kJ/mol

**$\Delta_{diss}H$ = -309.8 J/g**

The enthalpy of dissolution of CA:

$$CA + 4\ H_2O \rightleftharpoons Ca^{2+} + 2\ Al(OH)_4^-$$

$$-2327 - 4x286 \rightleftharpoons -543 - 2x1500.85$$

$\Delta_{diss}H$ = -73.7 kJ/mol

**$\Delta_{diss}H$ = -466.6 J/g**

The enthalpies of reaction of each species in Table 44 are described here.

**Table 44 : Enthalpies of reaction of dissolution in J/g for the calculation of degree of hydration and below enthalpies of reaction of precipitation in J/g at 25 °C and 1 bar [7].**

| Species | $\Delta_r H$ (J/g) | Ref. |
|---|---|---|
| *Dissolution* | | |
| $CA_2$ | −498 | [8, 9] |
| CA | −693 | [8, 9] |
| $C_{12}A_7$ | −703 | [10] |
| $C_3A$ | −868 | [11] |
| *Precipitation* | | |
| $CAH_{10}$ | −104 | [7] |
| $C_2AH_8$ | −61 | |
| $C_2AH_{7.5}$ | −320 | |
| $C_4AH_{19}$ | −590 | |
| $C_4AH_{13}$ | −855 | |
| $C_4AH_{11}$ | −1037 | |
| $C_4A\check{C}H_{11}$ | −291 | |
| $C_3AH_6$ | −609 | |
| $AH_3$ – Gibbsite | −94 | [8] |

# Appendix A.9 CEMDATA2018 database

Please follow the reference [7] to access the full database. Table 45 and Table 46 present only the phases of interest in this study.

**Table 45 : Cemdata18 database, reproduced from [7].**

| | $\Delta_f G°$ [kJ/mol] | $\Delta_f H°$ [kJ/mol] | S° [J/K/mol] | $a_0$ [J/K/mol] | $a_1$ [J/mol/K$^2$] | $a_2$ [J K/mol] | $a_3$ [J/K$^{0.5}$/mol] | V° [cm$^3$/mol] |
|---|---|---|---|---|---|---|---|---|
| **Clinkers** | | | | | | | | |
| $C_3A$ | −3382.35 | −3561 | 205 | 261 | 0.019 | $-5.06\cdot10^6$ | – | 89 |
| $C_{12}A_7$ | −18,451.44 | −19,414 | 1045 | 1263 | 0.274 | $-2.31\cdot10^7$ | – | 518 |
| CA | −2207.90 | −2327 | 114 | 151 | 0.042 | $-3.33\cdot10^6$ | – | 54 |
| $CA_2$ | −3795.31 | −4004 | 178 | 277 | 0.023 | $-7.45\cdot10^6$ | – | 89 |
| **AFm-phases** | | | | | | | | |
| $CAH_{10}$ | −4623.0 | −5288.2 | 610 | 151 | 1.113 | – | 3200 | 193 |
| $C_2AH_{7.5}$ | −4695.5 | −5277.5 | 450 | 323 | 0.728 | – | – | 180 |

| | | | | | | | | |
|---|---|---|---|---|---|---|---|---|
| $C_4AH_{13}$ | −7325.7 | −8262.4 | 831.5 | 208.3 | 3.13 | – | – | 274 |
| **Hydrogarnet** | | | | | | | | |
| $C_3AH_6$ | −5008.2 | −5537.3 | 422 | 290 | 0.644 | $-3.25\cdot10^6$ | – | 150 |
| **(Hydr)oxides** | | | | | | | | |
| $Al(OH)_3$(am) | −1143.2 | - | | Not defined | | | | 32 |
| $Al(OH)_3$(gibbsite) | −1151.0 | −1288.7 | 70.1 | 36.2 | 0.191 | – | – | 32 |
| CH (portlandite) | −897.01 | −985 | 83 | 187 | −0.022 | – | −1600 | 33 |

**Table 46 : Cemdata18 database, reproduced from [7].**

| Mineral | Dissolution reactions used to calculate solubility products $logK_{s0}$ |
|---|---|
| $C_3A$ | (CaO)3Al2O3 + 4H+ = 2AlO2- + 3Ca+2 + 2H2O@ |
| $C_{12}A_7$ | (CaO)12(Al2O3)7 + 10H+ = 14AlO2- + 12Ca+2 + 5H2O@ |
| CA | CaOAl2O3 = 2AlO2- + Ca+2 |
| $CA_2$ | CaO(Al2O3)2 + H2O@ = 4AlO2- + Ca+2 + 2H+ |
| $CAH_{10}$ | CaOAl2O3(H2O)10 = 2AlO2- + Ca+2 + 10H2O@ |
| $C_2AH_{7.5}$ | Ca2Al2(OH)10(H2O)2.5 + 2H+ = 2AlO2- + 2Ca+2 + 8.5H2O@ |
| $C_4AH_{13}$ | Ca4Al2(OH)14(H2O)6 + 6H+ = 2AlO2- + 4Ca+2 + 16H2O@ |
| $C_3AH_6$ | Ca3Al2O6(H2O)6 + 4H+ = 2AlO2- + 3Ca+2 + 8H2O@ |
| $Al(OH)_3$(am) | Al(OH)3 = AlO2- + H+ + H2O@ |
| $Al(OH)_3$(gibbsite) | Al(OH)3 = AlO2- + H+ + H2O@ |
| CH (portlandite) | Ca(OH)2 + 2H+ = Ca+2 + 2H2O@ |

# Appendix A.10 Solution compositions

The solution compositions at invariant points plotted in the solubility diagrams of the concerned chapters are given in Table 47 and Table 48.

**Table 47 : Solution compositions at invariant points for $CA_2$ and CA (w/c=25).**

| Time (h) | $[Ca^{2+}]$ (mmol/L) | $[Al(OH)_4^-]$ (mmol/L) | Time (h) | $[Ca^{2+}]$ (mmol/L) | $[Al(OH)_4^-]$ (mmol/L) |
|---|---|---|---|---|---|
| $CA_2$ | $CA_2$ | $CA_2$ | CA | CA | CA |
| **0.02** | 0.74 | 1.18 | **0.02** | 8.76 | 15.77 |
| **0.03** | 0.93 | 1.56 | **0.03** | 11.16 | 20.51 |
| **0.05** | 1.08 | 1.82 | **0.05** | 13.08 | 24.58 |
| **0.07** | 1.19 | 2.08 | **0.07** | 14.48 | 27.31 |
| **0.08** | 1.30 | 2.32 | **0.08** | 15.75 | 29.90 |

| | | | | | |
|---|---|---|---|---|---|
| **0.17** | 1.65 | 2.90 | **0.17** | 18.71 | 35.19 |
| **0.25** | 1.90 | 3.45 | **0.25** | 20.10 | 38.33 |
| **0.33** | 2.05 | 3.76 | **0.33** | 20.41 | 38.59 |
| **0.42** | 2.21 | 4.01 | **0.42** | 20.21 | 38.56 |
| **0.50** | 2.35 | 4.35 | **0.50** | 20.73 | 39.93 |
| **0.67** | 2.50 | 4.60 | **0.67** | 21.40 | 41.04 |
| **1.00** | 2.78 | 5.37 | **1.00** | 21.55 | 41.59 |
| **1.50** | 3.02 | 5.83 | **1.50** | 22.33 | 43.30 |
| **2.00** | 3.13 | 6.23 | **2.00** | 22.03 | 42.78 |
| **2.17** | 3.23 | 6.43 | **2.17** | 20.73 | 40.48 |
| **2.33** | 3.32 | 6.61 | **2.33** | 20.87 | 40.85 |
| **2.50** | 3.43 | 6.80 | **2.50** | 19.59 | 38.11 |
| **2.67** | 3.55 | 7.07 | **2.67** | 16.94 | 32.91 |
| **2.83** | 3.69 | 7.24 | **2.83** | 9.87 | 17.47 |
| **3.00** | 3.83 | 7.50 | **3.00** | 9.10 | 15.76 |
| **3.50** | 4.25 | 8.44 | **3.17** | 8.20 | 14.87 |
| **4.00** | 4.74 | 9.46 | **4.00** | 8.29 | 13.80 |
| **5.50** | 7.26 | 11.76 | **5.50** | 6.85 | 11.46 |
| **7.00** | 8.11 | 11.80 | **7.00** | 8.14 | 11.05 |
| **8.00** | 8.15 | 11.45 | | | |

**Table 48 : Solution compositions at invariant points for $C_{12}A_7$ and cubic-$C_3A$ (w/c=25).**

| **Time** | **$[Ca^{2+}]$** | **$[Al(OH)_4^-]$** | **Time** | **$[Ca^{2+}]$** | **$[Al(OH)_4^-]$** |
|---|---|---|---|---|---|
| **(h)** | **(mmol/L)** | **(mmol/L)** | **(h)** | **(mmol/L)** | **(mmol/L)** |
| **$C_{12}A_7$** | **$C_{12}A_7$** | **$C_{12}A_7$** | **$C_3A$** | **$C_3A$** | **$C_3A$** |
| **0.02** | 9.03 | 11.53 | **0.02** | 8.24 | 4.80 |
| **0.03** | 9.76 | 14.01 | **0.03** | 9.19 | 5.30 |
| **0.05** | 10.17 | 16.45 | **0.05** | 8.75 | 5.06 |
| **0.07** | 10.68 | 18.47 | **0.07** | 9.36 | 5.23 |
| **0.08** | 11.51 | 21.06 | **0.08** | 8.90 | 4.99 |
| **0.17** | 15.82 | 29.70 | **0.17** | 9.32 | 4.96 |
| **0.25** | 17.95 | 34.42 | **0.25** | 8.80 | 4.56 |
| **0.33** | 19.77 | 38.02 | **0.42** | 9.02 | 4.55 |
| **0.42** | 21.15 | 40.69 | **0.50** | 8.57 | 4.32 |
| **0.50** | 21.98 | 42.76 | **0.67** | 8.53 | 4.22 |
| **0.67** | 22.97 | 44.57 | **1.00** | 8.94 | 4.36 |
| **1.00** | 24.50 | 47.44 | **2.00** | 8.38 | 4.17 |
| **1.50** | 24.77 | 47.63 | **3.00** | 8.38 | 4.29 |

| | | | | | |
|---|---|---|---|---|---|
| **2.00** | 24.61 | 47.43 | **4.00** | 8.60 | 4.53 |
| **3.00** | 23.61 | 46.06 | **5.50** | 8.61 | 4.81 |
| **4.00** | 23.00 | 44.93 | **7.00** | 9.15 | 4.98 |
| **5.00** | 22.39 | 43.94 | | | |
| **5.50** | 21.45 | 42.28 | | | |
| **6.00** | 16.07 | 30.99 | | | |
| **6.50** | 10.57 | 17.60 | | | |
| **7.00** | 9.02 | 13.69 | | | |

## References


[1] D. Massiot *et al.*, "Modelling one- and two-dimensional solid-state NMR spectra," *Magnetic Resonance in Chemistry*, https://doi.org/10.1002/mrc.984 vol. 40, no. 1, pp. 70-76, 2002/01/01 2002.

[2] J. Zhang and G. W. Scherer, "Comparison of methods for arresting hydration of cement," *Cement and Concrete Research*, vol. 41, no. 10, pp. 1024-1036, 2011/10/01/ 2011.

[3] R. Snellings *et al.*, "RILEM TC-238 SCM recommendation on hydration stoppage by solvent exchange for the study of hydrate assemblages," *Materials and Structures*, vol. 51, no. 6, p. 172, 2018/12/13 2018.

[4] M. Atkins, F. P. Glasser, and A. Kindness, "Cement hydrate phase: Solubility at 25°C," *Cement and Concrete Research*, vol. 22, no. 2, pp. 241-246, 1992/03/01/ 1992.

[5] B. Lothenbach, L. Pelletier-Chaignat, and F. Winnefeld, "Stability in the system CaO–$Al_2O_3$–$H_2O$," *Cement and Concrete Research*, vol. 42, no. 12, pp. 1621-1634, 2012/12/01/ 2012.

[6] J. H. Ideker, K. L. Scrivener, H. Fryda, and B. Touzo, "12 - Calcium Aluminate Cements," in *Lea's Chemistry of Cement and Concrete (Fifth Edition)*, P. C. Hewlett and M. Liska, Eds.: Butterworth-Heinemann, 2019, pp. 537-584.

[7] B. Lothenbach *et al.*, "Cemdata18: A chemical thermodynamic database for hydrated Portland cements and alkali-activated materials," *Cement and Concrete Research*, vol. 115, pp. 472-506, 2019/01/01/ 2019.

[8] S. Klaus, "Quantification of CA hydration and influence of its particle fineness during early hydration of calcium aluminate cement," Friedrich-Alexander-Universität Erlangen-Nürnberg, 2015.

[9] S. Klaus, A. Buhr, D. Schmidtmeier, S. Kuiper, and F. Goetz-Neunhoeffer, "Hydration of calcium aluminate cement phase CA and $CA_2$ in refractory applications," presented at the UNITECR 2015 - 14th Biennial Worldwide Congress, Vienna, 2015.

[10] H. T. Nguyen, "Transfert hydrique dans le milieu poreux réactif : Application à l'étude de séchage d'une pâte pure ettringitique au jeune âge," Doctorat, Mécanique, Energétique, Génie Civil, Acoustique, INSA Lyon, Ecole Doctorale ED162, INSA Lyon, 2018LYSEI124, 2018.

[11] D. Jansen, F. Goetz-Neunhoeffer, B. Lothenbach, and J. Neubauer, "The early hydration of Ordinary Portland Cement (OPC): An approach comparing measured heat flow with calculated heat flow from QXRD," *Cement and Concrete Research*, vol. 42, no. 1, pp. 134-138, 2012/01/01/ 2012.

## RÉSUMÉ

Lorsque des déchets nucléaires irradiants sont conditionnés en matrice cimentaire, l'eau contenue dans la solution porale et dans les hydrates peut être radiolysée, conduisant notamment à la production de dihydrogène. Dans le cas de déchets fortement irradiants, la maitrise de ce terme source hydrogène dans un site d'entreposage et/ou de stockage peut constituer un enjeu de sûreté. Ce terme source hydrogène peut-être limité en diminuant la quantité d'eau mise en œuvre pour élaborer les matrices cimentaires de conditionnement, ou en choisissant un liant cimentaire dont les produits d'hydratation présentent un faible rendement de production radiolytique de dihydrogène. De ce point de vue, les ciments alumineux pourraient présenter un intérêt significatif par rapport aux ciments silico-calciques. En effet, l'hydratation des ciments alumineux conduit à des assemblages minéralogiques dont les hydrates présentent une bonne stabilité sous irradiation. Toutefois, la vitesse d'hydratation de ces ciments est parfois élevée et incompatible avec les contraintes d'un atelier de cimentation industriel. Il convient donc de mieux comprendre les mécanismes d'hydratation de ces phases pour éventuellement mieux les contrôler.

Dans le cadre de ce travail, le déroulement de l'hydratation de quatre aluminates de calcium anhydres synthétiques, se distinguant l'un de l'autre par leur rapport C/A, a été étudié. En particulier, ont été examinés, leur vitesse d'hydratation, leur degré d'hydratation et l'assemblage minéralogique formé. Les suivis d'hydratation ont été réalisés par microcalorimétrie isotherme et conductimétrie quand les phases ont été caractérisées par analyse thermogravimétrique, par diffraction des rayons-x et par résonance magnétique nucléaire du solide. Toutes les expériences ont été réalisées à 25 °C. Les résultats du suivi de l'hydratation de pâtes de ciment et de suspensions cimentaires nous ont permis de conclure que les vitesses d'hydratation sont d'autant plus grandes que le rapport C/A de l'anhydre considéré est élevé. De plus, l'étude de l'hydratation de ces phases anhydres en suspension a permis d'identifier les chemins réactionnels suivis par chacun des systèmes étudiés. Notamment, il a été démontré que la formation d'hydroxyde d'aluminium limite la cinétique d'hydratation des phases anhydres dont le rapport C/A est inférieur ou égal à 1. Les résultats obtenus dans le cadre de ce travail pourront permettre à terme d'orienter le choix du ciment alumineux à mettre en œuvre pour le conditionnement de déchets irradiants.



## MOTS CLÉS

ciment alumineux, hydratation, aluminates de calcium hydraté, degré d'hydratation, conductimétrie, microcalorimétrie, RMN du solide



## ABSTRACT

This Ph-D project takes place in the framework of nuclear waste conditioning in cementitious matrices. When an irradiating nuclear waste is stabilized and solidified in a cementitious matrix, the radiolysis of water molecules from the pore solution and from the hydrates themselves yields dihydrogen. In the case of highly irradiating wastes, the release of dihydrogen raises safety issues for storage and/or disposal facilities. The release of hydrogen gas by radiolysis can be limited by reducing the amount of water used for the elaboration of the cement or by choosing a cement binder with hydrates showing a good stability under irradiation. As far as radiolysis is concerned, calcium aluminate-based cements are of significant interest in comparison to calcium silicate cements. The hydration of calcium aluminate cements leads to mineralogical assemblages with a low radiolytic yield of dihydrogen. However, the hydration of these cements is sometimes too fast and incompatible with the industrial process requirements. The objective of this thesis is thus to better understand the underlying mechanisms of the hydration of the calcium aluminates present in calcium aluminate-based cements.

Specifically, the course of hydration of four synthetic anhydrous calcium aluminates, varying one from each other by their C/A ratio, is studied at 25°C from the point of view of their hydration rate, their degree of hydration and the resulting mineralogical assemblages by a combination of isothermal calorimetry, thermogravimetric analysis, x-ray diffraction and solid-state nuclear magnetic resonance. Monitoring the hydration by isothermal calorimetry in pastes and by conductometry in suspensions show that the higher the C/A ratio of the considered anhydrous phase, the higher the hydration rate. Finally, studying the hydration of each of these phases in suspension makes it possible to point out the reaction path followed by each studied system. This work also demonstrated that aluminium hydroxide formation limits the kinetics of hydration of anhydrous phases with a C/A ratio lower than or equal to 1. The results obtained in the framework of this thesis can help optimizing the design of a calcium aluminate cement-based matrix to be used for the conditioning of irradiating wastes.



## KEYWORDS

calcium aluminate cement, hydration, calcium aluminate hydrates, hydration degree, conductometry, isothermal calorimetry, solid-state NMR